

Università degli Studi di Napoli
“Federico II”



SCUOLA POLITECNICA E DELLE SCIENZE DI BASE
AREA DIDATTICA DI SCIENZE MATEMATICHE, FISICHE E NATURALI
Doctorate in Earth, Environmental and Resource Sciences
(XXXIII cycle)

Head of the Doctorate: Prof. Maurizio Fedi

Supervisor
Prof. Stefano Tavani

PhD student
Marco Snidero

ROLE OF INHERITANCES IN SHAPING THE
ZAGROS THRUST AND FOLD BELT

Contents

Abstract 4

Introduction 6

Methods 13

**Chapter 1: Temporal evolution of the Darmad-
dan salt diapir, eastern Fars region 15**

1.1 Abstract 15

1.2 Introduction 16

1.3 Geological Setting 20

1.4 The Darmadan anticline 26

1.5 Discussion: diapir evolution 38

1.6 Conclusions 42

**Chapter 2: The Zagros-Oman deformation front in the east-
ern Persian Gulf: role of structural inheritance 44**

2.1 Abstract 44

2.2 Introduction 45

2.3 Stratigraphic framework 49

2.4 Dataset 49

2.5 Seismic interpretation 50

2.6 Evolution of the Zagros-Oman related structures 59

2.7 Conclusions 60

**Chapter 3: Diapir kinematics in a multi-layer salt sys-
tem from the eastern Persian Gulf 63**

3.1 Abstract 63

3.2 Introduction 63

3.3 Dataset 68

3.4 Geological Setting 68

3.5 Salt structures 73

3.6 Discussion 81

3.7 Triggering mechanisms 86

3.8 Conclusions 89

**Chapter 4: The Mountain Front Flexure in the Lurestan region of the
Zagros belt: crustal architecture and role of structural inheritance 91**

4.1 Abstract 91

4.2 Introduction 91

4.3 Geological setting 94
4.4 Data and methods 98
4.5 Results 100
4.6 Balanced cross section 109
4.7 Discussion 112
4.8 Conclusions 118

Final remarks 119

Glossary 122

References 126

Abstract

The claim that a place has a unique geology is made often, and never incorrectly. The Zagros fold and thrust belt represents an exceptional example where different structural and stratigraphic inheritances co-exist along the same mountain range, playing a key role in determining the lateral variability of the thrust and fold belt. To the south-east, the Zagros mountains are limited by the Makran subduction zone. The subduction is pinned laterally by the continental collision of Arabia and Asia in the Straits of Hormuz area, where the Zagros and Oman chains meet. This zone of transition forms a major structural reentrant where the Zagros deformation front and the main Zagros thrusts converge.

This boundary represents the eastern limit of the Hormuz salt basin, characterized by a minimum of two kilometers thick salt unit deposited during the Neoproterozoic-Cambrian times. The Hormuz salt province aerially extends for over 500 km toward the north-west along the Fars Province, where spectacular diapirism developed previously to the Zagros contractive event. Besides, the presence of an effective basal decollement resulted in a wide detached thrust and fold belt shaping the structural salient of the Fars arc. The northwestern-ward thinning and finally pinch-out of the Hormuz salt is progressively taken over by the presence of the Mountain Front Flexure, a major structure of the Zagros orogenic system underlain by the deeply rooted and seismically active Mountain Front Fault system. These coupled structural features divide the belt from its foreland and their trace is sinuous, forming a sequence of salients and recesses, formally named, Dezful embayment, Lurestan arc and Kirkuk embayment.

In this work we combine the interpretation of on-shore and off-shore seismic reflection profiles, field data, earthquake data, geomorphic analysis, and, remote sensing interpretations, to build a series of geological maps, 3D geological reconstructions, geological and balanced cross-sections, and, sequential restorations in the eastern Fars province and the Lurestan region.

We provide new evidence from different structures of the Zagros fold-and-thrust belt, to stress the role of inheritances related with the previous rift architecture and the presence of the lateral facies change to the Hormuz salt sequence, as an important lateral variations of the mechanical properties of the multilayer, and a dramatic change in the structural style related with the pre-contractual Hormuz salt diapirism.

In the Fars province we propose new interpretations for several on-shore and off-shore pre-contractual salt structures. Our evolutionary models show how the deformation of inherited salt structures predates thrust wedging and leads to squeezing, roof arching, crestal extension and finally extrusion. Further shortening result on secondary welding as evidenced by the collapse of the extrusion summit dome and reverse faulting nucleated at the secondary welds. Regional cross sections across the eastern Hormuz salt pinch-out aim to understand the switch in structural style from a salt-detached thin- to thick-skinned thrusting.

In the Lurestan region we introduce a new interpretation of an hyperextended margin architecture segmented by inherited N-S and NE-SW striking faults, in an alternance of more proximal or distal rift domains. The integration of our results with previous knowledge indicates that the Mountain Front Fault system developed in the necking domain of the Jurassic rift system, ahead of an array of inverted Jurassic extensional faults, in a structural fashion which resembles that of a crustal-scale footwall shortcut. Within this structural context, the sinusoidal shape of the Mountain Front Flexure in the Lurestan area arises from the re-use of the original segmentation of the inverted Jurassic rift system.

Introduction

The term inheritance includes localized tecto-stratigraphic features that are reologically different from the surrounding rocks and/or that produce the lateral juxtaposition of different rheological domains. Inheritances are ubiquitous in the continental lithosphere and, during deformation, they force the development of structures differing from those that would develop an ideal layer-cake like geological framework. The notion of inheritance has its roots in the Wilson's cycle and, more in detail, in the concept of reuse of lithospheric-scale structures formed during previous rifting or collisional events (e.g. Wilson, 1966; Dewey and Bird, 1970).

It is very widely demonstrated that pre-existing mechanical discontinuities such as faults, shear zones, compositional layering undergo reactivation, therefore influencing fault-zone localization and development (e.g. Holdsworth et al., 1997). The influence of preexisting structures has been suggested at plate scales (e.g. Sykes, 1978; Daly et al., 1989; Snyder et al., 1997; Tikoff et al., 2001), regional scales (e.g. Doré et al., 1997; Needham and Morgan, 1997; Pinheiro and Holdsworth, 1997), outcrop scales (Shail and Alexander, 1997; e.g. Rubinat et al., 2013), grain scales and microscopic scales (e.g. Hippler and Knipe, 1990; Lloyd and Knipe, 1992; Knipe and Lloyd, 1994). The influence of pre-existing structures is particularly important in continental regions as the relatively buoyant quartzofeldspathic crust is rarely subducted, thereby imparting a long-lived architecture of inheritance that is not preserved in (mainly younger) oceanic lithosphere (e.g. Sutton and Watson, 1986). On the contrary, exposed regions of high-grade metamorphic basement rocks are generally believed to be representative of the continental crust that underlies most deformation zones and rifted basins at depth. Most basement complexes exhibit widespread circumstantial evidence for reactivation of pre-existing structures, playing a key role in determining the lateral variability of thrust-and-fold belts.

Since the 80's, the systematic documentation of faults reactivated with an opposite sense of slip, has shaped the idea of structural inheritances (e.g. Butler et al., 2006 and references therein), leading to the development of the concept of inversion tectonics (e.g. Glennie and Boegner, 1981; Cooper et al., 1989). Positive and negative inversion tectonics are nowadays widely documented worldwide, both in orogens and extensional basins, corresponding to extensional fault systems reactivated with a reverse sense of slip (e.g. Williams et al., 1989; Marshak et

al., 2000; Carrera et al., 2006) and thrusts reused as normal faults (e.g. Gamond, 1994; Curzi et al., 2020; Lucca et al., 2019), respectively. In shallow crustal levels, fault reactivation is controlled by frictional processes (Rutter, 1986), basically dependent on the cohesion, the coefficient of friction, and the orientation of the fault in respect to the stress field and the local pore-fluid pressures (Jaeger and Cook, 1979; Zoback, 2010).

Inversion tectonics occur when the regional shortening/stretching direction is oriented at a high angle with respect to the inherited fault system. When inheritances are highly oblique to the shortening/stretching direction, their most striking effect is the production of a marked lateral variation in the structural style, which does not limit to the strike-slip reactivation of inherited faults.

An example of this is the occurrence of salients and recesses in orogenic systems, which may retrace either the lateral segmentation of previous rift systems (e.g. Macedo and Marshak, 1999; Tavani et al., 2020) or the lateral pinch out of ductile decollement levels (e.g. McQuarrie, 2004; Muñoz et al., 2013). The same concept applies to rift systems, whose along strike architecture is frequently controlled by oblique inherited structures (e.g. Corti et al., 2007; Konstantinovskaya et al., 2007; Bellahsen et al., 2013; Mercier de Lépinay et al., 2016; Tavani et al., 2018; Heron et al., 2019).

Rifted margins are known to be systematically segmented by inherited features occurring at a variety of scales: from inherited basin-bounding fault systems (e.g. Corti, 2012), to crustal layering developed during the rifting process (e.g. Clerc et al., 2015). In detail, the segmentation of extensional structures occurring in continental rift systems can be achieved by transfer and/or accommodation zones (e.g. Morley et al., 1990; Gawthorpe and Hurst, 1993; Faulds and Varga, 1998; Acocella et al., 2005), both types being likely to the occurrence of previous discontinuities. Such inherited features are largely considered as the major parameters controlling the evolution of orogenic systems and their related foreland fold-and-thrust belts (Macedo and Marshak, 1999; Lacombe and Bellahsen, 2016).

In more detail, extensional fault systems tend to be segmented by soft- and hard-linked transfer faults (Gibbs, 1984; Morley et al., 1990). Fault segmentation results from the interaction of fault growth processes with pre-existing crustal features, and has a large impact on the sedimentary facies distribution of extensional basins (Gawthorpe and Hurst, 1993).

The deformation sequence leading to the formation of fold-and-thrust belts typically includes the involvement of the different structural domains of the passive

margin and their related fault systems, along with their corresponding sedimentary facies belts. The distribution of passive margin facies is strongly controlled by the geometry of the rift margin and its main extensional faults, as well as the amount of extension taken by the continental crust. Continental to shallow water facies prevail in the proximal domains of rifted margins where stretching of the continental crust is limited, whereas deeper water facies are deposited in more distal parts of the margin, where the continental crust undergoes significant amounts of extension. The transition between shallow water facies such as mixed carbonate-siliciclastic platforms, to deep water facies such as radiolarite basins is usually marked by the necking area of the rift margin, where the ductile parts of the continental crust have been completely thinned out during the final stages of rifting (e.g. Manatschal et al 2014; Peron-Pinvidic et al., 2020). From a rheological point of view, this necking area marks a strength discontinuity (i.e., Petri et al. 2019) between relatively weak upper crustal rocks and significantly stronger crystalline basement below; such strength discontinuity inherited from rifting that favors the localization of any subsequent contractional deformation.

In rift and passive margin settings, thick and aerially extensive deposits of evaporites have been deposited throughout geological history (Richter, 1970; Ziegler, 1989; Cartwright and Jackson, 2008; e.g. Brun and Fort, 2012; Quirk et al., 2012). The most important variable controlling salt structural style in rift basins and passive margins is the timing of salt deposition with respect to rifting (Jackson and Vendeville, 1994; Rowan, 2014). Three broad classifications are recognized: prerift salt, synrift salt, and late synrift/postrift salt (Figure 1). The relative timing of salt deposition strongly influences the lateral continuity of the salt detachment and the thickness of the salt source layer, both of which play a major role in subsequent salt tectonics. Synrift salt is found in interior rifts and along divergent continental margins (or their convergent successors). Before synrift evaporites accumulate, grabens and half-grabens partly fill with synrift, mostly continental deposits. Evaporites pond in half-grabens, forming wedges that end abruptly near fault scarps (Figure 2). High horsts are free of salt, whereas low horsts are draped by salt connecting thicker salt in flanking half-grabens. As evaporites continue to accumulate, initial sub-basins of salt thicken and can merge into broader salt basins. Synrift salt may vary extremely in primary thickness, both within a subbasin and between subbasins, depending on the basement fault throw versus salt thickness. In this case, the basement structural inheritances play a key role in the architecture and distribution of salt basins. One of the most well known,

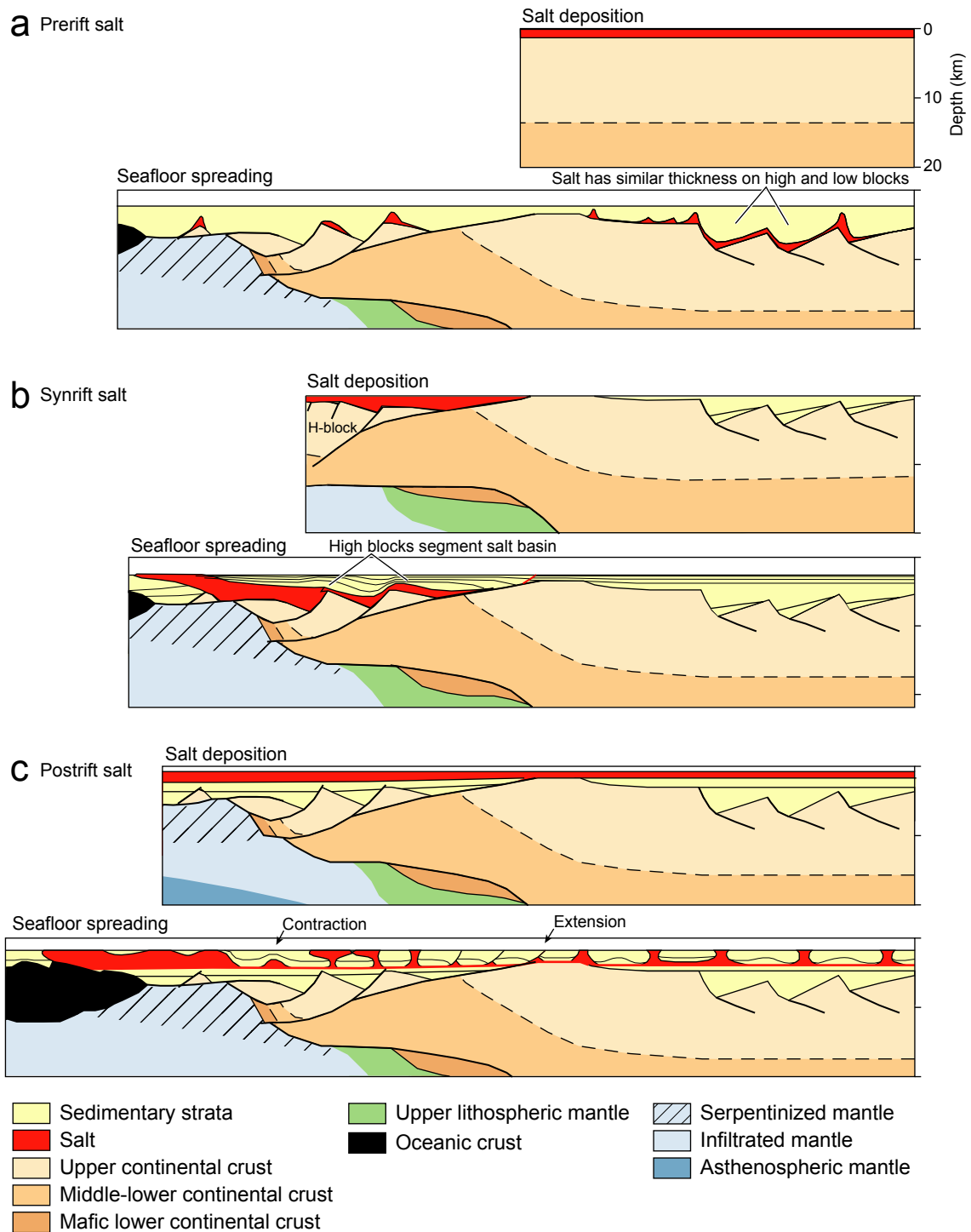


Fig.1: Salt geometry depends on the timing of salt deposition with respect to rifting. (a) Where salt is prerift, the salt layer is offset but there is little thickness change across faults, depending on the degree of structural coupling between basement and cover. Salt structures in upthrown and downthrown blocks thus have access to similar thicknesses of source layer. (b) Thicknesses of synrift salt can vary greatly across basement faults. Salt subbasins can be segmented by high blocks having thin salt or no salt. (c) A postrift salt layer is highly continuous. Linked kinematic systems having large magnitudes of translation are most common in this setting. After Rowan (2014).

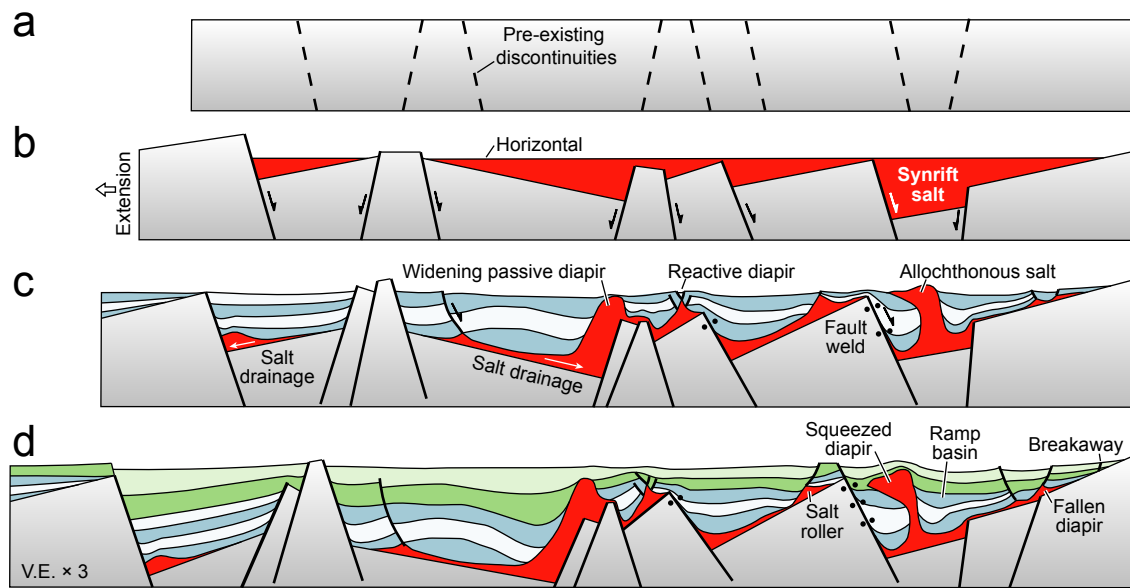
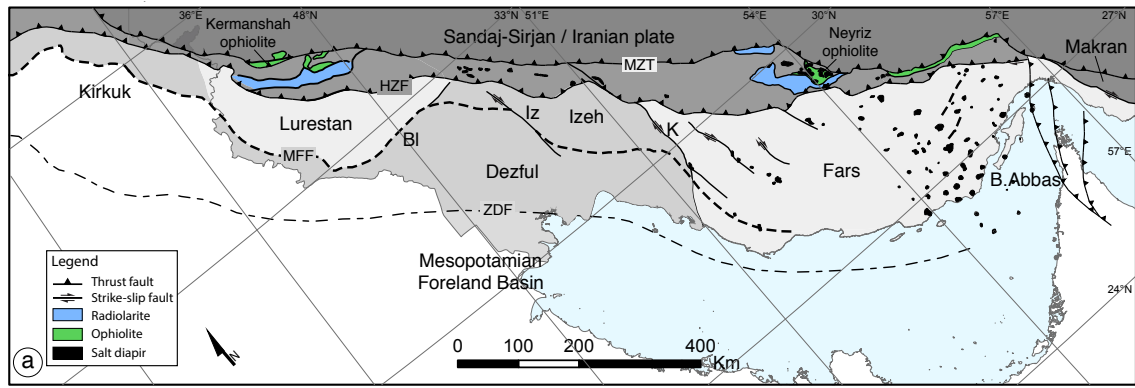
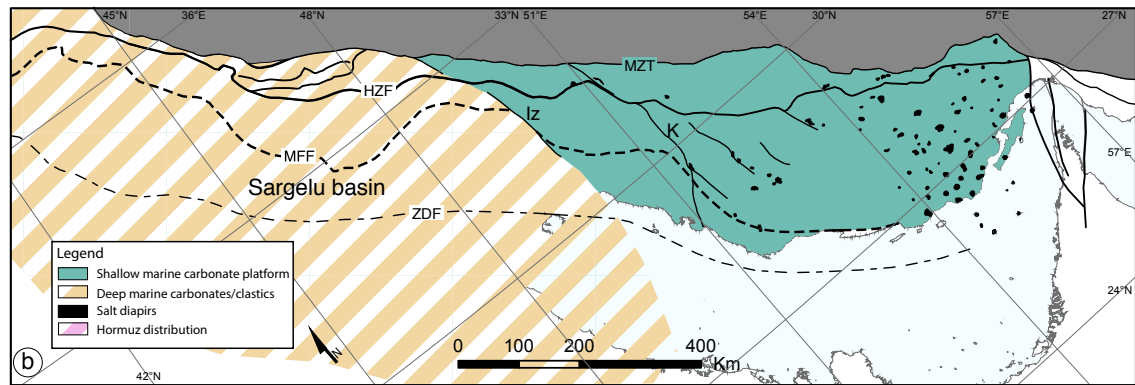


Figure 2: During rifting, subbasins of synrift salt accumulate in grabens and half-grabens so that salt thickness varies greatly. Reactive, falling, and extensional passive diapirs form in the synkinematic overburden. As rifting progresses, autochthonous salt thins and extension in the cover is increasingly coupled to that in the basement. Tilting may produce small linked kinematic systems in some subbasins. After Jackson and Hudec 2017.

otherwise still poorly understood syn to post-rift salt basin, is the Neoproterozoic to early Cambrian Hormuz Salt basin (Kent, 1958; Stöcklin, 1968; e.g. Falcon, 1969; Player, 1969). Extensive layered evaporitic sequences allow for the presence of regionally significant décollement horizons (e.g. Davis and Engelder, 1985). Salt is inherently weak (Jackson and Vendeville, 1994), and for the same matter, structural styles in salt-detached fold-and-thrust belts and rift systems are markedly different to those systems detached along frictional décollements (e.g. Vergés et al., 1992). Furthermore, the Hormuz Salt basin is characterized by the presence of numerous outcropping salt diapirs (Harrison, 1921; Richardson, 1926; e.g. De Böckh et al., 1929; Lees, 1931) often connected at depth as wide salt wall structures (e.g. Snidero et al., 2019). The presence of such structures powerfully influence the structural style, localizing the deformation through time (e.g. Callot et al., 2007). Consequently, the understanding of the diapirism deformation history is a key subject to address in order to understand the tectonic evolution where the presence of salt structures is significant. In the Zagros belt, the role of inheritances has long been associated with the original distribution of the Hormuz Salt at the base of an otherwise



Bajocian to Bathonian



Berriasian to Valanginian

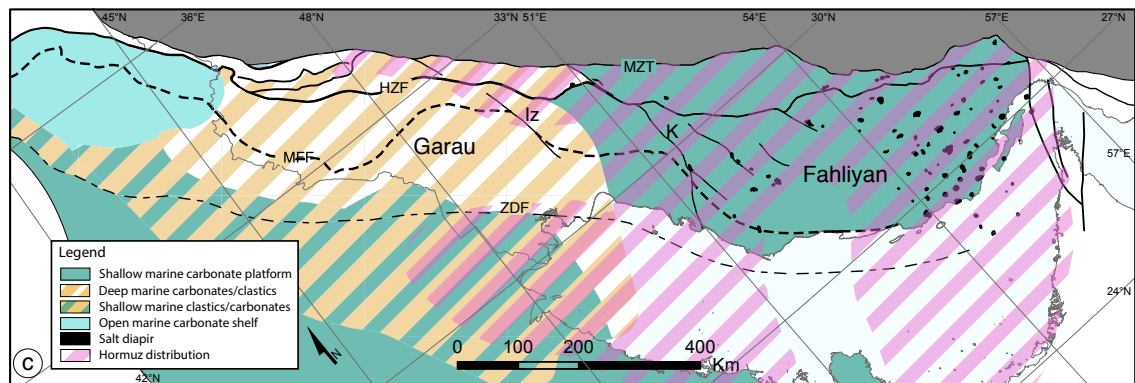


Figure 3: a) Syntetic structural map of Iran. The main structural elements outline the salients and embayment of the Zagros Fold and Thrust Belt. b) paleofacies reconstruction for the Middle Jurassic time. c) paleofacies reconstruction for the Lower Cretaceous time, overlaid and the distribution of the Hormuz salt. In detail, the extension developed during the opening of the Neo-Tethys reached its climax at the end of the Early Jurassic, when tectonically driven drowning of the long-lived Triassic to Early Jurassic carbonate platform led to the transition from shallow- to deep-water environments in large areas of the inner margin, coevally with the development of the Radiolarite Basin. During the Bajocian to Bathonian time the passive margin results separated in two main depositional environments, the deep marine carbonate to clastic deposits (over 200m depth) of the Sargelu basin to the NW and a shallow marine carbonate platform to the SE. Comparing the Middle Jurassic with the Early Cretaceous post-rift facies distribution map is highlighted that deep marine condition are preserved along the Lurestan arc in the Garau basin. Notice the analogy between the distribution of deep/shallow sedimentary environments and the nowadays distribution of salient and embayment between the Kirkuk, Lurestan and Fars regions, resembling the trend of the Mountain Front Flexure. Modified from: Koop and Stoneley, (1982); Ziegler, (2001); Barrier and Vrielynck (2008).

extremely thick sedimentary pile (figure 3c) (e.g. Bahroudi and Koyi, 2003), but also to the reactivation of deep-seated basement faults (e.g. figure 3a) (e.g. Berberian, 1995; Bahroudi and Talbot, 2003; Snidero et al., 2011; Tavani et al., 2018).

In this work we provide new evidence from different structures of the Zagros fold-and-thrust belt, to stress the role of inheritances related with: (i) faults previously formed within the Arabian plate, spanning in age from the Precambrian to the Mesozoic (e.g. figure 3a), and (ii) the presence of the lateral facies change to the Hormuz salt sequence, producing important lateral variations of the mechanical properties of the multilayer, and a dramatic change in the structural style related with the Hormuz salt diapirism. (figure 3b).

Methods

This study has been supported by a multidisciplinary methodological approach drawing from several independent datasets. These datasets include: onshore and offshore seismic reflection profiles calibrated with borehole data, geological data, geomorphic data, and earthquake hypocenter and focal mechanism data. Exhaustive field campaigns were performed in the eastern Fars and Lurestan areas. Both areas were characterized using geological maps 1:100,000 series from the Geological survey of Iran, 14-bands multispectral Aster images, Google Earth orthophotos, field observation and over 2000 field measured bedding dip data. In order to reduce uncertainties related with data projection during the construction of the geological cross-sections, a densification of the bedding dip-dataset has been performed. To digitally extract traces of layers and transform them in bedding dip orientation, publically available 0.5 m orthophotos draped onto 30 m resolution ASTER GDEM were used (e.g. Fernández, 2005; Snidero et al., 2011). This operation was performed by means of the OpenPlot software package (Tavani et al., 2011). The geological cross section and 3D surfaces have been built and balanced by means of the 3DMove software package. In detail, we have assumed flexural-slip folding (Donath and Parker, 1964) and preservation of bed thickness and line-length (Dahlstrom, 1969).

The geomorphological analysis was mainly performed in the Lurestan region (see Chapter 1). It was based on the inspection of the large-scale features (30 m resolution DEM), both active and relic, associated with the topography and drainage network within the study area. This analysis was carried out by means of investigation of satellite images (Google Earth, 2019) and orthophotos, aided by a GIS-based analysis of digital topography data (30 m resolution ASTER GDEM). Earthquake hypocentre and focal mechanism data were used to constrain the geometry of the fault systems at depth within the study area. These data are from the publically available USGS earthquake catalogue ([https://earthquake.usgs.gov/earthquakes.](https://earthquake.usgs.gov/earthquakes)) The seismic reflection profiles were acquired in different campaigns by the National Iranian Oil Company. The seismic data available in the eastern Fars area (chapter 1, 2, and 3), consist in 2D seismic reflection data covering around 34000 km². Maximum recorded depth is 7 seconds (two-way-time) and spacing of the seismic lines is 2 km in the offshore surveys, while onshore surveys show irregular distribution, orientation and spacing, grouped around the main structures, mostly along the coast and inside Qeshm island. The quality of the seismic data is generally

good in the offshore lines but variable in the onshore surveys, where most structures including the frontal limb of the Darmadan anticline (chapter 1), are poorly imaged and consequently not included in this manuscript. The seismic data was interpreted using Petrel E&P software by Schlumberger®. All data were integrated to identify and constrain the regional structure with emphasis on the Mesozoic and Lower Cenozoic basins (passive-to-active margin transition), the timing of the structures and their relationship with the main tectonic events occurred in the area. Moreover, attention was paid to the distribution of the evaporitic layers (Fars salt and Hormuz salt) concatenate with its impact on the geometry and distribution salt structures. The offshore interpretation was constrained to 16 exploration wells and aimed to achieve two main objectives: on one hand the interpretation of the main structures, their period(s) of activity and their relationship with the depocenter distribution; on the other hand, the detailed interpretation of the salt structures, their growth history, and how do they link with the geometry and distribution of the Hormuz salt layer at depth.

The onshore seismic dataset available in the Lurestan area (chapter 4) included 25 seismic reflection profiles, for a total length of about 1200 km. Although large portions of the study area are characterised by the occurrence of exposed karstified limestone (i.e. mostly the Asmari Formation), the seismic signal provide most sections with a resolution adequate for a reliable seismic interpretation. Furthermore, calibration of the seismic sections with surface geology data and the incorporation of seven wells providing further constraints for the firm interpretation of several portions of the study area. The seismic data was interpreted using 3D Move software package by Petroleum Experts® - Midland Valley®.

Chapter 1: Temporal evolution of the Darmadan salt diapir, eastern Fars region

This chapter is presented in the form of a manuscript, published in Tectonophysics (2019).

Snidero, M., Muñoz, J.A., Carrera, N., Butillé, M., Mencos, J., Motamedi, H., Piryaei, A., Sàbat, F.

1.1 Abstract

A wide range of diapirs crop out along the eastern Fars region. They are constituted by the Pre-Cambrian to Early Cambrian Hormuz Fm. and located in the transition from the frontal structures of the Zagros fold-and-thrust belt and the Oman Ranges. While, in different previous works about the Persian Gulf, off-shore diapirs the deformation history has been determined on the basis of subsurface data, onshore evidence for salt tectonics activity is often limited to post-Oligocene stratigraphic units and is significantly overprinted by shortening. The Darmadan diapir is one of the few salt structures where is possible to observe halokinetic sequences involving the pre-collision Mesozoic succession in the Fars region of the Zagros fold-and-thrust belt. The objective of our study was to characterize on the base of field data, the stratigraphic and structural relationships between the Hormuz salt and its overburden in order to establish its temporal evolution. The Darmadan diapir is interpreted as a salt stock connected to a salt wall structure at depth evolving to a passive diapir, at least since Late Jurassic-Early Cretaceous times. Expansional geometries toward the diapir reveal that primary welding was already occurred at the Albian time. The onset of contractional deformation in the internal part of the Zagros and Oman orogenic systems is recorded by the reactivation of the Darmadan diapir during the Late Cretaceous. The Darmadan diapir continued to be exposed during the Paleogene and was squeezed during the Neogene to recent Zagros deformation. Second-order contractional features and related growth geometries constrain the timing of the secondary welding during the early stages of the late Miocene Darmadan anticline development. The explained structure remarks that the present structural trends of the Zagros fold-and-thrust belt in the eastern Fars region are the result of the reactivation of preexistent salt structures.

Keywords: Iran ; Zagros fold-and-thrust belt; Darmadan; Hormuz; salt tectonics; diapirism

1.2 Introduction

The study area is located in the eastern termination of the Simply Folded Belt of the Zagros Mountains in the Fars region (Fig. 4a). The eastern Fars is characterized by the presence of numerous outcropping salt diapirs constituted by the evaporitic

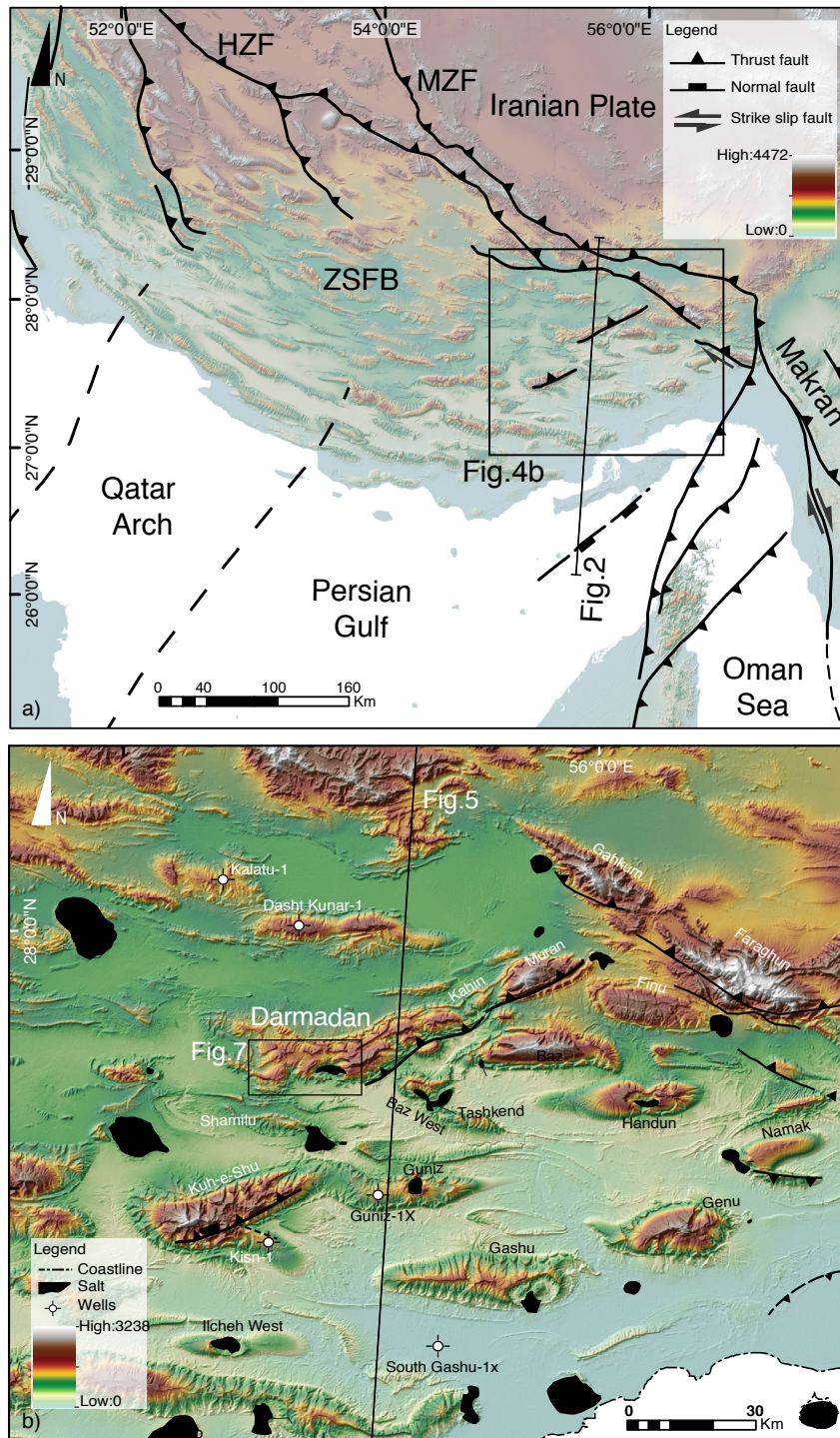


Fig. 4: a) Illustration of the major structural elements at a regional scale. ZSFB: Zagros Simply Folded Belt, HZF: High Zagros Fault, MZF: Main Zagros Fault. b) DEM of the study area with the main structures and wells used to build the regional cross section. Outcropping salt plugs are colored in black.

sequences of the Neoproterozoic to early Cambrian Hormuz Fm. (Richardson, 1926; De Böckh et al., 1929; Lees, 1931; Harrison, 1931; Kent, 1958; Gansser, 1960; Stöcklin, 1968; Player, 1969; Falcon, 1969; Fig. 4b). The eastern Fars is characterized by anticlines with variable trends departing from the regional E-W structural grain of the eastern part of the Zagros fold-and-thrust belt (Fig. 4b). Folds are punctuated by several salt diapirs which are located in different structural positions, such as the core of the anticlines, fold limbs, plunging terminations of anticlines, and in few cases also in synclines (Fig. 4b). In this area, the Hormuz Fm. is overlain by a thick Paleozoic to recent sedimentary overburden, from about 7-10 km onshore to as much as 15 km thick along the Arabian foreland (James and Wynd, 1965; Alavi, 2004; Jahani et al. 2009). All these sedimentary units have been incorporated in the Zagros fold-and-thrust belt (Fig. 5). Specifically, salt structures located in the foreland far from the orogenic front have been interpreted as controlled by the differential sedimentary rates associated with the foreland basin development of the Oman and Zagros collisional ranges (i.e., Perotti et al., 2016). On the other hand, salt structures observed in close proximity to the orogenic front present evidence for reactivation related to shortening since Late Cretaceous times (i.e., Letouzey et al, 2004; Callot et al., 2007; Callot et al. 2012).

The diachronous effect of the Mesozoic to present day shortening on the eastern Fars diapirism relates to its specific structural position, in the transition from the frontal NW-SE structures of the Zagros fold-and-thrust belt and the NE-SE Oman Ranges (Fig.4a)

The presence of emerging Hormuz salt diapirs at surface considering the thick (i.e., ~10 km) overburden led to suggest long-lasting periods of passive diapirism (Vendeville and Jackson 1992a). However, a remaining question is the potential triggering mechanism for salt diapirism responsible for the continuous and long-lasting mobilization of the Hormuz salt.

Strong supporting evidence for Paleozoic and Mesozoic halokinetic processes has been described from seismic data in the Persian Gulf, concluding that salt upwelling began by early Paleozoic times, persisting until today, with pulses of different intensities and rates strongly influenced by different sedimentary and tectonic events (Chiariotti et al., 2011; Perotti et al., 2016; Stewart, 2018). However, onshore evidence for salt tectonics activity is often limited to post-Oligocene stratigraphic units and is significantly overprinted by the late stages of shortening. Hence, in the onshore area of the eastern Fars little evidence for salt tectonics processes and diapirism prior to Oligocene times has been provided to date. Harrison (1930) and

Kent (1958), in this respect, were among the pioneering workers proposing a Late Cretaceous age for the development of Hormuz salt structures. In addition, Kent (1979) also provided first evidence for Early Cretaceous salt activity as inferred from isopach maps from around and in between salt structures. Koop and Stoonley (1982) provided evidence for Jurassic to Cenozoic salt tectonics and related changes in stratigraphic thickness. More recent works have documented thickness changes for the Jurassic to Cretaceous series, describing downbuilding geometries based on onshore seismic, field and well data (e.g., Piryaei et al., 2011; Motamedi et al., 2011).

All these previous studies have not provided a complete picture of the growth and detailed deformation history of these eastern Fars salt structures, in particular the relationship between diapirism and the main deformation events. In order to address this topic, the main aim of our study is to characterize the stratigraphic and structural relationships between the Hormuz salt and its stratigraphic overburden around the Darmadan (also referred as Harmadan) anticline (Fig. 4b). This anticline is one of the few examples in the whole Fars region where Late Jurassic to Pliocene stratigraphic series are well exposed around a Hormuz salt diapir. In the following we will show evidences for strong changes in the stratigraphic record around this fold, which include thickness and facies changes immediately around the diapir, as well as strong angular relationships that can be attributable to halokinetic sequences (e.g., Giles and Rowan 2012); in addition, contractional and extensional features of different orders have been identified at different positions around the salt structure. These stratigraphic and structural features are here interpreted as key evidence to constrain the driving mechanisms and the timing for long lived diapirism in the eastern Fars region, providing key insights for the structural evolution of the Fars region.

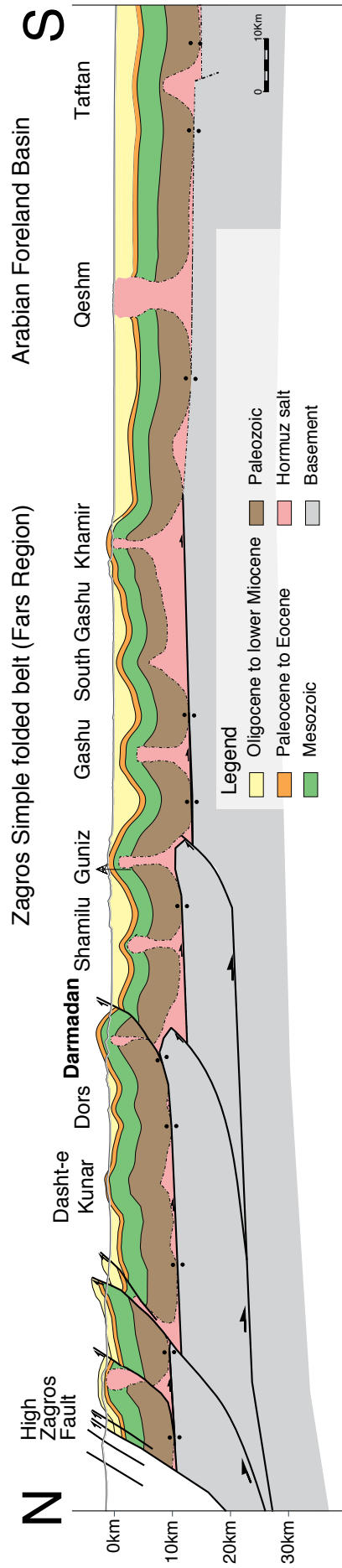


Fig.5: N-S Regional cross-section of the study area (location in Fig.4), built by the authors from field, well and seismic data. The sector included between the High Zagros Fault and the Dasht-e Kunar anticline is based on the Tavakoli-Shirazi et al. 2013 geological map. Notice the basement SE dipping normal fault in the off-shore Arabian Foreland Basin.

1.3 Geological Setting

1.3.1 Main tectonic events

The Darmadan anticline is situated in the Fars region (Fig. 4), in the more external structural domain of the Zagros Mountains commonly referred to as the Simply Folded Belt (Stöcklin, 1968). The stratigraphic pile consists of Paleozoic, Mesozoic and Cenozoic sediments that have been detached above the Neoproterozoic to Cambrian Hormuz Salt Series (Figs. 4, 5 and 6). The whole sequence lies above the crystalline basement of the Arabian Plate, which assembled during the Panafrican Orogeny in late Proterozoic times (640-620 Ma) as result of the E-W directed Amar collision, where a series of microcontinents and island arcs accreted to the Nubian (African) craton from the east (Stesser and Camp, 1985; Beydoun, 1991; Stern 1994; Hussein, 2000; Gray, 2008). During the late stages of this orogenic event (570-530 Ma) normal faulting was related to NW-trending left-lateral strike slip faults and NE-trending break away faults referred as the Najad Rift System (Hussein, 2000). All these fault systems had a strong influence during subsequent events (Ziegler, 2001; Bahroudi and Talbot 2003), such as the location of the Hormuz salt basin and its equivalent evaporites in the Middle East and Salt Ranges in Pakistan (Sepehr and Cosgrove, 2005).

During early Paleozoic times, the Paleotethys Ocean opened between Cimmeria (Laurasia) and Gondwana and a stable platform was established (Konert et al., 2001). Some authors propose a general uplift and erosion during the late Paleozoic, related to the far effect of the Variscan Orogeny in analogy to several major unconformities observed in other areas of the Arabian plate (Hussein, 1992; Konert et al., 2001; Faqira et al., 2009; Frizon de Lamotte, 2013; Tavakoli-Shirazi et al. 2013; Vennin et al., 2015). During late Permian-Lower Triassic times, the Neotethys Ocean formed between the Arabian and the Cimmeria plates. This rifting event was related to the northward drift of the Cimmeria plate which was constituted by Anatolia, Central Iran and Afghanistan (Hussein, 2000). The inherited basement heterogeneities strongly controlled the geometry of the main extensional faults of the Neotethys rift, which were distributed parallel to the older Precambrian basement trends (Berberian and King, 1981; Koop and Stoneley, 1982). These faults are NW-SE trending and mainly dip towards the northeast (Jackson, 1980) and are connected by NE-SW transform faults. The end of this event is regionally dated by an unconformity that seals the normal faults and

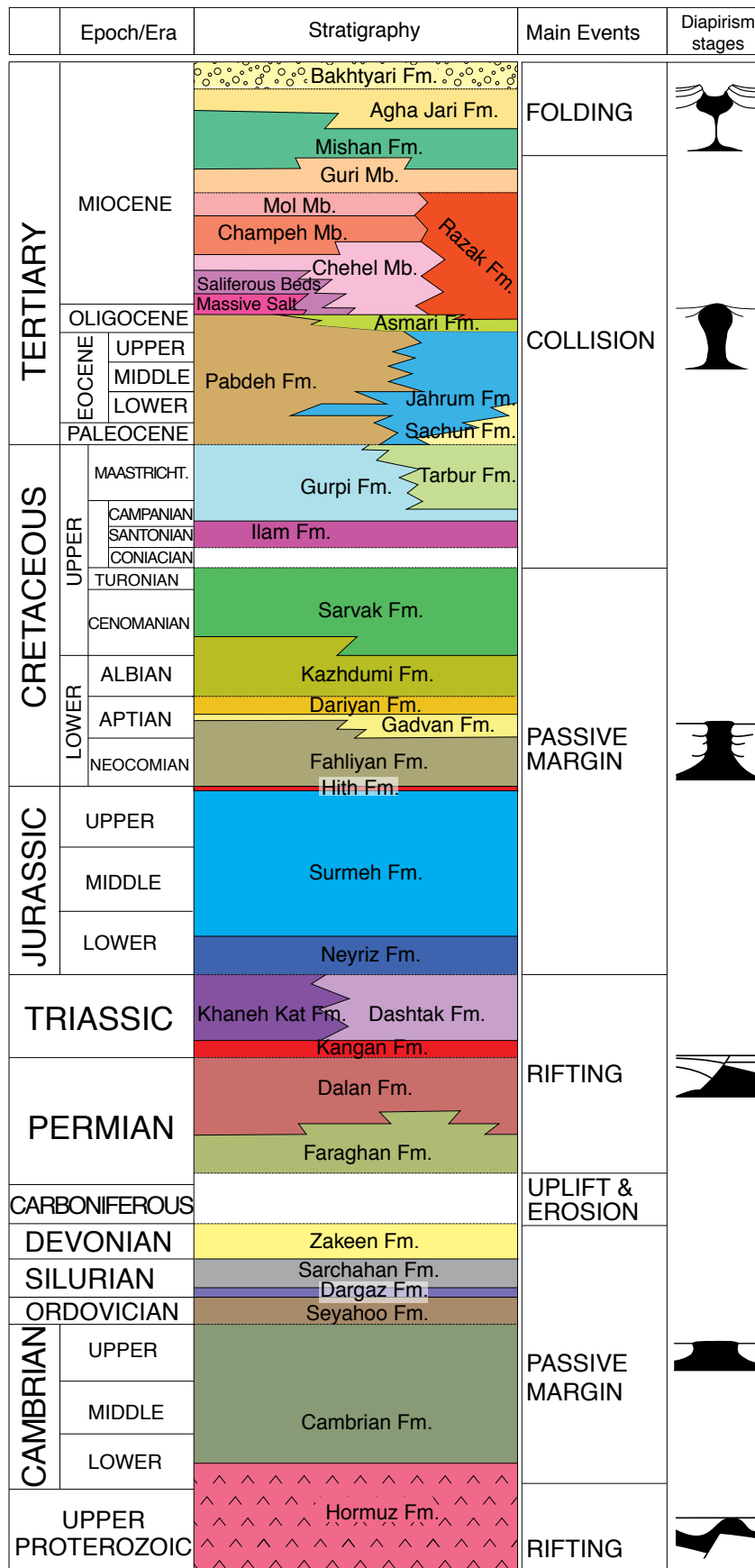


Fig.6: Stratigraphic chart of the eastern Fars region. Main tectonic events and possible mechanisms for the salt deformation in the area are shown.

separates it from the overlying Jurassic to Cretaceous continental shelf deposits (Alavi, 2004). In the Simply Folded Belt, evidence for Neotethyan Permo-Triassic extensional structures are limited to poor quality subsurface data located in the Dezful Embayment (Sepehr and Cosgrove, 2004), west of the study area.

By the Late Triassic, the Neotethys Ocean had opened up between Arabia (which included the present Zagros region as its northeastern margin) and Iran resulting in two continental margin basins on either side of the ocean. During most of the Mesozoic, the north-eastern margin of the Arabian plate (which included the present Zagros region) was relatively stable tectonically, which combined with a nearly equatorial location resulted in the development of a wide shallow carbonate ramp on the western margin of the Neotethys Ocean. During the Jurassic expansion of the Neotethys, the Paleotethys Ocean commenced subducting under the Eurasian Plate until the collision with the Cimmera Plate (e.g., Agard et al., 2011). The closing stage of the Neotethys began during the latest Jurassic–Early Cretaceous (Alavi et al., 2007). During the latest Turonian, obduction of thrust-stacked ophiolites onto the northeastern Arabian passive continental margin took place (Alavi, 2007), during a period of fast convergence between Arabia and Eurasia (Agard et al., 2011).

Obduction was located at the SW margin of the Neotethys Ocean, whereas Andean-type subduction continued at the NE side of it. Obduction ages young from Oman to NW Iranian Zagros, from Coniacian-Santonian (88-84 Ma) to Maastrichtian (68 Ma), respectively (Searle et al., 2007; Agard et al., 2011; Searle et al., 2014). Proto-foreland basins related to obduction were locally developed (Alavi, 2004) and a foreland basin setting was progressively established on the Arabian margin (Ziegler, 2001; Piryaei 2010; Saura, et al., 2015; Orang et al., 2018).

The first observed contractional deformation is coeval with the sedimentation of the Campanian-Maastrichtian Gurpi Fm. and the development of a foredeep basin that runs in front of what is usually referred to as the Oman and Zagros frontal structures. In the eastern Fars, the deformation front and consequently the foredeep depocenter progressively migrated toward the west during the Paleocene and Eocene sedimentation of the Pabdeh Fm. In Central and Northern Iran, different authors (i.e., Stoneley, 1990; McQuarrie et al. 2003; Agard et al., 2005; Mouthereau et al., 2012) propose that the final disappearance of the oceanic domain took place in the lower Oligocene and that collision must have taken place from late Oligocene to early Miocene. In Oman, compression was already finished by the early Miocene (Boote et al., 1990; Michaelis & Pauken, 1990; Searle et al.,

2014) whereas shortening related with the Arabia and the Central Iranian plate convergence lasted until recent days with the development of the Zagros fold-and-thrust belt and related Arabian foreland.

1.3.2 Stratigraphy

A synthetic review of the stratigraphic sequence along the eastern Fars areas has been compiled from bibliography and field observations (Fig. 6). The evaporitic Hormuz Fm. was deposited during the Precambrian to early Cambrian times but the lack of direct observations for most of the Hormuz basin and the mobilization of this evaporitic unit make challenging a proper evaluation of the depositional thickness. Different authors suggest a range between 1 to 4 km based on its lateral equivalents (e.g. Kent, 1970; Edgell, 1991) but the initial thickness of the Hormuz series remains highly speculative. It is composed by a sequence of massive halite, anhydrite, limestones, dark dolostones and some red sandstones and shales (Kent, 1970). Most of the sedimentary sequence from Ordovician to Devonian is made up of epicontinental siliciclastic units deposited in an intracratonic setting (Ghavidel-Syooki et al., 2014).

The Permian sequence starts with cycles of siliciclastics and dolomites of the Faraghan Fm., overlying by the bioclastic limestones, evaporites and dolostones of the Late Permian Dalan Fm. (Alavi, 2004; Zamanzadeh et al., 2009 and Kavooosi, 2013).. The Triassic sequence consists of carbonate facies of the Kangan Fm., and overlying Dashtak Fm. evaporites and their time equivalent shallow-water carbonates of the Khaneh Kat Fm. The lowermost Jurassic to upper Turonian strata are accumulated on the north- to northeast-facing shallow continental shelf of the Neotethys Ocean. The Lower Jurassic Neyriz Fm. consists of 3 units: a lower one dominated by thin-bedded dolostones and green shales, a middle sandy silty unit overlaid by an argillaceous, thin-bedded limestones to mudstones upper unit (James and Wynd, 1965). The Middle to Upper Jurassic Surmeh Fm. is the oldest unit outcropping around the Darmadan salt diapir and consist of a regressive carbonate cycle made up of open marine micritic limestones, often chalky and pyritic (Bowe, 1976, Lasemi and Jalilian, 2010) that is extensively dolomitized close to the Darmadan salt diapir. The Jurassic sequence ends with the Hith Fm. which is constituted sabkha-type anhydrites.

The base of the Lower Cretaceous succession consists of a transgressive deep-

water chalky to argillaceous limestone referred to as the Fahliyan Fm. This unit is overlain by Barremian to lower Aptian light gray marls interbedded with cryptocrystalline limestones of the Gadvan Fm.. The overlying Aptian Dariyan Fm. is characterized by thick bedded orbitolinid-bearing carbonates interbedded with pelletal and oolitic beds. Basinal conditions persisted until Aptian times, when the regressive Dariyan Fm. was deposited.

The Albian succession is a general shallowing-up cycle starting with the bituminous Kazhdumi shales and grading onwards to the thick carbonates of the late Albian to Cenomanian Sarvak Fm. The first stages of the foreland basin was infilled by a thick succession of marls represented by the Campanian to Maastrichtian Gurpi Fm. and the Paleocene to Eocene Pabdeh Fm., with its carbonate equivalent Tarbur Fm. The Pabdeh Fm. progressively grades NE-ward into the carbonate sequence of the Jahrum Fm. The presence of *Dictyoconus coskinolina* assemble zone shows a Middle Eocene age for the Jahrum Fm. in the Darmadan section. NE-ward the Jahrum Fm. grades in its lower part to the gypsiferous and terrestrial facies of the Paleocene to Eocene Sachun Fm. in a marginal restricted depositional setting. In the eastern Fars, the Jahrum Fm. is truncated by a regional unconformity during the Eocene-Oligocene boundary. This unconformity is equivalent to the AP10 and AP11 megasequences boundary in the Arabian Plate (Sharland et al., 2001). The Oligocene sequence is characterized by the marine carbonate unit of the Asmari Fm. overlaid by the Upper Oligocene and Lower Miocene Gachsaran Fm., equivalent southward to the evaporitic Fars Group (i.e., the Saliferous beds and Massive Salt in Fig.6).

In the Darmadan area, the Gachsaran Fm. is represented by three distinct members (Mbs.): a basal massive gypsum or anhydrite (i.e., Chehel Mb.), an alternating sequence of bedded limestones and green anhydritic marls (i.e., Champeh Mb.); and finally, a unit of alternating red shales with thin limestones (i.e., Mol Mb.). The middle Miocene succession is characterized by a fast transition to the cliff-forming limestones of the Guri Mb, the lowermost unit of the Mishan Fm. It consists of hard, creamy and fossiliferous limestones interbedded with rubbly limestones and marls (Rahmani et al., 2010). The middle to upper Miocene Mishan Fm. which overlies the Guri Mb., is essentially a sequence of shallow-water marine marls interbedded with bioclastic limestones and occasionally, with thin bioclastic sandstones. It varies remarkably in thickness, reaching up to 2000m as recorded from field and well data; this thickness value is very local and controlled by the early folding stages, as observed in the frontal limb of the Darmadan anticline. The upper

Miocene to Pliocene sediments consist of gray to brown calcareous sandstones, siltstones, silty marls and occasional sandstone beds and shelly limestones of the Agha Jari Fm. (Bozorgnia and Agah, 1973), overlain by massive, thick bedded and coarsening upwards fluvial deposits of the Bakhtyari Fm.

1.4 The Darmadan anticline

The Darmadan anticline is part of the southern sector of a prominent oblique E-W to NE-SW trend, composed of three major folds with three related outcropping diapirs, namely from west to east, Darmadan, Kahin and Muran (Fig. 4). The presented N-S regional cross sections (Fig. 5) passes through the Darmadan anticline about 10 km NW-ward of the study area. Taking as a reference the bottom of the synclines as a regional elevation, the Darmadan anticline shows, along this cross section, up to 1.5km of higher structural elevation than the southern structures (Leturmy et al. (2010) assert a vertical throw of 750m crossing the Kahin diapir). This structural relief progressively disappears following the plunge of the structure toward the SW and, in correspondence of the outcropping Darmadan diapir, the northern back limb is even lowered compared to the southern frontal syncline of more than 1 km.

In the area of our study (Fig. 7), the trend of the Darmadan anticline is arcuate and

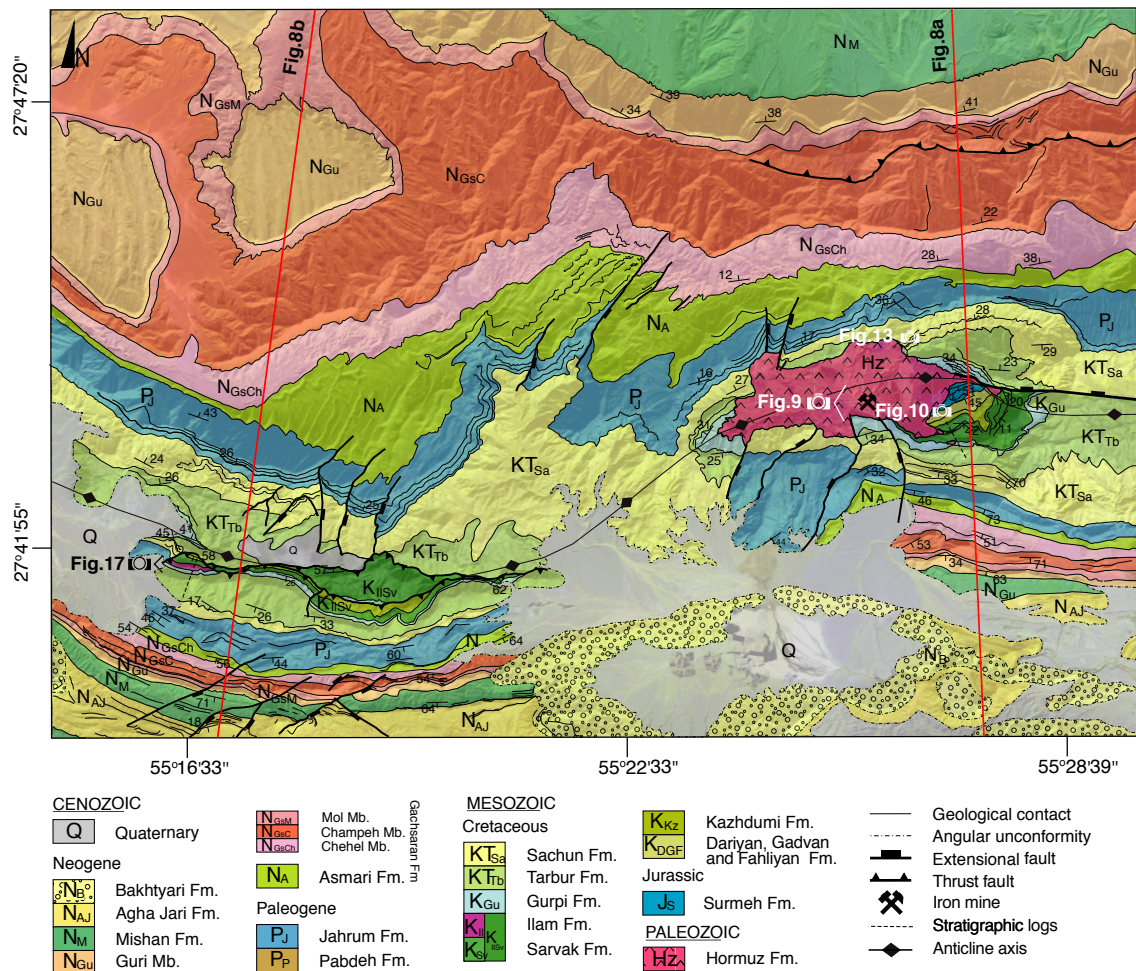


Fig.7: Geological map of the Darmadan structure (location in Fig. 4b).

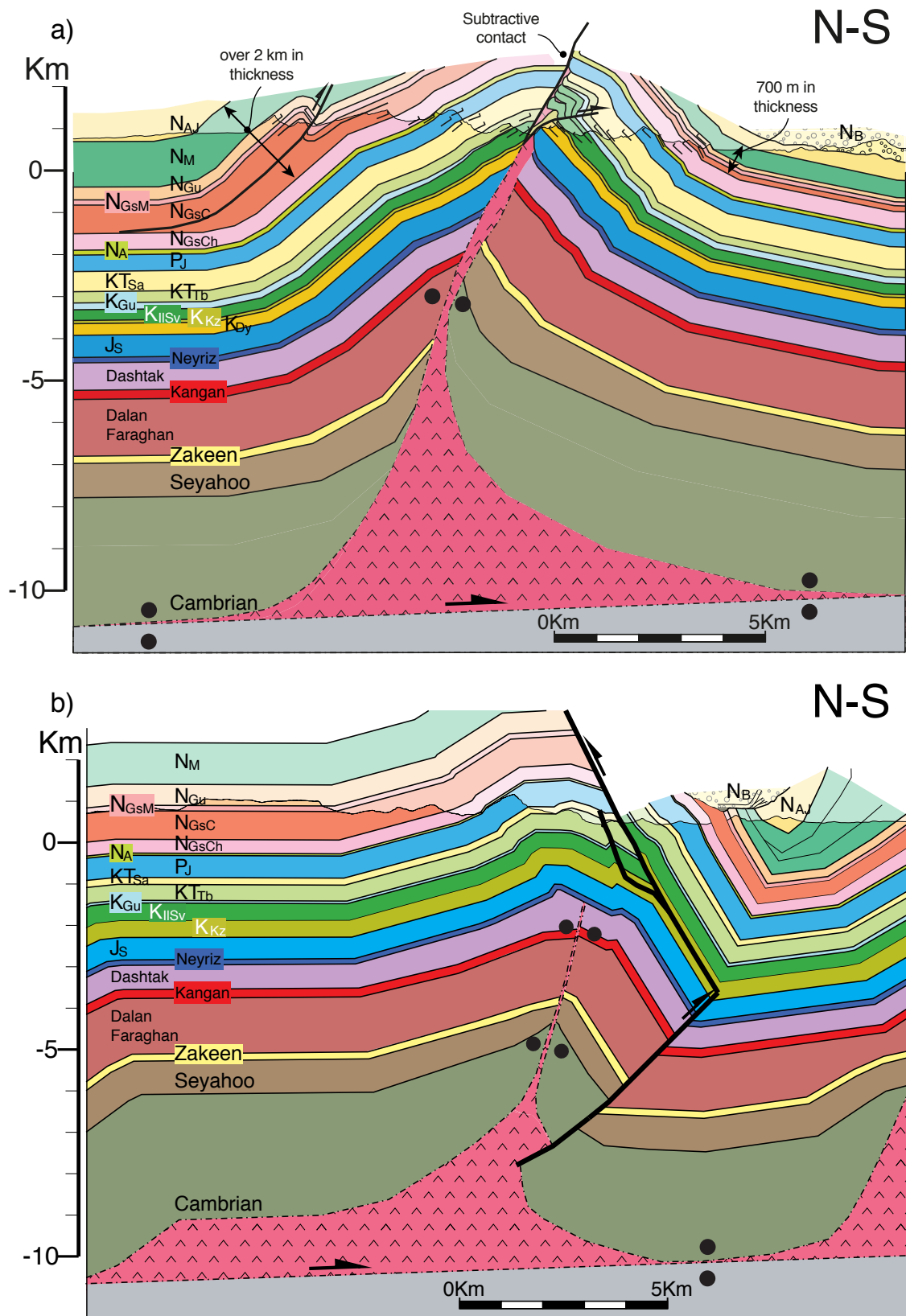


Fig.8: Cross-sections of the Darmadan structure in two different structural positions, a) Darmadan mine transect, b) Western sector. Location and stratigraphic codes are indicated in Fig.7. Black dots indicate the diapir primary/secondary welding.

progressively changes from east to west, being striking W-E around the Darmadan diapir, NE-SW in the central area and NW-SE in the westernmost part. The northern limb is gently to moderately dipping (i.e., 20° to 40°), whereas the southern limb presents significant dip variations along strike, from 30° S to overturned. The southern limb is almost completely covered by Quaternary sediments in the central part of the anticline, with outcrops occurring on either side of these deposits (Fig. 7). In the following, these areas of the Darmadan structure are described in detailed along two N-S striking profiles, namely eastern and western sectors (Fig. 8).

1.4.1 Eastern sector

On the eastern sector (Fig. 8a) the outcropping succession includes Hormuz Fm. and Upper Jurassic to Pliocene deposits (Figs. 6, 7). In this area, the Hormuz Fm. crops out in an iron ore mine where key relationships between the evaporitic formation and its sedimentary overburden are well exposed (Figs. 7 and 9). Its diapiric nature is revealed by the angular relationship with the different Mesozoic to Cenozoic stratigraphic units juxtaposed to it. The Hormuz Fm. describes an elliptical shape in map-view, defining the present-day geometry of the salt structure at surface as a salt stock (diapirs having a plan-form axial ratio < 2 , Trusheim, 1960). Around the salt stock several extensional faults display different orientations. Most of them are oriented approximately N-S, with the exception of a prominent N-dipping, W-E-trending fault that runs along the northern edge of the eastern termination of the Darmadan salt stock, separating the northern and the southern limbs of the anticline (Fig. 7 and 8a). The contact across this fault is subtractive with a maximum vertical throw of about 500m.

In the southern limb, and directly in contact with this normal fault and the Hormuz Fm., a pile of extensively dolomitized whitish well-bedded micritic carbonates with sparse crystalline basement clasts, crops out. These carbonates belong to the Upper Jurassic Surmeh Fm. and constitute the oldest exposed stratigraphic unit of the diapir overburden (Figs. 6, 7 and 9). Overlaying this formation, a sequence of dark massive carbonates crops out, probably corresponding to the Lower Cretaceous Fahliyan, Gadvan and Dariyan Fms. On top of those, a 30m thick dark green marly unit interbedded with two limestone banks (Figs. 6, 7 and 9) belonging to the Albian Kazhdumi Fm. includes orbitolinids, ammonites, echinoderms and large amounts of bivalve fragments. Above and in gradational contact, a sequence

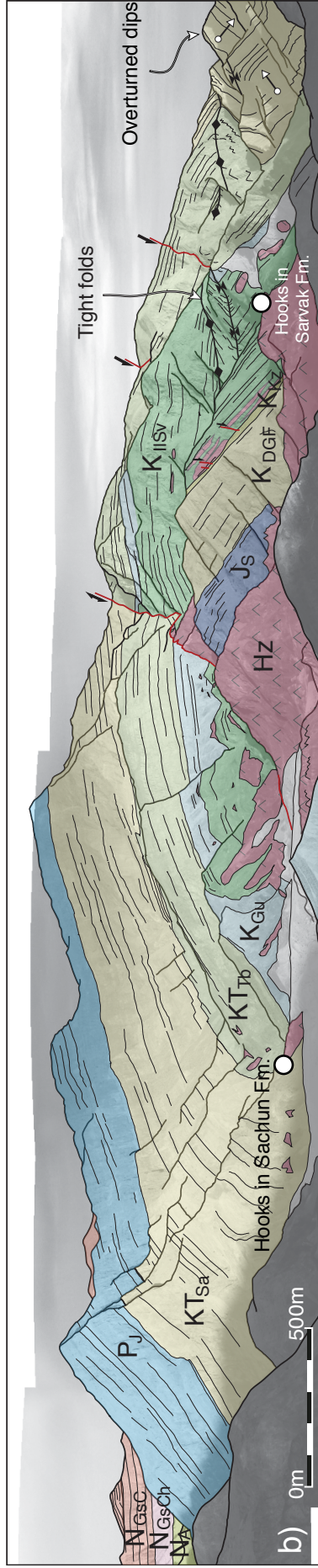
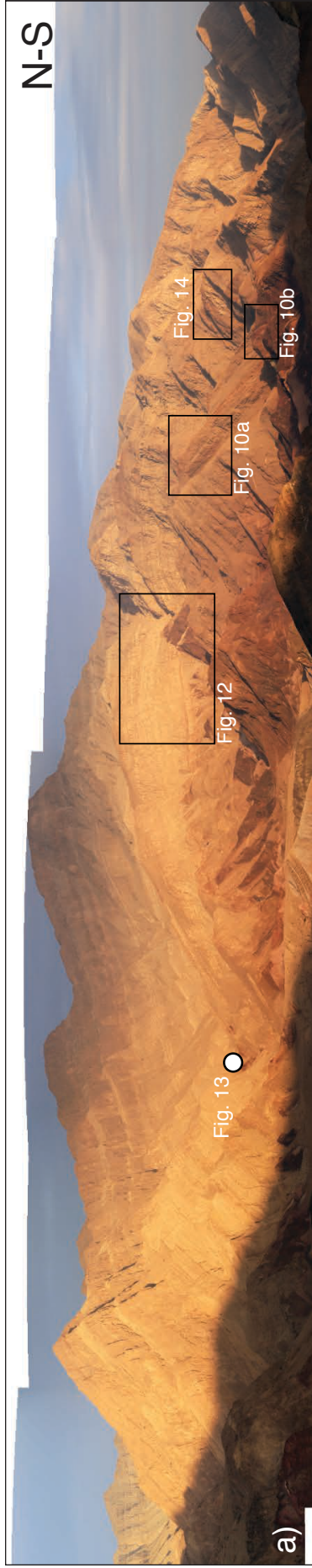


Fig.9: E-looking panoramic view of the Darmadan anticline on the eastern sector. a) Uninterpreted photograph. b) Linedrawing and main units and structures. For location and stratigraphic codes see Fig.7.

of ridge-forming neritic to shallow water wackestone and packstone carbonates containing rudists, gastropods and microfauna, corresponds to the upper Albian to Santonian Sarvak and Ilam Fms. (Figs. 6, 7 and 9). The Sarvak Fm. is constituted by several thickening upwards sequences of metric to decametric-scale thickness; the basal part of each of these sequences shows resedimented crystalline basement clasts sourced from the Hormuz Fm. in the nearby diapir (Fig. 10a and 11). Bedding-parallel chert bands within the lower parts of the Sarvak Fm. display soft-deformation structures and a cryptocrystalline texture, in close association with metric to decametric-scale normal faults that dip towards the diapir (Fig. 10a and 11). These features indicate early silicification close to the salt-sediment interface, coeval with syn-sedimentary extensional faulting.

Resedimented components of the Hormuz Fm. occur in the higher stratigraphic levels of the Sarvak Fm. in the range of coarse sand to cobble sizes, and can be followed around the diapir. These components are fundamentally constituted by resedimented crystalline basement and Albian orbitolinid-bearing limestones assigned to the Kazhdumi Fm. Moreover, the Sarvak Fm. is locally affected by tight decametric folds showing overturned limbs at the contact with the Hormuz Fm. (Fig. 10b and 11); these folded beds are unconformably overlain by younger sequences of the Sarvak Fm. and display Hormuz Fm. cusps at the edges of the diapir between the stacked Sarvak Fm. sequences. All these relationships, observed in the

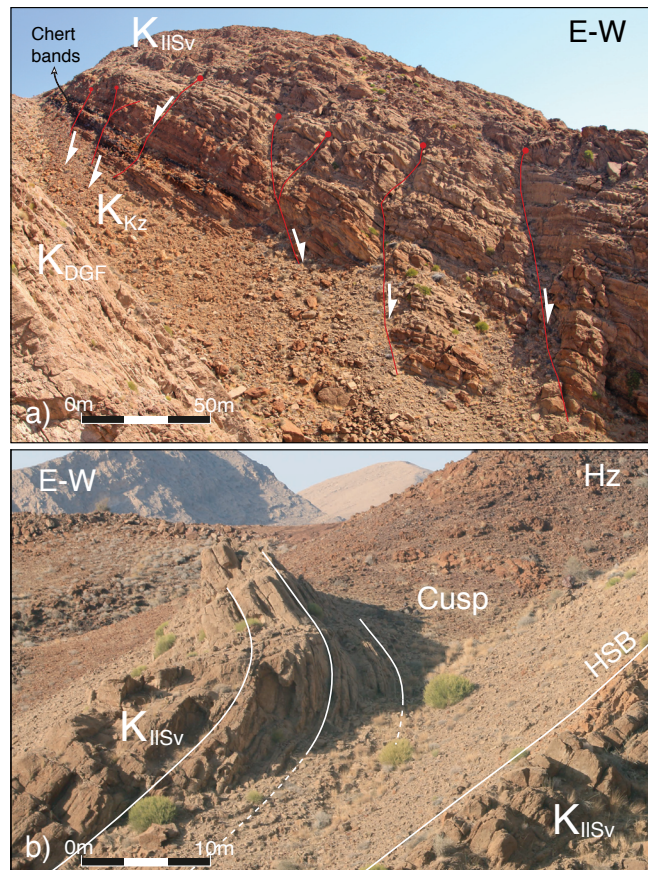


Fig. 10: Location of the field photographs in Fig. 7 and Fig. 8. a) Lower part of the Sarvak (KIIsv) sequence. Metric SW dipping normal faults are detached in the Kazhdumi marls (KIIsv). Notice the chert bands and the reddish colour of the Sarvak Fm. related with more abundant clasts sourced by the Hormuz Fm. (Hz) b) Detail of the hook geometry in Sarvak Fm. Notice how the carbonate beds below the hook sequence are not affected by the diapir growth, representing an halokinetic sequence boundary (HSB in the figure) with “cusp” like relationship with the overlying Hormuz salt.

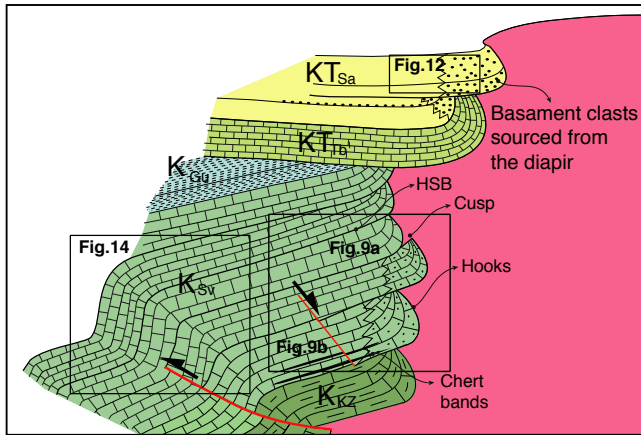


Fig. 11: Synthetic sketch of the observed relationships between diapir and overburden. The figure, not in scale, illustrates examples of the main elements of the observed halokinetic sequences. HSB: Halokinetic sequence boundary.

field, between the Hormuz Fm. and the Albian to Santonian Ilam-Sarvak Fms. suggest a series of stacked tabular halokinetic sequences up to 253m thick, with the decametric folds being hooks (Fig. 11, Giles and Rowan, 2012). To the south, the Sarvak and Ilam Fms. are overlain by the pelagic, whitish marls of the Campanian to Maastrichtian Gurpi Fm. The carbonates of the Campanian to Maastrichtian Tarbur Fm. are up to 80m thick, and are

unconformably overlying and truncating beds of the Gurpi Fm. Moreover, the Tarbur Fm. also presents internal unconformities; these being particularly well exposed at the northern limb of the Darmadan anticline (Fig. 12). The observed unconformities disappear few hundreds of meters away from the diapir along the anticline axis and are not present in the southern limb of the anticline, where the

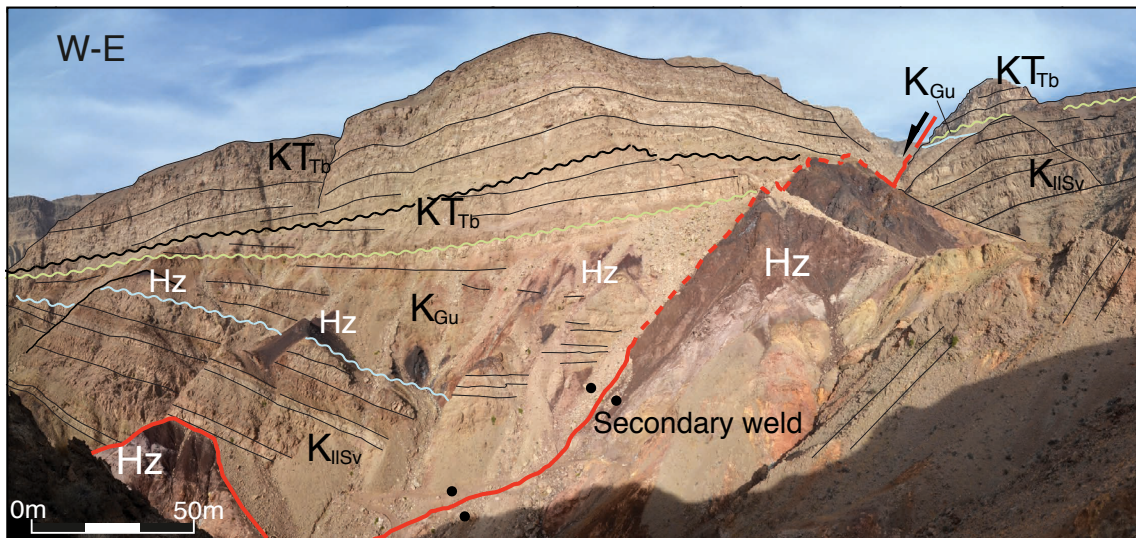


Fig. 12: N-looking view of the eastern edge of the Darmadan diapir and the N-dipping main normal fault eastward, (location in Fig.9). The Sarvak Fm. (KIISv) is tilted and unconformably overlaid by the Gurpi Fm. (KGu). Gurpi shows thickening toward the footwall of the fault and is truncated by the Tarbur Fm. (KTTb). Notice the intraformational angular unconformity in the Tarbur Fm. and the numerous overhangs of Hormuz Fm. (Hz), (dark patches) outcropping along different stratigraphic levels in the Gurpi Fm.

Maastrichtian unconformities occur in close proximity to the Darmadan salt stock, and disappear away from it.

In the southern limb of the Darmadan anticline, overlying these Upper Cretaceous units, white fine-grained and thin-bedded carbonates of the lower Paleogene Sachun Fm. occurs. Differently along the northern limb and next to the salt stock, the Sachun Fm. shows thickening (from 200m to 450m) and locally, is made up by conglomerates and sandstones of resedimented material sourced from the salt

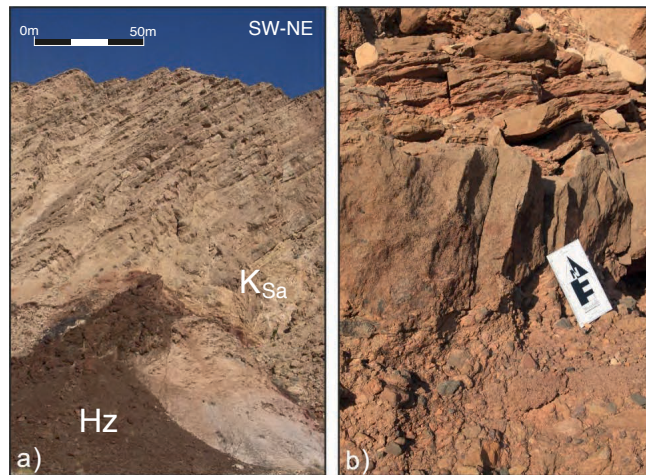


Fig.13: a) Sachun Fm. (K_{Sa}) is characterized by white thin bedded carbonates, probably accumulated in restricted shallow areas. b) Detailed photo of the Sachun Fm. in the western part of the Darmadan mine zone (see Figs. 7 and 9 for location). In that area Sachun Fm. is made up of conglomerates and sandstones with components derived from the erosion of the diapir's Hormuz Fm. (Hz). This coarse grained facies disappear away from the diapir.

stock (Fig. 13). These facies changes are clearly controlled by their distance to the diapir. In the northern flank, the Maastrichtian Tarbur Fm. and the lower Paleogene Sachun Fm. show drape folds in the immediate contact with the Darmadan salt stock, these being truncated at the top by angular unconformities (Fig. 9 and 11), in a similar fashion to the pattern observed for the Albian to Santonian Sarvak Fm. carbonates of the Eocene Jahrum Fm. conformably overlay the Sachun Fm. Above, the Asmari Fm. is in this area Rupelian in age, based on the presence of *Austrotrillina* and *Nummulites* intermedius fauna and overlaid by the Oligocene to Miocene Gachsaran and Mishan Fms.. These three units display a total thickness of 700m on the southern limb of the Darmadan anticline, whereas on the northern limb these units are as much as 2km thick (Fig. 8a). Part of such thickening (~500m) is structural as some minor south-directed thrusts and related folds occur (Figs. 7 and 8); however, the significant change in thickness requires a differential accommodation space during the Oligocene to Miocene. The Neogene sequence ends with the upper Miocene Agha Jari Fm. and the unconformably overlaying Bakhtyari Fm. conglomerates (Figs. 6 and 7).

The N-dipping W-E trending subtractive fault running along the northern edge of the eastern termination of the Darmadan salt stock brings the Maastrichtian Tarbur

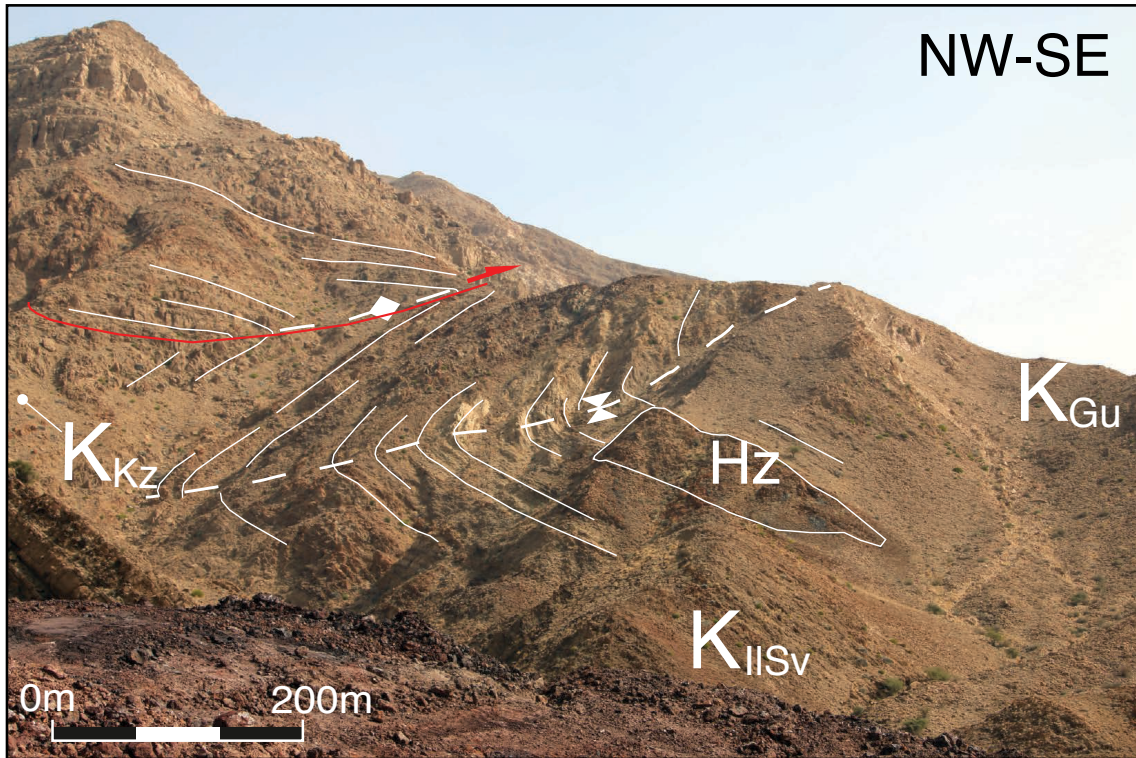


Fig.14: Detailed photo from the outcrop where folded Sarvak carbonates (KIIsv) detached over the Kazdumi Fm. are observed. The Hormuz Fm. (Hz) forms a salt wing emplaced in the Sarvak unit. Location in Fig.8. and stratigraphic codes from Fig.7.

Fm. on the northern limb of the anticline, in contact with the Albian to Santonian Ilam-Sarvak Fms. on the southern one, defining an extensional offset (Figs. 7, 8a and 12). To the north of this subtractive contact, the Sarvak Fm. is tilted and truncated underneath the Campanian to Maastrichtian Gurpi Fm. In turn, the Gurpi Fm. shows a stratigraphic expansion towards the south (Fig. 12). Along this contact several remnants of the Hormuz Fm. rocks can be observed (Figs. 7 and 12). Towards the east, the extensional offset decreases sharply, and a thrust splay off toward the southern flank of the anticline, dying out into a sequence of tight folds detached over the Albian Kazhdumi Fm. and involving the Ilam-Sarvak Fm. and sediments above (Figs. 14 and 15). These auxiliary folds present a gently ENE-dipping axial plane on the eastern side of the diapir. Eastward, the trend of these structures becomes almost E-W, affecting the forelimb of the Darmadan anticline that changes from moderately south-dipping to overturned (Figs. 7 and 15).

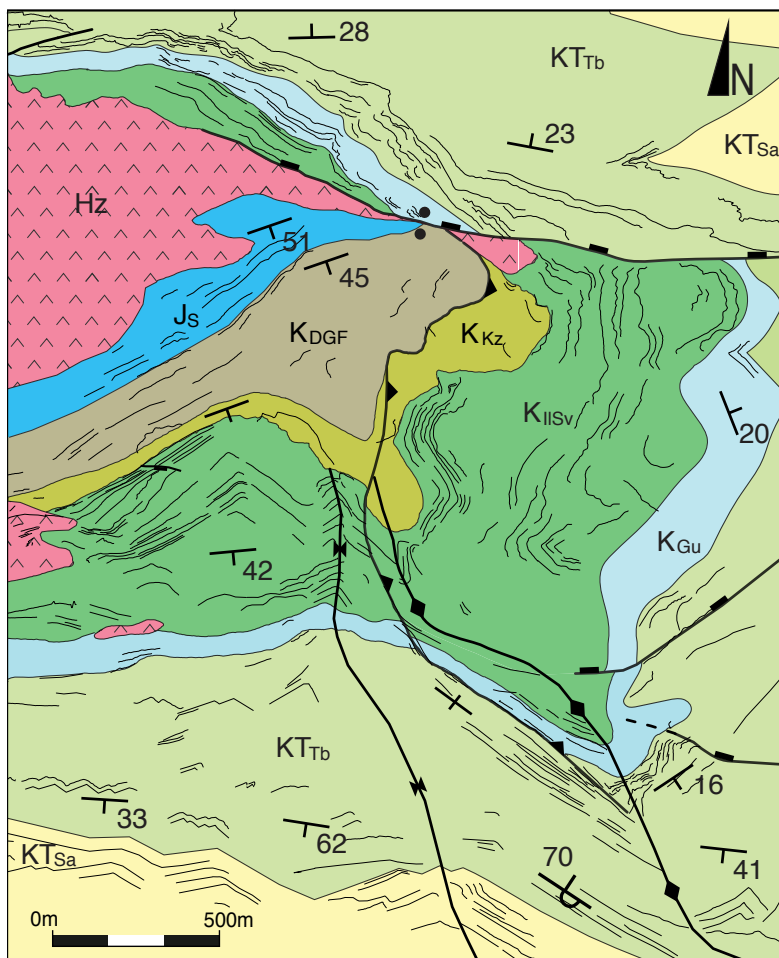


Fig.15: Structural map of the eastern side of the Darma-dan diapir. Colors and stratigraphic codes are indicated in Fig.5 and 7 respectively. The thrust and fold structures that splay from the N-dipping normal fault develop during the middle Miocene, dating the age of the diapir secondary welding.

1.4.2 Western sector

In the western sector (Fig. 8b), facies wise, the observed stratigraphic sequence is markedly similar to the eastern one, but there are no field evidences for the existence of sediments sourced from Hormuz Fm. Besides, differences in thicknesses have been reported from stratigraphic logs (Fig. 16). In this sense, the Albian Sarvak Fm. is about 140m thick and hence thinner than in the eastern sector. The Maastrichtian Tarbur Fm. is as well displaying differences in thickness with respect to the eastern sector; in the western sector, the Tarbur Fm. is about 250m in thickness (Fig. 16). Overall, there is a shift in sedimentary thickness from east to west from Albian to Maastrichtian times.

In addition, thickness variations are also observed for the Miocene Champeh Mbr. and Guri Mb., with thicker successions on the northern limb of the Darmadan anticline in the western sector (Figs. 7, and 8b). In the western sector the Darmadan anticline displays a strong asymmetry from a northern gently dipping backlimb to a steeper southern forelimb. The forelimb is affected by the presence of a steply-dipping and north-directed back-thrust system detached into the Kazhdumi Fm. marls (Figs. 7 and 8b). In the hanging wall of the main backthrust, a nice exposure of the Sarvak Fm. shows three stacked carbonate platforms with clinofolds prograding to the SW. At the bottom of these clinofolds metric blocks of

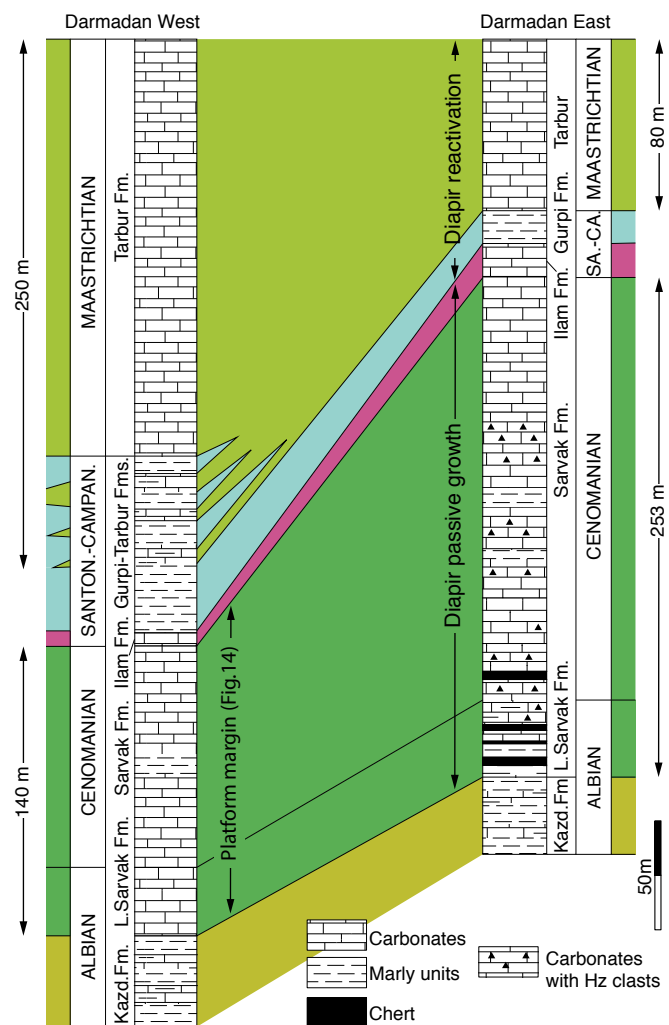


Fig.16: Stratigraphic correlation between logs representing the sedimentary succession of the Bangestan Group, Gurpi and Tarbur Fms along the two studied transects of the Darmadan anticline. The depocenter migration that happened during the Campanian is associated with the early stages of the compression affecting the Darmadan diapir.

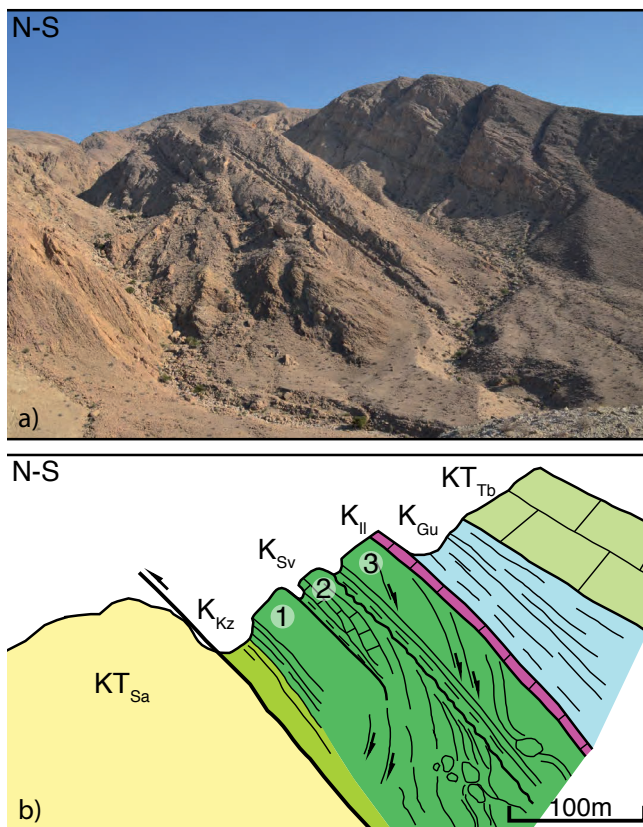


Fig.17: a) E-looking panorama of the mid Cretaceous series of the Darmadan western sector (location in Fig 4 and 13). b) Schematic cross-section across the outcrop where the mid to Upper Cretaceous sediments are thrust to the north on top of the Paleocene sediments of the Sachun Fm. (KTSa). The Sarvak Fm. (KSv) shows three stacked carbonate platforms with clinoforms prograding to the SW (numbered from 1 to 3). At its bottom several metric-sized resedimented blocks can be observed at the base of the platforms slope.

This sedimentary sequence suggests the destabilization of a platform margin during Albian times.

To the south, a tight syncline with Miocene strata belonging to the Mishan and Agha Jari Fms. is present (Fig. 7 and 8b). In its northern limb, these units present internal angular unconformities while they thicken towards the southern limb, defining a growth sequence (Fig. 8b). Above, the alluvial deposits of the Bakhtyari Fm. are folded in a syncline and unconformably overlie the complete sequence on top of an erosional surface. The Bakhtyari Fm. conglomerates also thicken southwards and present internal angular unconformities to the north, suggesting again a growth sequence. It must be highlighted the shift of the axial surface of the syncline through the unconformity at the bottom of the Bakhtyari Fm. (Figs. 8b).

Different sets of high angle normal faults, trending from N-S to NNE-SSW are crosscutting the outcropping succession (Fig.7). These faults are strictly confined to the flanks of the anticline and show an offset from decametric to hectometric-scale in a similar fashion of the N-S faults observed in the eastern sector.

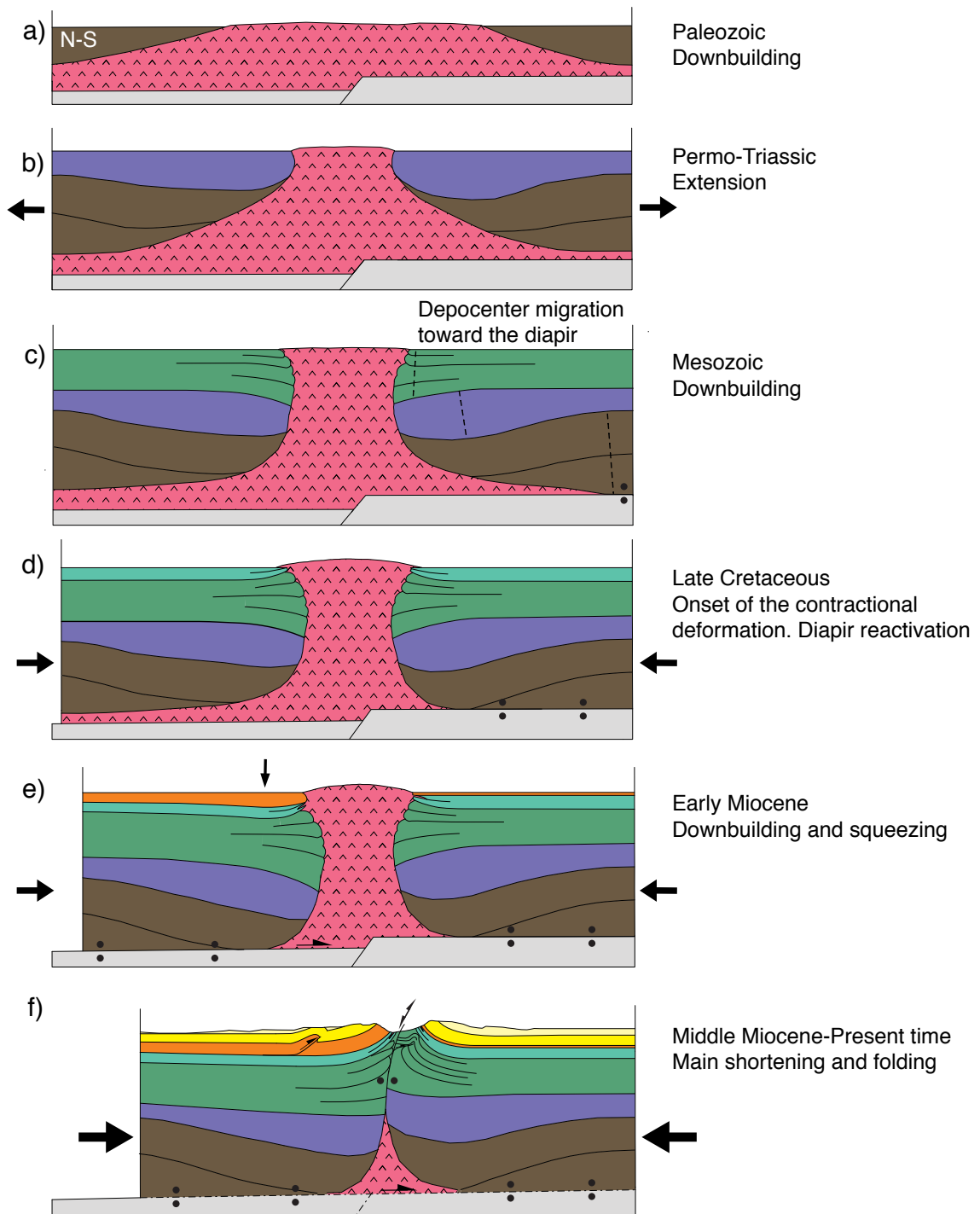


Fig.18: Evolutionary sketch of the Darmadan structure. a) Triggering of the salt structure and passive growth by sedimentary loading, during or just after the deposition of the Hormuz salt. b) Extension related with the Paleo-Tethyan rifting eased the diapir to remain emergent. The initial development of a wide geometry was followed by the emplacement of salt stock geometry by salt migration toward the Darmadan structure c) Touchdown of the minibasin and migration of the depocenter toward the diapir. d) Onset of the contractional deformation. The diapir remained emergent and the presence of numerous overhangs is related with diapir reactivation. e) Salt exhaustion on the southern flank of the diapir and thickening by dowbuilding at the northern side. f) Squeezing of the diapir and formation of a secondary weld. Subsequent anticline folding and development of second order structures that accommodate the shortening.

1.5 Discussion: diapir evolution

As stated in the introduction, the main aim of our study is to characterize the stratigraphic and structural relationships between the Hormuz salt and its stratigraphic overburden around the Darmadan diapir, aiming at establishing the temporal evolution of this salt structure. For this purpose, we propose a sequential restoration of the Darmadan salt stock outcropping in the eastern sector (Fig. 18) and investigate the main structural differences along strike with the Darmadan anticline.

The described geometries and relationships between the Darmadan diapir and its overburden are restricted to the Upper Jurassic to Recent outcropping succession. Hence, for understanding the pre-Jurassic evolution of the Darmadan structure, information from previous works in the frontal, less-deformed, parts of the Zagros fold-and-thrust belt have been used.

Onset of Hormuz salt tectonics could have started as early as the late stages of Hormuz salt deposition during the Precambrian extensional stages of the Najad Rift System, or during the Cambrian extension related with the Paleotethyan rifting. In such context, different authors highlight the influence of pre-existing base-salt discontinuities on the triggering and location of salt structures in the Fars region, (Jahani et al., 2017; Hassanpour et al., 2018).

Evidence for the continuous Hormuz salt evacuation during the entire Paleozoic in the SE sector of the Persian Gulf have been recently described by Perotti et al. (2011, 2016); these authors indicate that salt tectonics in the region probably started soon after the deposition of the Hormuz Fm., as suggested by seismic reflections with continuous and progressively downward increasing dips in the Permian and pre-Permian successions. Analogously, Stewart (2018) ascertain early salt evacuation in the western margin of the Hormuz salt basin as recorded by changes in the Cambrian strata thickness.

The significant structural relief observed between the back and frontal limb of the Darmadan, Kahin and Muran anticlines (Fig.5) suggests the presence of a deep-seated structure. Leturmy et al. (2010), propose the existence of a NE-SW reverse basement fault that controlled the development of these structures during the shortening. In analogy with this trend, south dipping NE-SW normal basement-involved faults controlled the initiation and orientation of salt structures in the off-shore of the southern Persian Gulf (Fig. 4a and Fig. 5) (Jahani et al. 2009). However, we have not evidences for the age of basement-involved fault that would

have triggered the Darmadan diapir (Fig. 18b).

Analogue models evidence how, especially in case of syn- to late- rift salt basins, pre-salt extensional faulting is one of the major factors controlling the initiation and orientation of salt structures (e.g. Jackson & Vendeville, 1994; Dooley et al., 2005). Based on these observations, we tend to consider the triggering of the Darmadan salt structure related to a NE-SW extensional north dipping basement-involved fault (Fig. 18a). This fault, may have been partially inverted during the shortening, with the displacement of the reactivated fault during contractional deformation disappearing laterally (e.g. toward the studied Darmadan salt stock), where the extensional throw is preserved.

Subsequently the Darmadan diapir developed by downbuilding during the deposition of the Lower Paleozoic sediments (Fig. 18a and b), in a similar fashion to the offshore structures as suggested by Perotti et al. (2011, 2016) and Stewart (2018). Passive diapirism driven by differential loading persisted through much of the Palaeozoic (Fig. 18b).

The Hormuz Fm. clasts found in the Surmeh Fm. emphasize that the Darmadan diapir was at surface already during the Late Jurassic time. Hooks (Fig. 10) observed in the Upper Cretaceous Sarvak-Ilam Fms., as well as the clasts sourced from the Hormuz Fm. and the synsedimentary extensional faults dipping towards the salt contact demonstrate that the Darmadan diapir was active and exposed during late Albian to Santonian times (Fig. 18c). These observations suggest that the Darmadan diapir grew passively at least during that time gap with a equal or higher salt rise rate relative to the sedimentary rate as confirmed by the presence of stacked tabular halokinetic sequences and associated Hormuz salt cusps; this higher salt rise rate would also be confirmed by the presence of Hormuz-derived blocks and overhangs in the upper levels of the Sarvak Fm. that would suggest that the diapir flared up at the time of Sarvak Fm. deposition (e.g. in Figs. 12 and 18c). At that time, the Sarvak Fm. expanded towards the salt stock to form a peripheral sink basin, which could suggest the development of a turtle structure (Trusheim, 1960) by primary welding away of the salt inflated area around the diapir. The platform margin observed in the Sarvak Fm. at the western part of the Darmadan anticline (Fig. 17) is synchronous with the development of this peripheral basin, suggesting the continuation of an inflated salt area (i.e., a salt wall) along strike of the diapir presently squeezed in the core of the anticline (Fig. 19).

A significant increase of the salt supply/sedimentation rate is observed during the Campanian to Maastrichtian as revealed by the numerous decametric to hectometric-

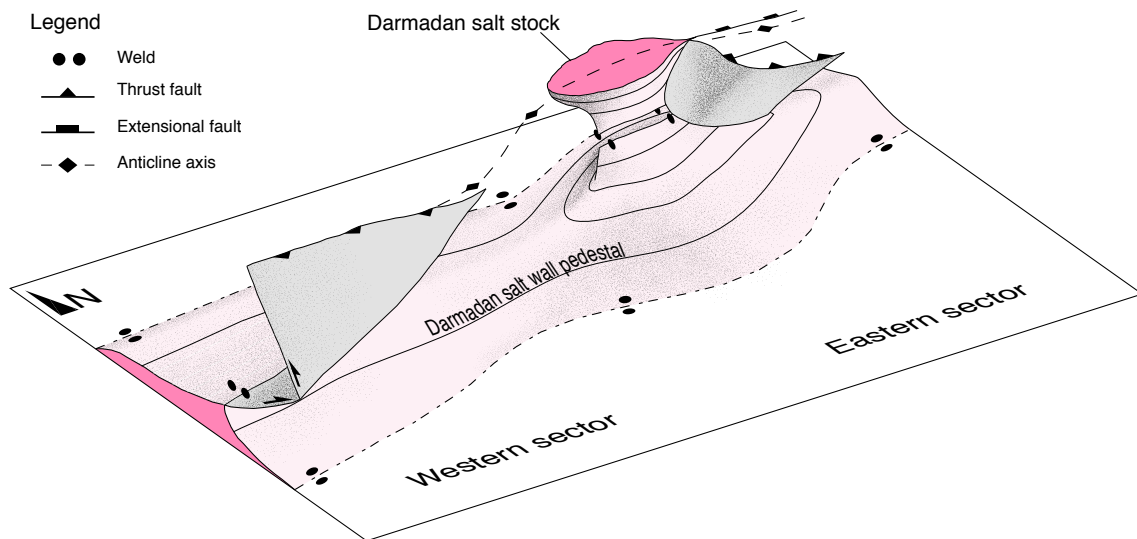


Fig.19: 3D Sketch of the studied Darmadan salt structure representing the top of the Hormuz salt and the main faults affecting the eastern and western sectors. The Darmadan salt structure initiated as a salt wall (or eventually salt anticline) and in any moment before the Albian, developed in the Darmadan salt stock outcropping in the eastern sector. The lateral changes of the salt structure geometry, resulted in different amount of shortening accomodated by thrusting and folding.

scale blocks of the Hormuz Fm. rocks embedded into the marly succession of the Gurpi Fm. (Fig. 9 and 12). During the Maastrichtian, the depocenter migration of the Tarbur Fm. away from the diapir (Fig. 16) suggests a phase of salt inflation. This feature, together with the observed angular unconformities and the presence of interbedded breccias cropping out in the Gurpi Fm. in the anticlines located northward the Darmadan structure suggest that the Darmadan diapir was reactivated and squeezed at the early stages of contractional deformation during the transition from obduction to the onset of collision along the NE edge of the Arabian plate at Santonian to late Maastrichtian times (Fig. 18d). At that time, the Darmadan diapir was located in a foreland position, farther south and west of the main depocenters related to the thrust front; however, the weakness of the salt diapir favored its squeezing recording the early stages of the contraction related with the obduction phase. The observed halokinetic sequences in the lower Paleogene Sachun Fm., the differences in thickness and the presence of clasts derived from the Hormuz Fm. in the northern limb of the Darmadan anticline demonstrate that the Darmadan diapir was continuously exposed from the Late Jurassic until the early Eocene. However, there are no evidence preserved of contractional deformation in the Darmadan structure during the Paleogene or salt evacuation/diapirism from early Eocene to Rupelian times. So, a question arises if the diapir underwent burial during the

deposition of the Eocene Jahrum and Rupelian Asmari Fms. to subsequently pierce the overburden during a rejuvenation phase related with the late Zagros contractional deformation.

During the Miocene but previous to the onset of folding in the Darmadan anticline, the higher accommodation space in the northern part of the Darmadan salt wall and diapir represented by the thicker Champeh and Guri Mb. could be explained by the evacuation of any remnants of Hormuz salt at depth (Fig 18e). The differential subsidence rate between the northern and the southern limb represents evidence that the thickness and availability of the Hormuz salt may be controlled by a deep-seated basement step, with an early primary welding along the southern flank. A second reason promoting the northern flank subsidence of the Darmadan salt structure is the extensional reactivation of the interpreted basement step, related to the foreland flexure ahead of the active frontal structures in the High Zagros.

The timing for the Darmadan anticline folding is constrained by the growth geometries described for the middle to upper Miocene Mishan Fm. south of the Darmadan structure. During this stage the diapir was squeezed until its stem was necked off forming a secondary weld, separating a diapir bulb from a deep-seated pedestal (Fig.18f).

The map view of the Darmadan diapir suggests the present day salt distribution at depth and the geometry of the Darmadan salt structure in the subsurface (Figs. 7 and 19). The diapir progressively welds eastward into the main E-W subtractive fault. In between this fault and the secondary weld, a small teardrop diapir is pinched off from its source layer, pointing out that the contractional deformation has been partially accommodated by squeezing and upward extrusion of the Hormuz salt. A thrust detached into the Kazhdumi Fm. and related tight folds splay off from the thrust weld (Fig. 15). Most probably, the north-dipping normal fault developed laterally in the diapir overburden, associated with the subsidence of the early Miocene successions by salt evacuation at depth, to be partially reactivated during the development of the Darmadan anticline, once the salt wall and diapir were secondary welded. Eastward, the shortening was transferred to the southern limb of the structure. This abrupt change in geometry from a south dipping to a strongly overturned southern flank (Figs. 9 and 15) is clearly controlled by the diapir location and represents an important temporal constrain that relates the timing of the secondary welding with the early folding of the Darmadan anticline in the middle Miocene.

The N-S trending normal faults observed in both, the eastern and western sectors

developed during this late stage. These faults crosscut at least up to the upper Miocene units and they are spatially confined to the Darmadan anticline fold. The fault pattern trend roughly parallel to the N-S shortening direction, similarly to the suggested distribution proposed by Withjack and Scheiner (1982) in analogue and analytical models on elliptical doming with regional compression. This observation is consistent with the presence of an elongated distribution of the salt structure in depth along eastern and western sectors, as depicted in Fig.19.

1.6 Conclusions

In this work we document for the first time halokinetic sequences involving the pre-collision Mesozoic succession in the Fars region of the Zagros fold-and-thrust belt. Our results emphasize the role played by preexisting passive diapirs in the structural development of the Zagros fold-and-thrust belt detached on the Hormuz salt layer, as already proposed by several authors (e.g., Koyi 1988, Letouzey et al. 1995, Callot et al., 2012). Salt structures most probably initiated by downbuilding since Paleozoic times. The presence of basement-involved discontinuities in the base-salt can have a deep influence in the initial geometry and orientation of such structures.

Independently of the triggering mechanisms for the salt structures, these evolved as passive diapirs at least during Late Jurassic-Early Cretaceous times before the ophiolite obduction at the northern and eastern edges of the Arabian plate.

Tabular halokinetic sequences developed as a result of the relatively high salt rise of the Darmadan diapir with respect the sedimentation rate. Laterally, salt upwelling to form a salt wall controlled facies and thickness distribution of the Cretaceous platform successions.

The onset of contractional deformation in the internal part of the Zagros and Oman orogenic systems is recorded by the reactivation of the Darmadan salt stock during the Late Cretaceous, regardless of the fact that it was located in the foreland at significant distance from the thrust front. The Darmadan salt stock continued active during the Paleogene and to be squeezed and partially welded during the Neogene to recent Zagros deformation, when the prominent detachment folds of the Zagros fold-and-thrust belt developed.

The deduced structural evolution of the Darmadan salt structure suggests the existence of a very thick Hormuz salt layer at depth able to source the salt structure

for a long time. First evidence of local primary welding would be related with the peripheral sink development at Albian-Cenomanian times. A more extensive primary weld to the south of the structure accounts for differences in subsidence rate related to salt evacuation during Miocene before the final squeezing and secondary welding. The trend and the location of the Darmadan anticline was possibly controlled by a preexisting salt structure. In addition the geometry of the anticline and related second order contractional features have been also controlled by the geometry of the diapir and salt wall and their squeezing as the contractional deformation progressed (Fig.19). Contractional deformation related with the squeezing of the Darmadan diapir was laterally transferred to a backthrust to the west and to a thrust and related folds to the east (Fig. 19). Pre-existing structures in the crystalline basement may have played a role in the orientation and location of the salt ridges and can be invoked to explain different amount of subsidence between the northern and southern limbs of the Darmadan diapir.

The explained structure emphasizes that the present structural features of the Zagros fold-and-thrust belt in the Fars region is the result of the reactivation of preexistent salt structures that developed in the Arabian passive margin before the onset of the collision.

Chapter 2: The Zagros-Oman deformation front in the eastern Persian Gulf: role of structural inheritance

This chapter is part of a manuscript that will be submitted to the Journal of Structural Geology

Snidero, M., Tavani, S., Muñoz, J.A., Mencos, J.

2.1 Abstract

The eastern limit of the Fars structural salient is formed by the Bandar Abbas structural embayment, converging into the Hormuz strait. This tight re-entrant underlined by the arched shape of the Oman peninsula represents the transition between the Zagros collisional belt and the Makran subduction-related prism. Within the foreland part of the Zagros fold thrust belt and the Oman Ranges, the transition is marked by a sudden change in structural trends and style and a rapid decrease in salt diapirism from west to east. Based on 2D seismic data, we present a NW-SE structural cross-section along this transect, intersecting the frontal structures of the Oman Ranges, here formed by the off-shore continuation of the Musandam peninsula. A sequence of structural highs are interpreted as rooted into normal faults that produced the compartmentalization of the Hormuz Salt basin and subsequently inverted during the Upper-Cretaceous to Miocene contraction. Specifically, we suggest that the Hormuz Dastan and Farshid (HD) structure would be located close to the Hormuz salt basin margin whereas the Hormuz Barez and Sepid (HBS) structure would be located outside the salt basin boundary. We finally propose a series of evolutive steps that include: i) Triggering of the Hormuz salt diapirism to be Paleozoic in age, ii) thickness variations show thickening toward the HD structure where normal fault act as roll-over for the rejuvenation of asymmetric reactive diapirs ii) Evidences of the Permo-Jurassic Neo-Tethyan rifting related to the Triassic unit thickening toward the HD salt structure, iii) onset of the Oman Mesozoic nappes emplacement, development of the Upper Cretaceous foredeep and consequent Paleogene depocenters migration toward the external part of the orogenic belt, iv) Continental collision and progressive increase of the flexural loading of the margin producing the northward lithospheric flexure.

2.2 Introduction

The Bandar Abbas syntaxis is located in the eastern sector of the Fars salient and constitutes a major structural feature within the Zagros orogen, marking the transition between the Zagros collision belt to the west and the Makran accretionary prism and Oman Mountains to the east (Fig. 20). It is marked by a sharp change in trend and style of the tectonic structures. The structures in this region describe a tight re-entrant underlined by the arched shape of the Oman peninsula jutting out into the Strait of Hormuz from the Arabian Peninsula (Molinaro et al. 2004; Piryaei et al. 2011). The onshore structures are characterized by a change in the structural trend of Zagros Thrust and Fold Belt front, from NW-SE to E-W (Fig. 20). Offshore, the frontal structures of the Zagros Fold and Thrust Belt deform the Arabian foreland and meet the NE-SW trending frontal structures of the Oman

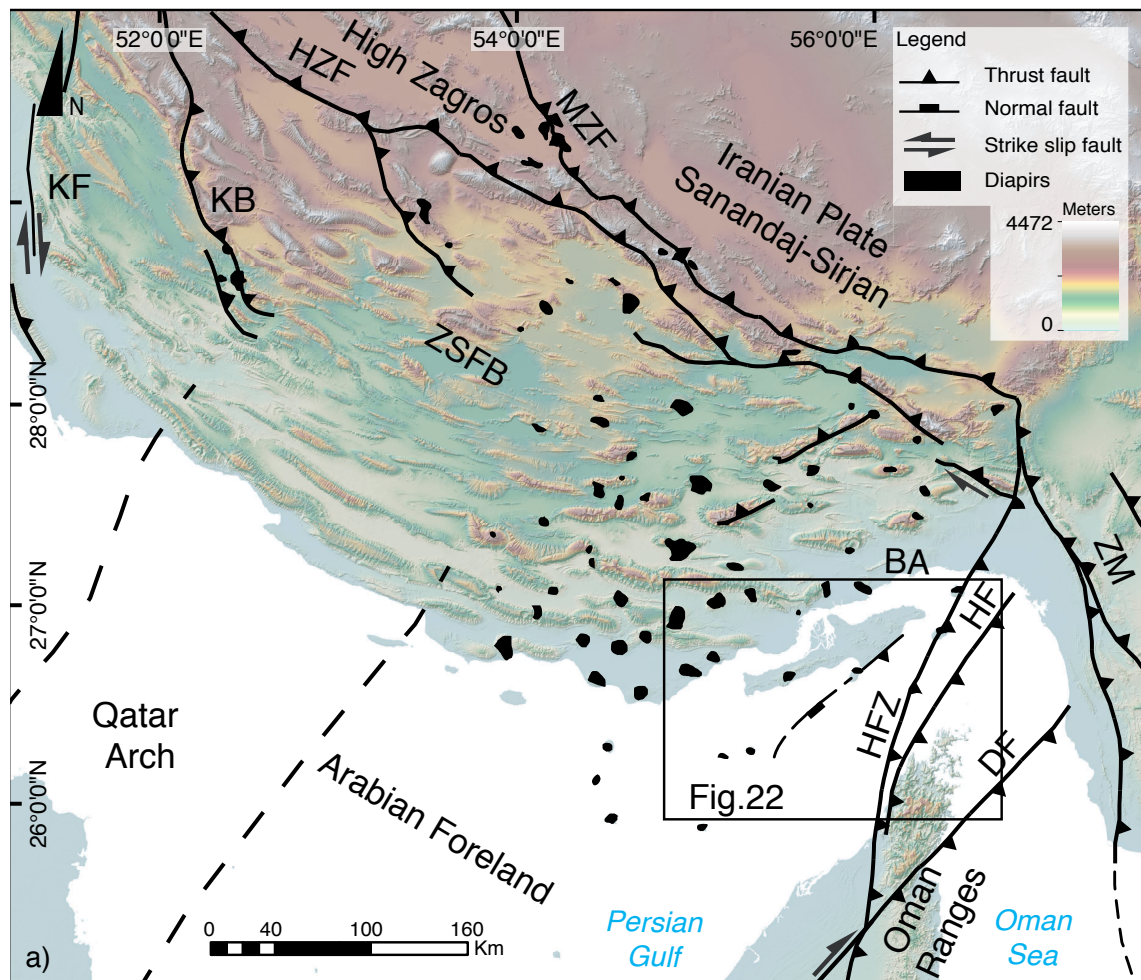


Fig.20: a) Digital elevation model showing the major structural elements of the southeastern Zagros fold and thrust belt, along the Fars Region. ZSFB: Zagros Simply Folded Belt. BA: Bandar Abbas syntaxis. HZF: High Zagros Fault, MZF: Main Zagros Fault. KF: Kazerun fault. KB: Karih Bas fault. HFZ: Hormuz fault zone. HF: Hagab fault. DF: Dibba fault. ZM: Zendan-Minab belt. The basemap was created using the Shuttle Radar Topography Mission dataset (Farr et al., 2007).

Range (Fig. 21).

The front of the Oman Ranges is characterized by a number of structural highs, which are often pierced by Hormuz Salt diapirs (Fig. 21). The most prominent of these structures are: (1) The Hormuz-Barez and Sepid high (HBS), (2) the Hormuz-Dastan and Farshid high (HD), (3) the Hormuz-Aras high (HA) and (4), the Zirang-Hulur anticline. The HBS high constitutes the most internal structure of the Oman front in the area and is interpreted as the northern prolongation of the Musandam high, exposed at the northern Oman mountains (Searle et al., 1983; Michaelis and Pauken, 1990). The HBS high is devoid of any Hormuz Salt structure. Conversely, the rest of the highs are pierced by salt diapirs, with the most important ones being the Larak and Hormuz diapirs in the HD highs and the Hengam diapir along the Zirang-Hulur/Taftan anticline (Fig. 22).

The timing of deformation of the Oman structures is marked by a southeasterly-directed thickening of the Campanian-Maastrichtian Gurpi and the Paleogene Pabdeh Formation, toward the Oman thrust fault system. The thicker intervals are located right above and in front of the HD and HA highs, respectively (Fig. 22). These structural and stratigraphic relationships record the shifting of the Campanian to Oligocene depocenters south-eastward, revealing the migration of the Oman

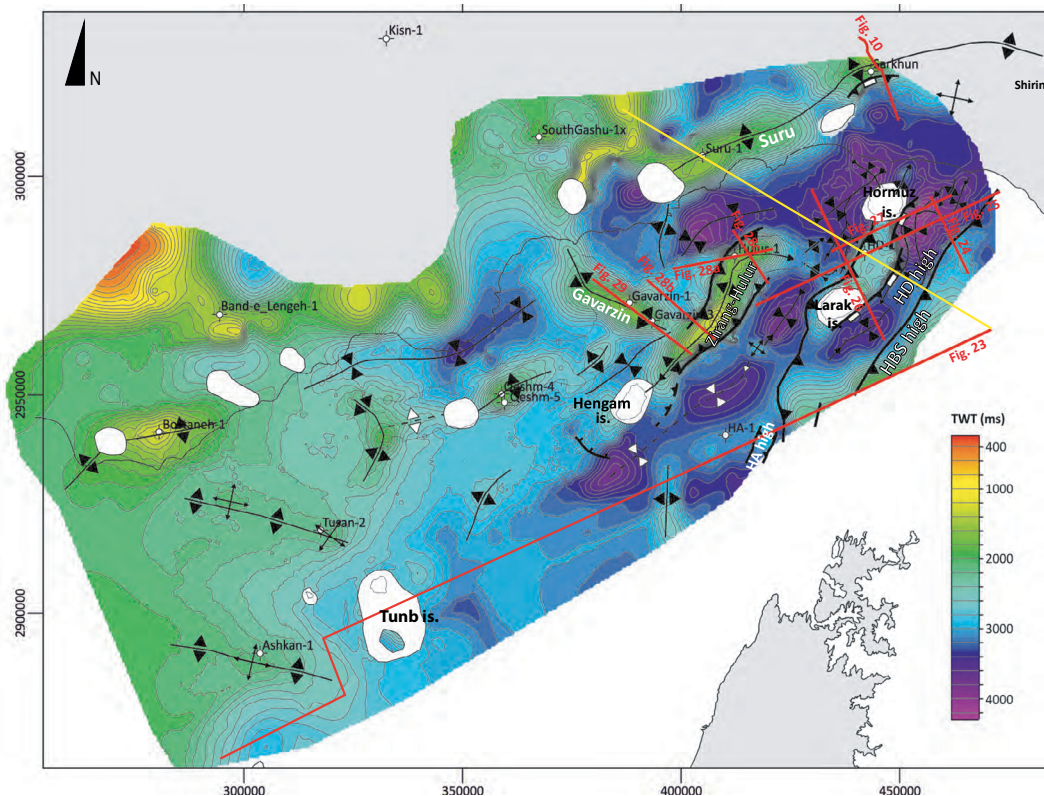


Figure 21: Time structural map of the top of the Santonian Ilam Fm. Seismic lines are highlighted in red. Diapirs are shown in white colour. The yellow line shows the location for the off-shore eastern cross section (Fig. 10).

foredeep toward the north-west (Fig. 22). At the eastern part of the Persian Gulf, the equivalent Upper Cretaceous, Paleogene, and Miocene successions are truncated by the Tortonian intra-Guri Member angular unconformity, and covered by a wedge of Neogene sediments (GU in Fig. 22). The overlying Neogene basin rapidly deepens from north-east to east directions (Ravaut et al., 1998) in response to the flexural loading related to the Zagros collision and the Makran prism (Molinaro et al., 2004). Using a regional 2D reflection seismic and well dataset, we depict the main structures along a NW-SE section, crossing the offshore Bandar Abbas and Hormuz strait re-entrant. This regional cross-section depicts the structural style of the Hormuz salt basin margin on the structural style off the Zagros-Oman Fold and Thrust belt. A sequential restoration of the main structures is presented in order to unravel the evolution of the area and the deformation history of the proximal diapirs to the Zagros-Oman mountain front.

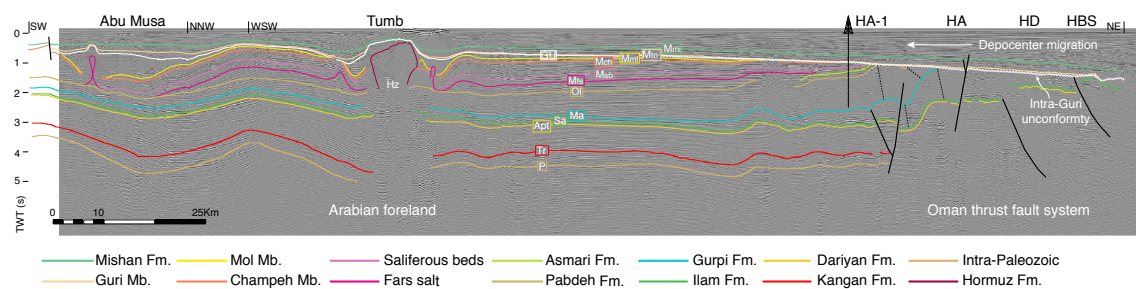


Figure 22: Composite seismic line along the southern edge of the study area. Location of the seismic line and of the well data is indicated Fig. 21. Dashed black lines are used to highlight thickness changes. The seismic profile shows, from ENE to WSW: the northwestwards-directed thrusts and folds related with the Oman-Zagros orogeny and associated foredeep in Gurpi and Pabdeh Fms. the Tunb salt structure, and a lateral section of the Abu Musa, structure both originated by the interference of the two evaporitic units (Fars salt and Hormuz salt). Hz: Hormuz; Tr: Kangan; Apt: Dariyan; Sa: Ilam-Sarvak; Ma: Gurpi; Ol: Pabdeh; Mfs: Fars Salt; Msb: Saliferous Beds; Mch: Champeh; Mml: Mol; Mtu: Guri; GU: Guri Unc.; Mmi: Mishan.

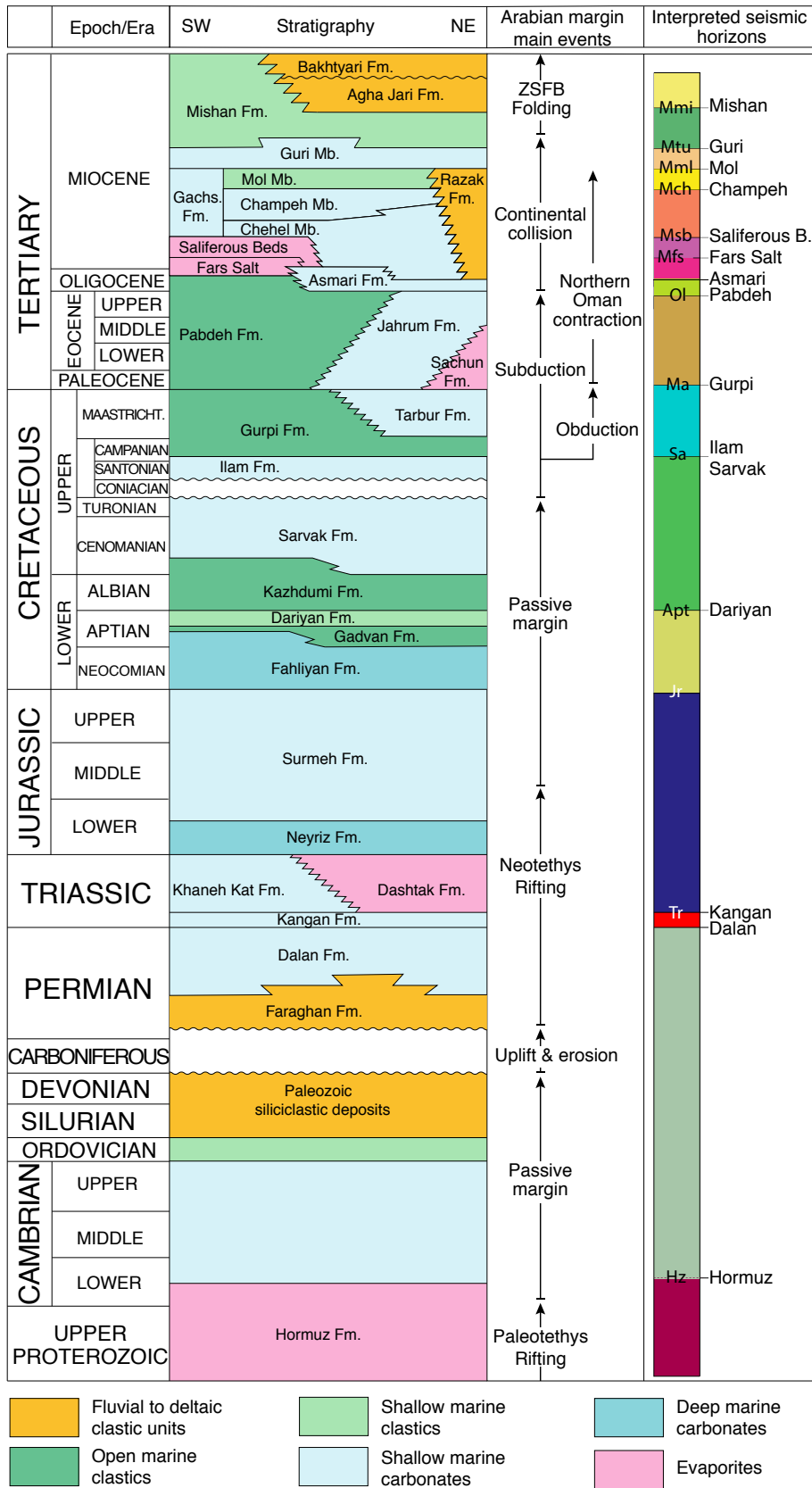


Figure 23: Stratigraphic chart of the eastern Fars region. The main tectonics event and the interpreted seismic horizons are shown. (Modified from James & Wynd, 1965; Ghavidel-yooki et al., 2011; Searle and Ali, 2014; Pirouz et al., 2015; Snidero et al., 2019).

2.3 Stratigraphic framework

In the study area, deposition of up to 12 km thick Paleozoic to Cenozoic sedimentary succession is deposited above a Neoproterozoic to Cambrian salt layer, referred to as the Hormuz Salt (Fig. 23). The Hormuz Salt consists of halite, anhydrite, limestones, dark dolostones, red sandstones, and shales (Ghavidel-Syooki et al., 2011 and 2014). During most of the Palaeozoic, a uniform clastic continental and shallow-marine sedimentation took place (e.g. Sharland et al., 2013; Ghavidel-Syooki et al., 2014). These deposits were overlain by distal siliciclastic deposits and dolostones of a Permian clastic system (Konert et al., 2001). Above, the Permian to Turonian succession consists of carbonates, evaporites, and marly units, deposited in a shallow to deep marine environment (James and Wynd, 1965; Alavi 2004; Kavooosi, 2013; Lasemi and Jalilian, 2010); these units are pre-orogenic deposits, and predate both the Oman and Zagros orogenies. The initial development of the Oman-Zagros foreland basins is recorded by a thick succession of Campanian to Oligocene marls, referred to as the Gurpi and Pabdeh formations (Piryaei et al., 2011). Above, the Oligocene-Miocene sequence is made up of the marine carbonate Asmari Formation. In the Qeshm Island (Fig. 21), the Asmari Formation is Chattian to early Aquitanian in age (Sajadi and Rashidi, 2019) and laterally equivalent to the upper part of the marly Pabdeh Formation basinward. The Pabdeh and Asmari formations are overlain by the Oligocene-Miocene Gachsaran Formation. The overlying middle Miocene succession is characterized by a fast transition into the limestones of the Guri Member, at the base of the Miocene to Pliocene Mishan Formation. These are characterized by shallow-water marine marls interbedded with bioclastic limestones (Pirouz et al., 2015).

2.4 Dataset

This study is based on a 2D seismic reflection survey covering ca. 34000 km² along the Hormuzgan coast, together with 16 exploration wells (Figs. 20 and 21). The spacing of the seismic lines in the offshore surveys is of 2 km. Onshore surveys have irregular distribution, spacing, and orientation, following the main structural trends. The maximum recorded depth is 7 seconds (tw). Some of the wells have relevant downhole logs for synthetic seismogram generation, whereas others include sonic logs and/or formation tops only. Depositional sequence boundaries were defined based on well intersections and the interpretation of

regional unconformities, seismic package internal architecture, seismic reflector geometries and facies, and their relationships with the structures studied (Figs. 23). Additionally, timelines have been tracked within selected depositional sequences to constrain the migration of the depocenters through time.

2.5 Seismic interpretation

2.5.1 Hormuz-Barez and Sepid high (HBS)

This structure has been interpreted as the northern prolongation of the Musendam High, cropping out at Oman mountains. The seismic coverage of this structure in the study area is poor and partial, as it is located at its far eastern end. Nevertheless, it is clearly depicted by the carbonates of the Bangestan Group, which are cut by a

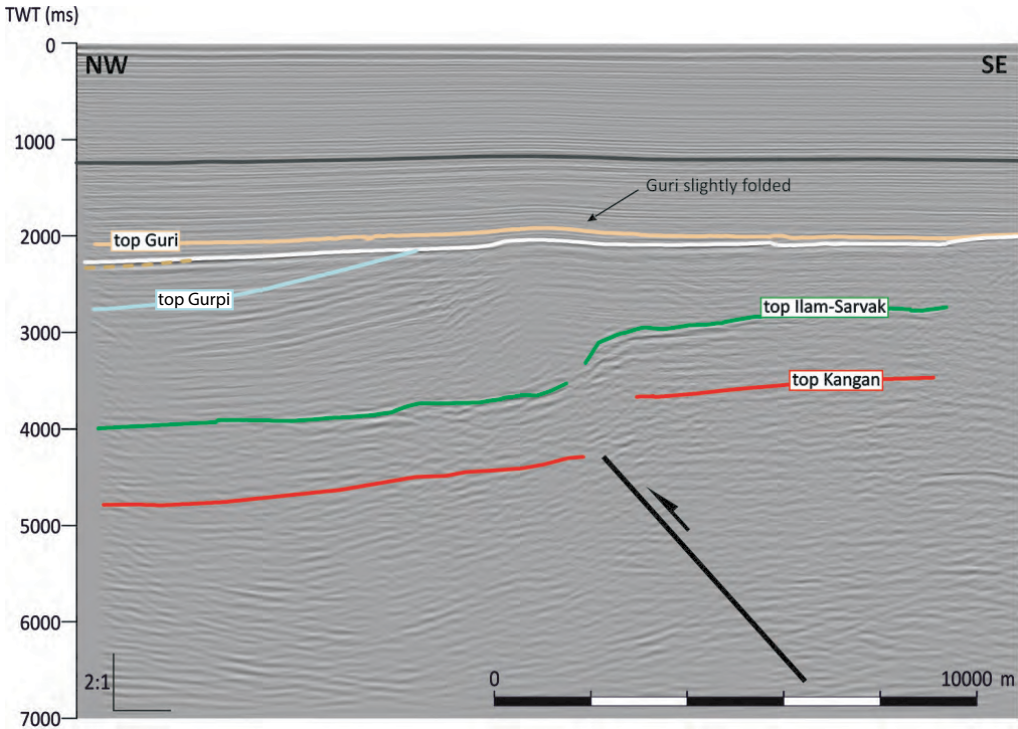


Figure 24: Seismic line 3112A along the eastern edge of the study area. HBS structure is shown (known as Hormuz-Barez high in this sector), well depicted by the Bangestan carbonates. Structural high and displacement along the thrust is less in this area than further south (Fig. 22). See location in Fig. 21.

steep thrust visible along the eastern section of the seismic line in Fig. 22. Further northeast, the top of the Bangestan Group is folded above the thrust suggesting the thrust is dying in that direction (Fig. 24). In front of this structure, the Gurpi succession shows the maximum thickness, and the internal reflections within this sequence are moderately inclined towards the NW and show clear downlap geometries on top of the Bangestan carbonates (Fig. 25). Despite the poor seismic coverage, no Hormuz salt inflation is recognizable at depth below the Hormuz Barez and Sepid highs. In addition, no Hormuz salt diapirs are present at surface along this structural trend (Fig. 20).

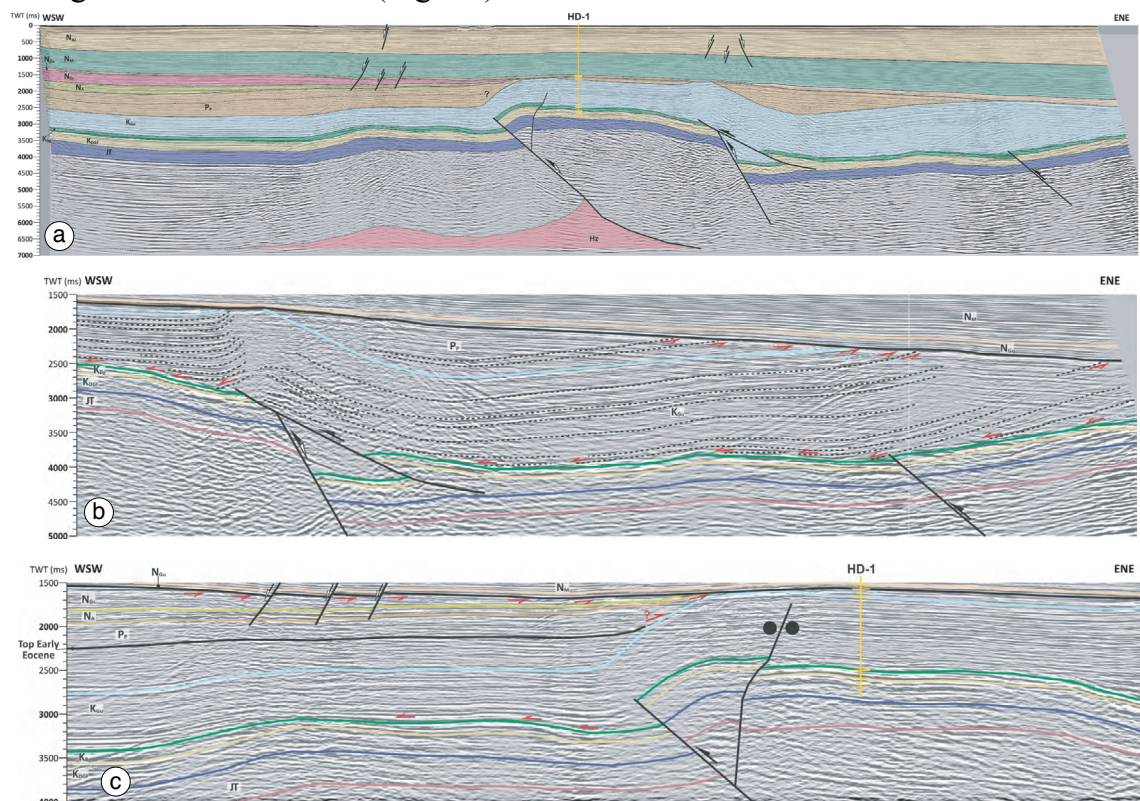


Figure 25: Seismic section across the HBS and HD structures. a) The HD structural high is very well imaged in this transect whereas the HBS structure has very low relief. Note that this seismic line is highly oblique with respect the trend of these structures. The by-passed extensional fault stands out. b) Detail of the folded geometry of the Gurpi reflectors (K) and their onlap over the top of the Bangestan Group (K). c) Detail of the HD high.

2.5.2 Hormuz-Dastan and Farshid (HD)

Northwestwards of the HBS structure there is an elongated NE-SW trending structural high drilled by the well HD-1 where two large Hormuz salt diapirs are located. These diapirs crop out at surface, at the Larak Island to the south and the

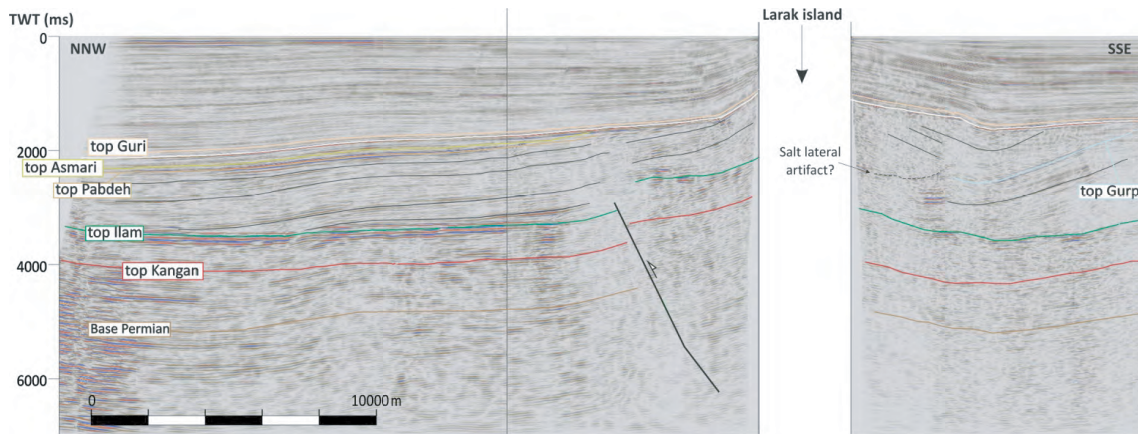


Figure 26: Approximately N-S seismic line across HD high and Larak island. Note the structure above the unconformity at the base of Guri carbonates and the structural position of the diapir. See location in Fig. 21.

Hormuz Island to the north (Figs. 20 and 25). Despite the necessary salt availability in this area to create such huge diapirs, the presence of salt coring this structure along strike the diapirs is not evident (Figs. 22 and 25). In fact, the structural high that is very well defined by the Bangestan carbonates, shows a quite consistent 4-way planar geometry close the the HD-1 well (Fig. 20). The HD high is bounded to the southeast by a SE-dipping normal fault, and to the northwest by a NW-

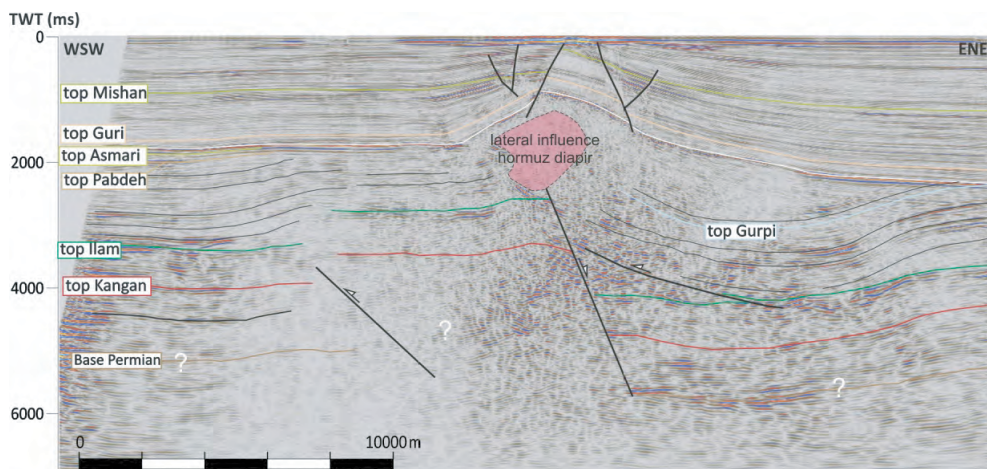


Figure 27: Approximately E-W seismic line across HD high close to the Hormuz island. This line reflexes the lateral influence of the Hormuz island diapir. See location in Fig. 21.

directed high-angle thrust (Figs. 26 and 27). Locally, the extensional fault is bypassed by a second-order NW-directed thrust, that forms a small-wavelength anticline depicted by the Gurpi and Pabdeh shales (Fig. 25b). The hangingwall of the NW-directed high-angle thrust, is characterized by a wide flat-lying panel as

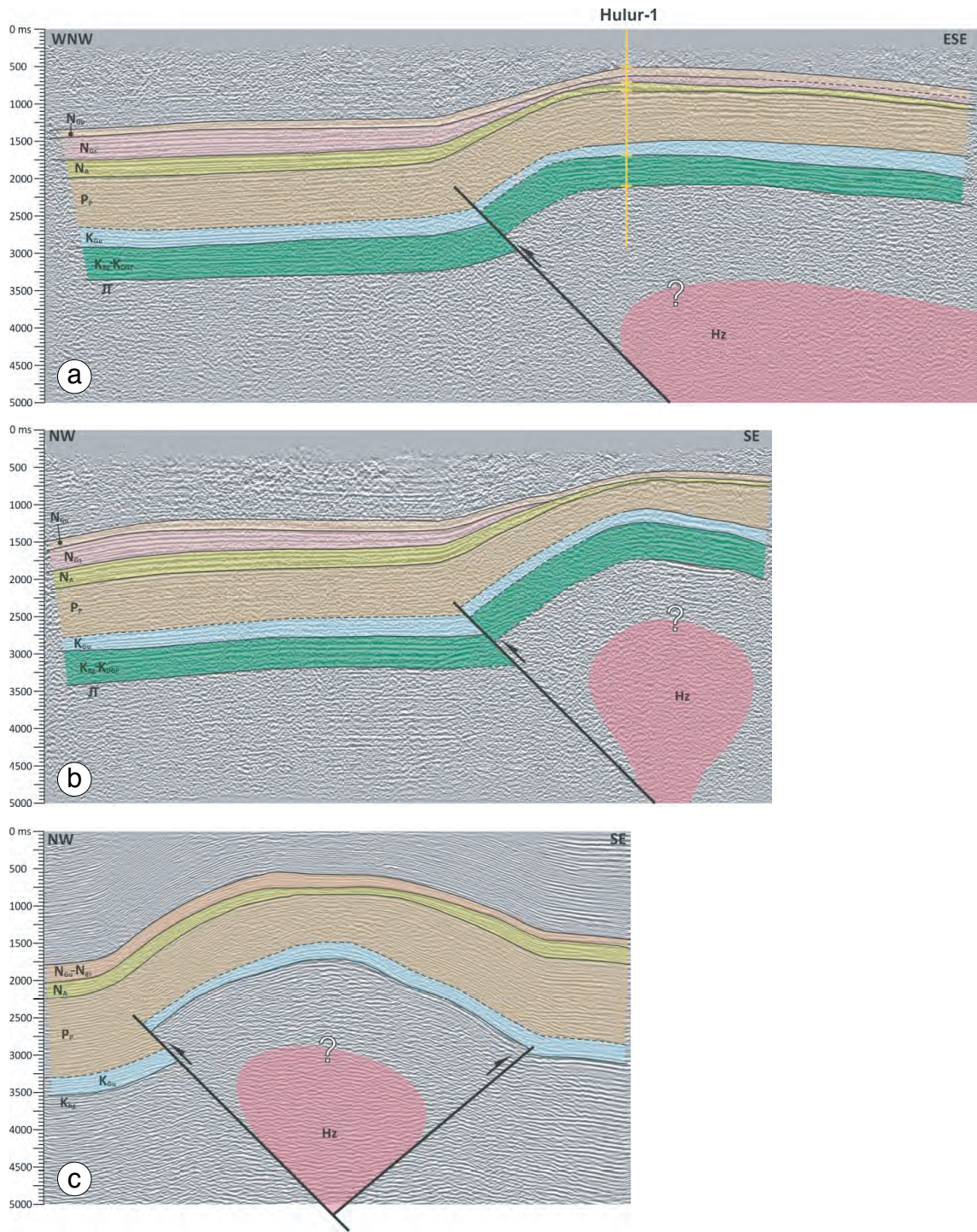


Figure 28: Seismic lines across the Zirang-Hulur anticline. This anticline is cored by Hormuz salt and bounded by a NW-directed thrust and a SE-directed second-order backthrust. The main thrust dies out within Pabdeh succession. Evidences of syntectonic deposition from Gurpi to Gachsaran deposits. See Fig. 21 for location.

very well depicted by Bangestan reflections and the internal reflections of the Gurpi and Pabdeh sequences (Fig. 27), especially along the 8013L seismic profile (Fig. 22). A thick Gurpi sequence is present above this high and drilled also by the

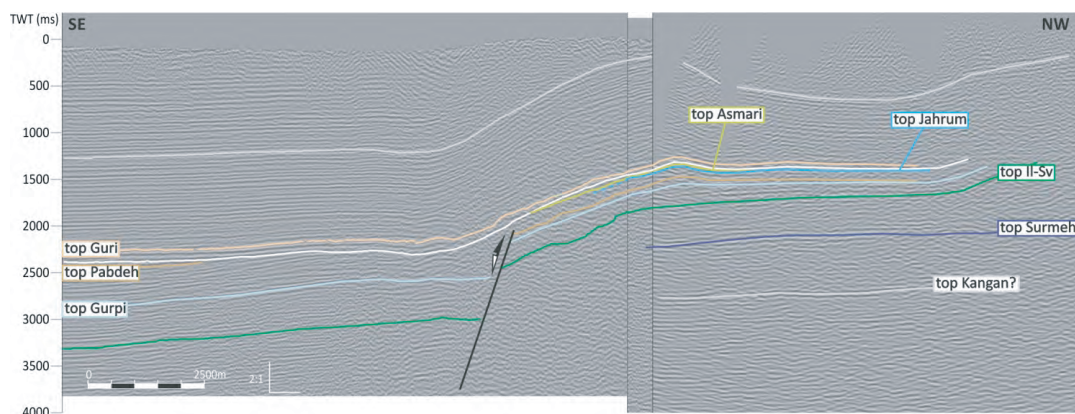
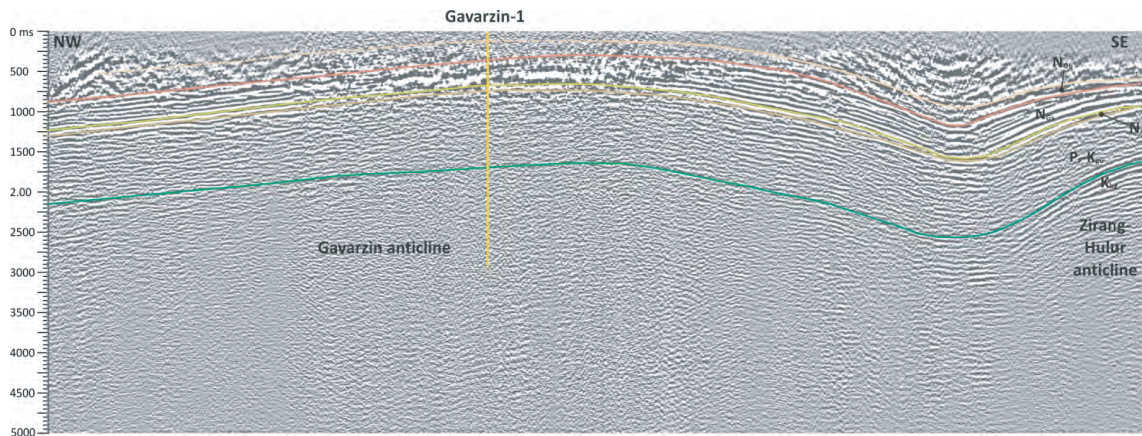


Figure 29: a) Seismic line along the Gavazzin anticline and across the Zirang -Hulur anticline. This line crosses the Zirang-Hulur anticline close to its southwestern end (see Fig. 21). Any thrust is interpreted along this line, at least affecting deposits younger than Middle to Upper Cretaceous Bangestan carbonates. See location in Fig. 21. b) Seismic line across the Sarkhun anticline. Note the extensional fault affecting Pabdeh and Gurpi sequences. This line also suggests the presence of a detachment level at the base of Guri Mb., similar to what is interpreted further east at Jallabi and Minab folds (Molinaro et al., 2004).

HD-1 well, so it may be assumed that the thrust was developed at least during the sedimentation of the Pabdeh Fm., presumably at late Pabdeh times, as suggested by well data. This structure is eroded and unconformably overlain by the Guri carbonates, although in their turn are slightly folded above the structural high (Figs. 22 and 25). The relationships between the HD-Farshid high and the Larak and Hormuz Islands diapirs are not straightforward, providing that these diapirs pierce up to the surface and clearly deform the whole post-Guri package, while the HD structure mainly developed before the sedimentation of the Guri Mb. (Figs. 25 to 27). The diapirs have developed in the footwall of the extensional faults that formed in the hangingwall of the thrust (Figs. 25 and 26). They have been subsequently squeezed after the unconformity at the bottom of the Guri Mb. This, together with the planar geometry of the HD-Farshid high and the very open fold

of the Guri Limestones and the succession above, synchronously with diapir squeezing, suggest the presence of the existence of two isolated preexisting Hormuz salt diapirs that have been squeezed during the contractional deformation associated with the development of the Zagros fold and thrust belt (Figs. 21, 22, 25, 27).

2.5.3 Zirang-Hulur anticline

The Zirang-Hulur and Sarkhun anticlines are interpreted to be cored by Hormuz salt, as suggested by typical semi-transparent seismic facies at their core, consistent with their rounded hinge and limbs, and supported by the presence of Hormuz salt diapirs nearby (Figs. 21 and 28). The Zirang-Hulur anticline is bounded by a northwestward-directed thrust cutting up to Pabdeh, and a smaller-order backthrust that affects the base of the Gurpi sequence (Fig. 27). The Pabdeh Formation shows thickness changes across the main thrust. Asmari up to at least Gachsaran sediments show growth and pinch out geometries against the fold limbs. Less evident is the thickness change of the Gurpi Formation, although it is suggested to thin against the anticlinal crest. For this reason, this anticline is interpreted to start growing perhaps during Gurpi deposition but mainly during the deposition of Pabdeh, with thrust development and fold growth continuing during Asmari and Gachsaran deposition. Although the seismic quality is not optimal, Guri carbonates show no evidences of thickness changes across the structure, thus indicating that fold growth may have stopped at this time. Nevertheless, the folded geometry of the Guri Fm. up to recent deposits indicates recent reactivation. The faults bounding the Zirang-Hulur anticline die out westwards, where the periclinal closure of the NW-SE-trending Gavarzin anticline comes upon (Figs. 20 and 29a). The westward continuation of the Zirang-Hulur anticline links with the Hengam diapir and the Taftan anticline, that are extensively discussed in the Chapter 4.

2.5.4 Sarkhun anticline

The Sarkhun-1 well located at the anticline crest drilled a very thin succession of Pabdeh, and also a thin Gurpi compared to wells located southwards. On the contrary, the thickness of the Gurpi-Pabdeh succession is remarkably larger immediately south of this structure, with good seismic control. This, together

with the geometry of the reflectors above the unconformity at the base of Guri Mb., suggest the presence of a blind extensional fault dipping southeastwards that controls the thickness of the Gurpi- Pabdeh sequences (Fig. 29b). This configuration is similar to what is observed further north, for example at Kush-e- Kuh structure, and southwards at HD high (Figs. 27 and 25).

2.5.5 Eastern Offshore Cross-Section

This cross-section, located offshore, runs SE-NW from the eastern end of the described area to the Hormuzgan coast (Fig. 30). It shows the Oman- related structures in the study area, that from SE to NW correspond to the Hormuz Barez High (HBS), the Hormuz Dastan high (HD) and ends at the Suru Anticline. In this cross-section, the eastern margin of the Precambrian to Cambrian Hormuz salt basin is illustrated. Deep-seated basement faults are interpreted to produce the compartmentalization of the Hormuz Salt basin and the control of the Hormuz salt sedimentary thickness. The HBS structure is located outside the basin and the relate thrust developed during the deposition of the Gurpi Fm. as evidenced by the thickening of this unit against the HBS structure and its onlap onto the Bangestan Group.

The HD structure, located at the Hormuz Salt basin margin is interpreted to be related to basement faults, despite the possibility of minor decoupling above a reduced sequence of the Hormuz salt. The existence or not of an efficient detachment at the Hormuz Fm. results in different detachment levels. The HD structure is developed at the hangingwall of an NW-directed thrust developed during the deposition of the Pabdeh Formation. This thrust is in its turn inverting a previous Triassic extensional fault. North of this structure an extensional fault has been interpreted cutting down the whole stratigraphic package. This normal fault has been developed during Upper Cretaceous, related with the forebulge of the Oman Orogen. This extensional fault is by-passed by a secondary thrust rooted at the Kazhdumi marls. Thinning of the Triassic sequence is related with the extension occurred during the opening of the Neo-Tethys ocean that could have rejuvenated the Hormuz salt diapirism in the area.

To the NW, the Suru anticline is developed above a Hormuz salt wall from Paleozoic until recent, when it has been squeezed. Close to the location of this cross-section the Hormuz salt pierce the surface and forms the Gachin diapir.

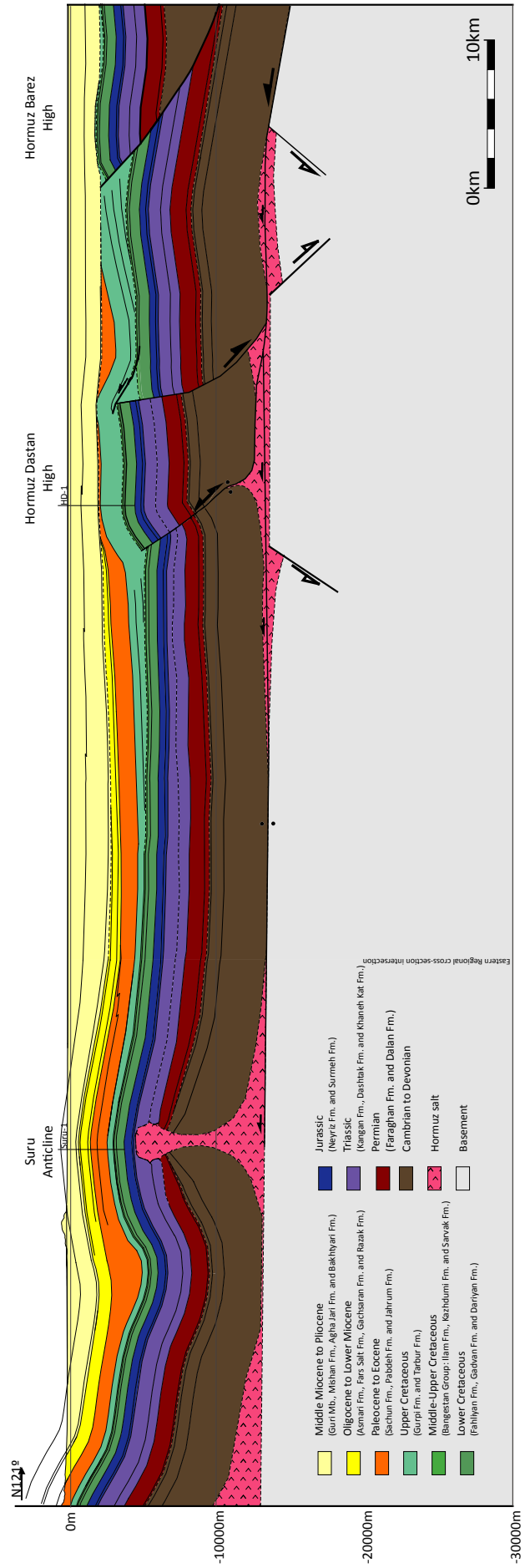
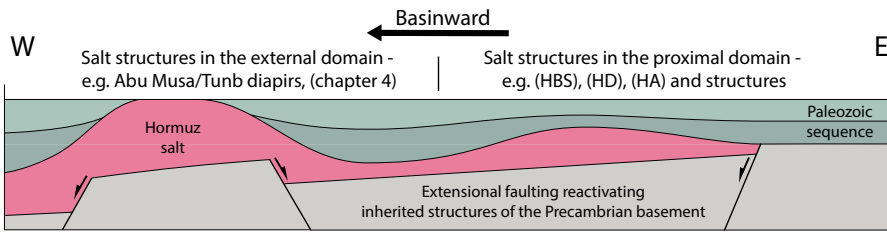
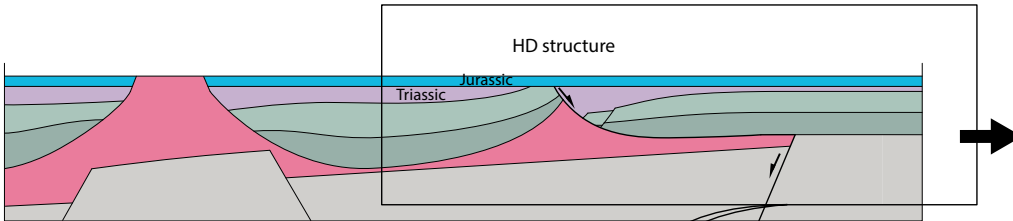


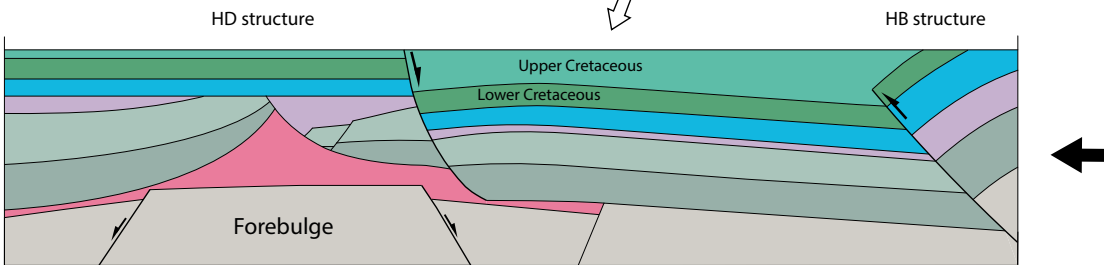
Figure 30: Eastern Offshore Crosssection. See location in Fig. 2.



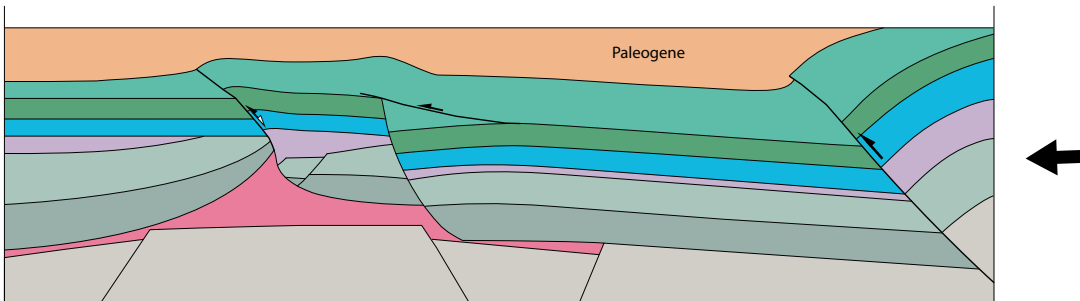
a) Neoproterozoic-Cambrian rifting, Hormuz salt deposition and Paleozoic triggering of the diapirism



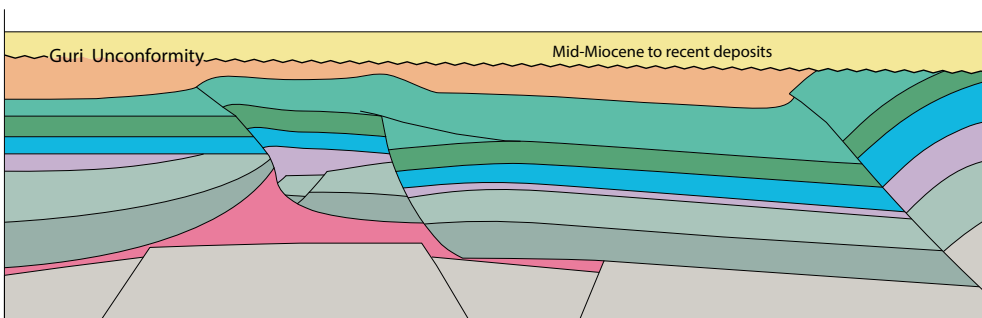
b) Triassic-Jurassic rifting. The Opening of the Neo-Tethys and Jurassic structures are located to the East.



c) Upper Cretaceous onset of the Oman-Zagros shortening. Lithospheric flexure, outer-arc extension and normal faulting in the external domain of the Gurpi Fm. foredeep.



d) Paleogene propagation of the Oman structures forward into the foredeep basin, producing inversion of the Upper Cretaceous extensional features.



e) The whole system is buried after the deposition of Guri carbonates (mid-Miocene) as consequence of the lithosphere flexure related to the Zagros mountain building.

Figure 31: Schematic restoration of the eastern Persian gulf structures, representing the transition above the Hormuz salt margin. The strata geometries are inspired in the seismic line in Fig. 25. The distances between the structures are not in scale.

2.6 Evolution of the Zagros-Oman related structures

We propose an evolution for the Hormuz Barez and Sepid (HBS), Hormuz Dastan and Farshid (HD), Hormuz Aras (HA) and Hular structures that are consistent with the available data and fits within the regional tectonic framework. The W-E schematic sequential restoration presented in Fig. 31 shows the main evolutive steps and structural relationships between the pre-existing structures and their control during the Zagros-Oman Front:

a) We consider the triggering of the Hormuz salt diapirism to be Paleozoic in age. Despite there is no direct information on the Paleozoic sequence in this area, the onset of Hormuz salt movement could have started as early as the late stages of Hormuz salt deposition during the Precambrian extensional stages of the Najad Rift System, or during the Cambrian extension related with the Paleotethyan rifting. In such context, different authors highlight the influence of pre-existing base-salt discontinuities on the triggering and location of salt structures in the Fars region, (e.g. Jahani et al., 2017). Evidence for the continuous Hormuz salt evacuation during the entire Paleozoic in the SE sector of the Persian Gulf have been recently described by Perotti et al. (2016), Snidero et al. (2020), see Chapter 4; these authors indicate that salt tectonics in the region probably started soon after the deposition of the Hormuz Fm., as suggested by seismic reflections with continuous and progressively downward increasing dips in the Permian and pre-Permian successions. Analogously, Stewart (2018) ascertain early salt evacuation in the western margin of the Hormuz salt basin as recorded by changes in the Cambrian strata thickness. Salt structures positioned close to the salt basin margin (e.g. HD high) are characterized by a minor salt availability and, on the other side an increased sedimentation rate with respect to the salt structures located basinward, forward to the west.

b) The Permo-Jurassic Neo-Tethyan rifting is recorded in the studied structures by the Triassic sequence. Minor thickness variations show thickening toward the HD structure where normal fault act as roll-over for the rejuvenation of asymmetric reactive diapirs. Laterally to this fault the Hormuz and Larak salt diapirs crop out at surface, where the HD structure is buried by the Jurassic isopach unit.

c) The Upper Cretaceous obduction of Tethys on the Arabian margin produces the

onset of the Oman Mesozoic nappes emplacement and consequent lithospheric flexure. The most internal structures of the Oman Ranges, (e.g. HBS and HB) propagate in a thick-skin fashion resulting in the development of the Gurpi foredeep. Extensional structures forms in the more external portion of the mountain range westward. The transition to the Hormuz salt basin is characterized by a certain degree of decoupling with the sedimentary cover, where normal fault Upper Cretaceous in age are observed (e.g. HD structure).

d) The Oman structures propagate northwestward, with the further uplift of the HD and Hular thrusts. The foredeep migrated progressively toward the external part of the orogenic belt and consequent deposition of the Pabdeh Fm. The shortening resulted in the inversion of the previous upper Cretaceous extensional faults and squeezing of the developed salt structures.

f) The climax of the NE-SW Oman related thrust system is reached during the lower Miocene, where the Zagros orogeny continued developing toward the North. The Oligocene-Miocene continental collision and progressive increase of the flexural loading of the margin produced the northward lithospheric flexure associated with the Middle Miocene Guri unconformity. This Neogene basin, represents the actual foreland of the Zagros Fold and Thrust Belt and produced the burial of the Oman related structures in this area.

2.7 Conclusions

a) Constraints on the Hormuz salt basin margin:

The geometry of the HBS and HD structures and the distribution of Hormuz diapirs at surface suggest that the HD structure would be located close to the Hormuz salt basin margin whereas the HBS structure would be located outside the basin boundary (Figs. 22, 25, and 27). From NW to SE, the HD structure is the last involving Hormuz salt in its core. Consequently, we do not expect salt available southeastwards (e.g. Fig. 31).

b) Diapir initiation and decoupling with the basement structures:

Different evidences for the diapirism initiation in the eastern Persian Gulf are presented in Chapter 3. We consider the triggering of the Hormuz salt diapirism

to be Paleozoic in age. The onset of Hormuz salt movement could have started as early as the late stages of Hormuz salt deposition during the Precambrian extensional stages of the Najad Rift System. A consequence of synrift salt deposition is that the overburden immediately above synrift salt is not prekinematic but is synkinematic, unless rifting ends with salt deposition. Thus, reactive diapirs start growing immediately after salt deposition ends as the overburden stretches by thick-skinned extension. Finally, the base of synrift salt is offset by basement faults. An uneven base of salt is less effective as a décollement and, this limitation intensifies as basement offset increases. Unless synrift salt is especially thick, it provides a stepped, discontinuous detachment. Most of the Hormuz salt basin was characterized by a minimum stratigraphic thickness of two kilometers, probably associated to a certain degree of decoupling during the initial extension. Indeed, the relationship between the basement fault throw versus salt thickness is especially important along the margin of the salt basin, where thinning and pinch-out of the Hormuz salt is expected. This relationship is especially evident during the Permian to Triassic time where thickness variations suggests that the extension was partially accommodated along the margin of the Hormuz salt basin, subsequently inverted during the Oman-Zagros related shortening.

c) Effects of the onset of the Zagros-Oman Orogeny:

Southeastward thickening of the Gurpi Formation, together with onlap of the Gurpi reflectors on top of the Bangestan carbonates suggest the development of a foredeep in this sector (Figs. 22, 24 and 25). Age and orientation of this foredeep is related with the onset of the Oman-Zagros orogeny southeastwards. Extensional faults interpreted in this area, together with thickness variations within Gurpi Fm. are interpreted as to be related with a forebulge related with the Oman orogen (Fig. 31c). As suggested by the distribution of the Pabdeh Formation, Oman structures propagated forward into the basin causing inversion of extensional features during Eocene (Pabdeh Fm.). This can be observed also in other locations (i.e. in the Sarkhun and Kush-e-Kuh anticlines). As evidenced by the geometries observed along the HD structure, compression against pre-existent Hormuz salt wall and diapir would have caused diapir reactivation and secondary welding.

d) Late reactivation:

The whole system was covered during the deposition of Guri carbonates, but these materials are locally folded, suggesting the late reactivation of this system (Fig. 22

and 24). Diapirs would have continued growing at certain locations (Hormuz and Larak islands, Figs. 26 and 27).

Chapter 3: Diapir kinematics in a multi-layer salt system from the eastern Persian Gulf

This chapter is presented in the form of a manuscript, published in Marine and Petroleum Geology (2020).

*Snidero M., Carrera N., Mencos J., Butillé M., Granado P.,
Tavani S., Sàbat F., Muñoz J.A.*

3.1 Abstract

The eastern Persian Gulf hosts several salt structures sourced from two different evaporite layers, the Neoproterozoic-Cambrian Hormuz Salt and the Oligocene-Miocene Fars Salt. Based on seismic interpretation, we discuss the kinematics and dynamics of this autochthonous multi-layer salt system for three case studies: the Tunb and Hengam diapirs, and the Taftan salt anticline. Halokinetic sequences related to Hormuz salt evacuation suggest three main stages of evolution: i) onset of Hormuz Salt diapirism (Paleozoic), ii) diapir squeezing, and emplacement of allochthonous Hormuz Salt (Late Cretaceous to Oligocene-Miocene), and iii) development of secondary and tertiary salt welds (Upper Miocene). Since Fars Salt structures are absent in areas devoid of allochthonous Hormuz Salt, our structural model interprets that the driving mechanism for Fars Salt diapirism is directly related to the emplacement of allochthonous Hormuz Salt during the Zagros-Oman contractional event. The related halokinetic sequences suggest that the Fars Salt diapir kinematic style depends on to the timing of Hormuz Salt extrusion with regards to Fars Salt deposition. Our results provide new insight into the interaction between salt structures sourced from two distinct autochthonous salt layers.

Keywords: Hormuz Salt; Fars Salt; Zagros-Oman Orogeny; Allochthonous salt; Diapir mechanics.

3.2 Introduction

Salt sheets are allochthonous salt bodies developed by salt extrusion from a source layer to a new stratigraphic position, resulting on complex salt-sediment systems. During salt sheet evolution, relocation of salt into new stratigraphic levels can

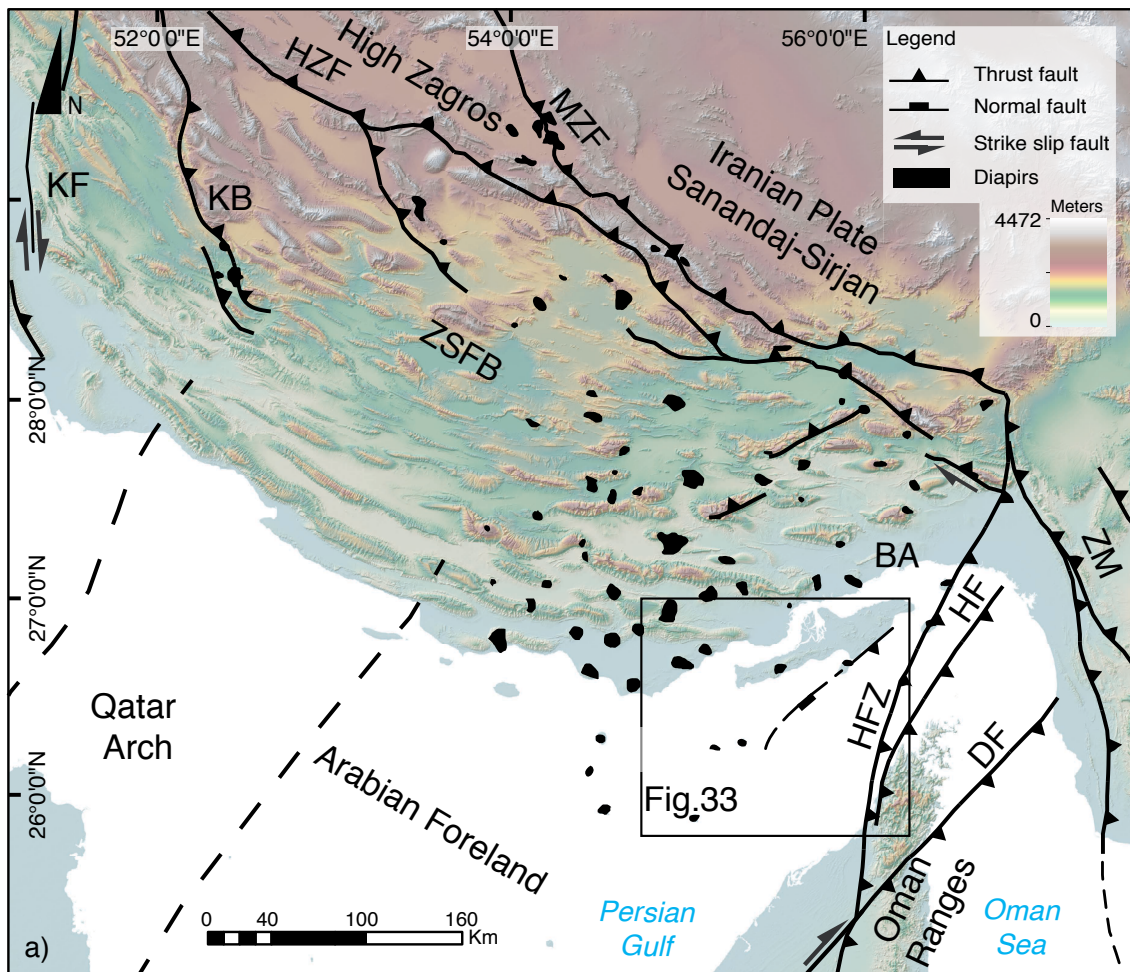


Fig.32: a) Digital elevation model showing the major structural elements of the southeastern Zagros fold and thrust belt, along the Fars Region. ZSFB: Zagros Simply Folded Belt. BA: Bandar Abbas Embayment. HZF: High Zagros Fault, MZF: Main Zagros Fault. KF: Kazerun fault. KB: Kareh Bas fault. HFZ: Hormuz fault zone. HF: Hagab fault. DF: Dibba fault. ZM: Zendan-Minab belt. The basemap was created using the Shuttle Radar Topography Mission dataset (Farr et al., 2007).

modify intermediate deformational stages, obscuring the original salt tectonic framework. Thanks to their economic importance to the hydrocarbon industry, recent advances on reflection seismic data (e.g. Leville et al., 2011), structural restorations (e.g. Rowan, 1993; Hossack, 1995; López-Mir et al., 2014), analogue modelling (e.g. Vendeville and Jackson, 1992a, b; Dooley, 2007, 2015), and field studies (e.g. Lawton et al., 2001; Giles and Lawton, 2002; Rowan et al., 2003b; Lopez-Mir et al. 2018, Callot et al., 2014; Caliteux, et al., 2018) have improved our understanding on salt sheet kinematics and dynamics, yet uncertainties remain. One of these uncertainties is the deformational mechanisms controlling the

emplacement, advance and collision of salt sheets with other salt bodies. To this end, investigating the overburden spatial distribution, the nature of the diapir-strata contacts and the regional stratigraphic framework by means of time-stepped structural restorations is fundamental [e.g. the offshore Gulf of Mexico and Santos Basin (e.g. Rowan et al., 1999; Rowan, 2014; Garcia et al., 2012; Jackson et al., 2015a)]. Moreover, several seismic and experimental examples of overriding salt sheets reveal that the differential loading introduced by extruded allochthonous salt can trigger subsidence and salt expulsion of underlying salt units (Jackson and Talbot, 1991; Dooley et al., 2012). Similar processes are observed in allochthonous salt sheets overriding diapirs that did not yet extrude, which deform the overridden diapir roof (Jackson and Hudec, 2017). However, research on the interaction between diapirs and salt extrusions sourced from two distinct autochthonous salt layers is scant.

In this paper, we present a case study for a multi-layer salt system located at the south eastern edge of the Persian Gulf, at the transition zone between the Arabian

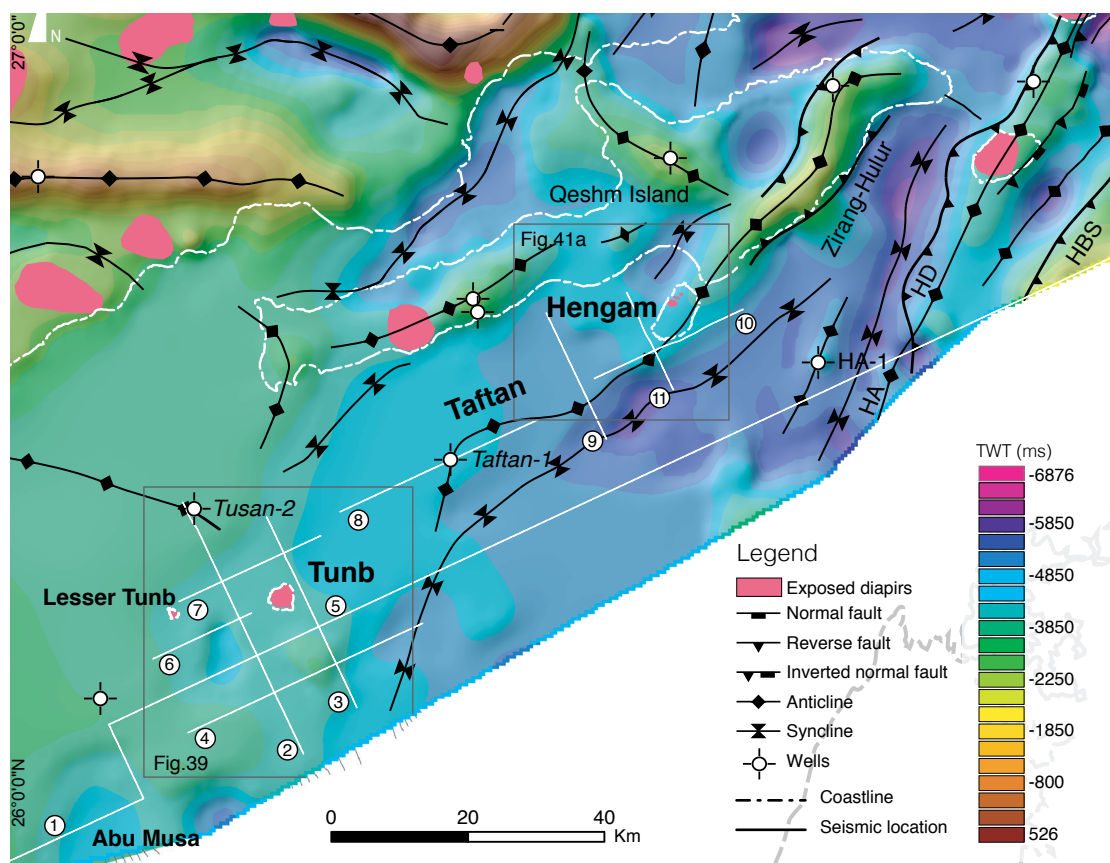


Figure 33: Time structural map of the top of the Santonian Ilam Formation. The illustrated seismic lines are highlighted in white and numbered as indicated in the text. HBS: Hormuz-Barez and Sepid high; HD: Hormuz-Dastan and Farshid high; HA: Hormuz-Aras high.

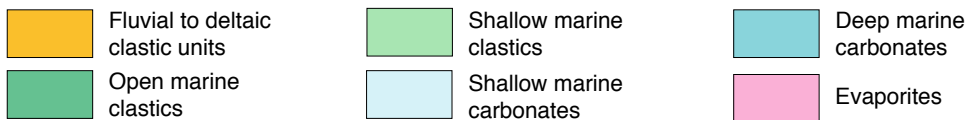
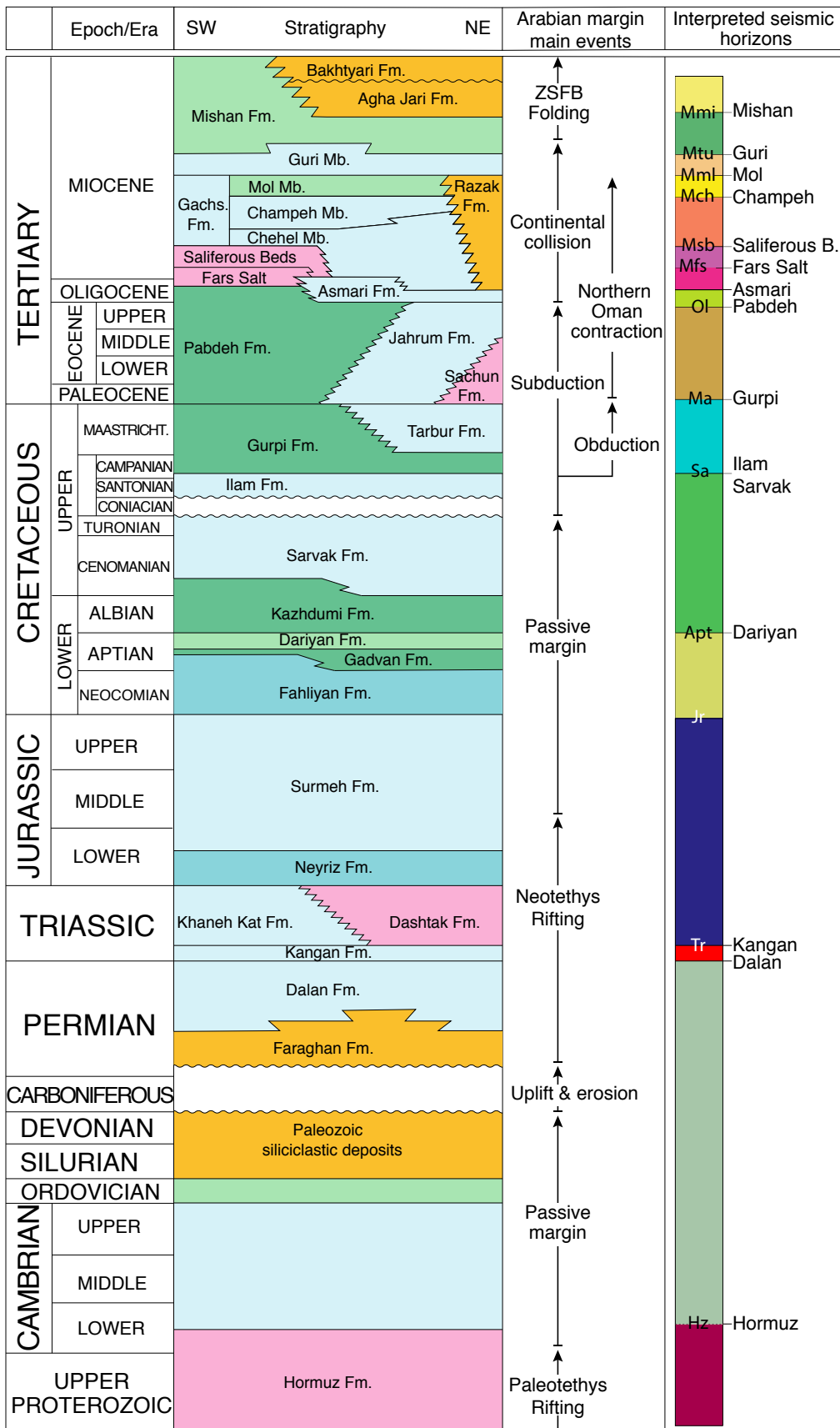


Figure 34: Stratigraphic chart of the eastern Fars region. The main tectonics event and the interpreted seismic horizons are showed. (Modified from James & Wynd, 1965; Ghavidel-syooki et al., 2011; Searle and Ali, 2014; Pirouz et al., 2015; Snidero et al., 2019).

foreland and the Zagros Fold and Thrust Belt to the north and the Oman Ranges to the east (Fig. 32). The salt structures consist of salt pillows and diapirs sourced from two autochthonous evaporitic units: the Neoproterozoic-Cambrian Hormuz Salt and the Late Oligocene-Early Miocene Fars Salt (Kashfi, 1980; Bahroudi and Koyi, 2004; Sajadi et al., 2016). These evaporitic units have very similar seismic facies and are difficult to distinguish once salt has been mobilized and is not in its original stratigraphic position. In these cases, the detailed interpretation of growth structures and salt migration pathways has been key for understanding the salt system evolution.

There is general agreement that diapirs sourced from the Hormuz Salt experienced a long-lasting phase of passive diapirism throughout Paleozoic and Mesozoic times (e.g. Perotti et al, 2016; Stewart, 2018; Snidero et al 2019). Hormuz Salt diapirs were squeezed by shortening related to the Late Cretaceous to Cenozoic Zagros-Oman contractional deformation, and some of them formed allochthonous salt bodies (Wenkert 1979; Talbot and Jarvis, 1984). The upper evaporite unit (Fars Salt) was deposited during Oligocene-Miocene times. Subsequently, in areas adjacent to several Hormuz Salt diapirs, it was mobilized during the Cenozoic contractional event, synchronously to the extrusion of Hormuz Salt allochthonous. However, there are very few detailed studies on the Fars Salt diapirs (Jahani et al., 2009; Alsouki et al., 2011; Orang et al., 2018; Faghieh et al., 2019) and neither the timing and nature of Fars Salt diapirism nor their interaction with Hormuz Salt structures is well understood.

Using a regional 2D reflection seismic and well dataset, this paper investigates three salt structures where both the Hormuz and Fars salt units are present: Tunb, Hengam, and Taftan (Fig. 33). The Tunb and Hengam diapirs are characterized by diachronous phases of Hormuz Salt extrusion, as recorded by two distinct stratigraphic levels, which pre-date and post-date the Fars Salt deposition, respectively. In both cases, emplacement of Hormuz allochthonous salt sheets led to the development of subsidiary Fars Salt structures. Conversely, the Taftan structure is an anticline cored by Hormuz Salt, where neither piercement nor significant movement of the overlying Fars Salt occurred.

Our main objective is to characterize the salt tectonic style of the Hormuz and Fars

salt levels for the three end-members (Tunb, Hengam, and Taftan). To this end, structural restorations were used to constrain the structural evolution of each end-member to ultimately hypothesize a triggering mechanism for the mobilization of the Fars Salt. Our results provide new insight into the interaction of salt structures sourced from different autochthonous salt layers. The examples provided provide excellent structural analogues for the salt-related hydrocarbon systems in the Zagros onshore, where the pre-Zagros salt tectonic framework was more severely overprinted by contractional deformation related to the Zagros Orogeny.

3.3 Dataset

This study is based on a 2D seismic reflection survey covering ca. 34000 km² along the Hormuzgan coast, together with 16 exploration wells (Figs. 32 and 33). The spacing of the seismic lines in the offshore surveys is of 2 km. Onshore surveys have irregular distribution, spacing, and orientation, following the main structural trends. The maximum recorded depth is 7 seconds (twt). Some of the wells have relevant downhole logs for synthetic seismogram generation, whereas others include sonic logs and/or formation tops only. Depositional sequence boundaries were defined based on well intersections and the interpretation of regional unconformities, seismic package internal architecture, seismic reflector geometries and facies, and their relationships with the structures studied (Figs. 33). Additionally, timelines have been tracked within selected depositional sequences to constrain the migration of the depocenters through time.

3.4 Geological Setting

3.4.1 Geodynamic setting

The study area is located in the eastern corner of the Persian Gulf, at the Bandar Abbas embayment of the Arabian foreland. This major embayment is bounded northward by the eastern edge of the Zagros Fold and Thrust belt and eastward by the NE-SW striking structures of the Oman Ranges (Fig. 32). In the study area, these oblique contractional systems interfere.

The basement consists of a pre-Cambrian Gondwana terrain, which was and

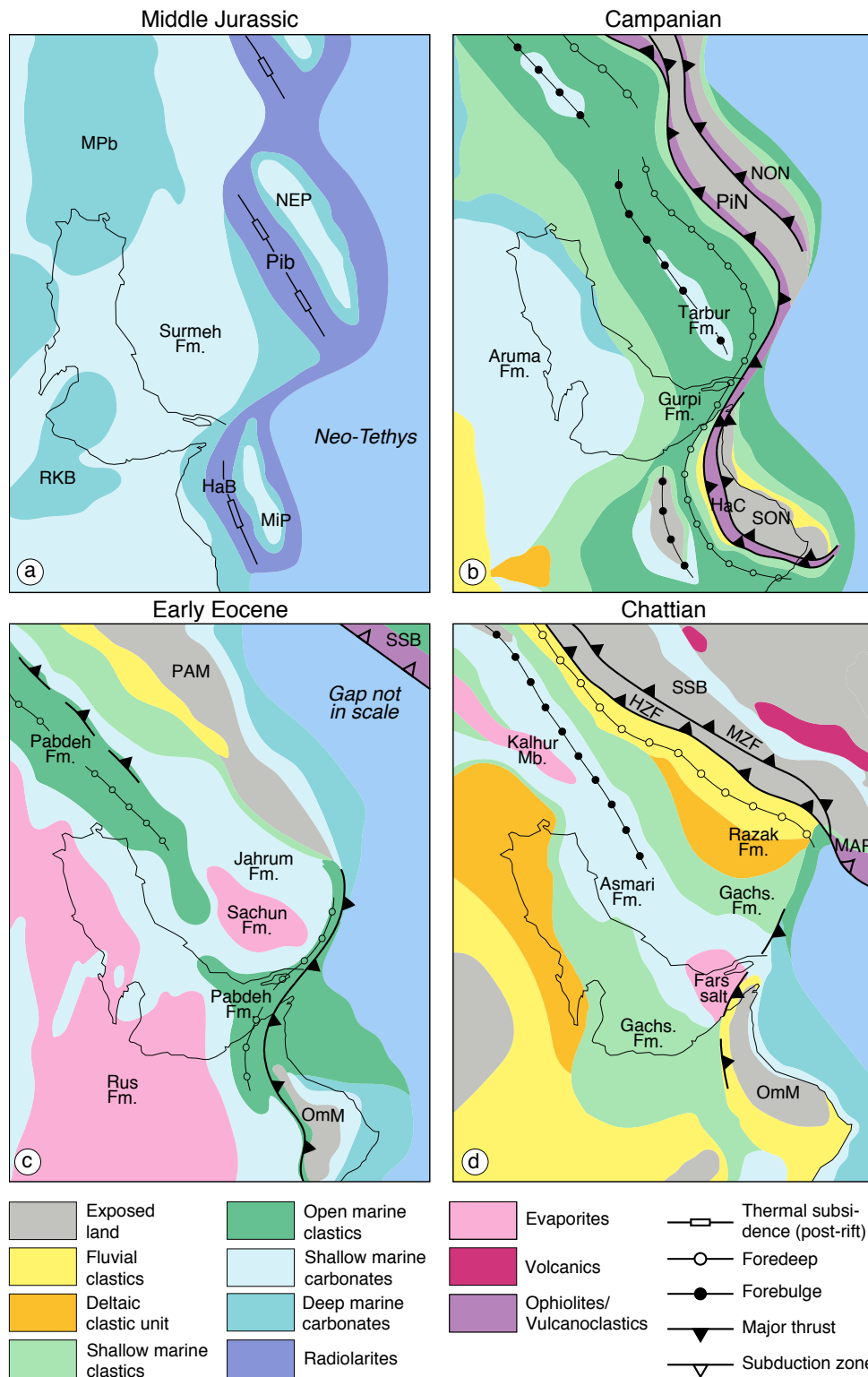


Figure 35: Paleogeographic reconstructions of the northeastern margin of the Arabian plate at the a) Middle Jurassic, b) Campanian, c) Early Eocene, and d) Chattian. Hab: Hawasina Basin; HaC: Hawasina Complex; HZF: High Zagros Fault; MAP: Makran Accretionary Prism; MiP: Misfah Platform; MPb: Mesopotamian Basin; MZF: Main Zagros Fault; NEP: Neyriz Exotics Platform; NON: Neyriz Ophiolites Nappe; OmM: Oman Mountains; PAM: Peri-Arabian Massif; PiN: Pichakun Nappe; RKB: Rub'Al Khali Basin; SSB: Sanandaj-Sirjan Block; SON: Semail Ophiolites Nappe. (modified from Barrier and Vrielynck, 2008; Saura et al., 2011)

dismembered during the break-up of Gondwana at the end of the Proterozoic (c. 570-530 Ma) (Stoeser and Camp, 1985; Beydoun, 1991; Hussein, 2000). In the study area, the Gondwana break-up led to the development of NW-trending left-lateral strike slip faults and NE-trending breakaway faults, referred to as the Njad Rift System (Hussein, 2000), and culminated with the deposition of the Hormuz Salt. These Neoproterozoic fault systems form the eastern boundary of the Hormuz Salt basin (Fig. 32).

The break-up of Gondwana was followed by a relatively stable passive margin during the early Paleozoic (Fig. 34). This was followed by diffuse extensional deformation during the Late Devonian, accompanied by an important uplift, related either to thermal effects (Tavakoli-Shirazi et al., 2013) or to the far effect of the Hercynian Orogeny (Faqira et al. 2009), and resulted in erosion, and peneplanation (Frizon de Lamotte et al., 2013). By the end of the Devonian, general subsidence led to the development of a Carboniferous/Permian sag basin (Frizon de Lamotte et al., 2013). During the Late Permian-Early Jurassic, rifting between the newly-formed Arabian and Cimmerian tectonic blocks led to the opening of the Neo-Tethys Ocean (Berberian and King, 1981; Koop and Stoneley, 1982; Tavani et al., 2018a). Subsequently, during the Upper Jurassic-Lower Cretaceous, the north-eastern margin of the Arabian plate (including the current Zagros region) was tectonically quiescent and located near the equator, at the western passive margin of the Neo-Tethys Ocean (Fig. 34 and Fig. 35a). During the Late Cretaceous to Cenozoic, convergence between the Arabian and Eurasian plates led to the closure of the Neo-Tethys Ocean, and the subsequent continental collision that formed the Oman and Zagros belts (e.g. Stöcklin, 1968; Ricou et al., 1977; Berberian and King, 1981; Alavi, 2007; Agard et al., 2005, 2011; Vergés et al., 2011; Mouthereau et al., 2012). This culminated with the obduction of ophiolite thrust sheets in the north-eastern Arabian continental margin (Coleman, 1981; Alavi, 2007; Searle 2014). The timing of obduction is diachronous, being Coniacian-Santonian (88-84 Ma) in Oman and Maastrichtian (68 Ma) in the north-western Iranian Zagros (Agard et al., 2011). Locally, Campanian-Maastrichtian proto foreland basins developed on the Arabian margin (Ziegler, 2001; Alavi, 2004; Saura et al., 2011). Subsequently during the Paleocene to the middle Oligocene, the foredeep deposits migrated progressively toward the external parts of the northern Oman and Zagros ranges (Orang et al., 2018) (Fig. 34 and Fig. 35c). The onset of continental collision between the Arabia and Central Iranian plates took place from the late Oligocene to the early Miocene (Stoneley, 1981; McQuarrie et al., 2003; Agard et al., 2005;

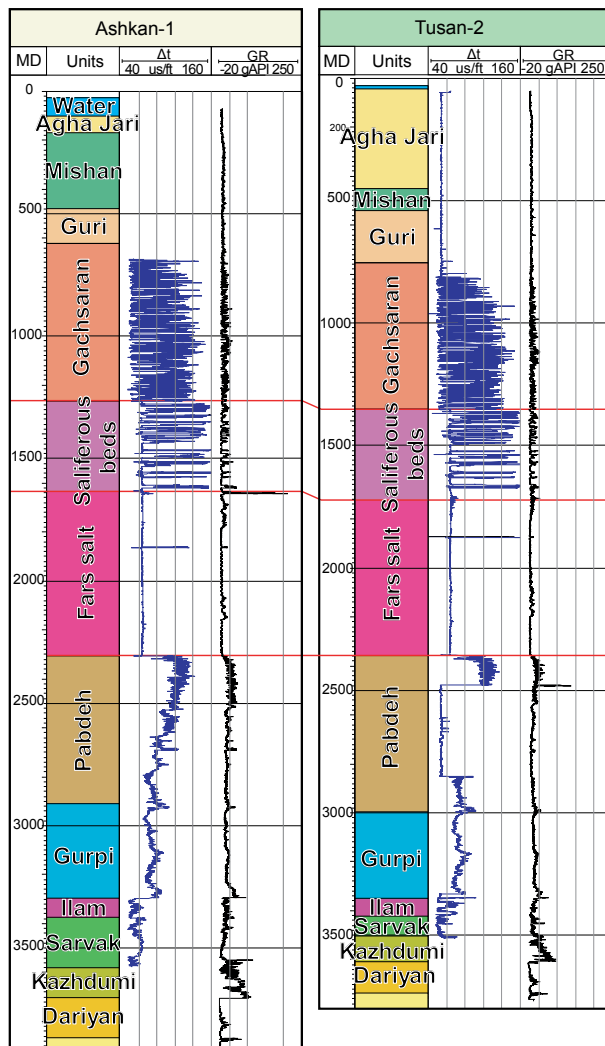


Figure 36: GR and acoustic logs for the Ashkan-1 and Tusan-2 wells. Notice the change in the signal of both GR and acoustic logs defining the boundary between the upper Saliferous beds and the lower Fars Salt. Wells location is indicated in Fig. 32.

limestones, dark dolostones, red sandstones, and shales (Ghavidel-Syooki et al., 2011 and 2014). During most of the Palaeozoic, a uniform clastic continental and shallow-marine sedimentation took place (e.g. Sharland et al., 2013; Ghavidel-Syooki et al., 2014). These deposits were overlain by distal siliciclastic deposits and dolostones of a Permian clastic system (Konert et al., 2001). Above, the Permian to Turonian succession consists of carbonates, evaporites, and marly units, deposited in a shallow to deep marine environment (James and Wynd, 1965; Alavi 2004; Kavooosi, 2013; Lasemi and Jalilian, 2010); these units are pre-orogenic deposits, and predate both the Oman and Zagros orogenies.

Mouthereau et al., 2012; Khadivi et al., 2012; McQuarrie and van Hinsbergen, 2013) (Fig. 34 and Fig. 35d). Such convergence lasted until Recent times with the development of the Zagros Fold and Thrust Belt, and related Arabian foreland basin (Mouthereau et al., 2007). Deformation in the northern Oman belt finished by the middle Miocene with the development of the out of sequence NE-SW trending Hagab thrust (Fig. 32) (Searle et al., 2014).

3.4.2 Tectono-stratigraphic framework

In the study area, the above-described geodynamic evolution led to the deposition of up to 14 km thick Paleozoic to Cenozoic sedimentary succession above a Neoproterozoic to Cambrian salt layer, referred to as the Hormuz Salt (Fig. 34). The Hormuz Salt consists of halite, anhydrite,

The initial development of the Oman-Zagros foreland basins is recorded by a thick succession of Campanian to Oligocene marls, referred to as the Gurpi and Pabdeh formations (Piryaei et al., 2011). Above, the Oligocene-Miocene sequence is made up of the marine carbonate Asmari Formation. In the Qeshm Island (Fig. 33), the Asmari Formation is Chattian to early Aquitanian in age (Sajadi and Rashidi, 2019) and laterally equivalent to the upper part of the marly Pabdeh Formation basinward. The Pabdeh and Asmari formations are overlain by the Oligocene-Miocene Gachsaran Formation, which in turn is sub-divided into three distinct members (Kashfi, 1980): a basal member made up of gypsum and anhydrite (i.e. Chehel Member), a middle member made up of marly limestone and dolostone succession interbedded with thin evaporite layers (i.e. Champeh Member) and an upper member made up of red shales alternated with thin limestones (i.e. Mol Member). These three members are only present in the south-eastern Fars region. The thickness of the Chehel Member decreases southward, toward the study area, due to a lateral transition into the Champeh Member and the evaporitic facies of the Fars Salt. In the literature, the Fars Salt is described as an Oligocene-Miocene evaporitic unit, made up of halite, sand, and subordinate anhydrite with thin interbedded marl layers (Kashfi, 1980). It has also been referred to as the Qeshm Formation (Kashfi, 1980; Bahroudi and Koyi, 2004) from the lower Fars Group (Harrison, 1924; Lees, 1950). Based on well data, we sub-divide the Fars Salt unit into two sub-units with characteristic GR and Δt signals. The upper sub-unit, referred here as Saliferous Beds is present throughout the entire Fars Salt basin and consists of an interlayered succession of evaporites and carbonates. These exhibit a characteristic jagged pattern for the GR and Δt logs (Fig. 36). The lower sub-unit, referred here simply as the Fars Salt, is only present in the Ashkan-1, Siri F-1, Taftan-1, and Tusan-2 wells, located in the central parts of the basin, where it shows a maximum stratigraphic thickness of 500 m (Fig. 37a). This is recognized by a drop on the Δt log and a distinctive straighter pattern, thus indicating a more homogeneous evaporitic composition. Toward the north and the east (proximal parts of the Fars Salt basin), the Fars Salt pinches out and the Saliferous Beds directly overlay the Pabdeh Formation or their lateral equivalent; the Oligocene-Miocene Asmari Formation (Fig. 37b). The overlying middle Miocene succession is characterized by a fast transition into the limestones of the Guri Member, at the base of the Miocene to Pliocene Mishan Formation. These are characterized by shallow-water marine marls interbedded with bioclastic limestones (Pirouz et al., 2015).

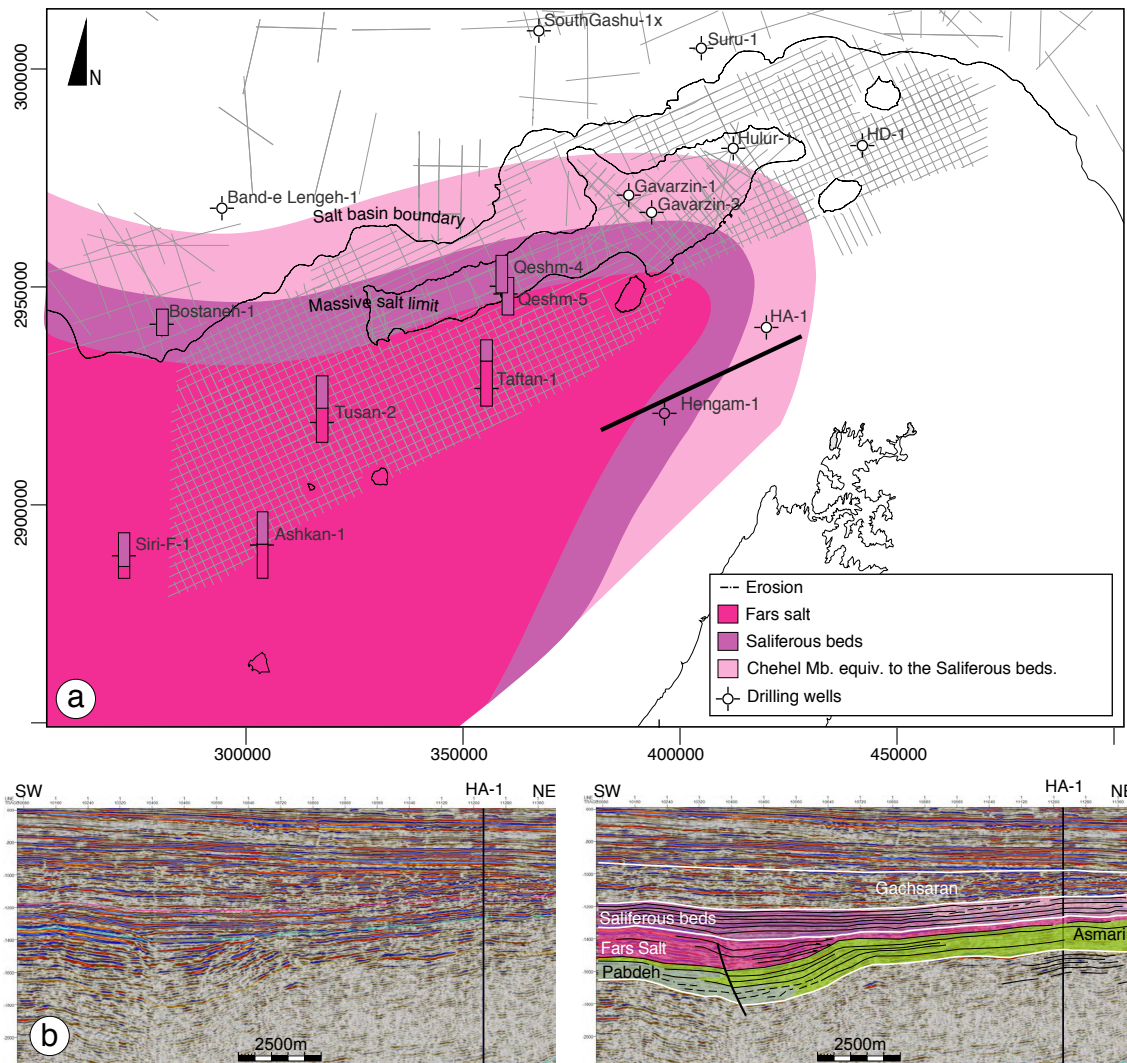


Figure 37. a) Facies map of the Fars evaporites. This maps is based on the interpreted seismic lines and the well data shown in the image. b) SW-NE Seismic line across the eastern Fars salt basin margin. Onlap geometries of the Fars Salt deposits onto the Asmari carbonates are highlighted. Above, the Saliferous beds unit grade laterally to Gachsaran Fm. drilled by the HA-1 well (Projected on the seismic profile). Below, the Asmari limestones grade eastwards to basinal facies underneath the Fars Salt unit.

3.5 Salt structures

The salt structures studied are located offshore, along the front of the Oman Ranges (Figs. 33 and 37). Here, the Hengam diapir pierces the Zirang-Hular/Taftan anticline and constitutes the western end of the Zirang-Hular anticline (Chapter 3), along the Fars Salt basin margin. To the west, the Hengam and the Taftan salt structures meet, so that they will be described together. To the south-west of Taftan, the Tunb salt structure constitutes an isolated salt diapir exposed in the homonymous Tunb

island, which is unrelated to the Oman structural highs (Fig. 33). Immediately to the north-west, another isolated but smaller salt diapir pierces the surface at the Lesser Tunb island. Several km south-west, the Abu Musa salt structure crops-out in an island (Fig. 33 and 37). However, the available seismic data do not cover the Abu Musa structure fully and, consequently, it is not describe throughout this work. Nevertheless, the few seismic geometries observed in Abu Musa diapir are comparable to those described for the Tunb salt structure, suggesting that the deformation history was similar.

3.5.1 Tunb salt structure

The Tunb salt structure consists of a central diapir made up of Hormuz Salt (i.e. the Central Tunb diapir, Tcd), which is surrounded by a ring of shallow Fars Salt structures referred here to as the Circular Belt (cb) (Figs. 38 and 39). The neighboring Lesser Tunb diapir is a minor Hormuz Salt diapir. It does not form any allochthonous salt sheet, and is not surrounded by Fars Salt structures (Figs. 33 and 39).

The Central Tunb diapir forms a relatively shallow salt sheet emplaced within the Oligocene-Miocene succession (referred hereafter as Tunb Salt sheet or Tss), which is recognizable by the seismic profiles 32, 33, and 35 as a 1250 ms to 500 ms nearly reflection-less zone (Figs. 38a,38b,38d, and 39). The top of the salt sheet is defined by strong reflectors that, based on well data and seismic interpretation, are considered Miocene. The base of the salt sheet is defined by weaker reflectors that cut through different levels of the Miocene sequence. These weaker reflectors define lateral salt ramps above several Miocene stratigraphic units, indicative of different periods of salt extrusion (Fig. 38b). For instance, in the eastern side, the Tunb Salt sheet overlies the Fars Salt unit to the south but the Champeh Member to the north, younging in a southerly direction (Fig. 38b).

Underneath the Tunb Salt sheet, the Central Tunb diapir feeder delineates a N-S trending elliptical map-view pattern, defined by the lowest points of the Tunb Salt sheet (Fig. 39). However, the geometry of the feeder at depth is uncertain due to the seismic wipeout zone so that the interpretation is largely based on the overburden geometries. The Tunb Salt Sheet around the Central Tunb diapir is interpreted to be fed from the emergent central dome, as observed in other diapirs onshore (Jahani et al., 2009). To the south, the diapir feeder is overlain by a secondary minibasin,

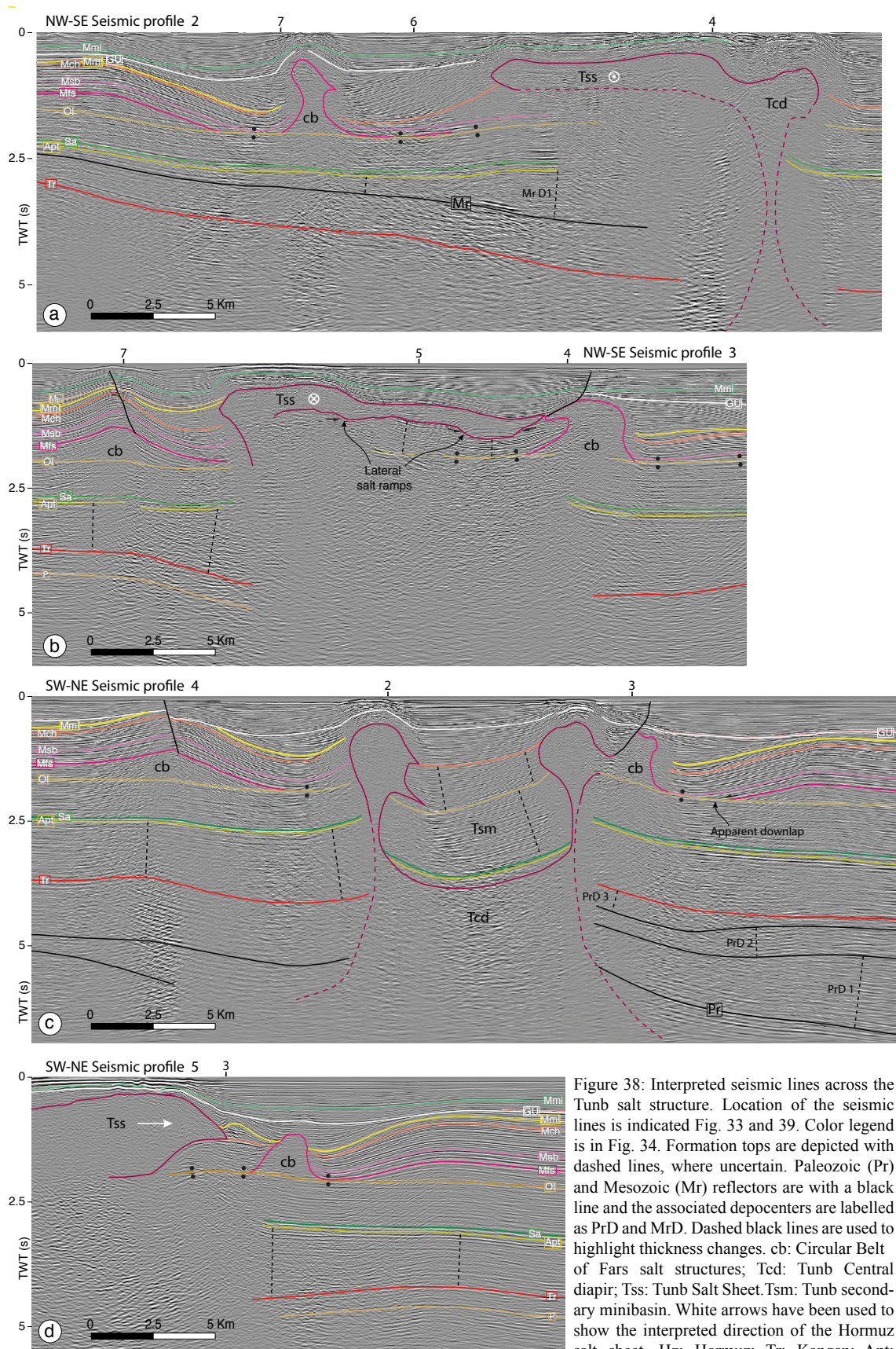


Figure 38: Interpreted seismic lines across the Tunb salt structure. Location of the seismic lines is indicated Fig. 33 and 39. Color legend is in Fig. 34. Formation tops are depicted with dashed lines, where uncertain. Paleozoic (Pr) and Mesozoic (Mr) reflectors are with a black line and the associated depocenters are labelled as PrD and MrD. Dashed black lines are used to highlight thickness changes. cb: Circular Belt of Fars salt structures; Tcd: Tunb Central diapir; Tss: Tunb Salt Sheet; Tsm: Tunb secondary minibasin. White arrows have been used to show the interpreted direction of the Hormuz salt sheet. Hz: Hormuz; Tr: Kangan; Apt: Daryan; Sa: Ilam-Sarvak; Ma: Gurpi; Ol: Pabdeh; Mfs: Fars Salt; Msb: Saliferous Beds; Mch: Champeh; Mmi: Mol; Mtu: Guri; Mmi: Mishan.

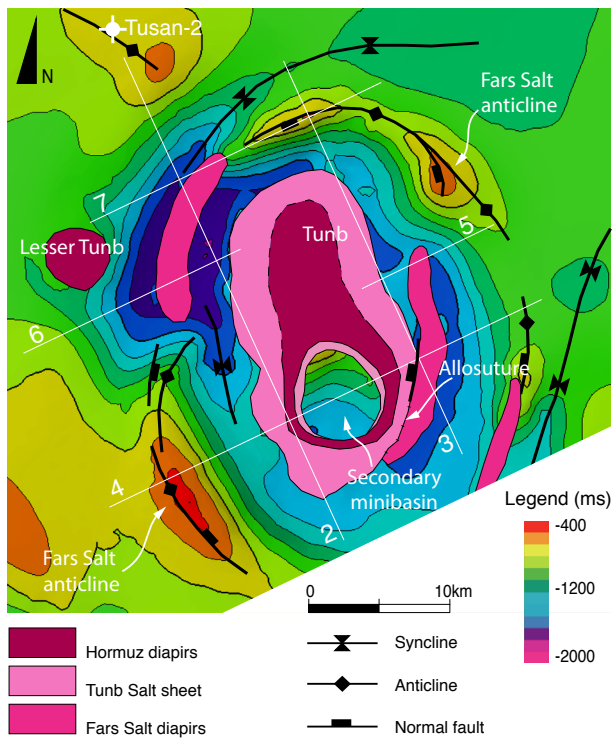


Figure 39: Time structural map of the Top Champeh Member for the Tunb and Lesser Tunb salt structures. The location of the seismic lines is indicated with white lines. The Fars Salt diapirs and salt anticlines form the Circular Belt around the Hormuz diapir. Notice the coalescence between the Fars Salt diapir and the Hormuz salt sheet at the eastern sector of the Circular belt.

by strata that thicken toward the Hormuz Tunb diapir (depocenter PrD 3 in Fig. 38c). Such features are indicative of the migration of the depocenter toward the diapir, and their geometry resembles that of a turtle structure (Trusheim, 1960). The specific age of the deep-seated Paleozoic overburden is unknown and their age is inferred based on their stratigraphic position.

Based on the correlated tops from the onshore Namak-1 and Finu-1 wells, the overlying reflectors are interpreted as the Lower Triassic Kangan Formation (reflector Tr in Fig. 38). However, the base of this unit cannot be clearly identified. This Lower Triassic unit forms a relatively thin isopach succession. Above, the Middle Triassic to Lower Cretaceous stratigraphic sequence thickens toward the diapir sides (e.g. depocenter MrD 1 in Fig. 38a). The overlying Upper Cretaceous to Oligocene sequence forms an almost 3 km thick relatively isopach succession, which is topped by the Pabdeh Formation, and pierced by the Central Tunb diapir

imaged in the seismic profile 4 (Tsm in Fig. 38c). The minibasin is sub-divided into a lower symmetric sedimentary package made up of approximately isopach strata, and an upper asymmetric package made up of sediment wedges that thicken toward the north-east. This change on the thickening trend is marked by a prominent Hormuz Salt wing, imaged at the south-west flank of the minibasin (Fig. 38c). Such geometry resembles those described for box type minibasins (sensu Pratson and Ryan, 1994)

The flanks of the Central Tunb diapir provide a good quality image until 6s (twt) (Fig. 38). The lowermost reflectors exhibit lenticular geometries, characterized by a flat-lying base and convex-upward tops (depocenters PrD 1 and PrD 2 in Fig. 38c). These are overlain

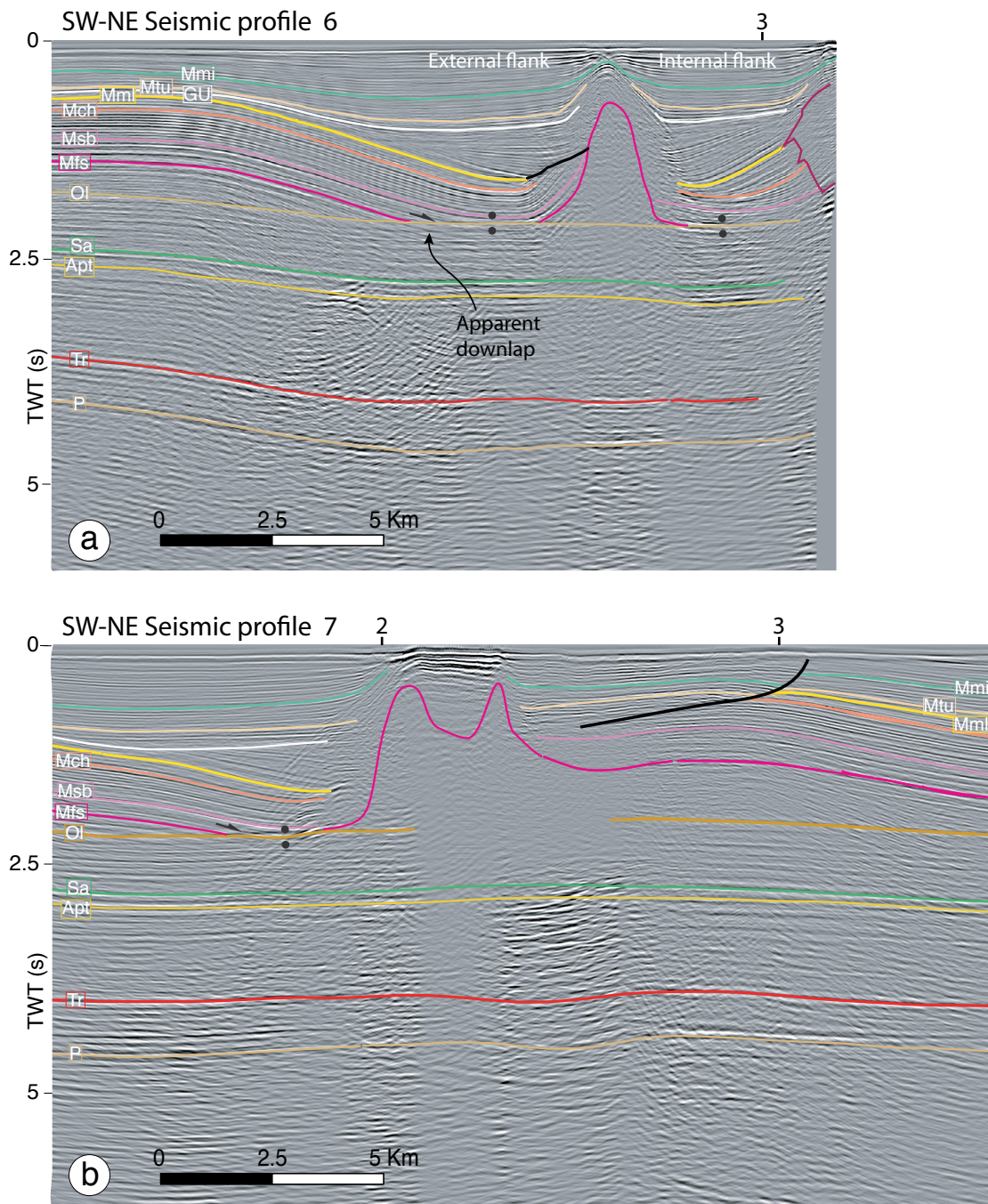


Figure 40: Interpreted seismic lines across the NW section of the Fars Circular Belt around the Central Tunb diapir. The location of the seismic lines is indicated in Fig. 32 and 38. See Fig. 33 for color legend. Colors of the interpreted formations tops are indicated in Fig. 33. a) Orthogonal profile of a salt wall. b) Oblique profile to the same salt wall and longitudinal to a Fars salt anticline. Hz: Hormuz; Tr: Kangan; Apt: Daryan; Sa: Ilam-Sarvak; Ma: Gurpi; Ol: Pabdeh; Mfs: Fars Salt; Msb: Saliferous Beds; Mch: Champeh; Mml: Mol; Mtu: Guri; Mmi: Mishan.

(Fig. 38).

The Circular Belt of Fars Salt structures, is located above this isopachous sequence that ends with the top of the Pabdeh Formation. It consists of a connected sequence

of salt anticlines and salt walls forming an approximately regular ring around the Tunb Salt sheet (Fig. 39). The Saliferous Beds and Champeh members overlie the Fars Salt and display minor thickness variations. Above, halokinetic sequences adjacent to the Fars Salt structure exhibit significant thickness variations on the Miocene Mol Member and the lower section of the Guri Member. These record the peak of Fars Salt evacuation. They display distinctive growth geometries, such as the salt wall in the north-west sector of the Circular Belt (Figs. 38 and 40), that resemble those described for expulsion rollovers (Ge et al., 1997) .

The eastern and western flanks of the Fars Salt diapir constitute the internal and external flanks of the Hormuz Salt diapir, respectively (Fig. 40a). Along the internal flank, the Fars Salt is completely depleted and an extended weld surface is present between both diapir flanks. The Saliferous Beds and Champeh Members rotate downward toward the Fars Salt diapir, and exhibit an apparent downlap above the Pabdeh Formation (Fig. 40a). This is indicative of salt inflation during the deposition of the Saliferous Beds followed by welding. Above, the sequence of the Champeh Member is also different between the two diapir flanks. In the external flank, the Champeh Member is isopach, concordant with the steep flank of the Fars Salt diapir and truncated by younger sediments of the Mol Member. Conversely, in the internal flank, the Champeh Member is truncated by the Fars Salt diapir and thickens toward the Hormuz Salt diapir (Fig. 41a). These observations suggest that the first depocenters associated to the evacuation of Fars Salt generally develop next to the Hormuz Salt diapir. Above, the Mol Member and the lower section of the Guri Member display of growth sequences characterized by a progressive shift of the depocenters toward the Fars Salt diapir.

The upper sequence of the Guri Member marks the burial of the Fars Salt diapir. The strata overlying the Guri unconformity onlap and thin toward the diapir, forming an arched roof above the diapir crest. The upper part of the sequence exhibits minor thickness changes and is affected by extensional faults above the diapir crest. Laterally, the Fars Salt does not pierce the overburden and the structure consists of salt anticlines on both sides of the diapir (Fig. 39, 40b, and 38c). These anticlines are affected by normal faults, which display a circular trend dipping toward the Hormuz Salt diapir. These faults accommodate different amounts of extension during the Middle to Upper Miocene. The Circular Belt of Fars Salt structures is usually located 5 to 10 km away from the Tunb Salt sheet, except at the eastern side of the Tunb diapir where the Fars Salt structure trend turns N-S, immediately before meeting the Hormuz Salt sheet (Fig. 39). As a result, the

Fars Salt structure and the Tunb Salt sheet in the seismic profile 5 (Fig. 40d) are clearly disconnected, whilst in the seismic profile 4 to the south, these structures merge. At shallower levels, they are separated by a small minibasin bounded by an extensional fault (Fig. 38c).

3.5.2 Taftan and Hengam salt structures

The Taftan and Hengam salt structures are located to the north-east of the Tunb structure (Fig. 33). The Taftan structure consists of a curved anticline cored by Hormuz Salt, that trends N20° in the south-east and N60° in the north-east (Fig. 41b and 41c). The western part of the Taftan anticline involves a thick Paleozoic to Oligocene isopach succession (Fig. 41b). However, it exhibits minor thickness variations at the anticline crest, revealing minor Fars Salt inflation. This Paleozoic to Oligocene succession is covered by an isopach succession made up of the Saliferous Beds and Champeh Member. The overlying Miocene Mol and Guri Members, and the post-Mishan sequence exhibit growth strata geometries, thinning toward the anticline crest (Fig. 41b), which are related to syn-sedimentary salt inflation.

To the east, the Taftan anticline links with the Hengam diapir and the Zirang-Hulur anticline (Fig. 32). At this sector, the Paleozoic to Oligocene sequence from the south-eastern limb of the Taftan anticline thickens and deepens toward a NE-SW trending depocenter, forming a synclinal trough along the anticline flank (Fig. 41a and 41c). At the junction with the Hengam diapir, the oldest layers identified correspond to the Ilam Formation (Fig. 41d and 41e). Toward the stem, they dip away from the diapir and reach lower depths in south-eastern flank than the north-western one (Fig. 41e). This resembles the asymmetric geometry described for the Taftan anticline. The Ilam horizons are eventually truncated by the diapir and form a salt keel, which is interpreted as a remainder of the upper part of the pinched-off salt feeder. Above, the diapir body forms a 10 km wide bulb, clearly imaged by the seismic lines. The diapir walls exhibit repeated episodes of salt extrusion within the Pabdeh and the overlying Miocene succession. In the seismic profile 10 (Fig. 41d), a larger extrusive salt wing is present above the Guri unconformity, indicating that salt extrusion occurred during the Tortonian, previous to the diapir burial.

In the seismic profile 10 (Fig. 41d), however, salt expulsion seems to have been

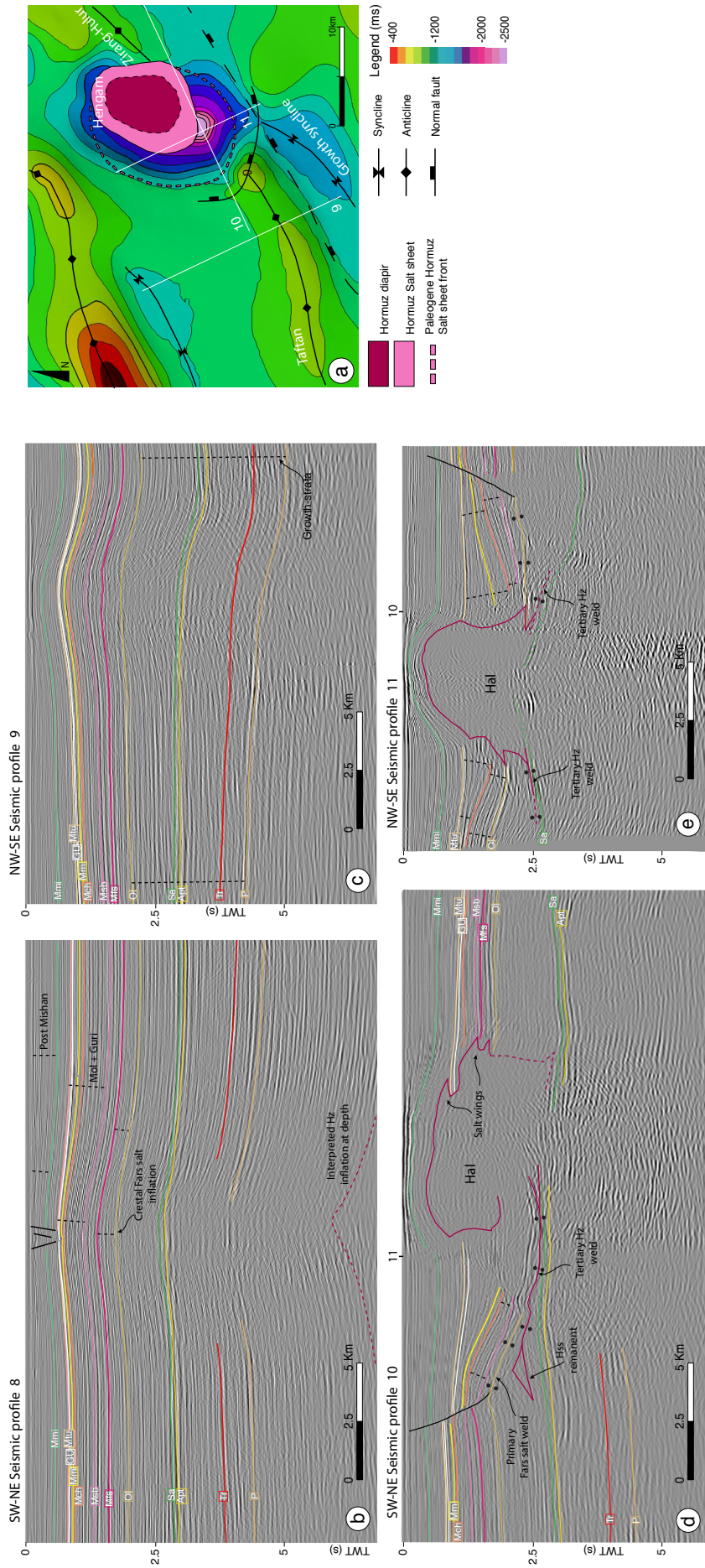


Figure 41: a) Time structural map of the Top Champe Member. b) Interpreted seismic line across the Taftan salt anticline. Notice the wedging geometries of the Mol and Guri Mbs. and the post-Mishan reflectors toward the anticline crest, where minor inflation of the Fars Salt occurs. Location is indicated in Fig. 33. c) Interpreted seismic line across the eastern sector of the Taftan salt anticline. d) and e) Interpreted seismic lines across the Hengam diapir. See Fig. 33 and 43c for location. See Fig. 34 for color legend. Hal: Hengam Allocthonous; Hss: Hengam Salt Sheet. Dashed black lines are used to highlight thickness changes. Hz: Hormuz; Tr: Kangan; Apt: Daryan; Sa: Ilam-Sarvak; Ma: Gurpi; Ol: Pabdeh; Mfs: Saliferous Beds; Meh: Champah; Mmi: Mol; Mtu: Guri; GU:Guri Unconformity; Mmi: Mishan.

more significant. A triangular area with a transparent facies within the Pabdeh Formation is interpreted as a remnant salt body, which is laterally equivalent to a larger Hormuz Salt sheet that is now welded. The salt weld forms a tertiary weld, climbing up-section within the Pabdeh Tertiary Formation toward the south-east, away from the diapir (Fig. 41d). The Miocene strata above the toe of this welded salt sheet form an anticline, affected by a syn-sedimentary normal fault, across which strata thicken (Figs. 41d and 41e). This fault is semi-circular in map-view, dips toward the Hengam diapir, and is interpreted to detach on the Fars Salt (Fig. 40a). Finally, the Mol and Guri Members thicken progressively toward the Hormuz diapir, indicating a shift of the depocenters (Fig. 41d and 41e). This coincides with the progressive welding of the Fars Salt unit. The overlying Mishan Formation thins and onlaps the inflated Hormuz Salt diapir, suggesting residual salt inflation.

3.6 Discussion

3.6.1 Tunb Deformation history

The geometries discussed throughout this paper indicate that salt flow in the Tunb structure started soon after the deposition of the Hormuz Salt. The strata architecture described underneath the Permian Dalan Formation indicates that shifting of depocenters related to wide salt structures already occurred in the Paleozoic. Furthermore, the identification of turtle anticlines in deep-seated Paleozoic strata around the Central Tunb diapir indicates that the Hormuz Salt approached the touchdown already before the Permian, forming partial welding, probably located in patches around the diapir (Fig. 42a). The continuous salt rise during the Paleozoic has also been interpreted in other salt structures from the Persian Gulf, based on the presence of rim basins and onlap surfaces, which progressively rotated and verticalized at depth (Carruba et al., 2007; Chiariotti et al., 2011). The growth geometries described for the Aptian Dariyan Formation and underlying strata, thickening toward the diapir stem, are indicative of ongoing salt expulsion, resulting in the lateral withdrawal of the Hormuz Salt (Fig. 42b). The constant thickness of the overlying Cretaceous to Oligocene units suggests that no lateral salt movement occurred during this time interval. Additionally, the Hormuz Salt overburden does not show any further subsidence in the external flanks of the Tunb diapir, supporting the development of primary welds, and the exhaustion of

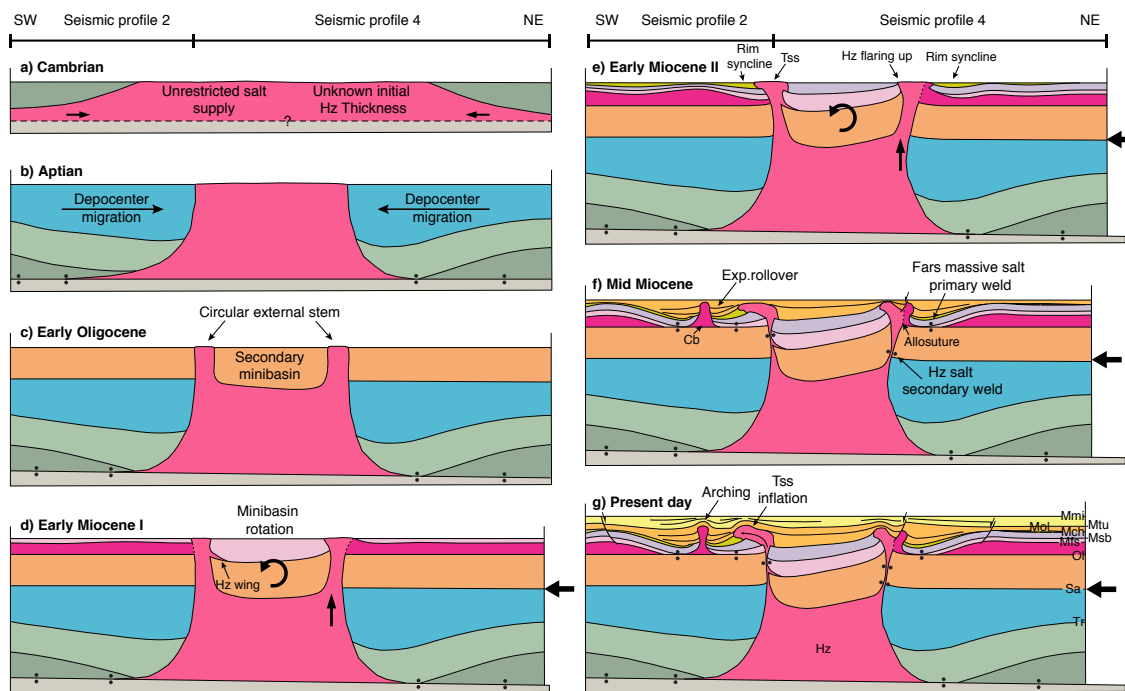


Figure 42: Schematic restoration of the Tumb salt structures. The strata geometries are inspired in the seismic line 2 and 4. Hz: Hormuz; Tr: Kangan; Sa: Ilam-Sarvak; Ol: Pabdeh; Mfs: Fars Salt; Msb: Saliferous Beds; Mch: Champeh; Mml: Mol; Mtu: Guri; Mmi: Mishan.

the Hormuz Salt source.

In spite of the interruption of Hormuz Salt supply, the Cretaceous to Oligocene units do not cover the Central Tunb diapir. A likely explanation is that the sink of secondary minibasins over the diapir feeder mobilized Hormuz Salt away from the Central Tunb diapir, and this evacuated salt formed a circular external stem (Fig. 42c). In such scenario, secondary minibasin initiation is interpreted to be marked by the basal strata corresponding to the Lower Cretaceous Dariyan Formation. Alternatively, the ongoing salt rise may have been enabled by the onset of contractional deformation at the Late Cretaceous. Here, salt would be sourced from the diapir stem.

This configuration continued during the Oligocene-Miocene, with the sedimentation of the Fars Salt unit, the Anhydrite Beds and the Champeh Member. Locally, this was coeval to minor Fars Salt inflation during or immediately after the Fars Salt deposition, as indicated by the onlapping relationship of the Saliferous Beds above the Fars Salt (Fig. 42d). Since the Oligocene, the increase of the salt-supply rate with regards to the sediment-accumulation rate led to the gradual flaring of Hormuz Salt on the eastern flank of the Tunb diapir, and the formation of a salt wing within the secondary minibasin. The estimated sedimentation rate during the Oligocene

is approximately three times higher (65 m/Ma) than during the Paleogene (20 m/Ma), as indicated by Perotti et al., (2016). This suggests a significant increase in the Hormuz Salt supply, which may have led to the development of allochthonous salt sheets. In turn, this is interpreted to be triggered by shortening related to the onset of the Zagros deformation (Fig. 42d). Such shortening also influenced the minibasin-subsidence mechanism, resulting in a differential salt uplift that led to the development of an asymmetric syncline (Hudec et al., 2009). The minibasin bathymetric low is offset toward the less uplifted side, resulting in the depocenter shift toward the south-west (Fig. 42d). Furthermore, salt wing extrusions on the western side of the minibasin produced an asymmetric load, enhancing the oblique sinking above salt.

During the deposition of the Miocene Mol and Guri members, the squeezing of the Central Tunb diapir and profuse supply of Hormuz Salt was coeval to the withdrawal of the younger Fars Salt. Fars Salt evacuation is indicated by growth strata geometries and the development of a shallow post-Oligocene rim syncline around the central Hormuz Salt diapir (Fig. 42e). The shift of the depocenters toward the external Circular Belt suggests that the evacuation of Fars Salt outward (away from the Central Tunb diapir) was related to the sedimentary loading produced by the extruding Hormuz Salt. The advance of the Hormuz Salt sheet and the progressive evacuation of Fars Salt produced the interpreted salt weld between the Saliferous Beds and the Pabdeh Formation (Fig. 42f).

At the middle Miocene, the Tunb diapir was almost totally buried, before the development of the Guri unconformity. During this period, the Guri Member was regionally deposited with an estimated sedimentation rate of 13 m/Ma (Perotti et al., 2016). This is significantly lower compared with the Oligocene to lower Miocene sedimentation rate. Consequently, the burial of Hormuz Salt structures implied a decrease in the Hormuz Salt supply, endorsing the interpretation of the progressive closure of the Central Tunb diapir by secondary welding, and the consequent end of the salt extrusion (Fig. 42f). With the drop of Fars Salt availability from the rim syncline, also the growth of the Circular Belt structures decreased. As a result, all the diapirs were buried (Fig. 42f). Further deformation related to ongoing shortening produced a switch to an active rise of both Fars and Hormuz Salt structures, as described for the strata above the Guri unconformity (Fig. 42g). Subsequently, the squeezing of the central Tunb diapir promoted folding of the thinned Neogene overburden and the arching of the Hormuz Salt sheet by salt inflation. Salt was imported laterally along strike, as described in similar salt

allochthonous structures (Jackson et al., 2008).

Along the Circular Belt, the connection between the Fars Salt structures enhanced the migration of the Fars Salt away from the salt anticlines, which collapsed by normal faulting, toward the salt walls. The latter underwent squeezing and roof arching. Wider salt walls experienced little arching because the displaced salt spread beneath a wide roof. Conversely, narrow salt walls experienced severe arching because the displaced salt was concentrated beneath a narrow roof, promoting crestal grabens.

3.6.2 Taftan and Hengam deformation history

The Paleozoic to Oligocene growth geometries described for the Taftan Hormuz Salt anticline record differential subsidence between the northern and southern flanks. The observed NE-SW growth syncline, previous to the Zagros continental collision, indicates that Hormuz Salt withdrawal predominantly occurred along the Taftan southeastern flank. The greater availability of Hormuz Salt along the Taftan southeastern flank is likely related to the depositional thickness of the Hormuz Salt, in turned controlled by the structural framework of the Neoproterozoic extensional system. In such way, the Hormuz Salt migrated laterally from the hanging wall of a basement-involved south-easterly dipping normal fault toward the Hengam salt structure, located in the footwall. We interpret that the differential subsidence described for the overlying Paleozoic to Oligocene depocenters was also controlled by salt evacuation related to these deep-seated basement normal faults (Fig. 43a and 43b).

In this area, the first Hormuz Salt sheet was extruded in the eastern and southern flanks of the Hengam Diapir, during the deposition of the Pabdeh Formation (Fig. 43b). Considering the increasing depositional rate of the Pabdeh foreland deposits, salt extrusion was probably related to the onset of the Zagros contractional event and consequent squeezing of the Hengam diapir. Differently to the Tunb diapir, the emplacement of the first salt sheet happened before the deposition of the Fars Salt unit, suggesting that salt structures closer to the Oman thrust front were squeezed earlier (Fig. 33).

Subsequently, the Hormuz salt sheet was buried by the upper portion of the Pabdeh Formation (Fig. 43b). Following the deposition of the Fars Salt unit, a semi-circular normal fault associated to a rollover anticline was developed above this buried salt

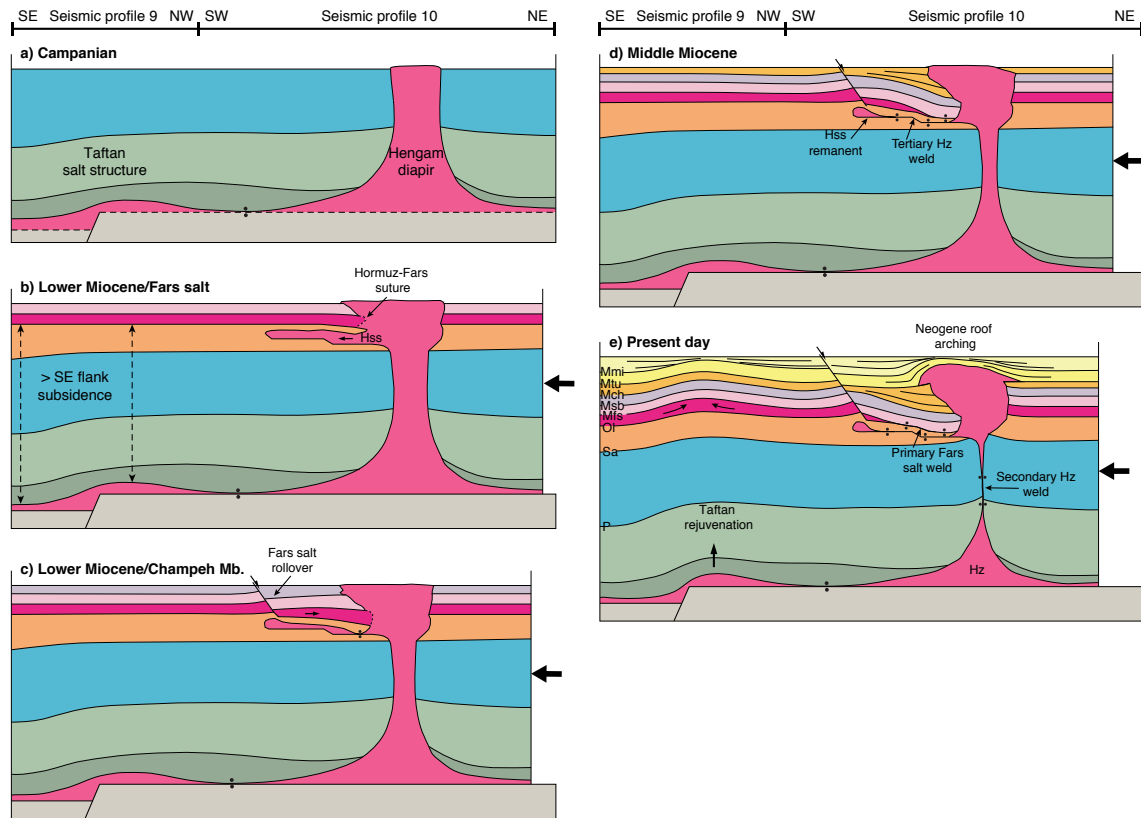


Figure 43: Schematic restoration of the Hengam and Taftan salt structures. The strata geometries are inspired in the seismic line 9 and 10. Hz: Hormuz; Tr: Kangan; Sa: Ilam-Sarvak; Ol: Pabdeh; Mfs:Fars Salt; Msb:Saliferous Beds; Mch: Champeh; Mml: Mol; Mtu: Guri; Mmi: Mishan.

sheet. The development of this extensional fault is interpreted to be related to the evacuation of salt from the underlying Hormuz salt sheet during the deposition of the Fars Salt unit, creating a slope gradient toward the central diapir. In this case, a suture should have formed between the extruding Hormuz Salt and the Fars salt (Fig. 43b). The lower Miocene Champeh Member growth strata record the onset of Fars Salt evacuation from the above-mentioned rollover toward the Hormuz Salt diapir (Fig. 43c).

Following the development of a Hormuz salt sheet tertiary weld, the shift of depocenters toward the Hormuz Salt diapir described for Miocene Mol and Guri members, indicates a major phase of Fars Salt expulsion (Fig. 43d). The development of salt wings above the Guri unconformity supports the continued availability of Hormuz Salt and ongoing squeezing of the Hengam diapir during the middle Miocene (Fig. 43e). The salt wings and most of the Taftan diapir bulb were subsequently buried by the Upper Miocene Mishan Formation. However, the arching of the overburden indicates that shortening continued until Recent times. Burial occurred during a period of relatively low sedimentation rate, as described

for the Tunb salt structure, suggesting a decrease on the salt supply. This decrease on salt supply suggests that the feeder may have pinched-off, forming a secondary weld (Fig. 43e).

Above, ongoing shortening is recorded by thinning and tapering of Guri Member growth strata and younger units toward the Taftan salt anticline. Minor thickness variations on the Miocene units indicate a shallow inflation of the Fars Salt along the anticline axis. However, no secondary Fars Salt structures developed. These features suggest that the Taftan structure underwent rejuvenation after the Guri Member deposition, with the major growth phase recorded by Recent deposits (Fig. 43e).

3.7 Triggering mechanisms

The described salt structures provide new insight into the triggering mechanisms for diapirism in multi-layer salt systems, where deeply-rooted overriding allochthonous salt sheets interact with a shallower salt layer. The Fars Salt structures in the eastern Persian Gulf are always developed next to pre-existing Hormuz Salt structures. Furthermore, in areas devoid of allochthonous Hormuz Salt sheets, the overburden of the Fars Salt has a near-constant thickness, indicating that quiescent Fars Salt was coeval to the passive growth of Hormuz Salt diapirs (e.g. Lesser Tunb diapir) and to their rejuvenation (e.g. Taftan anticline). In areas where Hormuz Salt sheets occurred (e.g. Central Tunb and Hengam diapirs), the distribution of the salt diapirs sourced from the Fars Salt resembles the shape of the adjacent Hormuz Salt sheet (e.g. Fars Circular Belt and Fars Salt structures surrounding Hengam). Accordingly, it can be argued that the driving mechanism for the Fars Salt mobilization is directly related to the emplacement of allochthonous Hormuz Salt, and not just the simple presence of a pre-existing Hormuz Salt diapir.

Starting from this major assumption, we examine the two possible scenarios that could have triggered Fars Salt diapirism (Fig. 44). The first scenario assumes that the allochthonous Hormuz Salt is emplaced after, or eventually during the Fars Salt deposition. The second scenario assumes that the allochthonous Hormuz Salt is emplaced before Fars Salt deposition. These represent end-members for the development of Fars Salt diapirs.

In the first scenario, flaring and extrusion of Hormuz Salt above a thickened Fars Salt overburden produced an increased gravitational loading, which resulted in

evacuation of the Fars Salt outward (Fig. 44a). Next to the Hormuz Salt diapir, a synformal minibasin sank above the Fars Salt by downbuilding, which was back fed by the Hormuz Salt source. Away from the diapir, instead, the syncline passed into an anticline, the wavelength of which is proportional to the overburden thickness (Fig. 44b). The migration of Fars Salt into the Hormuz feeder was unlikely, due to ongoing Hormuz Salt flow away from the diapir and increased salt pressure. Minibasin subsidence finished once primary welds were created. Afterward, the structure evolved as an expulsion rollover (Ge et al., 1997) with a progressive migration of the sedimentary depocenters toward the Fars Salt anticline by limb rotation. In the anticline, differential loading promoted salt migration upward, and the thinning of the overburden by faulting. This triggered the initiation of reactive diapirism. Subsequently, the Fars Salt actively pierced the anticline crest, forming a salt wall (Fig. 44c).

Conversely, assuming that the allochthonous Hormuz Salt sheet was emplaced just after the Fars Salt deposition above a thinned or nearly-unexisting overburden (i.e. above the Fars Salt), a different configuration was reached (Fig. 43d). In this case, the emplacement of Hormuz Salt above the Fars Salt resulted in the interaction between the two salt units, and the development of a wider salt inflation. Considering the Hormuz Salt flaring upward and the weight of the overriding Hormuz salt sheet, the suture between the Fars and Hormuz salt layers sank, forming a concave-upward geometry (Fig. 44e) (Dooley et al., 2012). However, a mixing between the two salt layers should not be excluded, especially if the Hormuz extrusion was synchronous to Fars Salt deposition. The younger halokinetic sequences onlap both the Hormuz salt sheet plus the Fars Salt diapir (Fig. 44e). This process explains the observed thinning, and apparent downlap above the Saliferous Beds unit (e.g. Fig. 38c). Diapirism of the combined Hormuz and Fars salt ended due to the development of primary welds. Then, subsequent withdrawal of Fars Salt occurred externally toward a second Fars Salt inflation (Fig. 44f).

In both cases, we hypothesize that the differential loading produced by the Hormuz Salt sheet was enough to displace the Fars Salt laterally. Then, Fars Salt structures were developed at different distances from the Hormuz Salt sheet, and folds with major wavelength formed in areas with a thicker overburden. This indicates that the Hormuz salt was extruded diachronically, as described in the eastern sector of the Tunb diapir, where the Fars Salt wall progressively merges the Hormuz Salt, forming an allosuture (Fig. 39). Here, the Hormuz Salt sheet was extruded earlier at the south-eastern diapir flank than the north-eastern one (Fig. 38b). We interpret

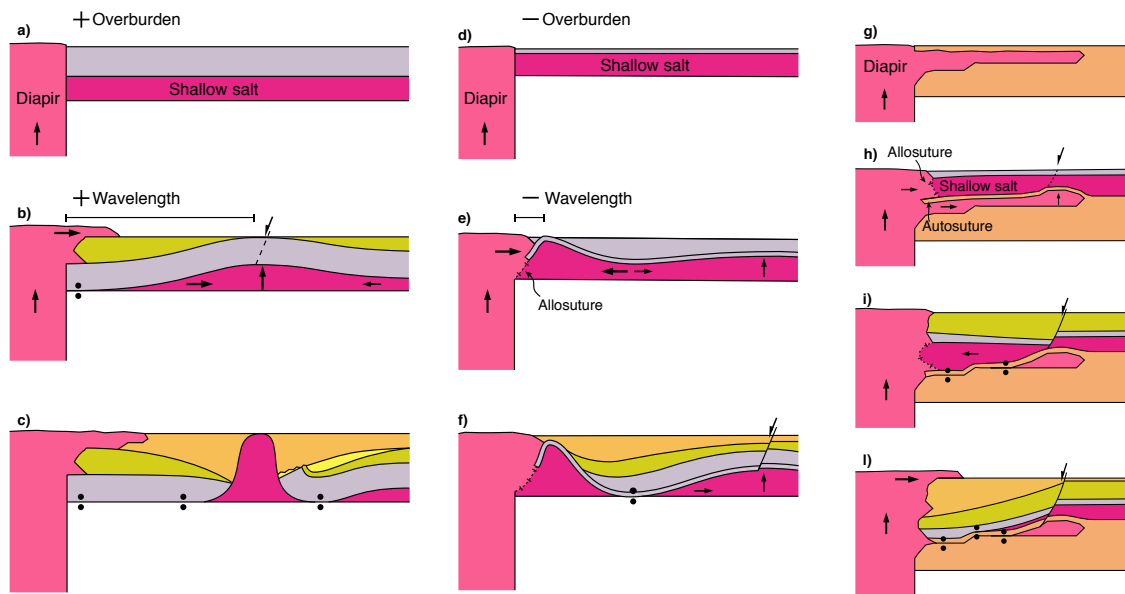


Figure 44: Sketches representing the triggering mechanism of the studied multi-layer salt system. For a), b) and c) a salt extrusion is emplaced after the deposition of the shallow salt unit, above a thick shallow salt overburden and for d), e), and f) above a thin/unexisting overburden. The g) to l) sketches, represent the triggering mechanism for a salt extrusion emplaced previously to the deposition of the shallow salt unit.

that the diachronous emplacement of the Hormuz Salt was related to the development of the secondary minibasin in the Central Tunb diapir. In such way, the squeezing of the Central Tunb diapir led to the rotation of the secondary minibasin toward the south-west, as consequence of the increased Hormuz Salt upwelling rate on its eastern flank. This local increase in salt supply produced the extrusion of Hormuz salt on the eastern side of the minibasin already during the deposition of Fars Salt. In the western sector of the Tunb diapir, the emplacement of the Hormuz Salt Sheet expanded progressively during the deposition of the Champeh and Guri Members. In the second scenario (Hormuz Salt sheet emplaced before the Fars Salt unit deposition), we assume that the first lobe of Hormuz Salt was extruded and buried by a thin roof of pre-Fars overburden, corresponding to the Pabdeh Fm (Fig. 44g). A subsequent Hormuz Salt extrusion overrode the suprasalt sediments, forming an autosuture and promoting the salt expulsion from beneath the overriding lobe (Fig. 44h). Moreover, the Fars Salt may have collided with the Hormuz Salt, forming an allosuture or eventually mixing together. The top of the Pabdeh Formation and the overlaying Fars Salt, progressively acquired a slope gradient toward the diapir, due to the extrusion of Hormuz salt away from the diapir (Fig. 44h). The initial mobilization of the Fars Salt toward the central Hormuz Salt diapir was produced by this downslope gradient, and was followed by extensional faulting up-dip. This

controlled the depocenter location of the Miocene Champeh Member (Fig. 44i). However, only a small amount of Fars Salt was evacuated and the Fars Salt did not undertake diapirism. The expulsion of the first Hormuz Salt sheet continued until tertiary welding occurred. Subsequent Hormuz Salt flaring and diapirism triggered the instability and the maximum evacuation of Fars Salt, resulting of the inward shift of the depocenters (Fig. 44l).

3.8 Conclusions

The structural model presented throughout this paper demonstrates that the driving mechanism for the evacuation of Oligocene-Miocene Fars Salt in the eastern Persian Gulf is directly related to the emplacement of salt sheets sourced from the Neoproterozoic-Cambrian Hormuz Salt during the Zagros-Oman contraction event. We infer that the triggering mechanism for Fars Salt withdrawal was determined by the timing of emplacement of Hormuz Salt sheets with regards to the Fars Salt deposition.

In the Hengam diapir, Hormuz Salt extrusion started at the Paleogene, synchronously to the development of the more external thrusts of the Oman Ranges, and pre-dates the Fars Salt deposition. The initiation of Fars Salt movement is interpreted to have been triggered by the downslope gradient produced by the emplacement of a Hormuz Salt sheet and the subsequent development of a tertiary weld. In the Tunb diapir, Hormuz Salt extrusion started in the early Miocene, after the onset of the Zagros continental collision, and post-dates or is coeval to the deposition of the Fars Salt. Here, Fars Salt diapirism is interpreted to have been triggered by the gravitational loading produced by an overriding allochthonous Hormuz Salt sheet, which pushed the Fars Salt outward forming a Circular Belt of Fars Salt structures. Around the Tunb diapir, the Hormuz Salt extruded diachronically over the Fars Salt overburden. This led to the development of folds with major wavelength in areas with a thicker overburden, explaining the development of Fars Salt structures at different distances from the Hormuz Salt sheet. Conversely, Fars Salt structures are absent around the Taftan salt anticline and the Lesser Tunb diapir, suggesting that Fars Salt diapirism did not occur in areas devoid of allochthonous Hormuz Salt structures.

Shortening during Miocene times led to the development of secondary welds and the burial of both the Hormuz and Fars salt diapirs. Prolonged contraction

reactivated the buried diapirs, which underwent active diapirism, bulb expansion, diapir roof arching and finally crestal normal faulting. Preexisting Hormuz salt structures that did not developed into piercing diapirs also underwent rejuvenation, but this did not trigger significant Fars Salt movement.

Chapter 4: The Mountain Front Flexure in the Lurestan region of the Zagros belt: crustal architecture and role of structural inheritance

This chapter is presented in the form of a manuscript, published in Journal of Structural Geology (2020)

Tavani, S., Camanni, G., Nappo, M., Snidero, M., Ascione, A., Valente, E., Gholamreza, G., Davoud, M., Mazzoli.

4.1 Abstract

The Mountain Front Flexure is a major structure of the Zagros orogenic system, and is underlain by the deeply rooted and seismically active Mountain Front Fault system. These coupled structural features divide the belt from its foreland and their trace is sinuous, forming salients and recesses. The origin and tectonic significance of the Mountain Front Fault system and its sinuosity are still unclear, with most of hypotheses pointing to a strong structural control exerted by geological inheritances. In this work we combine interpretation of seismic reflection profiles, earthquake data, geomorphic analysis, and geological observations, to build a balanced cross section across the Mountain Front Flexure in the Lurestan region. Our data are suggestive of a hybrid tectonic style for the Lurestan region, characterised by a major and newly developed crustal ramp in the frontal portion of the belt (i.e the Mountain Front Fault) and by the reactivation of steeply dipping pre-existing basin-bounding faults, along with a minor amount of shortening, in the inner area. Specifically, the integration of our results with previous knowledge indicates that the Mountain Front Fault system developed in the necking domain of the Jurassic rift system, ahead of an array of inverted Jurassic extensional faults, in a structural fashion which resembles that of a crustal-scale footwall shortcut. Within this structural context, the sinusoidal shape of the Mountain Front Flexure in the Lurestan area arises from the re-use of the original segmentation of the inverted Jurassic rift system.

4.2 Introduction

The Mountain Front Flexure (MFF) is a major structure of the Zagros folded belt, consisting of a topographic and structural step that divides the belt from its foreland basin (Falcon, 1961). The MFF runs for more than 1000 km, from Kurdistan to Fars,

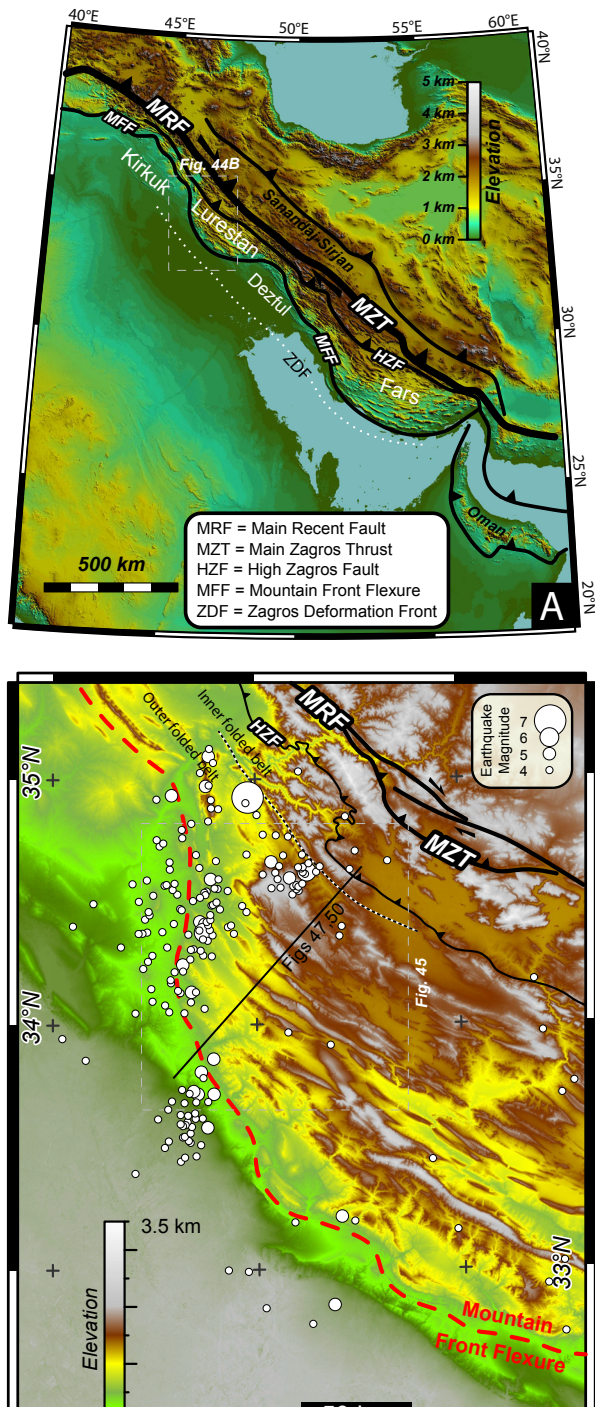


Figure 45: Tectonic sketch map of the Zagros Mts. (A) Elevation map with major structural features indicated. (B) Elevation map (source: ESDIS) showing the main structures of the NW portion of the Lurestan arc, with the Ezgeleh Mw 7.3 seismic sequence indicated (source: USGS, <https://earthquake.usgs.gov>).

to eventually disappear further to the SE, and is the surface expression of the active and deeply rooted Mountain Front Fault system (Fig. 45a). The trend of the Mountain Front Flexure is characterised by a sinusoidal shape defined by salients and recesses. From NW to SE these sinuosities are: the Kirkuk embayment, the Lurestan arc, the Dezful embayment, and the Fars arc (Fig. 45a). The Mountain Front Fault system which underlie the MFF comprises a seismically active basement-involving reverse fault system (e.g. Berberian, 1995; Talebian and Jackson, 2004; Sherkati and Letouzey, 2004; Molinaro et al., 2005; Mouthereau et al., 2006; Alavi, 2007; Vergés et al., 2011a; Tavani et al., 2018a), and the structural step across it is more than 3 km in the Kirkuk and Dezful embayments and in the Lurestan arc, and less than 2 km in the Fars area (e.g. Sherkati et al., 2006; Emami et al., 2010).

Although there is a general consensus in the literature on that the sinusoidal shape of the Mountain Front Flexure and the Mountain Front Fault system is controlled by geological inheritances, their exact nature is controversial and the origin of the flexure is still uncertain. For

example, McQuarrie (2004) has suggested that the position of the Mountain Front Flexure could be related to thickness variations of the Cambrian Hormuz salt, which is placed at the base of the sedimentary pile. Reactivation of steeply dipping N-S and E-W striking inherited basement faults, oriented obliquely to the NE-SW shortening direction, has been instead proposed by several authors (e.g. Hessami et al., 2001; Sepehr and Cosgrove 2004; Lawa et al., 2013), in accordance with the documented occurrence of inherited N-S and E-W striking faults exposed in the Arabian plate (e.g. Talbot and Alavi, 1996; Hessami et al., 2001). The Mw 7.3 Ezgeleh earthquake, that hit the Lurestan region on 12 November 2017, along with its aftershocks have illuminated the geometry at depth of one of the N-S striking oblique portions of the Mountain Front Fault system (Fig. 45b), which was revealed to consist of a low-dipping N-S striking oblique ramp, placed at about 20 km depth within the basement (e.g. Chen et al., 2018; Tavani et al., 2018a; Gombert et al., 2019; Vajedian et al., 2019). The low dip of this structure is suggestive of a model in which the Mountain Front Fault system is comprised of, at least in the Lurestan arc, newly-formed shallowly-dipping frontal (Blanc et al. 2003; Vergés et al., 2011a; Le Garzic et al., 2019) and oblique ramps (Tavani et al., 2018a). This apparently contrasts with the idea that the sinusoidal shape of the Mountain Front Fault system can be controlled by the reactivation of steeply dipping pre-existing basement faults or at least requires that steeply dipping faults are connected with shallow dipping faults at depth.

In this work, we explore the geometric complexities of the Mountain Front Fault system in the Lurestan arc, by integrating seismic reflection sections interpretation, cross section balancing, geomorphic analysis, and data from the aftershock sequence of the 2017 Ezgeleh Mw 7.3 earthquake. Limited shortening at the higher structural levels of the belt, where no remarkable far-travelled thrusts occur, allow to place constraints on the nature of the faults underlying the major topographic and basement steps of the area. Nodal planes of large earthquakes ($M_w > 5$) placed at short distances from the studied section constrain the Mountain Front Fault system at depth. Our results demonstrate that: (i) the low amount of shortening requires an inversion tectonic style along most portions of the studied section; (ii) the Mountain Front Fault system is comprised of a shallowly-dipping mid-crustal ramp splaying off the footwall of an inverting basement fault system; (iii) the Mountain Front Flexure is, in essence, the frontal limb of a slightly transported fault-propagation fold developing above the tip of the Mountain Front Fault system; (iv) the distribution of pre-existing faults is a primary factor in controlling

the development and the shape of the frontal structural features of the Zagros belt in the Lurestan area.

4.3 Geological setting

The Zagros belt extends from Turkey to SE Iran (Fig. 45a), and developed in Late Cretaceous to Cenozoic time. Convergence started with the closure of the Neo-Tethys ocean and evolved, during the late Eocene-Oligocene, in the continental collision between the Eurasian and Arabian plates (e.g. Stöcklin, 1968; Ricou et al., 1977; Berberian and King, 1981; Dercourt et al., 1986; Braud, 1987; Alavi, 1991, 1994; Stampfli and Borel, 2002; Agard et al., 2005; Allen and Armstrong, 2008; McQuarrie and van Hinsbergen, 2013; Koshnaw et al., 2018). The Zagros belt develops on the Arabian plate and it is bounded to the NE by the Main Recent Fault and the Main Zagros Thrust that represent the NW-SE trending suture zone that separates the Arabian plate from the Sanandaj-Sirjan Zone on the Eurasia plate to the NE (Fig. 45a) (e.g. Berberian and King, 1981; Ziegler, 2001; Blanc et al., 2003; Ghasemi and Talbot, 2006). The collisional zone is currently accommodating oblique convergence, with the 2 cm/yr N-ward motion of Arabia (considering fixed the Eurasia plate; Vernant et al., 2004) being partitioned between right-lateral motion along the NW-SE-striking suture zone and NE–SW-oriented shortening within the Zagros belt (Blanc et al., 2003; Vernant et al., 2004; Talebian and Jackson, 2002, 2004). In detail, shortening in the Zagros belt is about 5–10 mm/yr (Vernant et al., 2004), and it is accommodated by NW-SE oriented thrust and folds. Until the Cretaceous and before the closure of the Neo-Tethys, the Zagros Belt and the Sanandaj-Sirjan Zone formed the two conjugate passive margins of a southern branch of the Neo-Tethys (Berberian and King, 1981; Blanc et al., 2003; Sepehr and Cosgrove, 2004; Vergés et al., 2011a; Wrobel-Daveau et al., 2010). The Zagros belt is made up of terrains that originally belonged to the SW passive margin of the Neo-Tethys (NE Gondwana), i.e. the Arabian continental margin (Ziegler, 2001; Sepehr and Cosgrove, 2004; Ghasemi and Talbot, 2006; Vergés et al., 2011a; Mouthereau et al., 2006, 2012; English et al., 2015; Tavani et al., 2018b). This passive margin was characterised by different extensional domains. In particular, the distal portion of the margin included a deep-water radiolarite basin (Kermanshah Radiolarite basin), and an isolated carbonate platform (Bisotun Platform) interposed between the radiolarite basin and the oceanic domain (e.g. Ricou et al., 1977; Braud, 1987; Wrobel-Daveau et al., 2010). These extensional

domains developed during the Permo-Triassic (e.g. Alavi, 1980; Berberian and King, 1981; Ghasemi and Talbot, 2006) and, mostly, Early Jurassic (e.g. Tavani et al., 2018b) rifting events, which lead to the divergence of the Arabian margin and the Sanandaj-Sirjan Zone, and to the opening of the above mentioned southern branch of the Neo-Tethys. The distal portion of the Arabian margin is presently exposed in the hanging wall of the High Zagros Fault (Fig. 45), a fault that has been active since the Late Cretaceous (Karim et al., 2011; Saura et al., 2015). The

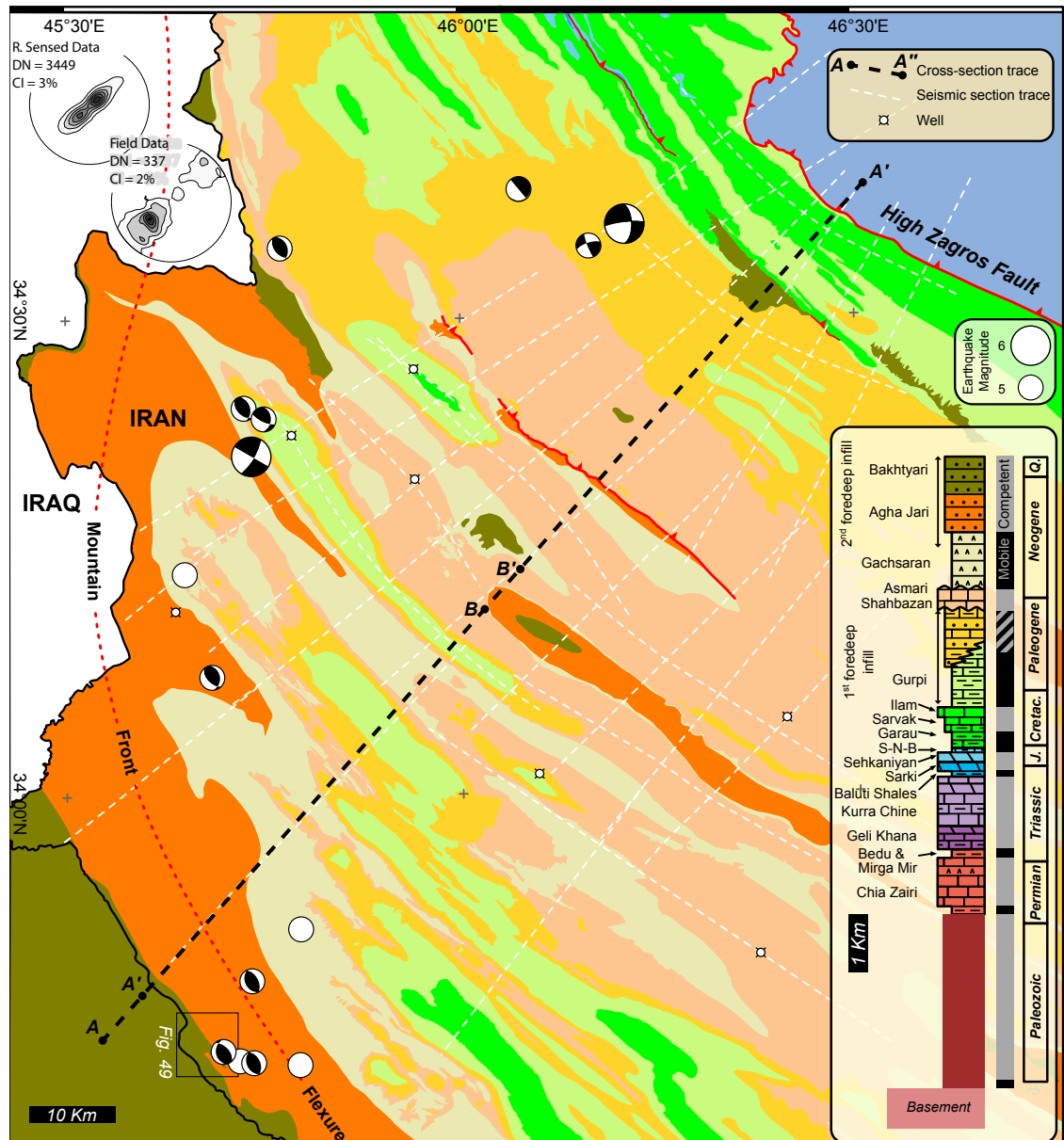


Figure 46: Geological map of the study area along with: (i) density contour of remotely sensed and field measured bedding data; (ii) Mw > 5 earthquakes with moment tensor solution (2017-2019 time interval; source: USGS, <https://earthquake.usgs.gov>); (iii) traces of near-vertical seismic profiles and wells; (iv) a trace of the geological section in Figs. 49 and 51; (v) stratigraphic succession of the area. The inset shows the normalised frequency distribution of earthquakes depth occurred in the map area, with no time range restriction. Data are from the USGS and Iranian Seismological Centre (<http://irsc.ut.ac.ir>) catalogues.

proximal domain of the Arabian margin is now cropping out in the footwall of the High Zagros Fault, which is the Simply Folded Belt, where NW-SE trending folds with up to 10 km wavelengths occur in a 200 km wide area, delimited to the SW by the Zagros Deformation Front (Fig. 45a).

The Mountain Front Flexure and the underlying Mountain Front Fault system, which are the object of investigation of this paper, are located between the NW-SE striking High Zagros Fault and the Zagros Deformation Front. In particular, the flexure represents a major topographic and structural divide that separates a north-eastern area, where thrust faults affect the basement, from a south-western area, mostly characterised by folds confined within the sedimentary sequence (or at least with no striking evidence of basement-involved reverse faults). In the Lurestan arc, one of the most prominent sinuosities of the mountain belt, the frontal features of the belt are characterised by a frontal portion striking NW-SE, and two lateral segments striking roughly E-W (SE segment, Bala Rud segment) and N-S (NW segment, Kanaquin segment), the latter being part of the study area of this work (Figs. 45b, 46). Fold traces are slightly bent approaching these oblique segments, but no remarkable offsets can be observed across them (e.g. Alavi, 2007; Allen and Talebian, 2011; Casciello et al., 2011; Casini et al., 2018). In the NW portion of the Lurestan arc, the folded belt in the footwall of the High Zagros Fault can be further divided into an outer and an inner folded belt (Fig. 45b), which are separated by a structural step marked by changes in elevation of nearly 2 km (Tavani et al., 2018a). In the study area, the High Zagros Fault is characterised by a major bend and by a more external position with respect to the NW. As a result, most of the inner folded belt is now located below the High Zagros Fault and our reconstruction is mostly limited to the outer folded belt (Fig. 46).

The sedimentary sequence of the Arabian margin exposed in the footwall of the High Zagros Fault, includes a pile of clastics and carbonates more than 10 km thick (James and Wynd, 1965; Stöcklin, 1968; Koop and Stoneley, 1982). In the south-eastern portion of the Zagros belt, i.e. in the Fars arc and in the Izeh domain (located immediately to the NE of the Dezful embayment), the base of the sedimentary sequence is represented by the late Proterozoic to early Cambrian Hormuz Salt, which does not occur in the Lurestan arc (e.g. Bahroudi and Koy, 2003; Alavi, 2007). In detail, the sedimentary sequence of the Lurestan arc area starts with an about 3 km thick succession of Paleozoic continental clastic deposits (up to 6 km to the NW of the study area, in the Kurdistan region, according to Le Garzie et al., 2019), overlain by nearly 1 km of shallow-water carbonates of the

Chia Zairi Formation, capped by the Triassic shales of the Bedu Shales and Mirga Mir formations (Fig. 46) (Jassim and Goff, 2006; Bordenave, 2008). The overlying Triassic-Jurassic multilayer is exposed 50 km to the north of the study area and includes (Tavani et al., 2018b): the about 400 m thick Middle Triassic Geli Khana Formation, consisting of thin-bedded limestones and dolostones; the 600-700 m thick Late Triassic thick-bedded dolostones and limestones of the Kurra Chine Formation; the 30 to 100 m thick Late Triassic shales and thinly bedded dolostones of the Baluti Shale Formation; the 300 m thick dolostones of the Upper Triassic-Lower Jurassic Sarki and Sehkaniyan formations. The above described Permian to Early Jurassic stratigraphic succession was deposited in a shallow-water to continental environment. At the end of the Early Jurassic, a major subsidence pulse associated with a rifting event led to the drowning of the margin (Tavani et al., 2018b) and the onset of deep-water conditions and the deposition of nearly 100 m of deep-water limestones, marls, shales, and deep water evaporites (Sargelu, Naokelekan, and Barsarin formations, Toarcian to Tithonian), followed by 400 to 1000 m of Cretaceous basinal limestones, shales and marls (Garau, Sarvak and Ilam Fms). To the SE of the study area, the upper portion of the Cretaceous sequence gradually passes from pelagic to neritic facies (Casciello et al., 2009). Further to the SW of the Mountain Front Flexure, the drowning of the carbonate platform was limited, and the Jurassic to Cretaceous stratigraphic succession was deposited mostly in a shallow marine environment (e.g. Ziegler, 2001). Onset of convergence during the Late Cretaceous caused the development of a first foredeep, filled by about 2 km of Maastrichtian to Eocene sediments (e.g. Homke et al, 2009; Vergés et al., 2011a; Saura et al., 2015). These are overlain by nearly 300 to 500 m of Oligocene-lower Miocene shallow-water carbonates (Shahbazan and Asmari formations), passing upward into lower to middle Miocene evaporites of the Gachsaran Formation. Renewed shortening affected this portion of the Zagros belt during Miocene (e.g. Barber et al., 2018) and led to the development of a second younger foredeep, filled by the Agha Jari and Bakhtiari clastic formations. The age of these formations in the study area has been determined by means of magnetostratigraphy, dating the base of the Agha Jari Formation at about 12-13 Ma and the base of the Bakhtiari at about 3 Ma (Homke et al., 2004). However, based on Sr strontium stratigraphy, a slightly older age (16 Ma) has been proposed for the lower part of the Agha Jari by Pirouz et al. (2015).

4.4 Data and methods

For determining the structure of the Mountain Front Flexure and of the underlying Mountain Front Fault system, we used a multidisciplinary methodological approach drawing from several independent datasets. These datasets include: seismic reflection profiles calibrated with borehole data, geological data, geomorphic data, and earthquake hypocenter and focal mechanism data. These datasets were analysed separately (see section 4) and, subsequently, combined together to construct the balanced cross section presented in section 5.

The seismic reflection profiles were acquired in different campaigns by the National Iranian Oil Company, in a time period spanning from the 2005 through to 2018. Twentyfive seismic reflection profiles (for a total length of about 1200 km) have been interpreted in this work for defining the deep geometry of faults and folds (Fig. 46). Nine and sixteen of the profiles are oriented, respectively, parallel (strike lines) and perpendicular (cross lines) to the traces of the folds that form the structural architecture of the belt. Although large portions of the study area are characterised by the occurrence of exposed karstified limestone (i.e. mostly the Asmari Formation), the seismic signal provide most sections with a resolution adequate for a reliable seismic interpretation. Furthermore, calibration of the seismic sections with surface geology data and the incorporation of seven wells (Fig. 46) which reached the Cenozoic (1 well), Cretaceous (1 well), Jurassic (3 wells), and Triassic (2 wells) units, provided further constraints for the firm interpretation of several portions of the study area.

Geological data comprise geological maps, and remotely sensed and field measured bedding dip data that were combined together to construct geological cross-sections across the study area. In particular, bedding dip data at a distance of < 2 km from the trace of the cross section have been projected onto it, and the geological cross section has been built by means of the 3DMove software package. To digitally extract traces of layers and transform them in bedding dip orientation, publically available 0.5 m orthophotos draped onto 30 m resolution ASTER GDEM were used (e.g. Fernández, 2005; Snidero et al., 2011). This operation was performed by means of the OpenPlot software package (Tavani et al., 2011). Measured (n: 337) and remotely sensed (n: 3499) bedding surfaces are NW-SE striking (Fig. 46), consistently with the trend of the fold traces as shown in the geological map of the area (Fig. 46). Notably, remotely sensed data tend to overestimate gently dipping bedding (Fig. 46), as the digital extraction of traces needs non col-linear traces,

which is hampered for steeply dipping strata.

The geomorphological analysis was based on the inspection of the large-scale features (30 m resolution DEM), both active and relic, associated with the topography and drainage network within the study area. This analysis was carried out by means of investigation of satellite images (Google Earth, 2019) and orthophotos, aided by a GIS-based analysis of digital topography data (30 m resolution ASTER GDEM). In particular, digital topography data were used to build a swath profile (generated by the SwathProfiler Add-in of Arcgis®; Pérez-Peña et al., 2017), a map showing the spatial distribution of elevation parameters, and to extract a digital stream network, which was validated through its comparison with a manually digitized drainage network constructed through the visual inspection of remotely sensed images. The satellite image inspection was also aimed at identifying relic stream paths and river bends. These features are of significant importance as they represent evidence of changes in flow orientations, which take place in response to local short-lived surface changes and/or regional long-term external processes driven by the differential influence of erosional or tectonic processes and, among the latter ones, fold growth (e.g. Lavé and Avouac, 2001; Miller and Slingerland, 2006; Prince et al., 2011; Forte et al., 2015; Burberry et al., 2010; Bretis et al., 2011; Buscher et al., 2017).

Earthquake hypocentre and focal mechanism data were used to constrain the geometry of the fault systems at depth within the study area. These data are from the publically available USGS earthquake catalogue (<https://earthquake.usgs.gov/earthquakes/search/>). In particular, in this study we selected seismic events with $M_w > 4$ occurred in the Lurestan region in a time period between 12 november 2017 and 9 June 2019, all of them being consistent with NE-SW oriented shortening. We chose this earthquake magnitude and this time frame, since the main aim here was to study earthquakes with a significantly high magnitude related to the $M_w 7.3$, 12 November 2017 earthquake that appeared to have activated a crustal shallowly-dipping fault within the study area of particular significance for this study. In addition, in the area of figure 46 we used the entire datasets in the catalogue of both the USGS and the Iranian Seismological Centre (<http://irsc.ut.ac.ir>) to determine the frequency of earthquake depth (inset in figure 46). This serves to place a rough limit between the brittle and ductile crust.

4.5 Results

4.5.1 Seismic reflection profiles

In this section, the interpretation of four representative seismic reflection sections is presented (Fig. 47): sections 1 and 2 are complementary and cross the whole study area largely overlapping with the trace of the balanced cross section (Fig. 46); sections 3 and 4 allow further constraining structures at the NE and SW edges of the balanced cross section, respectively. Where possible, up to five reliable (i.e. calibrated with borehole and/or surface geology data) stratigraphic horizons have been interpreted. From the youngest to the oldest, these stratigraphic horizons correspond to the Top Gachsaran (middle Miocene), the Top Asmari (lower Miocene), the Base Shahbazan (Oligocene), the Top Ilam (upper Cretaceous), and the Top Sehkaniyan (lower Jurassic) (Fig. 47). In addition, a reflector within the Triassic and three reflectors within the Paleozoic have been locally imaged, although they could have not been assigned to specific stratigraphic horizons. Finally, where possible, some intraformational horizons were also mapped to facilitate reconstructing geometries in specific areas.

Section 1 is characterised by a broad area in its central and NE parts that is affected by remarkable noise and poor resolution (Fig. 47). A few discontinuous reflectors can be traced in this area, although their stratigraphic attribution is harduous. In contrast, the southern part of the section shows a 20 km wide SW-dipping monocline, in which reflectors of the Agha Jari, Gachsaran, and Asmari formations are nearly parallel to one another. More in detail, folds with wavelengths of 1-2 km affect the Asmari Formation and they are apparently sealed by the Gachsaran Formation (Fig. 47). This apparent growth stratal geometry is arising from the decoupling taking place along the Gachsaran evaporites, as already documented in the area (e.g. Fig. 14c in Vergés et al., 2011b).

Section 2 is less affected by noise, and reflectors can be more easily traced and correlated across the section. Particularly, the Paleozoic to Early Jurassic (i.e. Top Sehkaniyan) stratigraphic package is characterised by nearly parallel reflectors. Nevertheless, some thickness variations do exist between the Paleozoic 1 and Paleozoic 2 reflectors, which could be related with growth structures, previously described in the Zagros, developed during the Permo-Triassic rifting (e.g. Seppehr and Cosgrove 2004). However, besides these variations and the local folding occurring at the Pataq Anticline, the Paleozoic to Early Jurassic sequence forms

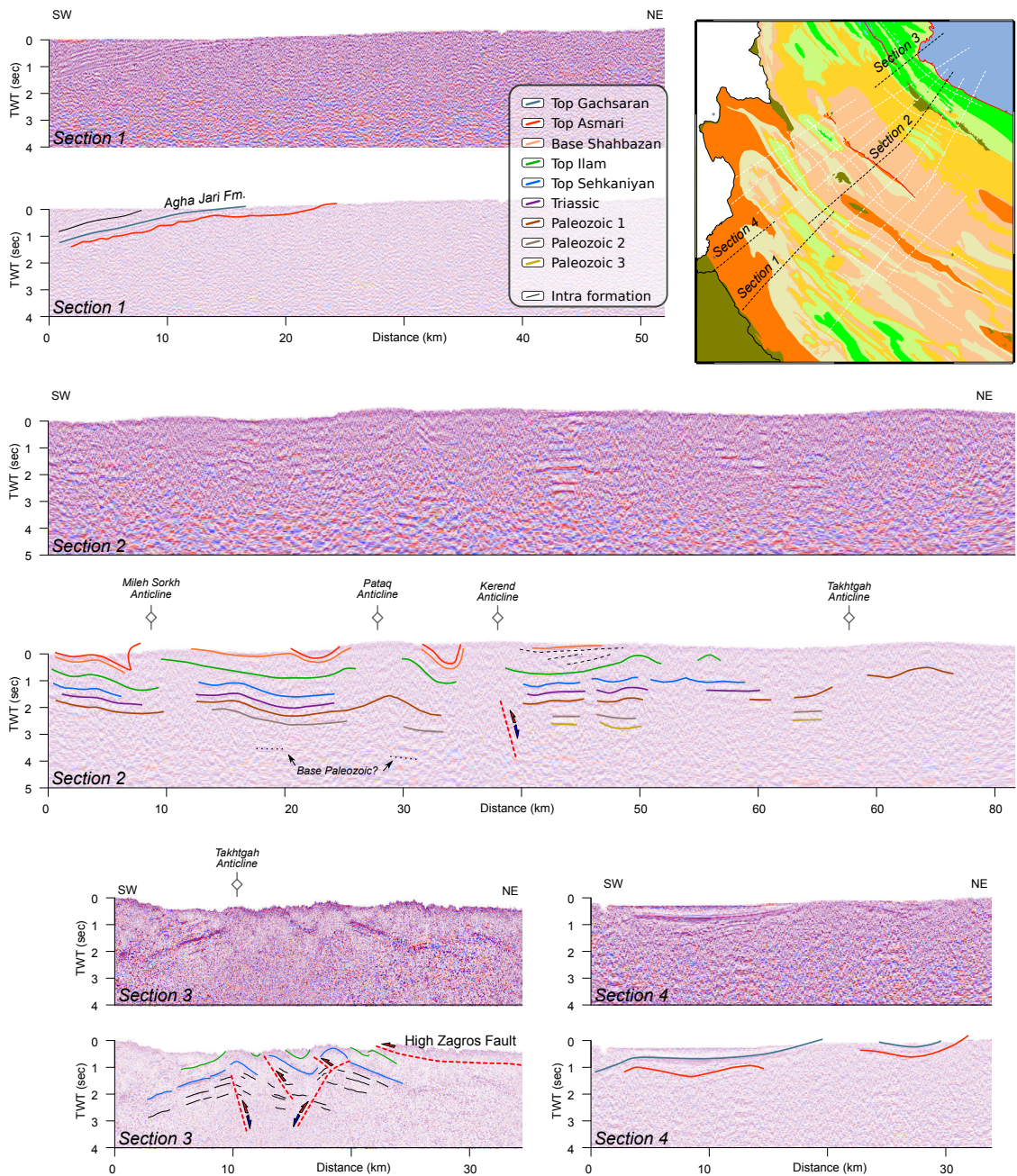


Figure 47: NE-SW-oriented near-vertical seismic profiles with along with line drawing.

a gently NE-dipping regional monocline which is particularly apparent in the SW portion of the section. This monocline is abruptly interrupted at the location of the Mileh Sorkh, Kerend, and Takhtgah anticlines. Moving upward in the stratigraphy, the Top Ilam reflector follows this general monoclinial trend although being not always parallel to the underlying Top Sehkaniyan reflector. This can be due to: (i) the partial decoupling between the Ilam and Sehkaniyan formations taking place at the Garau marls and shales, and which resulted in the development of diffuse disharmonic folding of the Ilam Fm (e.g. to the NE of the Kerend Anticline), and (ii)

the occurrence of Early Jurassic extensional troughs, filled by the Middle Jurassic to Cretaceous sediments (Tavani et al., 2018b). Similar disharmonic geometries occur between the Top Ilam and the Base Shahbazan reflectors, within the portion of the sedimentary sequence that was forming the first foredeep infill. This portion of the sequence is associated with the development of folds that appear to be partly decoupled from the underlying Ilam Formation (e.g. the small anticline to the SW of the Pataq Anticline) and with significant stratal thickness variations. The latter developed along with the local occurrence of growth geometries (e.g., to the NE of the Kerend Anticline), which suggests the existence of normal faults developed in the foredeep due to flexuring (e.g. Bradley and Kidd, 1991; Ranero et al., 2003; Tavani et al., 2015). Despite the low quality of the seismic line permits to place both low- and high-angle NE-dipping faults below the Kerend anticline, the above described extensional growth geometry indicates that the step across the Kerend Anticline can be the result of the positive inversion of a pre-existing normal fault. The two other sections here illustrated (i.e., sections 3 and 4) display features which are key for determining the structural style of the study area. Section 3 shows in detail the relationship between the Asmari and Gachsaran formations. The 20 to 30 km-wide gently SW-dipping monocline seen in section 1 projects to the location of three open anticlines occurring in the SW, central, and NE portions of the section. However, despite these three structures, the regional SW-dip is still recognisable. In the north-eastern syncline, reflectors of the Gachsaran Formation are parallel to the top of the Asmari Formation, whereas in the broad and gentle south-western syncline they are not. There, indeed, the Top Asmari forms a tighter syncline compared to reflectors within the Gachsaran and Agha Jari, mimicking a syn-kinematic geometry that, as mentioned for the seismic section 1, can be the result of the decoupling taking place within the evaporites of the Gachsaran Formation.

Section 4 (Fig. 47), which has been already published and discussed (Tavani et al., 2018b), includes three anticlines cored by the Garau Formation at the surface, which nearly project at the location of the Takhtgah Anticline seen in section 2. In details, these three anticlines are separated by two synclines cored by the Upper Cretaceous Gurpi Formation. The top of the Sehkanyian and Ilam formations are well marked in the seismic profile and are also well constrained from surface geology data. Reflectors ascribable to the Triassic and Paleozoic sedimentary succession are also recognisable. Overall, the structure illuminated in this section consists of two 10 km-wide monoclines bounding to the SW and to the NE a partly

inverted graben. Evidence which suggests the inversion of an inherited graben include (Tavani et al., 2018b): (i) the fact that the elevation of the Sehkanyian Formation in the central syncline of the graben is lower than that at the borders of the two external monoclines, (ii) the continuity of reflectors within the monoclines which point to the occurrence of steeply dipping faults located at the edge of the graben.

4.5.2 Geological cross section

The geological cross section is shown in figure 48. It traverses the whole study area and is oriented nearly perpendicular to the main structural features of this part of the Zagros belt. In detail, starting from the lower stratigraphic levels, the stratigraphic package including the Cretaceous Garau, Sarvak and Ilam formations is buried along most of the section, with the exception of the NE part of the study area where it crops out in the hinge zone of some anticlines. Despite the evidence of thickness variations as derived from the analysis of the seismic section profiles (Fig. 47, Section 2), in the geological cross section the thickness of this package is drawn as constant for the sake of simplicity, and due to the lack of constraints in large portions of the sections. To the north of the study area, where they are exposed, their cumulative thickness ranges from 400 to 2000 m, partly due to the variable accommodation space inherited from the Early Jurassic rifting (Tavani et al., 2018b). An average thickness of 700 m is used in the shallow section (and later in the balanced cross section) and the base of this package (i.e the base of the Garau Formation) corresponds to the bottom of the geological cross-section.

Similarly, the thickness of the Gurpi Formation is roughly constant along most of the section (ca. 1100 m), except than immediately to the north of the Kerend Anticline, where, as also evident on seismic section 2 (Fig. 47), a local remarkable thickening of the formation occurs (Fig. 47). Also, to the south of the Vizehnan Anticline, the exposed short-wavelength anticlines affecting the Asmari Formation are assumed to be confined to within the Gurpi to Asmari package and to develop above the roughly SW-dipping top of the Ilam Formation. The stratigraphic package between the Gurpi and the Shahbazan formations, which includes the Pabdeh, Kashkan, Taleh Zang, and Amiran formations, prominently thins SW-ward, passing from a maximum thickness of 700 m to the NE of the Pataq Anticline to a minimum one of 400 m to the SW of the Mileh Sorkh Anticline. The cumulative thickness of the

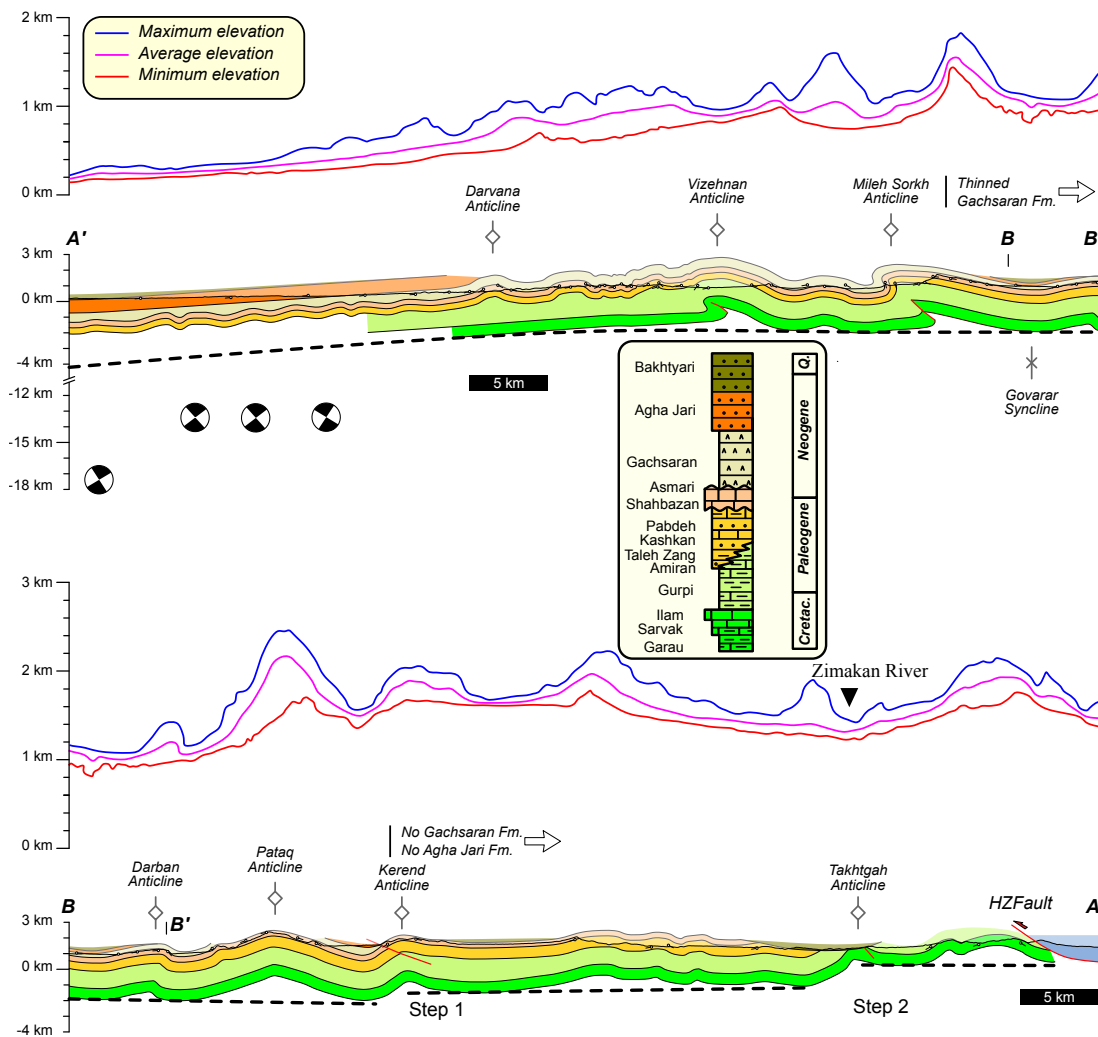


Figure 48: NE-SW-oriented geological section (the trace is shown in figure 46), with (i) projected $M_w > 5$ earthquakes (projection distance < 25 km, depth sourced by USGS, <https://earthquake.usgs.gov>), and swat profiles with (ii) maximum (blue), minimum (red), and average (magenta) elevation. The section is split in two parts, with an overlap zone (B-B').

Shahbazan and Asmari formations is constant across the entire geological cross section and it is nearly 350 m.

In the SW part of the section, stratigraphically on top of the Asmari Formation, the evaporites of the Gachsaran Formation are partially decoupled from the underlying formation, mimicking syn-kinematic geometries, as already seen in the seismic reflection profiles 1 and 4 (Fig. 47), and as previously described in the literature for the Lurestan arc (Emami et al., 2010; Vergés et al., 2011b). There is also a tendency for the Gachsaran Fm to vary in thickness towards the more internal structures. In particular, surface data indicate a rather constant thickness in between the Darvana and Mileh Sorkh anticlines and a gradual thinning northward. For example, across the Mileh Sorkh anticline the thickness of the Gachsaran

Formation strongly decreases. Furthermore, further to the NE (i.e. to the NE of the Kerend Anticline) the Gachsaran and the Agha Jari formations disappear and few patches of continental deposits, equivalent of the Bakhtiari Formation, directly rest on top of the Cretaceous to Miocene sequence. The northward thinning of the Gachsaran Fm suggests that the area to the NE of the Mileh Sorkh Anticline was already uplifted during the deposition of the Agha Jari Formation. To the SW, instead, strata of the Agha Jari and Gachsaran are parallel to one another, as seen in the seismic sections across the frontal portion of the study area (sections 1 and 3 in figure 47).

There is no available seismic section allowing to evaluate in detail the geometric relationship between the Agha Jari and the Bakhtiari formations, although at outcrops these formations are generally almost parallel to one another. Locally, however, growth geometries can be observed. An example of this is shown in figure 49, where gently SW-dipping strata of the Bakhtiari Formation seal a syncline which involves

in the deformation the Agha Jari Formation along with the lowermost portion of the Bakhtiari Fm itself. This evidence indicates that the folding of the Agha Jari and of the lower portion of the Bakhtiari formations took place at an earlier stage than that responsible for the development of the large-scale tilting observed in the southern portion of the geological cross section (of which this exposure form par), which also involves the uppermost portion of the Bakhtiari Formation (Figs. 48, 49). Finally, similarly to what can be seen in the seismic reflection section 2 (Fig. 47), the geological cross section indicates that: (i) with the exception of the High Zagros Fault, there is no remarkable exposed thrust in the area; (ii) the envelope of synclines

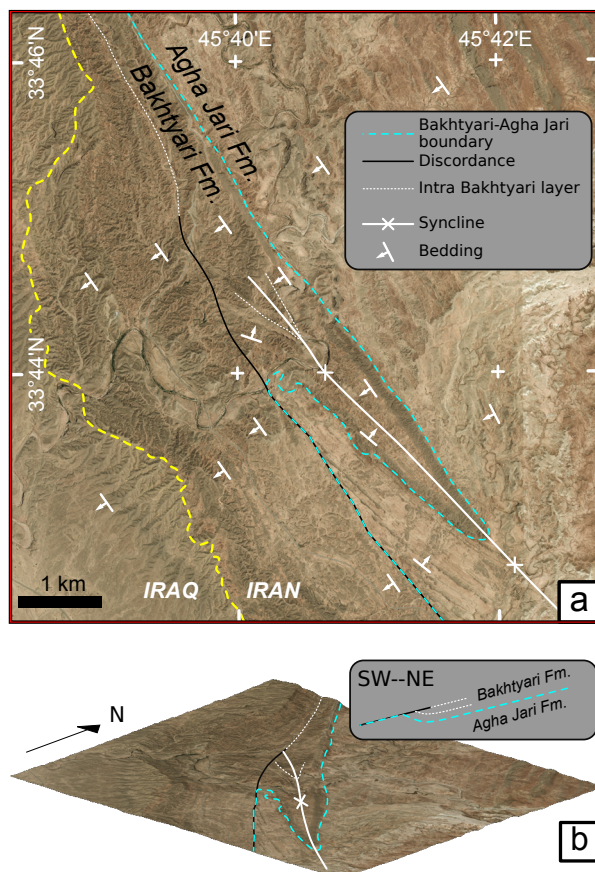


Figure 49: Orthophoto with structural scheme showing SW-dipping strata of the Bakhtiari Formation sealing a syncline cored by the Agha Jari Formation (location shown in figure 46).

indicates the occurrence of two structural steps located across the Kerend and the Takhtgah anticlines.

4.5.3 Geomorphic features

The studied area is elevated relative to adjacent sectors of the region (Fig. 45b), and underlines the regional water divide (Fig. 50a). Topography of the investigated area is influenced by the variable resistance to erosion of the outcropping rocks

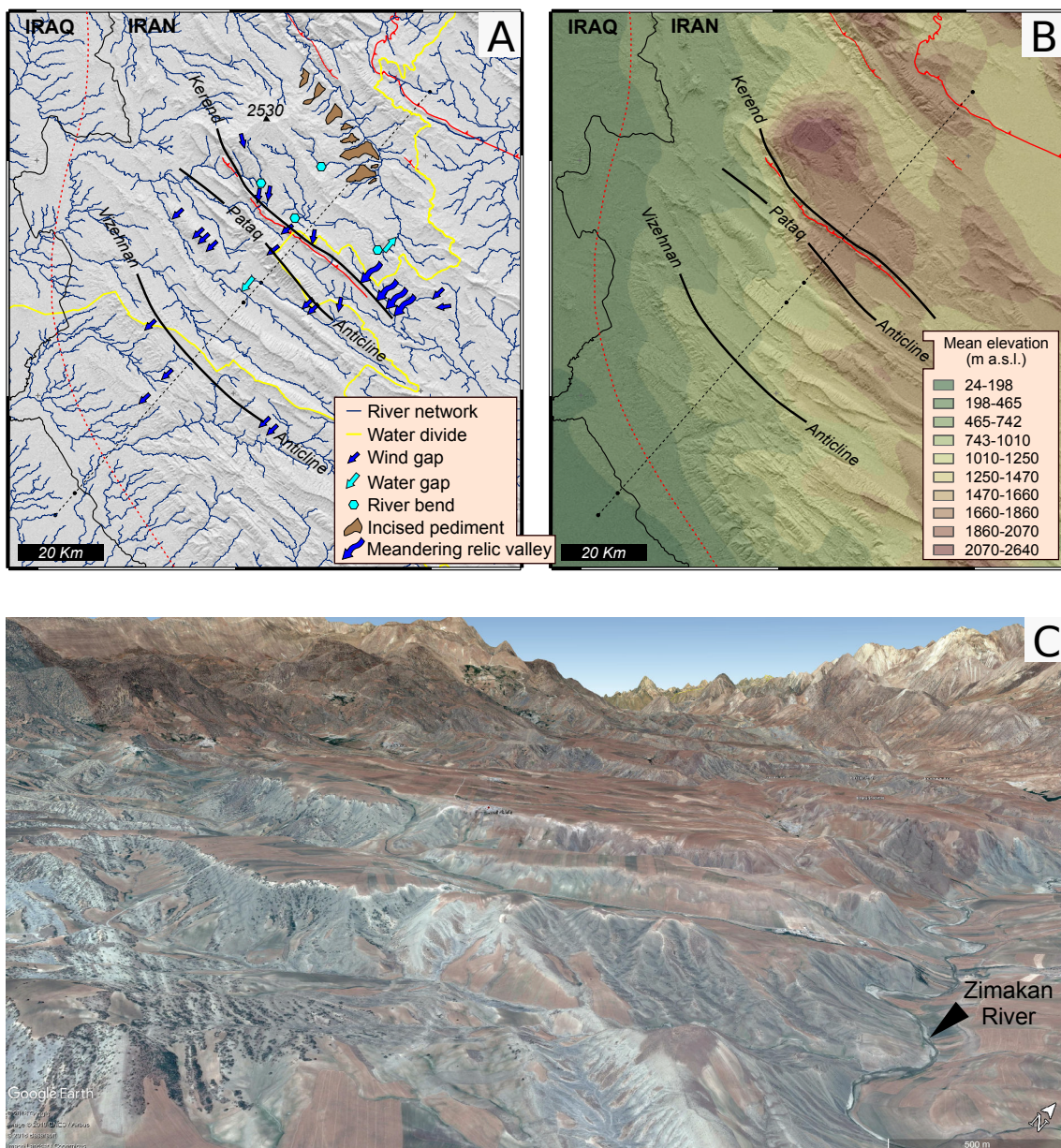


Figure 50: Main topographic and hydrographic features of the study area. (A) River network, with indication of the regional divide and main relic drainage and erosional features. (B) Mean elevation map. (C) Google Earth view of the incised pediment in the Zimakan River area (3X vertical exaggeration).

(e.g. Oberlander, 1985; Burberry et al., 2007; 2010; Zebari et al., 2019).

The large-scale topographic features of the study area are synthesised in the swath profile of Fig. 48, and in the Mean elevation map of Fig. 50b. The swath profile of Figure 48 condenses elevation data from a 30 km wide belt centred on the trace of cross section A'-A'' (location in Fig. 46) to a single profile. Comparison of the swath profile with the geological cross section (Fig. 48) shows that elevation curves are characterised by a net step marking a jump in elevation values at the location of the prominent Pataq Anticline, which only slightly diminish towards the NE, in the Zimakan River area (Fig. 48). When examined in map view (Fig. 50b), the spatial distribution of the mean elevation shows that values tend to increase from the boundary of the MFF towards the NE to attain the highest values (> c. 1700 m) in the area of the Pataq anticline and to the NE of it, in the area of the HZF.

The features of the fluvial network show that, consistent with the SW to NE topographic gradient, the southwestern part of the investigated area is drained by mainly SW-flowing, transverse rivers (Fig. 50a). Towards the NE, however, to the NE of the Vizehnan Anticline, the regional water divide is associated with a zigzag pattern with an overall SW-NE trend and the main rivers flow through longitudinal (i.e., NW-SE trending) valleys flanked by prominent carbonate ridges (Fig. 50a). In this region, the presence of wind gaps that incise the ridge crests, and river bends (Fig. 50a), are suggestive of drainage reorganization and river capture phenomena that could have been controlled by either base level fall or small/large scale uplift. The origin of the drainage reorganization remains unclear in the area spanning from the Vizehnan anticline, to the SW, to the Pataq anticline, to the NE. In that area both the features of the relief (which are strongly controlled by lithology) and, within it, of the valleys, which display concave bottoms and absence of fluvial terraces, point to the major role played by erosion in sculpting the topography. Conversely, in the region to the NE of the Pataq Anticline, the presence of several relic erosional landforms allow reconstruction of a multi-stage evolution of the land surface. The geomorphic elements that are significant to the reconstruction are river bends and a relic drainage net, which dissect the Kerend anticline and the elevated area to NE of it, and an incised pediment, which is identified in the Zimakan River area (Fig. 50a). The present-day drainage of the Kerend anticline and the elevated area to the NE of it is currently oriented towards both the NW (Zimakan River) and SE. However, that area is incised by a relic drainage net that consists of a series of abandoned transverse valleys originally draining towards the SW, irrespective of the underlying folds (Fig. 50a). These wind gaps are characterised

by incised meanders (the highest one located at around 1700 m a.s.l. and at about 50 m deep) that suggests the presence in that area of a low-gradient, SW-dipping land surface prior to the development of the topographic low in the Zimakán River area. In this area, an incised pediment gently dipping towards the NE, eroded on the soft foredeep sediments (mostly shales and marls) does occur (Fig. 46; Fig. a). The pediment, which is marked on top by a light-coloured duricrust, ranges in elevation from about 1600 m, in the SW, to c. 1380-1400 m towards the valley axis and stands at about 100-150 m higher than the main longitudinal rivers.

4.5.4 Earthquake data

In the Lurestan region, the Mw 7.3 12 November 2017 Ezgeleh earthquake was followed by more than 200 aftershocks with Mw > 4, which appear to be clustered in two main areas (Fig. 45b). The first area is located immediately to the west of the mainshock, and defines an about 150 km long N-S elongated ribbon positioned across the mountain front flexure. The second area is located nearly 50 km to the SE of the mainshock. The focal mechanisms of several events with Mw > 5 are also available and indicate strike-slip and thrust kinematics for the faulting occurring within the study area, both characterised by nodal planes consistent with a shortening direction oriented NE-SW (Fig. 46). In particular, seven Mw > 5 earthquakes have occurred along the Mountain Front Fault system at a distance < 25 km from the geological cross section (Fig. 46). Focal mechanism data are available for four of these earthquakes, all of them being characterised by a reverse fault plane solution. These focal mechanism data have been projected on the geological cross section shown in figure 48, using the strike of the NE-dipping nodal plane as the projection direction (as it is consistent with the first order geometry of the Mountain Front Fault system). Three of these events project at a similar location and have a homogeneous nodal plane geometry. In detail, these events have hypocentral depths ranging between 13 and 14 km, project onto the section at a distance of 10 - 20 km south of the Darvana Anticline, and the dip of the NE-dipping nodal plane ranges between 30° and 45°. We here interpret these events to be the geometric and kinematic expression of the Mountain Front Fault system.

4.6 Balanced cross section

The geological cross section shown in figure 48 has been extended at depth by using the cross-section balancing technique (e.g. Dahlstrom, 1969; Hossack, 1979; Elliot, 1983). In detail, we have assumed flexural-slip folding (Donath and Parker, 1964) and preservation of bed thickness and line-length (Dahlstrom, 1969). In order to ease the computation of beds length, a homogeneous thickness is assumed for all the stratigraphic units (whose values are provided in section 3.2), with the exception of the top Ilam to base Shahbazan interval for which we used 1500 m SW of the Mileh Sorkh Anticline and 1800 m NE of the Pataq Anticline. For the deeper portion of the section not shown in figure 48, we have used thickness values consistent with Tavani et al (2018a). In particular, a total thickness of 1350 m is assumed for the Triassic to Middle Jurassic sequence (i.e. from the base of the Geli Khana Formation to the base of the Garau Formation), which is well constrained by outcrop data from the immediate north of the study area (Tavani et al., 2018b). Thicknesses of 1 km for the Permian and 3 km for the pre-Permian sedimentary sequence are here used, which are also consistent with the observed depth of the base of the sedimentary sequence as observed in the seismic reflection sections presented in this article (Fig. 47). Finally, in agreement with the occurrence of a seismic gap between 20 and 30 km depth (Fig. 46), we estimated a thickness of 11

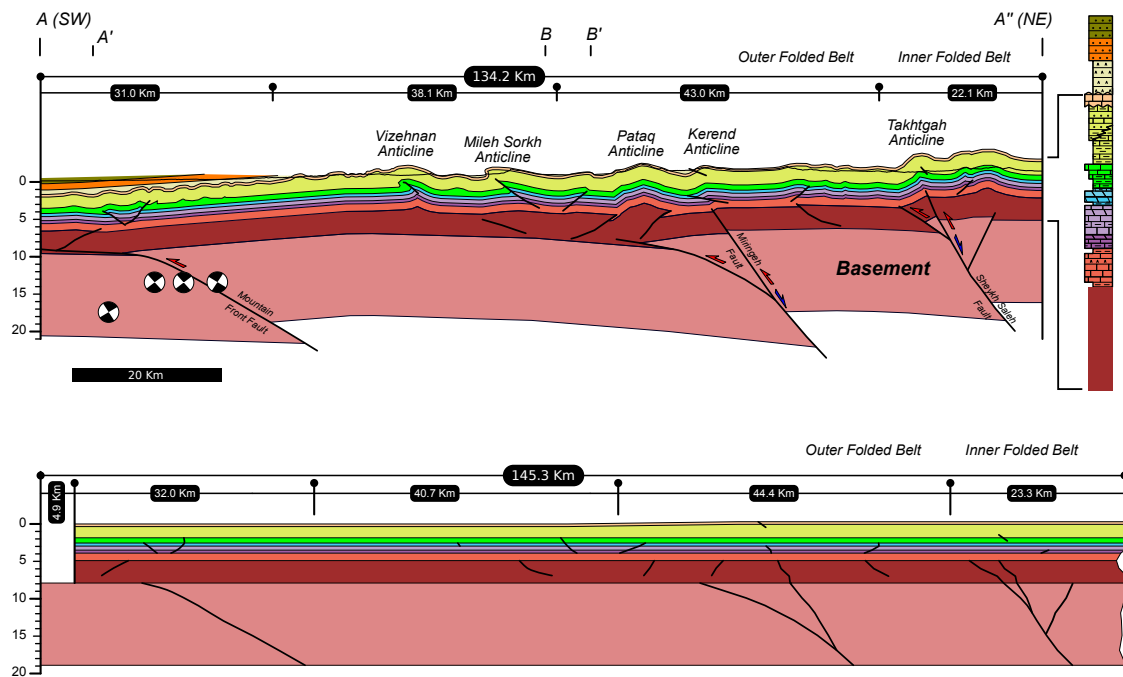


Figure 51: Balanced cross section along the direction of the geological section in Figure 48, and restored section. The stratigraphic succession shown in figure 46 is also illustrated.

km for the basement comprised between the base of the sedimentary sequence and the top of the ductile middle crust level. Such an inference being in agreement with previous work in the area (e.g. Talebian and Jackson, 2004; Nissen et al 2011). Our balanced cross section, along with its restoration, is shown in figure 51.

The Shahbazan to Asmari stratigraphic package is reconstructed along the entire section, also to the NE of the Takhtgah Anticline where there is no evidence that it was deposited. This was done as this package represents the best constrained portion of the multilayer, and we therefore took its length as a reference for cross section balancing. The present day length of the section is 134.2 km, whereas the unfolded and unfaulted length of the Shahbazan to Asmari package is 140.4 km, implying a shortening of 6.2 km. Surface geology data and the interpretation of seismic reflection profiles evidence some decoupling between competent and mobile packages, with folds having wavelengths of less than 5 km being confined to different portions of the sedimentary cover. Furthermore, the integration of surface geology, borehole data, and interpretation of seismic reflection profiles, indicates the occurrence of thrusts (underneath the Vizehnan, Mileh Sorkh, and Kerend Anticline) and backthrusts (SE of the Pataq Anticline). There is however, no evidence of large displacement associated with neither of them. The necessity for preserving line-length is also suggestive of very limited displacements associated with the thrust faults. Therefore, we confined them to within Mesozoic structural levels. Some low displacement thrusts are also assumed to occur within the Paleozoic sequence. The occurrence of deeply located thrusts are a geometric requirement for maintaining the length of the Paleozoic layers equal to that of the Meso-Cenozoic ones. In agreement with the geometries observed in the seismic reflection sections (Fig. 47), the two basement steps observed in the seismic section 2 of figure 47 and inferred in the geological cross section of figure 48, i.e. the steps across the Kerend (Step 1) and Takhtgah (Step 2) anticlines, are here interpreted as the result of the positive inversion of deeply rooted inherited extensional faults. A footwall shortcut occurs along both inverted faults. The interpretation of these two steps as inverted normal faults also fits with the extremely low amount of shortening observed in the Meso-Cenozoic stratigraphic sequence. In our reconstruction, structures affecting the Paleozoic to Cenozoic sedimentary succession between the Vizehnan and Takhtgah anticlines accommodated shortening transferred to the cover by the Sheykh Saleh and Miringeh inverted faults (Fig. 51). No major structures affecting the cover occurs to the SW of the Vizehnan Anticline, where shortening in the Asmari Formation is nearly 1 km.

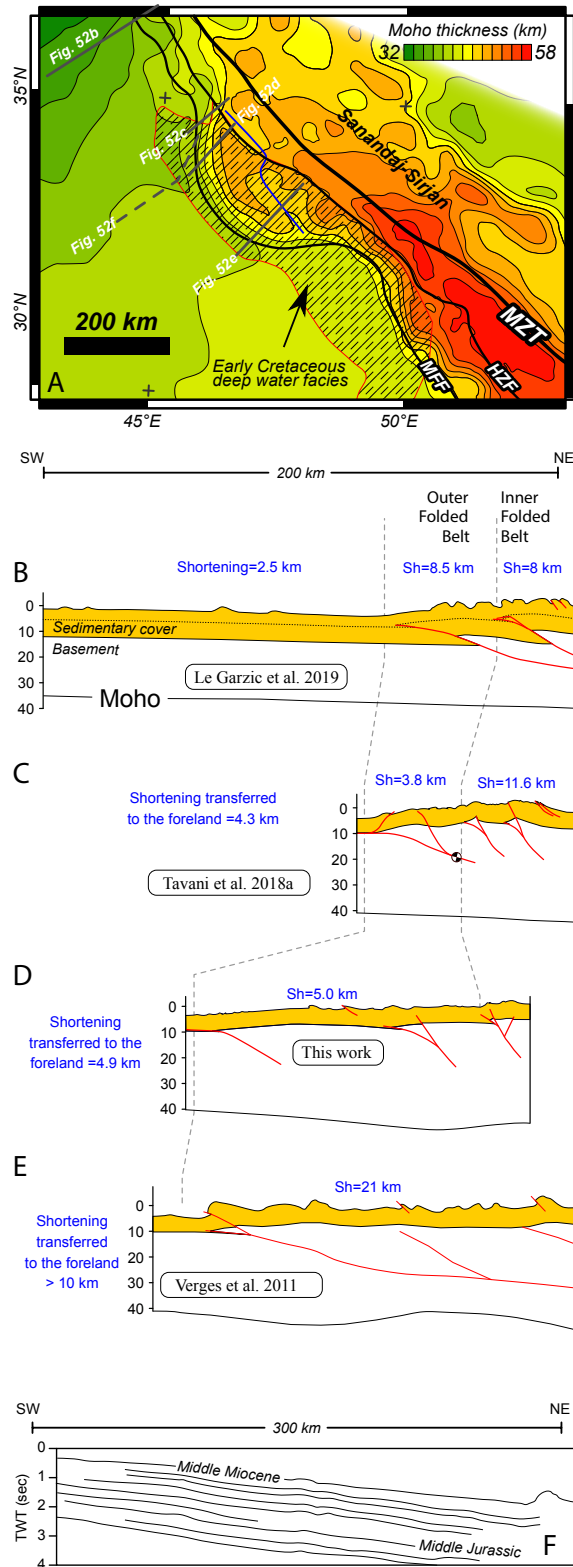


Figure 52: (A) Moho thickness in the Lurestan arc and surrounding zones (after Jiménez-Munt et al., 2012), with extent of Early Cretaceous deep-water facies indicated (after Ziegler, 2001), and thickness of the upper Tithonian - lower Turonian sequence (after English et al., 2015). (B-E) Schematic crustal scale cross sections across the Kirkuk embayment and the Lurestan arc, with Moho indicated. The Moho in sections B-D is from Jiménez-Munt et al., 2012, in section (E) it is redrawn from Paul et al., (2010)). (F) Line drawing of a seismic section across the foreland area (after Mohammed, 2006).

Scaling relationships between downdip rupture and earthquake magnitude (e.g. Wells and Coppersmith, 1994) indicate that the $M_w > 5$ events projected onto the section should have occurred along faults having a cross sectional length exceeding 3 km. The clustering of these events suggests that these faults form patches located along the main strand on the Mountain Front Fault system. Notably, the Mountain Front Fault system is located at the southwestern edge of the large anticlinorium that starts from the Kerend Anticlines and ends in the foredeep region.

The reconstructed geometry of the section implies a different amount of shortening for the basement and the sedimentary cover, the latter needing almost 5 km of additional shortening to occur SW of the section. The High Zagros Fault, which occurs in the NE portion of the section (Fig. 48), is not included in the balanced cross section for the sake of simplicity.

4.7 Discussion

4.7.1 Tectonic style and comparison with previous studies

The balanced cross section illustrated in figure 51 is almost entirely confined to within the outer Zagros folded belt, which in the study area appears to be associated with a hybrid deformation style. This composite tectonic style includes inversion tectonics and “pure” thrusting, in the central and NE, and in the SW portions of the balanced cross section, respectively.

In detail, in our reconstruction a slightly transported crustal-scale fault propagation fold is associated with the Mountain Front Fault. Such a scenario is constrained by the location of the hypocentres of the $M_w > 5$ earthquakes associated with the aftershock sequence of the M_w 7.3, 12 November 2017, earthquake that hit the Zagros belt in the Lurestan region (Figs. 45b, 48). These hypocentres, indeed, are located a few km to the NE of the trailing syncline of the crustal-scale anticline (Fig. 48), rather than underneath the crest-forelimb transition of this anticline (i.e. below the Vizehnan Anticline) as would be required by a fault-bend folding solution (in which the ramp underlies the crest). On the other hand, the inversion tectonics style adopted in the central and NE portions of the section is consistent with the structures imaged in the seismic reflection profiles (Fig. 47), and it is also a geometric requirement minimising the amount of shortening within the basement. This, in turn, serves as a mechanism for producing significant uplift in the interior

of the folded belt without transferring an excessive amount of shortening to its foreland. In our section, the shortening transferred to the foreland is < 5 km, in line or below the values adopted by other authors in the same area (Fig. 52). This value is compatible with the scarce shortening observed in the foreland region (Fig. 52f) and it could have been easily accommodated by meso-scale structures, such as tectonic stylolites or mesoscopic folds, which are widespread in the Mesozoic and Cenozoic multilayer of the Lurestan region (Tavani et al., 2018c). The amount of shortening for the sedimentary cover along the section can be estimated to be nearly 6 km, corresponding to about 5% of its original length. Several balanced cross sections have been provided in the literature for the whole Zagros mountain belt, which indicate up to 25% total shortening (Molinaro et al., 2005; Mouthereau et al., 2006; Allen et al., 2013; Bigi et al., 2018), including estimates for the Lurestan area (Blanc et al., 2003, Vergés et al., 2011a). However, most of this total shortening is thought to be accommodated by the High Zagros Fault (e.g. Vergés et al., 2011a), and published shortening values that exclusively take into account deformation associated with the folded belt are more in line with the results presented in this work. For example, balanced cross sections across the Lurestan arc (Vergés et al., 2011a; Tavani et al., 2018a) and the Kirkuk embayment (Le Garzic et al., 2019) suggest an amount of shortening in the sedimentary cover of the folded belt of nearly 15-20 km (Fig. 52). Furthermore, when considering only the shortening accommodated in the outer part of the folded belt, our reconstruction (~6 km of shortening) becomes consistent with the information from the NW Lurestan arc (~4 km of shortening, Tavani et al., 2018a; Fig. 52c) and from the Kirkuk embayment (8 km of shortening, Le Garzic et al., 2019; Fig. 52b. 5% of shortening according to Obaid and Allen, 2017).

In agreement with the seismic gap observed between 20 and 30 km depth (Fig. 46) (already illuminated by Niessen et al., 2011) and consistently with previous works in the Zagros (e.g. Mouthereau et al., 2006; Vergés et al., 2011a), we infer thrust and inverted normal faults sole down into a mid-crustal ductile detachment level. Concerning the timing of deformation, the northeastward thinning of the Gachsaran Formation across the Mile Sorkh and Kerend anticlines (e.g. Fig. 48) indicates that the NE portion of the section uplifted earlier than the SW one, probably already during the late Miocene. Consistent with such a chronology of deformation, elevation profiles and river network analysis allow identifying the area spanning from the Pataq anticline to the HZF as an uplifted area relative to the region to the SW of it. . In addition, the relic landforms in the area spanning from the Kerend

anticline to the Zimakan River area (i.e. immediately to the south of the Takhtgah Anticline) (Fig. 50) suggest that topographic growth has continued coeval with erosion. In particular, topographic growth can be inferred from the occurrence of an elevated land surface gently dipping towards the SW eroded in the Asmari Formation carbonates, which predates a first stage of deepening of the Zimakan River, and from the further deepening of the latter valley postdating formation of the pediment. Such a second stage of uplift could be related with the more recent activity of the Mountain Front Fault. In the NW portion of the Lurestan arc, onset of cover folding in the Mountain Front Flexure area is dated at about 8 Ma (Homke et al., 2004), i.e. syn Agha Jari. This is in agreement with the reduced thickness of the Gachsaran Formation observed in the northern portion of the geological cross section (Fig. 48), which suggest post-depositional uplift and erosion of the Gachsaran Formation. However, tilting of a fold-sealing unconformity in the Bakhtiari Formation during the flexure development (Fig. 49), indicates that folding within the cover sequence and the onset of the Mountain Front Flexuring were not coeval. In particular, such a feature shows that the development of the Mountain Front flexuring, and thus the development of the Mountain Front Fault system in the study area, can be traced back to approximately after 3 Ma (i.e. the age of the base of the Bakhtiari Formation; Homke et al., 2004). This is in agreement with Koshnaw et al. (2017) that, based on low-temperature thermochronology data, suggest a similar 5 ± 1 Ma age for the onset of the Mountain Front Fault system activity in the NW Zagros.

In summary, the study area is characterised by an hybrid style of deformation, in which folding of the cover sequence and inversion tectonics in the basement occurred together, in a piggy back propagation sequence. Later, during the final stages of shortening, the basement involving low-dipping Mountain Front Fault developed at the toe of the belt.

4.7.2 Early Jurassic inheritances and their influence in determining the sinuosities of the frontal Zagros belt

The structural architecture of a number of mountain belts worldwide, and in particular that of their foreland, has been shown to be largely affected by several modes of re-use of pre-existing basement faults inherited from the rifted margin (Williams et al., 1989; Cooper et al., 1989; Coward et al., 1991; Camanni et al., 2016; Brown

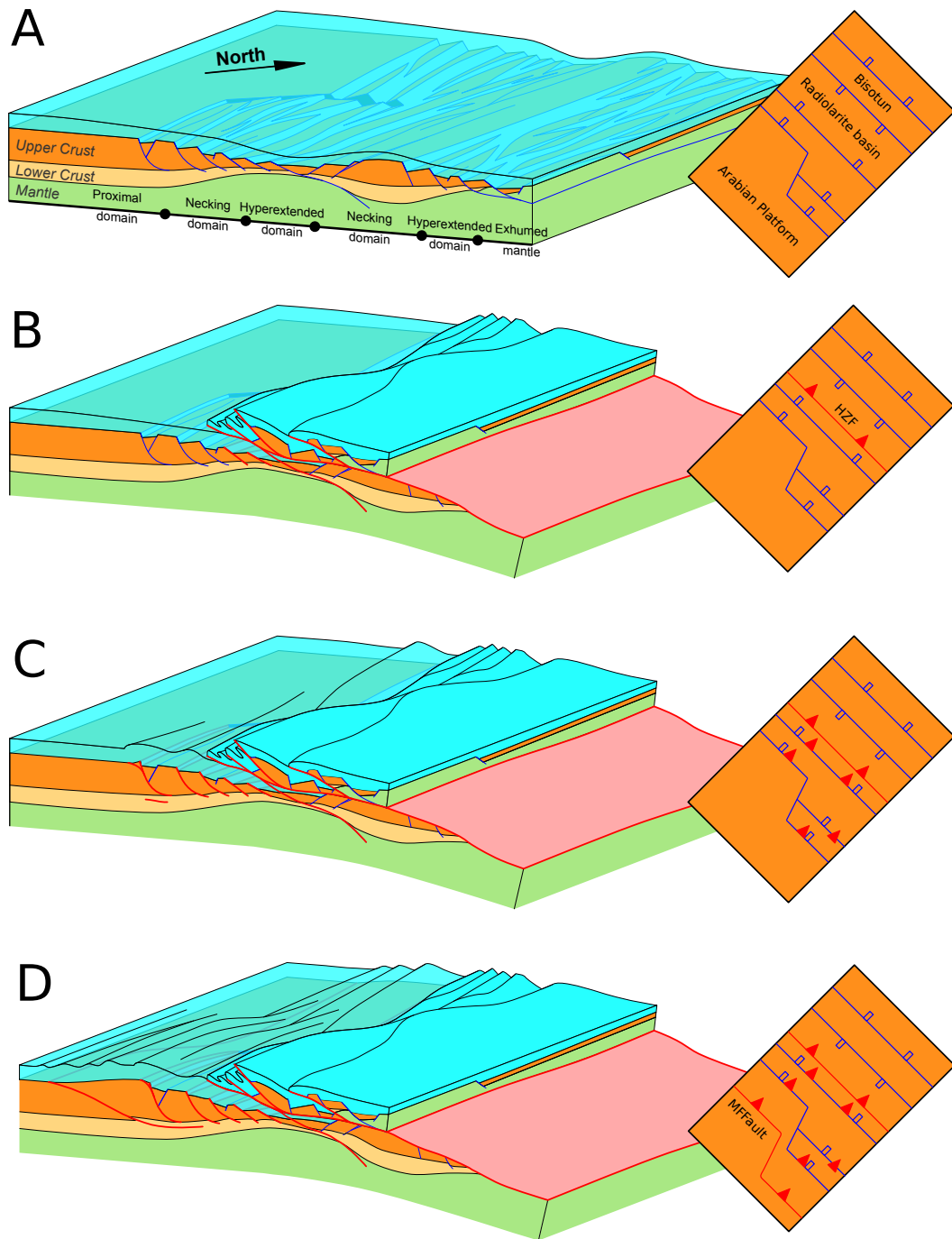


Figure 53: 3D scheme and map view showing the evolution of the Lurestan arc-Kirkuk embayment boundary region. (A) End of Early Jurassic rifting. (D) Development of the Mountain Front Fault during the Plio-Pleistocene. See text for details.

et al., 2017; Granado et al., 2017). In particular, it has been demonstrated that pre-existing basin-bounding extensional faults can be positively inverted during mountain building processes (Carrera et al., 2006; Tavani et al., 2013; Camanni et al., 2014 a,b), and that the structural complexity of the fault systems in the basement can locally forces the development of bends in the structural trend of an

otherwise roughly straight overlying fold and thrust belt (Macedo and Marshak, 1999; Jammes et al., 2014; Tugend et al., 2014; Alvarez-Marron et al., 2014). In the structural model that we present in this work for the foreland of the Zagros belt, the Mountain Front Fault system appears to correspond to a late stage gently NE-dipping crustal thrust that developed at the leading edge of an array of steeply dipping positively inverted extensional faults. Inheritances associated with the rift architecture could be, therefore, suitable candidates for explaining both structure and sinuosities of the Mountain Front Fault system also in the Zagros belt.

As already briefly mentioned, the Lurestan region underwent a major extensional pulse during the Early Jurassic, which resulted in the development of NW-SE oriented troughs (Tavani et al., 2018b) and in the shift of the depositional environment of a large area from shallow- to deep-water (e.g. Koop and Stoneley 1982; Ziegler, 2001; Barrier and Vrielynck, 2008). Extension and development of Early Jurassic basins required thinning of the crust in a widespread area, which was underfilled during the Middle and Late Jurassic. The map distribution of the overlying Early Cretaceous deep-water facies can be therefore used as a proxy for defining the rough shape of the area that experienced Early Jurassic crustal thinning. This area is overall oriented NW-SE, and its south-western border nearly coincides with the location of the Mountain Front Flexure (Fig. 52a), suggesting that the development of the Mountain Front Flexure is somewhat linked to the re-use of pre-existing fault systems that controlled the deposition of Early Cretaceous deep water facies. On the other hand, the relatively sudden NW-ward termination of Jurassic and Cretaceous deep water facies across the boundary between the Lurestan arc and the Kirkuk embayment, along with the NW-ward thinning of the Tithonian-Turonian sequence (Fig. 52a), can be attributed to the Jurassic rift segmentation, and in particular to the occurrence of NE-SW oriented faults or to inherited crustal scale N-S striking faults, which are widely documented in the Arabian Plate (e.g. Falcon, 1974; Talbot and Alavi, 1996; Hessami et al., 2001). Consistently with the lateral rift segmentation, despite the strong compressional overprint which has altered the original crustal thickness, the Moho depth below the Lurestan arc shows evidence of Jurassic NE-ward crustal thinning, which instead does not occur in the Kirkuk embayment, suggesting the lateral juxtaposition of different Early Jurassic rift domains. The sections across the Kirkuk embayment and the NW portion of the Lurestan arc (Fig. 52 b and c) are characterised by a rather linear increase of the Moho depth from SW to NE. Conversely, the two sections across the central part of the Lurestan Arc (Fig. 52 d and e) are characterised by a

region of crustal thinning, located immediately to the NE of the Mountain Front Fault system. This thinned area, when observed in map view, defines two NW-SE elongated regions (marked by the blue line in Fig. 52 a), which could correspond to regional graben structures.

All the above described features suggest a key role of the Early Jurassic rift structure in shaping the Mountain Front Flexure and in determining its sinuosity in the western portion of the Lurestan arc. In detail, according to our interpretation, the pre-orogenic architecture of the Arabian margin in the NW portion of the Lurestan arc was largely defined by NW-SE elongated extensional domains, with secondary N-S to NE-SW striking fault systems segmenting the proximal domain of the margin (Fig. 53a). The Mountain Front Fault system, and thus the flexure, developed with a sinusoidal shape that follows the boundary between the Jurassic thinned (and drowned) crust and the area that did not experience remarkable thinning and drowning. In essence, the Mountain Front Flexure follows the trend of the laterally segmented boundary between the Jurassic proximal and necking domains of the margin (Fig. 53b).

As the Mountain Front Fault system is not an inherited fault but, instead, it is a newly generated fault rooted in the middle to lower crust, the reason of the parallelism between Mountain Front Fault system and extensional domains should be found in the inherited rheology of the passive margin. In particular, as pointed out by several authors (e.g. Cloetingh et al., 2005; Sutra et al., 2013; Lacombe and Bellahsen, 2016; Lescoutre, 2019), thinning of the crust during rifting and its subsequent cooling significantly reduces the rock volumes that can undergo deformation by ductile processes. Consequently, the weak zones in the middle and lower crust thin oceanward and, eventually, in the distal domains of rift systems almost the entire crust shows a brittle behaviour and becomes coupled with the mantle (Sutra et al., 2013). We speculate that in the distal portions of the Arabian margin, the mid-crustal ductile layer is not well developed and cannot, therefore, provide a suitable level of weakness for the activation of a large and interconnected basal detachment. Instead, in the innermost portion of the necking domain and in the proximal domain, the ductile middle crust layer is thick and well developed and can therefore provide a significant mechanical weakness for the development of detachment levels. Accordingly, in the Lurestan arc of the Zagros belt, when this area became involved in the deformation, such basal decollement rapidly developed and allowed for the development of a frontal thrust that mimics the trend of the basin boundary.

4.8 Conclusions

In this work, we have integrated information from near-vertical seismic reflection profiles, surface geology, geomorphic, and earthquake data to build a balanced cross section across the NW portion of the Lurestan arc. The amount of shortening in the section does not exceed 10 km, with partial decoupling between the sedimentary cover and the basement. In our reconstruction, the Mountain Front Flexure is the frontal limb of a crustal-scale, slightly transported, fault propagation anticline, associated with the NE-dipping Mountain Front Fault. Such a fault developed as a late stage structure and splays off from a mid-crustal decollement level, ahead of a system of positively inverted normal faults. Our study suggests a strong control of the Early Jurassic rift architecture on the structure of the belt. In particular, the Mountain Front Fault nucleates in the inner portion of the necking domain of the Jurassic rift, where the mid-crustal ductile level is sufficiently thick to promote the development of a large and interconnected decollement, from which the Mountain Front Fault emanates. Lateral segmentation of the Jurassic rift, accommodated by transfer faults, promoted a differential advancement of the necking domain between the Kirkuk embayment and the Lurestan arc, which resulted in the sinusoidal shape of the Mountain Front Fault and in its different position in the two regions.

Final remarks

In this work we analyzed different structures along the Zagros fold-and-thrust belt in order to stress the role of structural inheritances. We specially focused on two areas of study: (i) the Lurestan, where basement faults previously formed within the Arabian plate controlled the segmentation of the Triassic to Early Jurassic rift and the subsequent shape of the deformation front during the ZFTB development; (ii) the Fars Arc, where the evaporitic sequence of the Hormuz Fm. represents a significant décollement horizons and, together with the extensive diapirism, markedly change ZFTB structural style.

From our study in Lurestan we could reconstruct the Mountain Front Flexure as the frontal limb of a crustal-scale, slightly transported, fault propagation anticline related with the NE-dipping Mountain Front Fault. Such a fault developed as a late stage structure and splays off from a mid-crustal decollement level, ahead of a system of positively inverted normal faults.

We interpret the Mountain Front Fault to nucleates in the inner portion of the necking domain of the Jurassic rift, where the mid-crustal ductile level is sufficiently thick to promote the development of a large and interconnected decollement, from which the Mountain Front Fault emanates. The resulting rift architecture explains the observed segmentation of the belt structure. Besides, the lateral segmentation of the Jurassic rift, accommodated by transfer faults, promoted a differential advancement of the necking domain between the Kirkuk embayment and the Lurestan arc, which resulted in the sinusoidal shape of the Mountain Front Fault and in its different position in the two regions.

Differently, in the Fars Arc there are no clear evidences of the Mountain Front Flexure presence. Off-shore, along the Arabian foreland the deformation is mainly localized around salt structures. Onshore, the stratigraphic package is folded, maintaining the same regional level until the more internal structures in proximity of the Main Zagros Thrust (e.g. the Darmadan anticline).

The change in structural style from faults reactivation, controlled by frictional processes, and, a subhorizontal decoupling above the Hormus Salt is well depicted along ENE-WSW transect across the Oman-Zagros deformation front in the eastern Persian Gulf. Here, the inherited basement normal fault of the pre-Cambrian rifting

controlled the boundary of the Hormuz basin and consequently the pinch-out of the salt.

To the east of the pinch-out, thrusting develops during the deposition of the Upper Cretaceous Gurpi Fm. and the onset of the Oman-Zagros contraction related to the obduction phase. Structures located at the Hormuz Salt basin margin are interpreted to be related to basement faults, despite the possibility of minor decoupling above a reduced sequence of the Hormuz salt. Besides, variations in the Triassic sedimentary sequence thickness suggest activity of these normal faults, also during the Triassic rifting. The subsequent inversion occurs during the deposition of the Paleocene Pabdeh Fm. as a consequence of the northwestward migration of the foredeep. Further to the west, along the Arabian foreland and above a thicker Hormuz sequence, diapirism records the compressive events where the adjacent country rocks show little or no deformation. We conclude that, the salt pinch-out and the inherited basement discontinuities along the eastern Persian Gulf worked as a strain-lock, enucleating most of the shortening during the Oman-Zagros Upper Cretaceous to Paleocene contractional event.

In eastern Fars, the onset of the continental collision occurred along the NW-SE Zagros trend approximately at Oligocene time. Many preexisting diapirs encased into the sedimentary package were reactivated as deformation progressed from the internal parts of the fold and thrust belt to the undeformed foreland. Pre-existing diapirs modified the expected fold and thrust pattern resulting into changes of the trend and wavelength of the structures, as observed in the transition from central Fars to Eastern Fars.

Strong supporting evidence for presence of pre-orogenic diapirism are the Paleozoic and Mesozoic halokinetic processes described from seismic data in the Tunb diapir and the field observations in the Darmadan diapir. The shortening and squeezing of the eastern Fars diapirs resulted in a strong variability of the folds geometry and orientation. Buckle folds tend to curve around pre-existing salt bodies. Thrusts can jump forward to join a pre-existing diapir, which act as nucleating point for faulting. Salt stocks and country rocks absorb shortening in different ways but always maintaining kinematic compatibility. To maintain it, thrusts and folds, which trend nearly perpendicular to the shortening direction, curve and merge into the salt stock and its secondary welded equivalent as observed in the Darmadan diapir. Moreover, the Darmadan anticline geometry, and the presence several salt stocks along the structure, pointed out that nearly circular evolved from initially

continuous salt ridges during the Mesozoic and Cenozoic. This implies that buried and currently extruding salt stocks are connected through a framework of salt ridges or salt walls at depth.

Diapirs located in the undeformed foreland recorded the compression since the Paleocene, showing (i) diachronous extrusions and emplacements of Hormuz salt sheets, (ii) development and squeezing of second order salt structures formed by the upper Fars Salt evaporitic level, and (iii) rotation of secondary minibasins, and (iv) active diapirism, bulb expansion, diapir roof arching and finally crestal normal faulting.

Glossary

The terminology related to the salt tectonic world is relatively young and in some cases still under debate or eventually very specific for a certain context. Several terms included in this manuscript have been listed in this glossary in order to avoid misconceptions. The definitions reported here are attributed to various authors and in particular to the work of synthesis carried out by Jackson and Hudec (2017).

active diapirism. Diapir rise by arching, uplifting, or shouldering aside its roof (Nelson 1989). Active diapirism occurs in two ways. Halokinetic active diapirism is driven by overburden load on the source layer. When the average density of this overburden exceeds the average density of the diapir and its roof, diapiric salt is pressurized and pushes upward against the roof. If this buoyancy force is greater than the strength and weight of the roof, then the roof is pushed up and the diapir rises actively. Halokinetic active diapirism occurs in relatively tall diapirs overlain by relatively thin roofs. Compressional active diapirism is driven by regional shortening, which squeezes the diapir, forcing salt upward to uplift, arch, or intrude into the roof. Because regional tectonic forces are typically much greater than buoyancy forces, compressional active diapirism can deform a much thicker roof than can halokinetic active diapirism.

allochthonous salt. Subhorizontal or moderately dipping, sheetlike salt diapir emplaced at stratigraphic levels above the autochthonous source layer. Allochthonous salt overlies stratigraphically younger strata. The term can be applied even if the salt sheet remains attached to its source layer. Compare with autochthonous salt and parautochthonous salt (Naumann 1858; Wilckens 1912; Van de Fliert 1953).

allosuture. Suture between salt sheets having separate feeders.

autosuture. Suture between two lobes of the same salt sheet.

bulb. Swollen, crestal part of a salt diapir. Its enlarged periphery is an overhang. Extremely broad bulbs grade into salt sheets (Jackson and Talbot 1986).

crestal graben. Dominantly planar normal faults that dip toward one another and root into the crest of a salt structure.

differential loading. Application of a variable load on a salt body from any direction. All salt flow is produced by some combination of three types of differential

loading: displacement loading, gravitational loading, and thermal loading. Which combination is most important depends on the depth of salt burial, geometry of the salt body, geologic setting, and thermal conditions of the salt (Hudec and Jackson, 2007).

downbuilding. *see passive diapirism.*

drape fold. (a) Fold produced in layered rocks by an underlying block rising at high angles to the layering; a type of forced fold. (b) as used in this manuscript (Chapter 1), a zone of upturned strata adjacent to a diapir. Upturning results from arching of the diapir roof above flanking strata and is an important process forming halokinetic sequences (Rowan et al. 2003). **halokinesis.** Type of salt tectonics in which salt flow is powered entirely by gravitational forces (release of gravitational potential energy) in the absence of significant lateral tectonic forces (Trusheim 1957).

halokinetic sequence. Relatively conformable succession of drapefolded growth strata genetically influenced by near-surface or extrusive salt flow and equivalent in scale to a parasequence. Halokinetic sequences are locally bounded at the top and base by angular unconformities that become disconformable to conformable with increasing distance from the diapir (Giles and Lawton 2002). Hook halokinetic sequences have narrow zones of deformation (50–200 m), >70 degrees of angular discordance, common mass-wasting deposits, and abrupt facies changes. **Hook sequences** stack into a tabular composite halokinetic sequence, which has subparallel boundaries, thin roofs, and local deformation (Giles and Rowan 2012).

minibasin. Small intrasalt basin largely surrounded by and subsiding into relatively thick allochthonous or autochthonous salt. Such basins can merge over time into larger, composite basins. Salt expelled from beneath a minibasin wells up around the minibasin margin, forming a network of salt walls, massifs, or welds that surround the minibasin.

overburden. Strata younger than the salt source layer. “Overburden” is generally used as a stratigraphic rather than structural term; for example, allochthonous salt overlies part of its overburden.

overhang. *See bulb.*

passive diapirism (downbuilding). Syndepositional growth of a diapir whose exposed crest rises as sediments accumulate around it. The diapir’s crest can be periodically buried, but the diapir repeatedly breaks through this thin, ephemeral

roof. The diapir's base subsides, together with encasing strata, as the basin fills with sediment (Barton 1933; Nelson 1989).

pedestal. Triangular base of a diapir, where the diapir widens downward to merge with the source layer (Vendeville and Nilsen 1995).

peripheral sink. Locally thickened, synkinematic strata accumulating in a rim syncline as a result of salt withdrawal.

piercement. Emplacement of a salt diapir to create a discordant salt contact, in which the diapiric margin crosscuts surrounding strata.

reactive diapirism. Emplacement of an elongated, sharp-crested diapir of salt or shale into the space created by regional extensional thinning during rifting or gravity spreading (Jackson and Vendeville 1990; Vendeville and Jackson 1992a).

rollover. Stratal interval that thickens and bends downward toward a normal fault, diapir, or salt weld. An extension rollover results from rotation of hanging-wall strata as they slide down a listric fault surface (Hamblin 1965). An expulsion rollover results from expulsion of underlying salt by prograding strata (Ge et al. 1997).

roof. That part of a diapir's overburden that overlies the widest part of the diapir and has structure or stratigraphy affected by diapirism (Hudec and Jackson 2006).

salt anticline. Elongated (planform axial ratio of 2 or more) mound of salt having concordant overburden. *Compare with salt pillow.*

salt diapir. Mass of salt that has flowed in a ductile manner and has discordant contacts with the encasing overburden. In its broadest sense, a diapir includes intrusions or extrusions of any shape, upwelling of either buoyant or nonbuoyant rock, or emplacement by downbuilding, upbuilding, or faulting of overburden (Mrazec 1907).

salt expulsion. *See salt withdrawal.*

salt feeder (canopy feeder, feeder diapir). Diapir supplying salt to an overlying salt sheet or salt canopy (Sumner et al. 1990).

salt sheet. Allochthonous salt sourced from a single feeder whose breadth is several times greater than its maximum thickness; a broad, nongenetic term that includes salt glacier, namakier, salt sill, and salt nappe (Hudec and Jackson 2006).

salt stock (salt plug). Pluglike salt diapir having subcircular planform (axial ratio of less than 2) (Trusheim 1960).

salt structure. Map-scale body of salt that has changed shape by salt flow from its depositional configuration. Salt structures include salt diapirs, salt pillows, salt anticlines, salt sheets, and salt canopies.

salt tectonics. Strictly defined as large-scale deformation involving salt or other evaporites as a source layer, but in its loosest sense, any deformation involving evaporites. Salt tectonics includes halokinesis (Jackson and Talbot 1986).

salt wall. Broad ridge of diapiric (discordant) salt having a planform axial ratio of 2 or more. Walls can form sinuous, parallel rows (Trusheim 1960).

salt wing. Subhorizontal wedge of allochthonous salt protruding from the steep flanks of a salt diapir. Most salt wings record episodes of salt extrusion over underlying strata. Repeated extrusions create stacked salt wings, forming a serrated salt contact or Christmas-tree structure (Ladzekpo, et al. 1988).

salt withdrawal. (or, more accurately, salt expulsion). Evacuation of salt due to the weight of its overburden. Salt withdrawal creates accommodation space for an overlying withdrawal basin. Salt is expelled from regions of salt withdrawal into salt structures. This flow is typically three-dimensional, so the cross-sectional area of salt can increase or decrease over time. Expulsion eventually forms salt welds or fault welds. See salt deflation.

secondary minibasin. Minibasin whose base rests on allochthonous salt or an equivalent salt weld. See also minibasin, primary minibasin, and encased minibasin.

source layer. Layer of autochthonous or allochthonous salt supplying salt for the growth of salt structures.

stem. Comparatively slender part of a salt diapir below the bulb.

suprasalt. Lying above autochthonous or allochthonous salt.

turtle-structure anticline (turtle structure). Mounded strata between salt diapirs, typically having a flat base and rounded crest. The sedimentary sequence is thick in its core and thins laterally. The anticline may or may not be cored by a low salt pillow. The turtle structure forms between diapirs whose flanks subside because of regional extension (see diapir fall) or between salt structures whose withdrawal basins migrate and widen through time (Trusheim 1960). Compare with mock-turtle anticline.

upbuilding. See active diapirism.

weld. Surface or zone joining strata originally separated by autochthonous or allochthonous salt (Jackson and Cramez 1989). The weld is a negative salt structure resulting from complete or nearly complete removal of intervening salt.

withdrawal basin. See salt withdrawal.

References

Acocella, V., Hus R., Funicello R., De Batist, M., 2005. Sandbox models of relay ramp structure and evolution. *Journal of structural geology*, 27, 459-473.

Alavi, M. (1980). Tectonostratigraphic evolution of the Zagrosides of Iran. *Geology*, 8, 144-9. DOI:10.1130/0091-7613(1980)8<144:TEOTZO>2.0.CO;2

Alavi, M. (1991). Sedimentary and structural characteristics of the Paleo-Tethys remnants in northeastern Iran. *Geological Society of America Bulletin*, 103, 983-992. DOI:10.1130/0016-7606(1991)103<0983:SASCOT>2.3.CO;2

Alavi, M. (1994). Tectonics of Zagros orogenic belt of Iran, new data and interpretation. *Tectonophysics*, 229, 211-238. DOI:10.1016/0040-1951(94)90030-2

Alavi, M., 2004. Regional stratigraphy of the Zagros Fold-Thrust Belt of Iran and its proforeland evolution. *American Journal of Science*, 304, 1-20.

Alavi, M., 2007. Structures of the Zagros Fold-Thrust belt in Iran. *American Journal of Science*, 307, 1064-1095, DOI 10.2475/09.2007.02].

Allen, M. B., Armstrong, H. A. (2008). Arabia–Eurasia collision and the forcing of mid-Cenozoic global cooling. *Palaeogeography, Palaeoclimatology, Palaeoecology*, 265, 52-58, DOI:10.1016/j.palaeo.2008.04.021

Allen, M. B., Talebian, M. (2011). Structural variation along the Zagros and the nature of the Dezful Embayment. *Geological Magazine*, 148, 911-924, DOI:10.1017/S0016756811000318Allen, M. B., Saville,

Alsouki, M., Riahi, M.A. and Yassaghi, A. (2011). Seismic imaging of sub-circular salt-related structures: evidence for passive diapirism in the Straits of Hormuz, Persian Gulf. *Pet. Geosci.*, 17(1), 101-107. Doi:10.1144/1354-079309-799.

Agard, P., Omrani, J., Jolivet, L., Mouthereau, F., 2005. Convergence history across

Zagros (Iran): Constrains from collisional and earlier deformation. *International Journal of Earth Sciences*, 98, 401-419. doi: 10.1007/s00531-005-0481-4.

Agard, P., Omrani, J., Jolivet, L., Whitechuck, H., Vrielyck, B., Spakman, W., Monié, P., Meyer, B., Wortel R., 2011. Zagros orogeny: a subduction-dominated process. *Geological Magazine*, 148 (5-6), 692-725.

Bahroudi, A., Talbot, C. J., 2003. The configuration of the basement beneath the Zagros Basin. *Journal of Petroleum Geology*, 26 (3), 257-282.

Bahroudi, A., Koyi, H., 2003. Effect of spatial distribution of Hormuz Salt on deformation style in the Zagros fold and thrust belt: an analogue modelling approach., *Journal of the Geological Society*. <https://doi.org/10.1144/0016-764902-135>

Bahroudi, A., Talbot, C.J., 2003. THE CONFIGURATION OF THE BASEMENT BENEATH THE ZAGROS BASIN., *Journal of Petroleum Geology*. <https://doi.org/10.1111/j.1747-5457.2003.tb00030.x>

Barber, D. D., Stockli, D. F., Horton, B. K., Koshnaw, R.I. (2018). Cenozoic Exhumation and Foreland Basin Evolution of the Zagros orogen during Arabia-Eurasia collision, Western Iran. *Tectonics*, 37, 4396-4420. DOI:10.1029/2018TC005328

Barrier, E., Vrielynck, B. (2008). Paleotectonic maps of the Middle East: Atlas of 14 maps. Middle East Basin Evolution (MEBE) Programme

Barton, D. C., 1933, Mechanics of formation of salt domes with special reference to Gulf Coast salt domes of Texas and Louisiana: *American Association of Petroleum Geologists Bulletin*, 17, 1025–1083.

Berberian, M. (1995). Master “blind” thrust faults hidden under the Zagros folds: Active basement tectonics and surface morphotectonics. *Tectonophysics*, 241, 193-224. DOI:10.1016/0040-1951(94)00185-C

Berberian, M., and King, G. C. P. (1981). Towards a paleogeography and tectonic evolution of Iran. *Canadian Journal of Earth Sciences*, 18, 210-265. DOI:10.1139/e81-019

Bigi, S., Carminati, E., Aldega, L., Trippetta, F., Kavooosi, M. A. (2018). Zagros fold and thrust belt in the Fars province (Iran) I: Control of thickness/rheology of sediments and pre-thrusting tectonics on structural style and shortening. *Marine and Petroleum Geology*, 91, 211-224. DOI:10.1016/j.marpetgeo.2018.01.005

Blanc, E. P., Allen, M. B., Inger, S., Hassani, H. (2003). Structural styles in the

Zagros simple folded zone, Iran. *Journal of the Geological Society*, 160, 401-412.
DOI:10.1144/0016-764902-110

Bordenave, M.L. (2008) The origin of the Permo-Triassic gas accumulations in the Iranian Zagros Fold belt and contiguous offshore areas: A review of the palaeozoic petroleum system. *Journal of Petroleum Geology*, 31, 3-42.
DOI:10.1111/j.1747-5457.2005.tb00087.x

Bozorgnia, H., Agah, S., 1973. Geological Information on Lar Block (Gr-360). National Iranian Oil Company Exploration and Production Affairs, 95.

Beydoun, Z.R., 1991. Arabian Plate hydrocarbon geology and potential, a plate tectonic approach. *AAPG. Studies in Geology*, 33, 77.

Bellahsen, N., L. Husson, J. Autin, S. Leroy, and E. d'Acremont. 2013. "The Effect of Thermal Weakening and Buoyancy Forces on Rift Localization: Field Evidence from the Gulf of Aden Oblique Rifting." *Tectonophysics*. <https://doi.org/10.1016/j.tecto.2013.05.042>.

Berberian, M., 1995. Master "blind" thrust faults hidden under the Zagros folds: active basement tectonics and surface morphotectonics., *Tectonophysics*. [https://doi.org/10.1016/0040-1951\(94\)00185-c](https://doi.org/10.1016/0040-1951(94)00185-c)

Boote, D.R.D., Mou, D., Waite, R.I., 1990. Structural evolution of the Suneinah foreland, central Oman Mountains. In: A.H.F. Robestson, M.P. Searle & A.C. Ries (Eds.). *The Geology and Tectonics of the Oman Region*, Geology Society of London, Special Publication, 49, 397-418.

Bowe, R.J., 1976. Geological Report Bandar Abbas Agreement Area, Iran (GR-5515-25). Phillips Petroleum Company Iran, 105.

Bradley, D.C., Kidd, W.S.F. (1991). Flexural extension of the upper continental crust in collisional foredeeps. *Geological Society of America Bulletin*, 103, 1416-1438. DOI:10.1130/0016-7606(1991)103<1416:FEOTUC>2.3.CO;2

Braud, J. (1987). La suture du Zagros au niveau de Kermanshah (Kurdistan Iranien): Reconstitution paléogéographique, evolution géodynamique, magmatique et structural. PhD thesis, Université Paris-Sud.

Bradley, D.C., Kidd, W.S.F. (1991). Flexural extension of the upper continental crust in collisional foredeeps. *Geological Society of America Bulletin*, 103, 1416-1438. DOI:10.1130/0016-7606(1991)103<1416:FEOTUC>2.3.CO;2

Braud, J. (1987). La suture du Zagros au niveau de Kermanshah (Kurdistan Iranien):

Reconstitution paléogéographique, evolution géodynamique, magmatique et structural. PhD thesis, Université Paris-Sud.

Bretis, B., Bartl, N., Grasemann, B. (2011). Lateral fold growth and linkage in the Zagros fold and thrust belt (Kurdistan, NE Iraq). *Basin Research*, 23, 615-630. DOI:10.1111/j.1365-2117.2011.00506.x

Brown, D., Alvarez-Marron, J., Schimmel, M., Wu, Y. M., Camanni, G. (2012). The structure and kinematics of the central Taiwan mountain belt derived from geological and seismicity data. *Tectonics*, 31, TC5013. DOI:10.1029/2012TC003156

Brown, J Alvarez-Marron, C Biete, H Kuo-Chen, G Camanni, CW Ho (2017) How the structural architecture of the Eurasian continental margin affects the structure, seismicity, and topography of the south central Taiwan fold-and-thrust belt. *Tectonics*, 36, 1275-1294

Brun, J.-P., Fort, X., 2012. Salt tectonics at passive margins: Geology versus models – Reply., *Marine and Petroleum Geology*. <https://doi.org/10.1016/j.marpetgeo.2012.04.008>

Burberry, C. M., Cosgrove, J. W., Liu, J. G. (2007). Stream network characteristics used to infer the distribution of fold types in the Zagros Simply Folded Belt, Iran. *Journal of Maps, Student Edition*, 32–45. DOI:10.1080/jom.2007.9711027

Burberry, C.M., Cosgrove, J.W., Liu, J.G. (2010). A study of fold characteristics and deformation style using the evolution of the land surface: Zagros Simply Folded Belt, Iran. *Geological Society, London, Special Publications*, 330, 139-154. DOI:10.1144/SP330.8

Buscher, J.T., Ascione, A., Valente, E. (2017). Decoding the role of tectonics, incision and lithology on drainage divide migration in the Mt. Alpi region, southern Apennines, Italy. *Geomorphology*, 276, 37–50. doi: 10.1016/j.geomorph.2016.10.003

Butler, R.W.H., Mazzoli, S. (2006). Styles of continental contraction: A review and introduction, in Mazzoli, S., and Butler, R. W. H., *Styles of Continental Contraction: Geological Society of America Special Paper 414*, 1–10. DOI:10.1130/2006.2414(01)

Callot, J.P., Jahani, S., Letuzey, J., 2007. The role of pre-existing diapirs in fold and thrust belt development. In: *Thrust Belts and Foreland Basins* (Ed. by O. Lacombe, J. Lavè, F. Roure & J. Vergès). Springer, Berlin, pp. 309-325.

- Callot, J.-P., Trocme, V., Letouzey, J., Albouy, E., Jahani, S., Sherkati, S., 2012. Pre-existing salt structures and the folding of the Zagros Mountains. *Geological Society of London Special Publication*, 363, 545-561.
- Callot, J.-P., Ribes, C., Kergaravat, C., Bonnel, C., Temiz, H., Poisson, A., Vrielynck, B., Salel, J.-F. and Ringenbach, J.C. (2014). Salt tectonics in the Sivas basin (Turkey): crossing salt walls and minibasins. *Bull. Soc. Geol. Fr.*, 185(1), 33-42.
- Camanni, G., Brown, D., Alvarez-Marron, J., Wu, Y-M., Chen, H-A. (2014a). The Shuilikeng fault in the central Taiwan mountain belt. *Journal of the Geological Society*, 171, 117-130
- Camanni, G., Chen, C-H., Brown, D., Alvarez-Marron, J., Wu, Y-M., Chen, H-A., Huang, H-H., Chu, H-T., Chen, M-M., Chang, C-H. (2014b). Basin inversion in central Taiwan and its importance for seismic hazard. *Geology*, 42, 147-150. DOI:10.1130/G35102.1
- Camanni, G., Alvarez-Marron, J., Brown, D., Ayala, C., Wu, Y-M., Hsieh, H-H. (2016). The deep structure of south-central Taiwan illuminated by seismic tomography and earthquake hypocenter data. *Tectonophysics*, 679, 235-245
- Carosi, R., Montomoli, C., Iaccarino, S., Visonà, D. (2018). Structural evolution, metamorphism and melting in the Greater Himalayan Sequence in central-western Nepal. *Geological Society, London, Special Publications*, 483. DOI:10.1144/SP483.3
- Carrera, N., Muñoz, J. A., Sàbat, F., Mon, R., Roca, E. (2006). The role of inversion tectonics in the structure of the Cordillera Oriental (NW Argentinean Andes). *Journal of Structural geology*, 28, 1921-1932. DOI:10.1016/j.jsg.2006.07.006
- Carruba, S., Bertozzi, G., Perotti, C.R., & Rinaldi, M. (2007). Alcuni aspetti del diapirismo salino nel Golfo Persico. *Rendiconti della Società Geologica Italiana*, 4, 188-190.
- Cartwright, J.A., Jackson, M.P.A., 2008. Initiation of gravitational collapse of an evaporite basin margin: The Messinian saline giant, Levant Basin, eastern Mediterranean., *Geological Society of America Bulletin*. <https://doi.org/10.1130/b26081x.1>.
- Casciello, E., Vergés, J., Saura, E., Casini, G., Fernández, N., Blanc, E. P., Homke, S., Huntet, D.W. (2011). Fold patterns and multilayer rheology of the Lurestan

Province, Zagros simply folded belt (Iran). *Journal of the Geological Society*, 166, 947–959. DOI:10.1144/0016-76492008-138.

Casini, G., Casciello, E., Saura, E., Vergés, J., Fernandez, N., Hunt, D. W. (2018). Fracture characterization in sigmoidal folds: Insights from the Siah Kuh anticline, Zagros, Iran. *AAPG Bulletin*, 102, 369-399. DOI:10.1306/0503171615817076.

Chen, K., Xu, W., Mai, P. M., Gao, H., Zhang, L., Ding, X. (2018). The 2017 Mw 7.3 Sarpol Zahāb Earthquake, Iran: A compact blind shallow-dipping thrust event in the mountain front fault basement. *Tectonophysics*, 747, 108-114.

Chenin, P., Manatschal, G., Picazo, S., Müntener, O., Karner, G., Johnson, C., Ulrich, M. (2017). Influence of the architecture of magma-poor hyperextended rifted margins on orogens produced by the closure of narrow versus wide oceans. *Geosphere*, 13, 559-576. DOI:10.1130/GES01363.1

Chiariotti, L., Perotti, C.R., Carruba, S., Cattaneo, L., 2011. Age and structural evolution of salt diapirism in the Iranian sector of the Persian Gulf. *Rendiconti Online della Società Geologica Italiana*, 15, 26-29.

Ciarcia, S., Mazzoli, S., Vitale, S., Zattin, M. (2012). On the tectonic evolution of the Ligurian accretionary complex in southern Italy. *Geological Society of America Bulletin*, 124, 463-483.

Clerc, C., Jolivet, L., Ringenbach, J.-C., 2015. Ductile extensional shear zones in the lower crust of a passive margin., *Earth and Planetary Science Letters*. <https://doi.org/10.1016/j.epsl.2015.08.038>

Coleman, R.G. (1981). Tectonic setting for ophiolite obduction in Oman. *Journal of Geophysical research*, 86, B4, 2497-2508. Doi: 10.1029/JB086iB04p02497.

Cloetingh, S., Ziegler, P., Beekman, F., Andriessen, P., Matenco, L., Bada, G., Garcia-Castellanos, D., Hardebol, N., Dezes, P. Sokoutis, D. (2005). Lithospheric memory, state of stress and rheology: neotectonic controls on Europe's intraplate continental topography. *Quaternary Science Reviews*, 24, 241–304. DOI:10.1016/j.quascirev.2004.06.015.

Cooper, M. A., Williams, G. D., De Graciansky, P. C., Murphy, R. W., Needham, T., De Paor, D., Stoneley, R., Todd, S. P., Turner, J.P., Ziegler, P.A. (1989). Inversion tectonics-a discussion. *Geological Society of London, Special Publications*, 44, 335-347. DOI:10.1144/GSL.SP.1989.044.01.18.

Corti, G., 2012. Evolution and characteristics of continental rifting: Analog

modeling-inspired view and comparison with examples from the East African Rift System., *Tectonophysics*. <https://doi.org/10.1016/j.tecto.2011.06.010>.

Corti, G., van Wijk, J., Cloetingh, S., Morley, C.K., 2007. Tectonic inheritance and continental rift architecture: Numerical and analogue models of the East African Rift system., *Tectonics*. <https://doi.org/10.1029/2006tc002086>.

Curzi, M., and Aldega, L., and Bernasconi, S., Berra, F., Billi, A., Boschi, C., Franchini, S., Van der Lelij, R., Viola, G., Carminati, E. 2020. Architecture and evolution of an extensionally-inverted thrust (Mt. Tancia Thrust, Central Apennines): Geological, structural, geochemical, and K–Ar geochronological constraints. *Journal of Structural Geology*. 104059. [10.1016/j.jsg.2020.104059](https://doi.org/10.1016/j.jsg.2020.104059).

Coward, M.P.A., Gillcrist, R., Trudgill, B. (1991). Extensional structures and their tectonic inversion in the Western Alps. Geological Society of London, Special Publication, 56, 51-77. DOI:10.1144/GSL.SP.1991.056.01.07

Dahlstrom, C. D. A. (1969). Balanced cross sections, *Canadian Journal of Earth Sciences*, 6, 743–757. DOI:10.1139/e69-069.

Daly, M.C., Chorowicz, J., Fairhead, J.D., 1989. Rift basin evolution in Africa: the influence of reactivated steep basement shear zones., Geological Society, London, Special Publications. <https://doi.org/10.1144/gsl.sp.1989.044.01.17>

Davis, D.M., Engelder, T., 1985. The role of salt in fold-and-thrust belts., *Tectonophysics*. [https://doi.org/10.1016/0040-1951\(85\)90033-2](https://doi.org/10.1016/0040-1951(85)90033-2)

De Böckh, H., Lees, G., Richardson, F.D.S., 1929. Contribution to the stratigraphy and tectonics of the Iranian ranges., J. W. Gregory, ed.. *The structure of Asia*: London, Methuen.

Dewey, John F., and John M. Bird. 1970. “Mountain Belts and the New Global Tectonics.” *Journal of Geophysical Research*. <https://doi.org/10.1029/jb075i014p02625>.

Dercourt, J., Zonenshain, L. P., Ricou, L.-E., Kazmin, V. G., Le Pichon, X., Knipper, A. L., Grandjacquet, C., Sbertshikov, I.M., Geysant, J., Lepvrier, C. and Pechersky, D.H. (1986). Geological evolution of the Tethys belt from the Atlantic to the Pamirs since the Lias. *Tectonophysics*, 123, 241-315. DOI:10.1016/0040-1951(86)90199-X

Donath, F. A., Parker, R. B. (1964). Folds and folding. *Geological Society of America Bulletin*, 75, 45-62.

- Dooley, T.P., McClay, K.R., Hempton, M., Smit, D. 2005. Salt tectonics above complex basement extensional fault systems: results from analogue modelling. *Petroleum Geology, North-West Europe and Global Perspectives*, Geol. Soc. Lond., 6, 1631-1648, doi:10.1144/0061631.
- Dooley, T. P., Jackson, M. P. A. and Hudec, M. R., (2007). Initiation and growth of salt-based thrust belts on passive margins. Results from physical models: *Basin Research*, 19, 165-177. Doi:10.1111/j.1365-2117.2007.00317.x.
- Dooley, T. P., Hudec M. R. and Jackson, M. P. A., (2012). The structure and evolution of sutures in allochthonous salt. *AAPG Bulletin*, 96, 1045-1070. Doi:10.1306/09231111036.
- Dooley, T.P., Jackson, M.P.A., Hudec, M.R., (2015). Breakout of squeezed stocks: dispersal of roof fragments, source of extrusive salt and interaction with regional thrust faults. *Basin Research* 27, 3-25. Doi: 10.1111/bre.12056.
- Doré, A.G., Lundin, E.R., Fichler, C., Olesen, O., 1997. Patterns of basement structure and reactivation along the NE Atlantic margin., *Journal of the Geological Society*. <https://doi.org/10.1144/gsjgs.154.1.0085> Edgell, H.S., 1991. Proterozoic salt basins of the Persian Gulf area and their role in hydrocarbon generation. *Precambrian Research*,54, 1-14.
- Elliot, D. (1983). The construction of balanced cross-sections. *Journal of Structural Geology*, 5, 101. DOI:10.1016/0191-8141(83)90035-4
- Emami, H., Vergés, J., Nalpas, T., Gillespie, P., Sharp, I., Karpuz, R., Blanc, E.P., Goodarzi, M.G.H. (2010). Structure of the Mountain Front Flexure along the Anaran anticline in the Pusht-e Kuh Arc (NW Zagros, Iran): insights from sand box models. *Geological Society of London, Special Publications*, 330, 155-178. DOI:10.1144/SP330.9.
- England, P., Molnar, P. (1990). Surface uplift, uplift of rocks, and exhumation of rocks. *Geology*, 18, 1173–1177. DOI:10.1130/0091-7613(1990)018<1173:SUUO RA>2.3.CO;2
- English, J.M., Lunn, G.A., Ferreira, L., Yacu, G. (2015). Geologic evolution of the Iraqi Zagros, and its influence on the distribution of hydrocarbons in the Kurdistan region. *AAPG Bulletin*, 99, 231–272. DOI:10.1306/06271413205.
- Falcon, N.L. (1961). Major earth-flexuring in the Zagros mountains of South-West Iran. *Q. J. Geol. Soc.*, 117, 367-376. DOI:10.1144/gsjgs.117.1.0367.

Falcon, N. L., 1969. Problems of the relationship between surface structure and deep displacements illustrated by the Zagros Range. P. E. Kent, G. E. Satterthwaite, and A. M. Spencer, eds.: Special Publication 3, Time and place in orogeny: Geological Society of London, 9-22.

Falcon, N. L., (1974). Southern Iran: Zagros Mountains. *Journal of the Geological Society*, 4, 199-211. DOI:10.1144/GSL.SP.2005.004.01.11

Faqira, M., Rademakers, M., Kader, M. A. 2009. New insights into the Hercynian Orogeny, and their implications for the Paleozoic Hydrocarbon System in the Arabian Plate. *GeoArabia*, 14, (3), 199-228.

Faghih, A., Ezati-Asla, M., Mukherjee, S., Soleimany, B., (2019). Characterizing halokinesis and timing of salt movement in the Abu Musa salt diapir, Persian Gulf, offshore Iran. *Marine and Petroleum Geology*, 105 (2019) 338-352.

Farr, T. G., Rosen A. P., Caro, E., Crippen, R., Duren, R., Hensley, S., Kobrick, M., Paller, M., Rodriguez, E., Roth, L., Seal, D., Shaffer, S., Shimada, J., Umland, J., Werner, M., Oskin, M., Burbank, D., Alsdorf, D., (2007). The Shuttle Radar Topography Mission, *Rev. Geophys.* 45, Doi:10.1029/2005RG000183.

Fernández, O. (2005). Obtaining a best fitting plane through 3D georeferenced data. *Journal of Structural Geology*, 27, 855-858. DOI:10.1016/j.jsg.2004.12.004.

Frizon de Lamotte, D., Tavakoli-Shirazi, S., Leturmy, P., Averbuch, O., Mouchot, N., Raulin, C., Leparmentier, F., Blanpied, C., Ringenbach, J.C., 2013. Evidence for Late Devonian vertical movements and extensional deformation in northern Africa and Arabia: Integration in the geodynamics of the Devonian world. *Tectonics*, 32, 107-122, <http://doi.org/10.1002/tect.20007>.

Gamond, J-F. 1994. "Normal Faulting and Tectonic Inversion Driven by Gravity in a Thrusting Regime." *Journal of Structural Geology*. [https://doi.org/10.1016/0191-8141\(94\)90013-2](https://doi.org/10.1016/0191-8141(94)90013-2).

Garcia, S.F.M., Letouzey, J., Rudkiewicz, J.-L., Filho, A.D. and Frizon De Lamotte, D. (2012). Structural Modeling Based on Sequential Restoration of Gravitational Salt Deformation in the Santos Basin (Brazil). *Marine and Petroleum Geology*, 35, 337-353. Doi:10.1016/j.marpetgeo.2012.02.009.

Gawthorpe, R.L., Hurst, J.M., 1993. Transfer zones in extensional basins: their structural style and influence on drainage development and stratigraphy., *Journal of the Geological Society*. <https://doi.org/10.1144/gsjgs.150.6.1137>

- Ge, H., Jackson, M. P. A. and Vendeville, B. C. (1997). Kinematics and dynamics of salt tectonics driven by progradation. *AAPG Bulletin*, 81, 398-423.
- Ghasemi, A., Talbot, C.J. (2006). A new tectonic scenario for the Sanandaj–Sirjan Zone (Iran). *J. Asian Earth Sci.*, 26, 683–693. DOI:10.1016/j.jseae.2005.01.003.
- Ghavidel-Syooki, M., Popov, L.E., Mohammad, G.P., Suyarkovae, H.E.A., (2011). Stratigraphic evidence for the Hirnantian (latest Ordovician) glaciation in the Zagros Mountains, Iran. *Palaeogeography, Palaeoclimatology, Palaeoecology*. 307, 1-4, 1-16.
- Ghavidel-Syooki, M., Popov, L.E., Álvaro, J.J., Pour, M.G., Tolmacheva, T.Y., Ehsani, M.H., 2014. Dapingian-lower Darriwilian (Ordovician) stratigraphic gap in the Faraghan Mountains, Zagros Ranges, south-eastern Iran. *Bulletin of Geosciences*, 89(4), 679-706.
- Gibbs, A.D., 1984. Structural evolution of extensional basin margins., *Journal of the Geological Society*. <https://doi.org/10.1144/gsjgs.141.4.0609>
- Giles, K.A. and Lawton, T.F. (2002) Halokinetic sequence stratigraphy adjacent to the El Papalote diapir, north-eastern Mexico, *AAPG Bull.*, 86(5), 823-840.
- Giles, K.A., Rowan, M.G., 2012. Concepts in halokinetic-sequence deformation and stratigraphy. *Salt Tectonics, Sediments and Prospectivity*. Geological Society, London, Special Publications, 363, 7–31. <http://dx.doi.org/10.1144/SP363.2>.
- Gansser, A., 1960. *Über Schlammvulkane und Salzdome: Naturf. Gesell. Zurich Vierteljahrsschr.* 106, (1), 1-6.
- Glennie, K. W. and Boegner, P. L. E. (1981) Sole Pit inversion tectonics. In: *Petroleum Geology of the Continental Shelf of North-West Europe* (Eds L. V. Illing and G. V. Hudson), Institute of Petroleum, London, 110-120.
- Gombert, B., Duputel, Z., Shabani, E., Rivera, L., Jolivet, R., Hollingsworth, J. (2019). The impulsive source of the 2017 (MW= 7.3) Ezgeleh, Iran, earthquake. *Geophysical Research Letters*, 46, 5207– 5216. DOI:10.1029/2018GL081794
- Goodarzi, M.H. (2009). Late Cretaceous–Paleocene formation of the proto–Zagros foreland basin, Lurestan Province, SW Iran. *Geological Society of America Bulletin*, 121, 963-978. DOI:10.1130/B26035.1
- Google Earth (2019). <https://earth.google.com/web>
- Granado, P., Ferrer, O., Muñoz, J.A., Thöny, W., Strauss, P. (2017). Basin

inversion in tectonic wedges: Insights from analogue modelling and the Alpine-Carpathian fold-and-thrust belt. *Tectonophysics*, 703-704, 50-68. DOI:10.1016/j.tecto.2017.02.022

Gray, D.R., Foster, D.A., Meert, J.G. Goscombe, B.D., Armstrong, R., Trouw R.A.J., Passchier, C.W., 2008. A Damara orogen perspective on the assembly of southwestern Gondwana. Geological Society of London, Special Publications, 294, 257-278.

Jackson, J.A., (1980). Reactivation of basement faults and crustal shortening in orogenic belts. *Nature*, 283, 343-346.

Jackson, M. P. A., and C. Cramez, 1989, Seismic recognition of salt welds in salt tectonics regimes, in Gulf of Mexico salt tectonics, associated processes and exploration potential: Society of Economic Paleontologists and Mineralogists Gulf Coast Section, 10th annual research conference program and abstracts, 66–71.

Jackson, M.P.A., Vendeville, B.C., (1994). Regional extension as a geologic trigger for diapirism. *Geological Society American Bull.*, 106, 57-73.

Jackson, A.-L.C., Jackson, M.P.A. and Hudec, M.R., (2015a). Understanding the Kinematics of Salt-Bearing Passive Margins: A Critical Test of Competing Hypotheses for the Origin of the Albian Gap, Santos Basin, Offshore Brazil. *Geological Society America Bulletin*, 127, (11-12), 1730-1751. Doi:10.1130/B31290.1.

Jackson, M. P. A.; Hudec, M. R.; Jennette, D. C. and Kilby, R. E. (2008). Evolution of the Cretaceous Astrid thrust belt in the ultradeep-water Lower Congo basin, Gabon: *AAPG Bulletin*, 92, 487-511.

Jackson, M.P.A. and Hudec, M.R. (2017). *Salt Tectonics: Principles and Practice*. Cambridge University Press, Cambridge. Doi:10.1017/9781139 003988.

Jackson, M. P. A., and C. J. Talbot, (1986), External shapes, strain rates, and dynamics of salt structures: *Geological Society of America Bulletin*, 97, 305–323.

Jackson, M. P. A., and C. J. Talbot, (1991). A glossary of salt tectonics. University of Texas at Austin, Bureau of Economic Geology Geological Circular, 91-4, 44.

Jackson, M. P. A., and B. C. Vendeville, 1990, The rise and fall of diapirs during thin-skinned extension (abs.): *American Association of Petroleum Geologists Bulletin*, 74, 683.

Jaeger, J. C., and Cook, N. G. W., 1979. *Fundamentals of Rock Mechanics*.

3rd edition. xix 593 pp., numerous figs. London: Chapman and Hall. ISBN 0 412 22010 5. Price £9.95. Geological Magazine, 117(4), 401-401. doi:10.1017/S001675680003274X.

Jahani, S., Callot, J. P., Letouzey, J., Frizon De Lamotte, D., 2009. The eastern termination of the Zagros Fold-and-Thrust Belt, Iran: Structures, evolution, and relationships between salt plugs, folding, and faulting. *Tectonics*, 28 (6), TC6004. doi:10.1029/2008TC002418.

Jahani, S., Hassanpour, J., Mohammadi-Firouz, S., Letouzey, J., Frizon de Lamotte, D., Alavi, S.A., Soleimany, B., 2017. Salt tectonics and tear faulting in the central part of the Zagros Fold-Thrust Belt, Iran. *Mar. Pet. Geol.*, 86, 426-446.

James E. Faulds, Robert J. Varga, 1998. The role of accommodation zones and transfer zones in the regional segmentation of extended terranes. *Accommodation zones and transfer zones; the regional segmentation of the Basin and Range Province*, James E. Faulds, John H. Stewart.

James, G. A., Wynd J. G., 1965. Stratigraphic nomenclature of Iranian Oil Consortium Agreement Area. *AAPG Bulletin*, 49, 2182–2245.

Jammes, S., Huismans, R. S., Muñoz, J.A. (2014). Lateral variation in structural style of mountain building: controls of rheological and rift inheritance. *Terra Nova*, 26, 201-207. DOI:10.1111/ter.12087

Jassim, S. Z., Goff, J. C. (2006). *Geology of Iraq*. Brno, Czech Republic: DOLIN, distributed by Geological Society of London.

Jiménez-Munt, I., Fernández, M., Saura, E., Vergés, J., Garcia-Castellanos, D. (2012). 3-D lithospheric structure and regional/residual Bouguer anomalies in the Arabia-Eurasia collision (Iran). *Geophysical Journal International*, 190, 1311-1324. DOI:10.1111/j.1365-246X.2012.05580.x.

Hamblin, W. K., 1965, Origin of reverse drag on the downthrown side of normal faults: *Geological Society of America Bulletin*, 76, 1145–1163.

Hassanpour, J., Jahani, S., Reza Ghassemi, M., Ahmad Alavi, S., Zeinali, F., 2018. Evolution of the Karebas Fault System and adjacent folds, central Zagros fold-and-thrust belt, Iran: Role of pre-existing halokinesis (diapirs and minibasins) and detachment levels. *Journal of Asian Earth Sciences* (2018), <https://doi.org/10.1016/j.jseaes.2018.06.024>.

Harrison, M.R.J.V., 1921. Salt domes in Persia. In *Symposium on Salt Domes*,

Institute of Petroleum Technologists Journal 17, 300–320.

Harrison, J., V., (1924). Gypsum deposits of south-west Persia. *Econ. Geology*, 19, 259-274.

Harrison, MR. J. V., 1930. The Geology of some salt-plug in Laristan (Southern Persia). *Geological Society of London. Quart. Jour.*, 86, 463-522.

Harrison, MR. J. V., 1931. Salt domes in Persia, in Symposium on salt domes. *Inst. Petroleum Technologists Journal*, 17, 300-320.

Hessami, K., Koyi, H. A., Talbot, C. J. (2001). The significance of strike-slip faulting in the basement of the Zagros fold and thrust belt. *Journal of Petroleum Geology*, 241, 5–28. DOI:10.1111/j.1747-5457.2001.tb00659.x

Hippler, S.J., Knipe, R.J., 1990. The evolution of cataclastic fault rocks from a pre-existing mylonite., *Geological Society, London, Special Publications*. <https://doi.org/10.1144/gsl.sp.1990.054.01.08>

Heron, Philip, Alexander Peace, Ken J. W. McCaffrey, J. K. Welford, R. Wilson, and R. N. Pysklywec. n.d. “Segmentation of Rifts through Structural Inheritance: Creation of the Davis Strait.” <https://doi.org/10.31223/osf.io/6mkc8>.

Holdsworth, R.E., Butler, C.A., Roberts, A.M., 1997. The recognition of reactivation during continental deformation., *Journal of the Geological Society*. <https://doi.org/10.1144/gsjgs.154.1.0073>

Holdsworth, R.E. Grant, C. J. (1990). Convergence-related ‘dynamic spreading’ in a mid-crustal ductile thrust zone: a possible orogenic wedge model. *Geological Society of London, Special Publications*, 54, 491-500. DOI: 10.1144/GSL.SP.1990.054.01.45

Hossack, J.R., (1979). The use of balanced cross-sections in the calculation of orogenic contraction: a review. *Journal of the Geological Society*, 136, 705-711.

Hossack, J., 1995, Geometric rules of section balancing for salt structures. M. P. A. Jackson, D. G. Roberts, and S. Snelson, eds., *Salt tectonics: A global perspective*: Tulsa, OK, American Association of Petroleum Geologists, Memoir 65, 29-40.

Husseini, M.I., 2000. Origin of the Arabian Plate structures: Amar Collision and Najd Rift. *GeoArabia*, 5 (4), 527-542.

Homke, S., Vergés, J., Garcés, M., Emami, H., Karpuz, R. (2004). Magnetostratigraphy of Miocene-Pliocene Zagros foreland deposits in the front

of the Push-e Kush Arc (Lurestan Province, Iran), *Earth and Planetary Science Letters*, 225, 397-410. DOI:10.1016/j.epsl.2004.07.002.

Homke, S., Vergés, J., Serra-Kiel, J., Bernaola, G., Sharp, I., Garcés, M., Monetro-Verdú, I., Karpuz, R. and Goodarzi, M.H. (2009). Late Cretaceous-Paleocene formations of the proto-Zagros foreland basin, Lurestan Province, SW Iran. *GSA Bulletin* 121 (7/8), 963-978. Doi: 10.1130/B26035.1.

Hudec, M. R., and M. P. A. Jackson, 2007, *Terra infirma: Understanding salt tectonics: Earth-Science Reviews*, 82, 1–28, doi:10.1016/j.earscirev.2007.01.001.

Hudec, M.R., Jackson, M.P.A., Schultz-Ela, D.D., (2009). The paradox of minibasin subsidence into salt: Clues to the evolution of crustal basins. *GSA Bulletin*, 121 (1-2), 201-221. Doi: 10.1130/B26275.1.

Huisman, R. S., Beaumont, C. (2014). Rifted continental margins: The case for depth-dependent extension. *Earth and Planetary Science Letters*, 407, 148-162. DOI:10.1016/j.epsl.2014.09.032.

Husseini, M.I., (2000). Origin of the Arabian Plate structures: Amar Collision and Najd Rift. *GeoArabia* 5 (4), 527-542.

Kashfi, M. S. (1980). Stratigraphy and Environmental Sedimentology of Lower Fars Group (Miocene), South-South-west Iran. *AAPG Bulletin*, 64, 2095-2107.

Karim, K. H., Koyi, H., Baziany, M. M., Hessami, K. (2011). Significance of angular unconformities between Cretaceous and Tertiary strata in the northwestern segment of the Zagros fold–thrust belt, Kurdistan. *Geological Magazine*, 148, 925-939, DOI:10.1017/S0016756811000471.

Knipe, R.J., Lloyd, G.E., 1994. Microstructural analysis of faulting in quartzite, Assynt, NW Scotland: Implications for fault zone evolution., *Pure and Applied Geophysics PAGEOPH*. <https://doi.org/10.1007/bf00874330>

Kavoosi, M.A., 2013. Evidence for volcanic activity in the Upper Permian Nar Member of the Dalan Formation, southeast Iran. In: Poppelrieter M (Ed), *Permo-Triassic sequence of the Arabian Plate*. EAGE Publications, Houten, the Netherlands, 147-162.

Khadivi, S., F. Mouthereau, J. Barbarand, T. Adatte, and O. Lacombe (2012). Constraints on palaeodrainage evolution induced by uplift and exhumation on the southern flank of the Zagros-Iranian plateau, *J. Geol. Soc.*, 169(1), 83-97.

Kent, P.E., 1958. Recent studies of South Persian salt plugs. *AAPG*, 42, 2951-

2972.

Kent, P.E., 1970. The salt plugs of the Persian Gulf region. *Trans. Leic. Literao Philos. Soc.*, 64, 65-88.

Kent, P.E., 1979. The emergent salt plugs of southern Iran. *Journal of Petroleum Geology*, 2 (2), 117-144.

Koyi, H.A., 1988. Experimental modelling of role of gravity and lateral shortening in Zagros mountain belt. *AAPG Bulletin*, 72, 1381-1394.

Konert, G., Afifi, A.M., Al-Hajri, S.A., Droste, H.J., 2001. Paleozoic Stratigraphy and Hydrocarbon Habitat of the Arabian Plate. *GeoArabia*, 6, 407-442.

Konstantinovskaya, Elena A., Lyal B. Harris, Jimmy Poulin, and Gennady M. Ivanov. 2007. "Transfer Zones and Fault Reactivation in Inverted Rift Basins: Insights from Physical Modelling." *Tectonophysics*. <https://doi.org/10.1016/j.tecto.2007.06.002>.

Koop, W. J., Stoneley, R., Ridd, M. F., Murphy, R. W., Osmaston, M. F., Kholief, M. M., 1982. Subsidence History of the Middle East Zagros Basin, Permian to Recent [and Discussion]. *Philosophical Transaction of the Royal Society of London A.*, 305, 149-168. Doi: 10.1098/rsta.1982.0031.

Koshnaw, R. I., Horton, B. K., Stockli, D. F., Barber, D. E., TamarAgha, M. Y., Kendall, J. J. (2017). Neogene shortening and exhumation of the Zagros fold-thrust belt and foreland basin in the Kurdistan region of northern Iraq, *Tectonophysics*, 694, 332–355. DOI:10.1016/j.tecto.2016.11.016, 2017.

Koshnaw, R.I., Stockli, D.F., Schlunegger, F. (2018). Timing of the Arabia-Eurasia continental collision—Evidence from detrital zircon U-Pb geochronology of the Red Bed Series strata of the northwest Zagros hinterland, Kurdistan region of Iraq. *Geology*, 47, 47-50. DOI:10.1130/G45499.1

Imber, J., Holdsworth, R. E., Butler, C. A. (2001). A reappraisal of the Sibson-Scholz fault zone model: The nature of frictional to viscous ("brittle-ductile") transition along a long-lived crustal-scale fault, Outer Hebrides, Scotland. *Tectonics*, 20, 601-624.

Lacombe, O., Bellahsen, N. (2016). Thick-skinned tectonics and basement-involved fold–thrust belts: insights from selected Cenozoic orogens. *Geological Magazine*, 153, 763-810. DOI:10.1017/S0016756816000078.

Ladzekpo, D. H., K. K. Sekharan, and G. H. F. Gardner, 1988, *Physical modeling*

for hydrocarbon exploration: Society of Exploration Geophysicists, 58th annual meeting, SEG Abstracts 1, 586–588.

Lawton, T. F., Vega, F. J., Giles K. A., and Rosales-Domínguez, C., (2001). Stratigraphy and origin of the La Popa basin, Nuevo León and Coahuila, Mexico. Tectonics, sedimentary basins, and petroleum systems, American Association of Petroleum Geologists, Memoir 75, 219-240.

Lees, G.M., (1950). Some structural and stratigraphical aspects of the oil fields of the Middle East. 18th Internat. Geol. Cong. of London, Proc., pt.6, p. 26-33.

Lavé, J., Avouac, J.P. (2001). Fluvial incision and tectonic uplift across the Himalayas of central Nepal. *Journal of Geophysical Research, Solid Earth*. 106, 26,561–26,591. DOI:10.1029/2001JB000359

Lavier, L.L., Manatschal, G. (2006). A mechanism to thin the continental lithosphere at magma-poor margins. *Nature*, 440, 324-328. DOI:10.1038/nature04608

Leveille J. P., Ian F. Jones, Zheng-Zheng Zhou, Bin Wang and Faqi Liu4Leville (2011). Subsalt imaging for exploration, production, and development: A review. *Geophysics*, vol. 76, no. 5. Doi: 10.1190/GEO2011-0156.1

Lawa, F. A., Koyi, H., Ibrahim, A. (2013). Tectono-stratigraphic evolution of the NW segment of the Zagros fold-thrust belt, Kurdistan, NE Iraq. *Journal of Petroleum Geology*, 36, 75-96. DOI:10.1111/jpg.12543.

Le Garzic, E., Vergés, J., Sapin, F., Saura, E., Meresse, F., Ringenbach, J.-C. (2019). Evolution of the NW Zagros Fold-and-Thrust Belt in Kurdistan Region of Iraq from balanced and restored crustal-scale sections and forward modelling. *Journal of Structural Geology*, 124, 51-69. DOI:10.1016/j.jsg.2019.04.006.

Lescoutre, R. (2019). Formation and reactivation of the Pyrenean-Cantabrian rift system: inheritance, segmentation and thermal evolution. PhD thesis, Université Strasbourg.

Lacombe, O., Bellahsen, N., 2016. Thick-skinned tectonics and basement-involved fold–thrust belts: insights from selected Cenozoic orogens., *Geological Magazine*. <https://doi.org/10.1017/s0016756816000078>

Lasemi, Y., Jalilian, A. H., (2010). The Middle Jurassic basinal deposits of the Surmeh Formation in the Central Zagros Mountains, southwest Iran: facies, sequence stratigraphy, and controls. *Carbonates Evaporites*, 25, 283-295, doi: 10.1007/s13146-010-0032-3

Lees, G.M., 1931. Salt - some depositional and deformational problems. Symposium on salt domes: Institute of Petroleum Technologists Journal, 17, 259-280.

Lépinay, Marion Mercier de, Marion Mercier de Lépinay, Lies Loncke, Christophe Basile, Walter R. Roest, Martin Patriat, Agnès Maillard, and Philippe De Clarens. 2016. "Transform Continental Margins – Part 2: A Worldwide Review." *Tectonophysics*. <https://doi.org/10.1016/j.tecto.2016.05.038>.

Lloyd, G.E., Knipe, R.J., 1992. Deformation mechanisms accommodating faulting of quartzite under upper crustal conditions., *Journal of Structural Geology*. [https://doi.org/10.1016/0191-8141\(92\)90052-x](https://doi.org/10.1016/0191-8141(92)90052-x)

Letouzey, J., Colletta, B., Vially, R., Chermette, J.C., 1995. Evolution of salt-related structures in compressional settings. In: Martin, M.P.A., Roberts, D.G., Snelson, S. (Eds.), *Salt Tectonics: A Global Perspective*. AAPG Memoir, 65, 41-60.

Letouzey, J., Sherkati, S., 2004. Salt Movement, Tectonic Events, and Structural Style in the Central Zagros Fold and Thrust Belt (Iran). 24th Annual Bob F. Perkins Research Conference, pp. 753-778, doi: 10.5724/gcs.04.24.0753.

Leturmy, P., Robin, C., 2010. Tectonic and Stratigraphic Evolution of Zagros and Makran during the Mesozoic–Cenozoic. Geological Society, London, Special Publications, 330, 121-138, doi: 10.1144/SP330.7.

López-Mir, B., Muñoz, J. A. and García-Senz, J. (2014). Restoration of basins driven by extension and salt tectonics: Example from the Cotiella Basin in the central Pyrenees. *J. Struct. Geol.*, 69, 147-162. Doi:10.1016/j.jsg.2014.09.022.

Lopez-Mir, B., Schneider, S., Hülse, P., (2018). Fault activity and diapirism in the Mississippian to Late Cretaceous Sverdrup Basin: New insights into the tectonic evolution of the Canadian Arctic. *Journal of Geodynamics*, 118, 55-65. Doi:10.1016/j.jog.2017.11.002.

Lucca, A., Storti, F., Balsamo, F., Clemenzi, L., Fondriest, M., Burgess, R., Di Toro, G., 2019. From submarine to subaerial out-of-sequence thrusting and gravity-driven extensional faulting: Gran Sasso massif, central Apennines, Italy. *Tectonics* 38, 4155–4184.

Macedo, J., Marshak, S., 1999. Controls on the geometry of fold-thrust belt salients., *Geological Society of America Bulletin*. [https://doi.org/10.1130/0016-7606\(1999\)111<1808:cotgof>2.3.co;2](https://doi.org/10.1130/0016-7606(1999)111<1808:cotgof>2.3.co;2)

Marshak, S., Karlstrom, K., and Timmons, J.M., 2000, Inversion of

Proterozoic extensional faults: An explanation for the pattern of Laramide and Ancestral Rockies intracratonic deformation: *Geology*, v. 28, p. 735–738, doi: 10.1130/0091-7613(2000)28<735:IOPEFA>2.0.CO;2

Manatschal, G. (2004). New models for evolution of magma-poor rifted margins based on a review of data and concepts from West Iberia and the Alps. *International Journal of Earth Sciences*, 93, 432-466. DOI:10.1007/s00531-004-0394-7

Macedo, J., Marshak, S. (1999). Controls on the geometry of fold-thrust salients. *Geological Society of America Bulletin*, 111, 1808-1822. DOI:10.1130/0016-7606(1999)111<1808:COTGOF>2.3.CO;2

Manatschal, G., Lavier, L., and Chenin, P. (2014). The role of inheritance in structuring hyperextended rift systems: some considerations based on observations and numerical modeling. *Gondwana Res.* 27, 140–164. doi: 10.1016/j.gr.2014.08.006

Masini, E., Manatschal, G., Tugend, J., Mohn, G., Flament, J. M. (2014). The tectono-sedimentary evolution of a hyper-extended rift basin: the example of the Arzac–Mauléon rift system (Western Pyrenees, SW France). *International Journal of Earth Sciences*, 103, 1569-1596. DOI:10.1007/s00531-014-1023-8

McQuarrie, N., Stock, J.M., Verdel, C., Wernicke, B.P., 2003. Cenozoic evolution of Neotethys and implications for the causes of plate motions. *Geophysical Research Letters*, 30 (20), 2036, doi: 10.1029/2003GL017992.

McQuarrie, N. (2004). Crustal scale geometry of the Zagros fold–thrust belt, Iran. *Journal of Structural Geology*, 26, 519–535, DOI:10.1016/j.jsg.2003.08.009.

McQuarrie, N., van Hinsbergen, D. J. (2013). Retrodeforming the Arabia-Eurasia collision zone: Age of collision versus magnitude of continental subduction. *Geology*, 41, 315-318. DOI:10.1130/G33591.1

Michaelis, P.L., Pauken, R.J., 1990. Seismic interpretation of the structure and stratigraphy of the Strait of Hormuz. In: A.H.F. Robestson, M.P. Searle & A.C. Ries (Eds.), *The Geology and Tectonics of the Omen Region*, Geological Society of London, Special Publication, 49, 387-395

Miller, S.R., Slingerland, R.L. (2006). Topographic advection on fault-bend folds: inheritance of valley positions and the formation of wind gaps. *Geology*, 34, 769–772. DOI:10.1130/G22658.1

Mohammed, S.A.G. (2006). Megaseismic section across the northeastern slope of

the Arabian plate, Iraq. *GeoArabia*, 11, 77-90

Molinaro, M., Guezou, J.C., Leturmy, P., Eshraghi, S.A. and Frizon de Lamotte, D. (2004). The origin of changes in structural style across the Bandar Abbas syntaxis, SE Zagros (Iran). *Marine and Petroleum Geology*, 21, 735-752.

Molinaro, M., Leturmy, P., Guezou, J.-C., Frizon de Lamotte, D., Eshraghi, S. A. (2005). The structure and kinematics of the southeastern Zagros fold-thrust belt, Iran: From thin-skinned to thick-skinned tectonics. *Tectonics*, 24, TC3007. DOI:10.1029/2004TC001633

Motamedi, H., Sepehr, M., Sherkati, S., Pourkermani, M., 2011. Multi-phase Hormuz salt diapirism in the southern Zagros, SW Iran. *Journal of Petroleum Geology*, 34 (1), 29-44.

Morley, C.K., Nelson, R.A., Patton, T.L., Mann, S.G., 1990. Transfer Zones in the East African Rift System and Their Relevance to Hydrocarbon Exploration in Rifts (1)., *AAPG Bulletin*. <https://doi.org/10.1306/0c9b2475-1710-11d7-8645000102c1865d>

Mouthereau, F., Lacombe, O., Meyer, B. (2006). The Zagros folded belt (Fars, Iran): constraints from topography and critical wedge modelling. *Geophysical Journal International*, 165, 336–356. DOI:10.1111/j.1365-246X.2006.02855.

Mouthereau, F., J. Tensi, N. Bellahsen, O. Lacombe, T. de Boisgrollier, and S. Kargar (2007). Tertiary sequence of deformation in a thin-skinned/thick-skinned collision belt: The Zagros Folded Belt (Fars, Iran), *Tectonics*, 26, TC5006, Doi: 10.1029/2007TC002098.

Mouthereau, F., Lacombe, O., Vergés, J., 2012. Building the Zagros collisional orogen: timing, strain distribution and the dynamics of Arabia/Eurasia plate convergence. *Tectonophysics*, 532, 27–60. doi:10.1016/j.tecto.2012.01.022.

Mrazec, L., 1907, Despre cute cu simbure de străpungere [On folds with piercing cores]: *Buletinul Societății de Științe din București*, 16, 6–8.

Muñoz, J.A., Beamud, E., Fernández, O., Arbués, P., Dinarès Turell, J., and Poblet, J. 2013. The Ainsa Fold and thrust oblique zone of the central Pyrenees: Kinematics of a curved contractional system from paleomagnetic and structural data, *Tectonics*, 32, 1142– 1175, doi:10.1002/tect.20070.

Navabpour, P., Angelier, J., Barrier, E. (2011). Brittle tectonic reconstruction of palaeo-extension inherited from Mesozoic rifting in West Zagros (Kermanshah,

Iran). *Journal of the Geological Society*, 168, 979-994. DOI:10.1144/0016-76492010-108

Naumann, C. F., 1858, *Lehrbuch der Geognosie*, Vol. 1 (2nd ed.): Leipzig, Wilhelm Engelmann.

Needham, T.I.M., Morgan, R., 1997. The East Irish Sea and adjacent basins: new faults or old?, *Journal of the Geological Society*. <https://doi.org/10.1144/gsjgs.154.1.0145>

Nelson, T. H., and L. H. Fairchild, 1989, Emplacement and evolution of salt sills in northern Gulf of Mexico (abs.): *American Association of Petroleum Geologists Bulletin*, 73, 395

Nissen, E., Tatar, M., Jackson, J. A., Allen, M. B. (2011). New views on earthquake faulting in the Zagros fold-and-thrust belt of Iran. *Geophysical Journal International*, 186(3), 928-944, DOI:10.1111/j.1365-246X.2011.05119.x

Oberlander, T.M. (1965). *The Zagros streams: a new interpretation of transverse drainage in an orogenic zone*. Syracuse University Press, 168 p.

Obaid, A. K., Allen, M. B. (2017). Landscape maturity, fold growth sequence and structural style in the Kirkuk Embayment of the Zagros, northern Iraq. *Tectonophysics*, 717, 27-40, DOI:10.1016/j.tecto.2017.07.006

Orang, K., Hossein, M., Azadikhah, A., Royatvand, M., 2017. Structural framework and tectono-stratigraphic evolution of the eastern Persian Gulf, offshore Iran. *Marine and Petroleum Geology*, 91, 89-107, doi:10.1016/j.marpetgeo.2017.12.014.

Paul, A., Hatzfeld, D., Kaviani, A., Tatar, A., Pequegnat, C. (2010). Seismic imaging of the lithospheric structure of the Zagros mountain belt (Iran). *Geological Society of London, Special Publication*, 330, 5-18

Pérez-Peña, J.V., Al-Awabdeh, M., Azañón, J.M., Galve, J.P., Booth-Rea, G., Notti, D. (2017). Swath Profiler and NProfiler: Two new ArcGIS Add-ins for the automatic extraction of swath and normalized river profiles. *Computer and Geosciences*, 104, 135-150. DOI:10.1016/j.cageo.2016.08.008

Péron-Pinvidic, G., Manatschal, G., (2009). The final rifting evolution at deep magma-poor passive margins from Iberia-Newfoundland: A new point of view. *International Journal of Earth Sciences*, 98, 1581-1597. DOI:10.1007/s00531-008-0337-9.

Peron-Pinvidic, G., Manatschal, G., Osmundsen, P. T. (2013). Structural comparison

- of archetypal Atlantic rifted margins: A review of observations and concepts. *Marine and Petroleum Geology*, 43, 21-47. DOI:10.1016/j.marpetgeo.2013.02.002
- Peron-Pinvidic G., Manatschal G., the “IMAGinING RIFTING” Workshop Participants, (2020). *Rifted Margins: State of the Art and Future Challenges*. *Front. Earth Sci.*, 22 August 2019 | <https://doi.org/10.3389/feart.2019.00218>
- Perotti, C., Carruba, S., Rinaldi, M., Bertozzi, G., Feltre, L., Rahimi, M., 2011. The Qatar–South Fars Arch Development (Arabian Platform, Persian Gulf): insights from seismic interpretation and analogue modelling. Schattner, U. (Eds.), *New Frontiers in Tectonic Research - At the Midst of Plate Convergence*, InTech., pp. 325-352.
- Perotti, C., Chiariotti, L., Bresciani, L., Cattaneo, L., Toscani, G., 2016. Evolution and timing of salt diapirism in the Iranian sector of the Persian Gulf. *Tectonophysics*, 679, 180-198
- Petri, B., Duretz, T., Mohn, G., Schmalholz, S., Karner, G., et al.. Thinning mechanisms of heterogeneous continental lithosphere. *Earth and Planetary Science Letters*, Elsevier, 2019, 512, pp.147-162. [ff10.1016/j.epsl.2019.02.007](https://doi.org/10.1016/j.epsl.2019.02.007)ff. [ffinsu-02044661f](https://doi.org/10.1016/j.epsl.2019.02.007)
- Piryaei, A., Reijmer, J. J. G., Van Buchem, F. S.P., Yazdi-Moghadam, M. , Sadouni, J., Danelian, T., 2010. The influence of Late Cretaceous tectonic processes on sedimentation patterns along the northeastern Arabian plate margin (Fars Province, SW Iran). *Geological Society, London, Special Publications*, 330, 211-251.
- Piryaei, A., Reijmer, J. J. G., Borgomano, J., Van Buchem, F. S. P., 2011. Late Cretaceous tectonic and sedimentary evolution of the Bandar Abbas area, Fars Region, Southern Iran. *Journal of Petroleum Geology*, 34 (2), 157-180.
- Pirouz, M., Simpson, G., Chiaradia, M. (2015). Constraint on foreland basin migration in the Zagros mountain belt using Sr isotope stratigraphy. *Basin Research*, 27, 714-728. DOI:10.1111/bre.12097
- Pinheiro, R.V.L., Holdsworth, R.E., 1997. Reactivation of Archaean strike-slip fault systems, Amazon region, Brazil., *Journal of the Geological Society*. <https://doi.org/10.1144/gsjgs.154.1.0099>
- Player, R.A., 1969. The Hormuz salt plugs of southern Iran: Ph.D. thesis, Reading University, pp. 300.
- Pratson, L. F., and W. B. F. Ryan, (1994). Pliocene to recent infilling and subsidence

of intraslope basins offshore Louisiana. AAPG Bulletin, 78, 1483-1506.

Prince, P.S., Spotila, J.A., Henika, W.S. (2011). Stream capture as driver of transient landscape evolution in a tectonically quiescent setting. *Geology*, 39, 823–826. DOI:10.1130/G32008.1.

Quirk, D.G., Schødt, N., Lassen, B., Ings, S.J., Hsu, D., Hirsch, K.K., Von Nicolai, C., 2012. Salt tectonics on passive margins: examples from Santos, Campos and Kwanza basins., Geological Society, London, Special Publications. <https://doi.org/10.1144/sp363.10>

Rahmani, Z., Vaziri-Moghaddam, H., Taheri, A., 2010. Facies Distribution and Palaeoecology of the Guri Member of the Mishan Formation, in Lar area, Fars province, SW Iran. *Iranian Journal of Science and Technology. Transaction A.*, 34 (A3), 257-266.

Ranero, C. R., Morgan, J. P., McIntosh, K., Reichert, C. (2003). Bending-related faulting and mantle serpentinization at the Middle America trench. *Nature*, 425, 367. DOI:10.1038/nature01961

Ravaut, P., Carbon, D., Ritz, J. F., Bayer, R., and Philip, H. (1998). The Sohar Basin. Western Gulf of Oman: Description and mechanisms of formation from seismic and gravity data. *Marine and Petroleum Geology*, 15, 359-377.

Richardson, R.K., 1926. Die geologie und die salzdome im südwestlichen teile des Persischen Golfes: Verhandlungen der Naturhistorischen. Medizin Verein Heidelberg, n.s., 15, 51.

Richter, M., 1970. Bericht über die 119. Hauptversammlung der Deutschen Geologischen Gesellschaft vom 9. bis 13. Oktober 1967 in Berlin., *Zeitschrift der Deutschen Geologischen Gesellschaft*. <https://doi.org/10.1127/zdgg/119/1970/462>.

Ricou, L. E., Braud, J., Brunn, J. H. (1977). Le Zagros. *Mémoires de la Société Géologique de France*, 8, 33–52.

Rowan, M.G., (1993). A systematic technique for the sequential restoration of salt structures. *Tectonophysics*, 228(3-4), 331-348. Doi:10.1016/0040-1951(93)90347-M.

Rowan, M.G., Jackson M.P.A. and Trudgill, B.D. (1999) Salt-Related Fault Families and fault welds in the Northern Gulf of Mexico. *AAPG Bulletin*, 83(9), 1454-1484.

Rowan, M.G., Lawton, T.F., Giles, K.A., Ratliff, R.A., (2003). Near-salt deformation

in La Popa basin, Mexico, and the northern Gulf of Mexico: a general model for passive diapirism. *AAPG Bulletin* 87, 733-756.

Rowan, M.G., 2014. Passive-margin salt basins: hyperextension, evaporite deposition, and salt tectonics., *Basin Research*. <https://doi.org/10.1111/bre.12043>

Rubinat, M., Roca, E., Escalas, M., Queralt, P., Ferrer, O., Ledo, J.J., 2013. The influence of basement structure on the evolution of the Bicorn-Quesa Diapir (eastern Betics, Iberian Peninsula): contractive thin-skinned deformation above a pre-existing extensional basement fault., *International Journal of Earth Sciences*. <https://doi.org/10.1007/s00531-012-0789-9>.

Rutter, E. H. 1986. On the nomenclature of mode of failure transitions in rocks. *Tectonophysics* 122, 381-7.

Sajadi, S.H., Baghbani, D., Daneshian, J., Keramati Moezabad, M., (2016). Stratigraphy of Oligocene–miocene salt deposits in the SE Persian Gulf. *Carbonates Evaporites* 31, 277-288. Doi:10.1007/s13146-015-0263-4.

Sajadi, S.H. and Rashidi, H.S. (2019). Paleocology and Sedimentary Environments of the Oligocene-Miocene Deposits of the Asmari Formation (Qeshm Island, SE Persian Gulf). *New Insights into the Stratigraphic Setting of Paleozoic to Miocene Deposits*, Gemma Aiello. IntechOpen, Doi: 10.5772/intechopen.81402.

Saura, E., et al. (2011). Basin architecture and growth folding of the NW Zagros early foreland basin during the Late Cretaceous and early Tertiary. *Journal of the Geological Society, London*, 168, 235–250. Doi: 10.1144/0016-76492010-092.

Saura, E., D.Garcia-Castellanos, E. Casciello, V. Parravano, A. Urruela, and J. Vergés, 2015. Modeling the flexural evolution of the Amiran and Mesopotamian foreland basins of NW Zagros (Iran-Iraq). *Tectonics*, 34, 377-395, doi:10.1002/2014TC003660.

Searle, M. P., James, N. P., Calon, T. J., and Smewing, J. D. (1983). Sedimentological and structural evolution of the Arabian continental margin in the Musandam Mountains and Dibba zone, UAE. *Geological Society of America Bulletin*, 94, 1381-1400.

Searle, M.P., Cherry, A.G., Ali, M.Y. and cooper, D.J.W. (2014). Tectonics of the Musandam Peninsula and northern Oman Mountains: From ophiolite obduction to continental collision. *GeoArabia*, 19, 135-174.

Searle, M.P., 2007. Structural geometry, style and timing of deformation in

the Hawasina Window, Al Jabal al Akhdar and Saih Hatat culminations, Oman Mountains. *GeoArabia*, 12 (2), 99–130.

Searle, M.P., Ali, M.Y. (2009). Structural and tectonic evolution of the Jabal Sumeini–Al Ain–Buraimi region, northern Oman and eastern United Arab Emirates. *GeoArabia*, 14, 115-142.

Searle, M.P., Cherry, A.G., Ali, M.Y., Cooper, D.J.W. 2014. Tectonics of the Musandam Peninsula and northern Oman Mountains: From ophiolite obduction to continental collision. *GeoArabia*, 19, 135-174.

Sepehr, M., Cosgrove, J.W., 2004. Structural framework of the Zagros fold–thrust belt, Iran. *Mar. Pet. Geol.*, 21(7), 829-843, doi:10.1016/j.marpetgeo.2003.07.006.

Sepehr, M., J.W., Cosgrove, 2005. Role of the Kazerun Fault in the formation and deformation of the Zagros Fold-Thrust Belt, Iran. *Tectonics*, 24, 5. Doi:10.1029/2004TC001725.

Sherkati, S., Letouzey, J. (2004). Variation of structural style and basin evolution in the central Zagros (Izeh zone and Dezful Embayment), Iran. *Marine and Petroleum Geology*, 21(5), 535–554. DOI:10.1016/j.marpetgeo.2004.01.007

Sherkati, S., Letouzey, J., Frizon de Lamotte, D. (2006). Central Zagros fold–thrust belt (Iran): New insights from seismic data, field observation, and sandbox modelling. *Tectonics*, 25, TC4007. DOI:10.1029/2004TC001766.

Sharland, P.R., Archer, R., Casey, D.M., Davies, R.B., Hall, S.H., Heward, A.P., Horbury, A.D., Simmons, M.D., 2001. Arabian Plate Sequence Stratigraphy. *GeoArabia Special Publication*, 2, 371.

Sharland, P.R., Archer, R., Casey, D.M., Davies, R.B., Hall, S.H., Heward, A.P., Horbury, A.D. and Simmons, M.D. (2013) Arabian plate sequence stratigraphy. *GeoArabia, J. Middle East Pet. Geosci.*, 18(4).

Shail, R.K., Alexander, A.C., 1997. Late Carboniferous to Triassic reactivation of Variscan basement in the western English Channel: evidence from onshore exposures in south Cornwall., *Journal of the Geological Society*. <https://doi.org/10.1144/gsjgs.154.1.0163>

Snidero, M., Amilibia, A., Gratacos, O., -P. Blanc, E.J., Muñoz, J.A., 2011. The 3D reconstruction of geological structures based on remote sensing data: example from the Anaran anticline, Lurestan province, Zagros fold and thrust belt, Iran., *Journal of the Geological Society*. <https://doi.org/10.1144/0016-76492010-107>.

- Snidero, M., Muñoz, J.A., Carrera, N., Butillé, M., Mencos, J., Motamedi, H., Piryaei, A., Sàbat, F., 2019. Temporal evolution of the Darmadan salt diapir, eastern Fars region, Iran., *Tectonophysics*. <https://doi.org/10.1016/j.tecto.2019.06.006>
- Snyder, D.B., England, R.W., McBRIDE, J.H., 1997. Linkage between mantle and crustal structures and its bearing on inherited structures in northwestern Scotland., *Journal of the Geological Society*. <https://doi.org/10.1144/gsjgs.154.1.0079>
- Stampfli, G. M., Borel, G. D. (2002). A plate tectonic model for the Paleozoic and Mesozoic constrained by dynamic plate boundaries and restored synthetic oceanic isochrons. *Earth and Planetary Science Letters*, 196, 17-33. DOI:10.1016/S0012-821X(01)00588-X
- Stesser, D. B., Camp, V. E., 1985. Pan-African microplate accretion of the Arabian shield: *GSA Bulletin*, 96, 817-826.
- Stern, R.J., 1994. Arc assembly and continental collision in the Neoproterozoic East African Orogen: implications for consolidation of Gondwanaland. *Annu. Rev. Earth Planet. Sci.*, 22, 319-351.
- Stewart, S. A. (2018). Hormuz Salt distribution and influence on structural style in NE Saudi Arabia. *Petroleum Geoscience*. Doi:10.1144/petgeo2017-011
- Stoneley, R. (1981). The Geology of the Kuh-e Dalneshin Area of Southern Iran, and Its Bearing on the Evolution of Southern Tethys. *Journal of the Geological Society*, 138, 509-526. <http://dx.Doi.org/10.1144/gsjgs.138.5.0509>
- Stoneley, R., (1990). The Arabian continental margin in Iran during the Late Cretaceous. *The Geology and Tectonics of the Oman Region*. (eds.) Robertson, A.H.F., Searle, M.P., Ries, A.C., Geological Society Special Publication, 49, 787-795.
- Stöcklin, J. (1968). Structural history and tectonics of Iran: A review. *AAPG Bulletin*, 52, 1229-1258.
- Sumner, H. S., B. A. Robison, W. K. Dirks, and J. C. Holiday, (1990), Morphology and evolution of salt/mini-basin systems: Lower shelf and upper slope, central offshore Louisiana (abs.): Geological Society of America, Abstracts with Programs, A48.
- Suppe, J. (1983). Geometry and kinematics of fault-bend folding. *American Journal of Science*, 283, 684-721. DOI:10.2475/ajs.283.7.684
- Sutra, E., Manatschal, G., Mohn, G., Unternehr, P. (2013). Quantification and

restoration of extensional deformation along the Western Iberia and Newfoundland rifted margins. *Geochemistry, Geophysics, Geosystems*, 14, 2575-2597. DOI:10.1002/ggge.20135

Sutton, J., Watson, J.V., 1986. Architecture of the Continental Lithosphere., *Philosophical Transactions of the Royal Society A: Mathematical, Physical and Engineering Sciences*. <https://doi.org/10.1098/rsta.1986.0020>

Sykes, L.R., 1978. Intraplate seismicity, reactivation of preexisting zones of weakness, alkaline magmatism, and other tectonism postdating continental fragmentation., *Reviews of Geophysics*. <https://doi.org/10.1029/rg016i004p00621>

Talbot, C. J., and R. J. Jarvis, (1984). Age, budget and dynamics of an active salt extrusion in Iran. *Journal of Structural Geology*, 6, 521-533.

Talbot, C. J., Alavi, M. (1996). The past of a future syntaxis across the Zagros. *Geological Society of London, Special Publication*, 100, 89-109. DOI:10.1144/GSL.SP.1996.100.01.08.

Talebian, M., Jackson, J.A. (2002). Offset on the Main Recent Fault of the NW Iran and implications for the late Cenozoic tectonics of the Arabia-Eurasia collision zone. *Geophysical Journal International*, 150, 422-439. DOI:10.1046/j.1365-246X.2002.01711

Talebian, M., Jackson, J.A. (2004). A reappraisal of earthquake focal mechanisms and active shortening in the Zagros mountains of Iran. *Geophysical Journal International*, 156, 506–526. DOI:10.1111/j.1365-246X.2004.02092

Tavakoli-Shirazi, S., Frizon de Lamotte, D., Wrobel-Daveau, J.-C., Ringenbach, J.-C., 2013. Pre-Permian uplift and diffuse extensional deformation in the High Zagros Belt (Iran): integration in the geodynamic evolution of the Arabian plate. *Arab. J. Geosci.*, 6 (7), 2329-2342. doi:10.1007/s12517-012-0542-5.

Tavani, S., Snidero, M., Muñoz, J.A., 2014. Uplift-induced residual strain release and late-thrusting extension in the Anaran mountain front anticline, Zagros (Iran)., *Tectonophysics*. <https://doi.org/10.1016/j.tecto.2014.08.018>

Tavani, S., Camanni, G., Nappo, M., Snidero, M., Ascione, A., Valente, E., Gholamreza, G., Davoud, M., Mazzoli, S., 2020. The Mountain Front Flexure in the Lurestan region of the Zagros belt: Crustal architecture and role of structural inheritances. *Journal of Structural Geology*. 104022. 10.1016/j.jsg.2020.104022.

Tavani, S., Arbués, P., Snidero, M., Carrera García de Cortázar, N., Muñoz, J. A.

(2011). Open Plot Project: an open-source toolkit for 3-D structural data analysis. *Solid Earth*, 2, 53-63. DOI:10.5194/se-2-53-2011

Tavani, S., Carola, E., Granado, P., Quintà, A., Muñoz, J. A. (2013). Transpressive inversion of a Mesozoic extensional forced fold system with an intermediate décollement level in the Basque-Cantabrian Basin (Spain). *Tectonics*, 32, 146-158. DOI:10.1002/tect.20019

Tavani, S., Storti, F., Lacombe, O., Corradetti, A., Muñoz, J. A., Mazzoli, S. (2015). A review of deformation pattern templates in foreland basin systems and fold-and-thrust belts: Implications for the state of stress in the frontal regions of thrust wedges. *Earth-Science Reviews*, 141, 82-104. DOI:10.1016/j.earscirev.2014.11.013

Tavani, S., Parente, M., Puzone, F., Corradetti, A., Gharabeigli, G., Valinejad, M., Morsalnejad, D., Mazzoli, S. (2018a). The seismogenic fault system of the 2017 Mw 7.3 Iran-Iraq earthquake: constraints from surface and subsurface data, cross-section balancing and restoration. *Solid Earth*, 9, 821–831. DOI:10.5194/se-9-821-2018.

Tavani, S., Parente, M., Vitale, S., Iannace, A., Corradetti, A., Bottini, C., Morsalnejad, D., Mazzoli, S. (2018b). Early Jurassic rifting of the Arabian passive continental margin of the Neo-Tethys. Field evidence from the Lurestan region of the Zagros fold-and-thrust belt, Iran. *Tectonics*, 27, 2586–2607. DOI:10.1029/2018TC005192.

Tavani, S., Corradetti, A., Sabbatino, M., Morsalnejad, D., Mazzoli, S. (2018c). The Meso-Cenozoic fracture pattern of the Lurestan region, Iran: The role of rifting, convergence, and differential compaction in the development of preorogenic oblique fractures in the Zagros Belt. *Tectonophysics*, 749, 104-119. DOI:10.1016/j.tecto.2018.10.031.

Tikoff, B., Kelso, P., Manduca, C., Markley, M.J., Gillaspay, J., 2001. Lithospheric and crustal reactivation of an ancient plate boundary: the assembly and disassembly of the Salmon River suture zone, Idaho, USA., Geological Society, London, Special Publications. <https://doi.org/10.1144/gsl.sp.2001.186.01.13>

Trusheim, F., 1960. Mechanism of salt migration in northern Germany: *American Association of Petroleum Geologists Bulletin*, 44, 1519-1540.

Tugend, J., Manatschal, G., Kusznir, N. J., Masini, E., Mohn, G., Thinon, I. (2014). Formation and deformation of hyperextended rift systems: Insights from rift domain mapping in the Bay of Biscay-Pyrenees. *Tectonics*, 33, 1239-1276.

DOI:10.1002/2014TC003529

Valente, E., Buscher, J.T., Jourdan, F., Petrosino, P., Reddy, S.M., Tavani, S., Corradetti, A., Ascione, A. (2019). Constraining mountain front tectonic activity in extensional setting from geomorphology and Quaternary stratigraphy: A case study from the Matese ridge, southern Apennines. *Quaternary Science Reviews*, 219, 47-67, DOI:10.1016/j.quascirev.2019.07.001

Vajedian, S., Motagh, M., Mousavi, Z., Motaghi, K., Fielding, E., Akbari, B., Wetzell, H.H., Darabi, A. (2018). Coseismic deformation field of the MW 7.3 12 November 2017 Sarpol-e Zahab (Iran) earthquake: A decoupling horizon in the northern Zagros Mountains inferred from InSAR observations. *Remote Sensing*, 10, 1589. DOI:10.3390/rs10101589.

Van de Fliert, J. R., 1953, Tectonique d'écoulement et Trias diapir au Chetthaabas, sud-ouest de la ville de Constantine, Algérie, in 19th International Geological Congress, Algeria, 3, 71–92.

Vendeville, B. C., and Jackson, M. P. A. (1992a). The rise of diapirs during thin-skinned extension. *Marine and Petroleum Geology*, 9, 331-353.

Vendeville, B. C., and Jackson, M. P. A. (1992b). The fall of diapirs during thin-skinned extension: *Marine and Petroleum Geology*, 9, 354-371.

Vergés, J., Muñoz, J.A., Martínez, A., 1992. South Pyrenean fold and thrust belt: The role of foreland evaporitic levels in thrust geometry., *Thrust Tectonics*. https://doi.org/10.1007/978-94-011-3066-0_23

Vergés, J., Saura, E., Casciello, E., Fernández, M., Villaseñor, A., Jiménez-Munt, I., García-Castellanos, D. (2011a). Crustal-scale cross-sections across the NW Zagros belt: Implications for the Arabian margin reconstruction. *Geological Magazine*, 148, 739–761. DOI:10.1017/S0016756811000331

Vergés, J., Goodarzi, M. G. H., Emami, H., Karpuz, R., Efstathiou, J., Gillespie, P. (2011b). Multiple detachment folding in Pusht-e Kuh arc, Zagros: Role of mechanical stratigraphy, in K. McClay, J. Shaw, and J. Suppe, eds., *Thrust fault related folding*. AAPG Memoir, 94, 69-94. DOI:10.1306/13251333M942899

Vendeville, B. C., and M. P. A. Jackson, 1992a, The rise of diapirs during thin-skinned extension: *Marine and Petroleum Geology*, 9, 331–353.

Vendeville, B. C., Jackson, M. P. A., 1992b. The rise of diapirs during thin-skinned extension. *Marine and Petroleum Geology*, 9, 331-353.

- Vendeville, B., H. Ge, and M. P. A. Jackson, 1995, Scale models of salt tectonics during basement-involved extension: *Petroleum Geoscience*, 1, 179–183.
- Vennin, E., Kolodka, C., Asghari, A., Thomazo, C., Buoncristiani, J.F., Goodarzi, H., Desaubliaux, G., 2015. Discussion on Palaeozoic discontinuities in the Kuh-e Surmeh area (Zagros, Iran). *Marine and Petroleum Geology*, 66, 1073-1092.
- Vernant, P., Nilforoushan, F., Hatzfeld, D., Abbassi, M.R., Vigny, C., Masson, F., Nankali, H., Martinod, J., Ashtiani, A., Bayer, R., Tavakoli, F., Chéry, J. (2004). Present-day crustal deformation and plate kinematics in the Middle East constrained by GPS measurements in Iran and northern Oman. *Geophysical Journal International*, 157, 381-398, DOI:10.1111/gji.2004.157
- Viola, G. and Henderson, I. C. (2010). Inclined transpression at the toe of an arcuate thrust: an example from the Precambrian ‘Mylonite Zone’ of the Sveconorwegian orogen. *Geological Society of London, Special Publications*, 335, 715-737. DOI: 10.1144/SP335.29
- Wells, D. L. Coppersmith, K. J. (1994). New empirical relationships among magnitude, rupture length, rupture width, rupture area, and surface displacement. *B. Seismol. Soc. Am.*, 84, 974–1002.
- Wenkert, D. D., (1979). The flow of salt glaciers. *Geophysical Research Letters*, 6, 523-526.
- Williams, G.D., Powell, M.A., Cooper, M.A. (1989). Geometry and kinematics of inversion tectonics. *Geological Society of London, Special Publications*, 44, 3-15. DOI:10.1144/GSL.SP.1989.044.01.02
- Whitmarsh, R. B., Manatschal, G., Minshull, T. (2001). Evolution of magma-poor continental margins from rifting to seafloor spreading. *Nature*, 413, 150–154. DOI:10.1038/35093085.
- Wilckens, O., 1912, *Grundzüge der tektonischen Geologie*: Jena, Fischer.
- Williams, G.D., Powell, M.A., Cooper, M.A. (1989). Geometry and kinematics of inversion tectonics. *Geological Society of London, Special Publications*, 44, 3-15. DOI:10.1144/GSL.SP.1989.044.01.02
- Wilson, J. Did the Atlantic Close and then Re-Open? 1966. *Nature* 211, 676–681. Doi: 10.1038/211676a0
- Withjack, M. O., Scheiner, C., 1982. Fault patterns associated with Domes – An experimental and Analytical Study. *AAPG Bulletin*, 66 (3), 302-316.

Wrobel-Daveau, J.-C., Ringenbach, J.-C., Tavakoli, S., Ruiz, G. M. H., Masse, P., Frizon de Lamotte, D. (2010). Evidence for mantle exhumation along the Arabian margin in the Zagros (Kermanshah area, Iran). *Arabian Journal of Geosciences*, 3, 499–513. DOI:10.1007/s12517-010-0209-z

Zebari, M., Grützner, C., Navabpour, P., Ustaszewski, K. (2019). Relative timing of uplift along the Zagros Mountain Front Flexure (Kurdistan Region of Iraq): Constrained by geomorphic indices and landscape evolution modeling. *Solid Earth*, 663-682. DOI:10.5194/se-10-663-2019

Ziegler, M.A., 2001. Late Permian to Holocene paleofacies evolution of the Arabian Plate and its hydrocarbon occurrences. *GeoArabia* 6, 445–504

Zamanzadeh, S.M., Amini, A., Ghavidel Syooki, M., 2009. Sequence stratigraphic controls on early-diagenetic carbonate cementation of shallow marine clastic sediments (the Devonian Zakeen Formation, southern Zagros, Iran). *Geosciences Journal*, 13 (1), 31-57.

Ziegler, P.A., 1989. Evolution of the Arctic — North Atlantic Rift System., Earthquakes at North-Atlantic Passive Margins: Neotectonics and Postglacial Rebound. https://doi.org/10.1007/978-94-009-2311-9_3

Ziegler, M.A., 2001. Late Permian to Holocene Paleofacies Evolution of the Arabian Plate and its Hydrocarbon Occurrences. *GeoArabia*, 6 (3), 445-503.

Zoback M.D. (2010) Reservoir geomechanics, Cambridge University Press, Cambridge, UK.